DOCTORAL DISSERTATION SERIES

TITLE HEAT TRANSFER AND PRESSURE DROP FOR SUPERHEATED STEAM FLOWING IN PLAIN AND MODIFIED ANNULI

AUTHOR GEORGE W. GOVIER, JR.

UNIVERSITY U of Michigan DATE 1948

DEGREE Sc.D. PUBLICATION NO. 1106

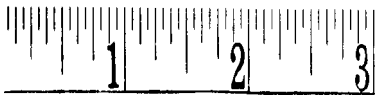

HEAT TRANSFER AND PRESSURE DROP

FOR SUPERHEATED STEAM

FLOWING IN PLAIN AND MODIFIED ANNULI

BY

George W. Govier

A Dissertation Submitted in Partial Fulfillment of the Requirements for the Degree of Doctor of Science, in the University of Michigan.

Committee in Charge:
Professor Robert R. White, Chairman
Professor Donald L. Katz
Professor Alan S. Foust
Assistant Professor William W. Hagerty

August, 1948
Ann Arbor, Michigan

To my wife

Doris

THE PROBLEM

This study is concerned with an evaluation of the heat transfer and pressure drop factors involved in the general problem of superheating medium pressure steam through its contact, under flow, with heated bare and extended metallic surfaces. A simple geometry, that of the annulus in various modifications, is chosen for detailed study.

SUMMARY

Heat transfer coefficients and associated pressure drops are determined for superheated steam flowing in the plain and modified annuli formed between a 4.026-inch I. D. shell and a 1.500-inch O. D. tube, and three 1.500-inch O. D. tubes supporting extended surfaces of various types. The transfer section is 15.0 feet long in the case of the plain tube and 13.0 feet long for the various finned tubes. The Reynolds number of the steam is varied from 5000 to 102,000 over the temperature range of 294°F. to 460°F. at two pressures of 50 and 100 psi. abs. Temperature differences between the heated inner tube and the steam vary from 30°F. to 160°F.

The gas phase heat transfer coefficients, based upon the total exposed surface, are found to range from 2.85 to 26.2. A simple graphical method is developed for separating these coefficients into their radiation and convection components. This method indicates that from 6.6 to 59 percent of the total heat transfer is accomplished by radiation.

The radiation components of the heat transfer coefficients are also calculated from radiation theory, and the convection components obtained by difference. The validity of the method is established by the correlation of the convection data. The necessary absorptivities and emissivities of steam are obtained by extrapolating available data on the emissivity of water vapor in air by means of a theoretical equation. The extrapolated values are substantiated by the correlations of the data

and by the good agreement between calculated values of the emissivity of steel and values recorded in the literature. In the modified annuli the rigorous application of fundamental radiation theory is hopelessly tedious for engineering purposes. It is shown, however, that these cases may be handled as plain annuli by considering the extended surface as equivalent to a bare surface of unit emissivity.

The convection heat transfer coefficients are analyzed and correlated by Dittus-Boelter type equations as follows:

Bare Tube Annulus: $$h = .0220 \frac{K}{D_v}\left(\frac{C\mu}{K}\right)^{0.4}\left(\frac{D_v W}{\mu S_{min}}\right)^{0.80}$$

Longitudinal Fin Tube Annulus: $$h = .0117 \frac{K}{D_v}\left(\frac{C\mu}{K}\right)^{0.4}\left(\frac{D_v W}{\mu S_{min}}\right)^{0.80}$$

"Star" Fin Tube Annulus: $$h = .0078 \frac{K}{D_v}\left(\frac{C\mu}{K}\right)^{0.4}\left(\frac{D_v W}{\mu S_{min}}\right)^{0.91}$$

Helical Fin Tube Annulus: $$h = .00494 \frac{K}{D_v}\left(\frac{C\mu}{K}\right)^{0.4}\left(\frac{D_v W}{\mu S_{min}}\right)^{0.91}$$

The pressure drop data are correlated in the conventional manner by the equations:

Bare Tube Annulus: $$f = 0.133 \left(\frac{D_v W}{\mu S_{min}}\right)^{-0.16}$$

Longitudinal Fin Tube Annulus: $$f = 0.133 \left(\frac{D_v W}{\mu S_{min}}\right)^{-0.16}$$

ACKNOWLEDGMENT

The author wishes to express appreciation to Professor R. R. White who supervised this work and to other members of the Doctorate Committee, Professors A. S. Foust, W. W. Hagerty, and D. L. Katz, for their interest and guidance.

Acknowledgment is also made to Professor H. C. Hottel of the Massachusetts Institute of Technology for his guidance in the theoretical radiation studies.

The author is indebted to

American Structural Products Company for their sponsorship of this work and especially to Mr. U. E. Bowes, President, Mr. E. C. Shuman, Director of Research, and Mr. J. K. Selden of this organization;

to The Engineering Research Institute of the University of Michigan under whose immediate auspices the work was conducted;

and to The Brown FinTube Company,
The Foster Wheeler Corporation, and
The Griscom-Russell Company
who furnished the finned tubes for the heat exchanger.

Appreciation is also expressed to the following, who helped with the construction of the equipment and with the collection of much of the data:

Mr. T. H. Elferdink

Mr. S. Miner

Mr. H. M. Noritake

Mr. W. R. Studhalter

Mr. L. Wenzel

and to Mr. D. I. Saletan for his assistance with the calculations.

TABLE OF CONTENTS

LIST OF TABLES

LIST OF FIGURES

APPENDIX B

I. INTRODUCTION

The problems of superheating steam, and of maintaining steam in a superheated condition while heat is being extracted from it, are of increasing interest in the light of new industrial process developments in which superheated steam plays an important role. A case in point is the use of superheated steam as a drying medium. Such a use necessitates a continuous input of heat to the circulating drying medium in order to maintain the superheat level desired for optimum drying performance.

In a process of this type piping and pressure drop difficulties generally prevent the use of conventional superheaters which pass the steam through tubes heated externally by convection and radiation from hot combustion gases. Much simpler circuits may be devised in which the steam is circulated over bare or extended metallic surfaces maintained hot by condensing higher pressure steam, condensing Dowtherm vapor, or circulating hot oil, molten salt, etc.

The magnitudes of the heat transfer coefficients and the pressure drops realized by the flow of superheated steam over plain and extended metallic surfaces can not at present be predicted with any reasonable degree of certainty. There are several reasons for this situation:

1. Uncertainties in our knowledge of certain of the physical properties of superheated steam. This is especially true in the case of viscosity and thermal conductivity.

2. Uncertainties and wide gaps still remaining in the generalized correlations of heat transfer coefficients and friction factors in terms of fluid properties, geometrical parameters, and flow rate.

3. Uncertainty as regards the magnitude and relative importance of direct radiant heat transfer to superheated steam.

In addition to the difficulty of predicting heat transfer rates and pressure drops, there is the additional (although related) problem of surface arrangement. It is well known that increased surface, or increased turbulence (as caused by a high degree of surface roughness, baffles transverse to the fluid flow, etc.), causes an increase in the heat transfer rate at the same flow mass velocity. It is also known that such increased surface or turbulence causes an increase in the pressure drop and hence in the power required to maintain flow. The question arises as to whether, with certain types of surface arrangements and turbulence promoters, the gain in heat transfer rate is sufficient to compensate for the increased power requirement.

This question and others may be answered provided the heat transfer coefficients and the friction factors can be correlated in terms of fluid properties and flow rate for the various geometries.

The present study is undertaken to determine these relations for superheated steam flowing in plain annuli and in the modified annuli formed between various finned tubes and a constant outer shell.

A general outline of the program of study is as follows:

1. For each of the annuli shown in Figure 2 (see next section), the collection of experimental data to yield gas (steam) phase heat transfer coefficients and friction factors for superheated steam flowing at Reynolds numbers over the range of 5000 to about 100,000.

2. The interpretation of these coefficients in terms of their radiation and convection components.

3. The correlation of the convection heat transfer coefficients, the radiation heat transfer coefficients, and the friction factors in terms of the fluid properties, the flow rate, and the geometry of the system.

4. The interpretation of the data to indicate the relative merits of the various surface arrangements from the viewpoint of their industrial utility.

II. INTRODUCTORY THEORY AND REVIEW OF LITERATURE

Heat Transfer Mechanisms in Annuli

The general case of heat transfer to a fluid flowing through an annular space involves all modes of heat transmission: conduction, convection, and radiation. In many instances the proportion of heat transferred by one or more of these mechanisms is small and may be neglected. It is necessary, however, to have a rather thorough understanding of the role played by all mechanisms in order to determine those of importance in a given case.

With this object in view, the case of a fluid, such as superheated steam, being heated in an annulus by the circulation of a hotter fluid through the inner tube will be considered in detail. Consider the annulus shown in Figure 1 formed between an inner 1-1/2-inch tube and an outer 4-inch pipe carrying external insulation. Assume fluids flowing in both the inner tube and the annular space and that the inner fluid is hotter than the annular fluid and that both are hotter than the environment. With reference to the figure, the following streams of heat may then be identified:

q_1, representing heat which flows by convection* from the inner fluid to the inside of the metal wall and thence, by conduction, through the metal wall to its outer surface.

q_{RT}, representing the net radiant energy emitted from the outer surface of the 1-1/2-inch tube.

---

*convection, as used here, includes heat transferred by the mechanism of fluid conduction. This is the generally accepted concept.

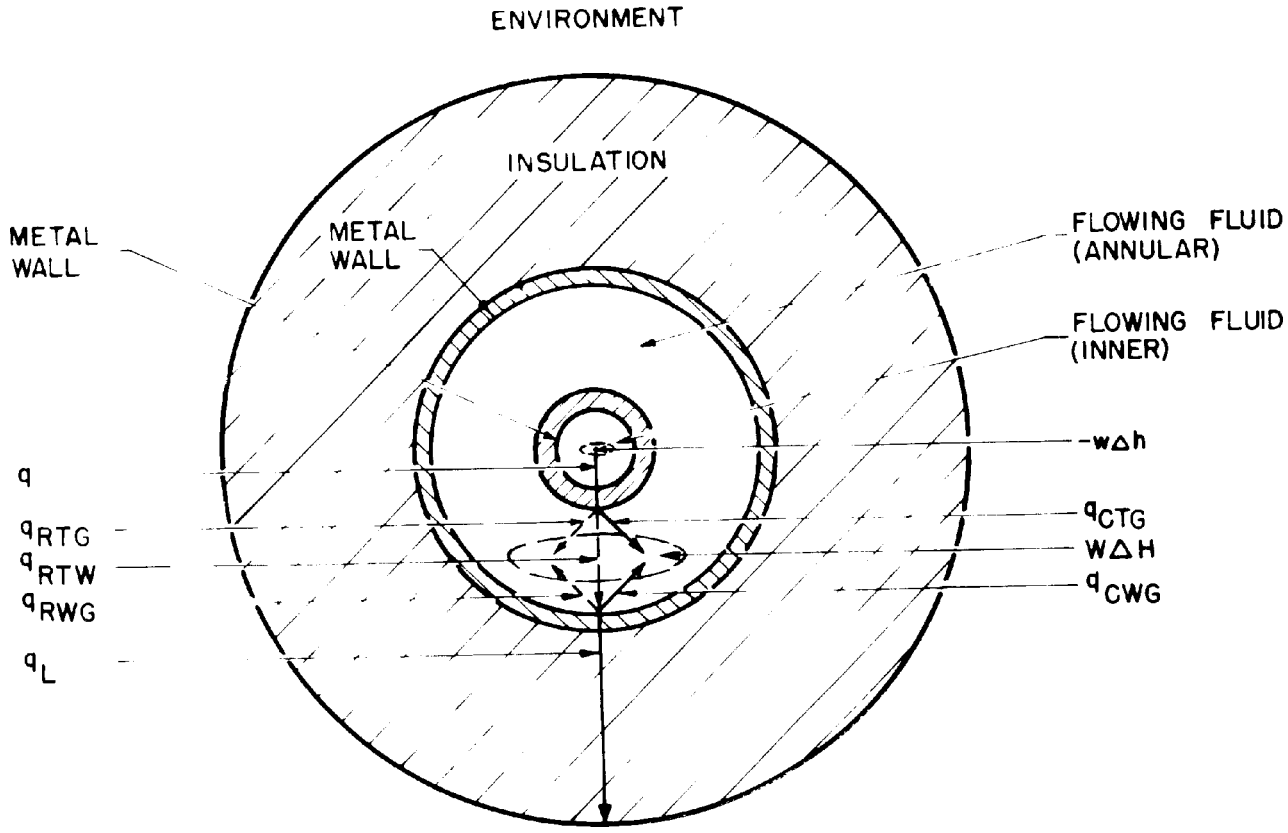

FIGURE 1.

HEAT TRANSFER MECHANISMS IN AN ANNULUS

DOTTED LINES REPRESENT RADIANT STREAMS. SOLID LINES REPRESENT CONVECTION AND/OR CONDUCTION STREAMS.

q_{RTW}, representing that net portion of q_{RT} which passes through the annular fluid and is absorbed by the inner wall of the 4-inch pipe.

q_{RTG}, representing that net portion of q_{RT} which is absorbed by the annular fluid.

q_{RWG}, representing the net radiant energy emitted by the inner wall of the 4-inch pipe and absorbed by the annular fluid.

q_{RW}, representing the total net radiant energy received by the inner wall of the 4-inch pipe.

q_{CTG}, representing the heat which is transferred by convection from the outer wall of the 1-1/2-inch tube to the annular fluid.

q_{CWG}, representing the heat which is transferred by convection from the inner wall of the 4-inch pipe to the annular fluid.

q_L, representing the heat loss from the system which is transferred by conduction through the wall of the 4-inch pipe and the layer of insulation and thence, by convection and radiation, to the environment.

$-w\Delta h$, representing the net amount of heat transferred from the inner fluid by all mechanisms.

Here w = rate of flow of inner fluid,
Δh = increase in enthalpy of inner fluid.

$W\Delta H$, representing the net amount of heat transferred to the annular fluid by all mechanisms.

Here W = rate of flow of annular fluid,
ΔH = increase in enthalpy of annular fluid.

Under conditions of steady state, heat balances may be written on (1) the inner fluid, (2) the inner tube, (3) the annular fluid, and (4)

the outer pipe. These balances and (5) the dependent over-all balance are as follows:

Inner Fluid:

$$- w\Delta h = q \qquad (1)$$

Inner Tube:

$$q = q_{RT} + q_{CTG} = q_{RTG} + q_{RTW} + q_{CTG} \qquad (2)$$

Annular Fluid:

$$W\Delta H = q_{RTG} + q_{CTG} + q_{CWG} + q_{RWG} \qquad (3)$$

Outer Pipe:

$$q_{RW} = q_{RTW} - q_{RWG} = q_L + q_{CWG} \qquad (4)$$

Over-all:

$$- w\Delta h = W\Delta H + q_L \qquad (5)$$

Before proceeding further with a discussion of the heat balances it is expedient to inquire more closely into the significance and relative importance of certain of the terms.

The quantities q_{RTG} and q_{RWG} which represent respectively the radiant energy transfer to the annular fluid from the tube and the outer wall, merit particular mention. These quantities are significant only in the case where the annular fluid is a gas which is at least partially opaque, i.e., one capable of absorbing radiant energy. Many gases such as air, oxygen, hydrogen, etc. are almost completely transparent to radiant energy and in such cases q_{RTG} and q_{RWG} would be negligibly small regardless of the temperature differentials. Other gases, including water vapor,

carbon dioxide, etc., are partially opaque to radiation and for these, particularly if the temperature differentials are large, say 50°F. or more, the terms q_{RTG} and q_{RWG} may be quite large.

In the case of liquids, radiant energy is almost completely absorbed in a very short distance of travel through the liquid, and for this reason the effect of radiant heat transfer is not separable from that of normal conduction. For liquids, therefore, q_{RTG} and q_{RWG} are zero since the equivalents of these quantities of heat are included in the conduction (i.e., convection*) term.

The quantity q_{RTW}, on the other hand, is significant only when the annular fluid exhibits some degree of transparency. For the case of air, oxygen, nitrogen, etc. the term may be of considerable importance, depending upon the temperature differential. The same is true, but to a lesser extent, for gases such as water vapor which exhibit partial transparency. The term is completely negligible in the case of liquids.

Returning now to a consideration of the heat balances in the general case where all terms are significant, it may be seen that only $-w\Delta h$, $W\Delta H$, and q_L are ordinarily capable of direct separate measurement. The over-all balance shows the necessary relationship which must exist between these three quantities under steady state conditions. Equation (1) indicates that the term $-w\Delta h$ is equal to q, the total heat transferred, which in turn, by Equation (2), equals the total radiation transfer from the inner tube plus the convection transfer. Combination of Equations (1), (2), and (5) indicates that:

---

*convection, as used here, includes heat transferred by the mechanism of fluid conduction. This is the generally accepted concept.

$$W\Delta H + q_L = - w\Delta h$$
$$= q$$
$$= q_{RTG} + q_{RTW} + q_{CTG}$$
$$= q_{RT} + q_{CTG} \qquad (6a)$$

Equation (6a) shows that q_{CTG}, the convection heat transfer from the inner tube to the annular fluid is:

$$q_{CTG} = (W\Delta H + q_L) - q_{RT} \qquad (6b)$$

i.e., is equal to the total heat transferred, less the total net radiant transmission from the inner tube.

This equation is significant in that it shows that the convective transfer from the inner tube is equal to the enthalpy gain only when both q_L, the heat loss, and q_{RT}, the total net radiant transfer from the inner tube, are negligibly small or equal. In measurements for the purpose of determining the convective heat transfer from the inner tube, efforts are normally made to keep the heat loss term small, but the importance of the radiation quantity may easily be overlooked.

Review of the Literature

The technical literature contains no specific references to the problem of superheating steam through its contact with heated surfaces in either plain or modified annuli. There are, however, numerous references to the general problems of turbulent heat transfer and pressure drop of other fluids in plain annuli and one or two such references to modified annuli.

Plain Annuli: Heat transfer between the walls of a plain annulus and an annular fluid, under conditions where both q_L and q_{RT} (see discussion above) are small or negligible, has been investigated by Dufinez and Marcus in 1938 (9), Thompson and Foust in 1940 (40), Foust and Christian in 1940 (10), Zerban in 1940 (47), Wiegand and Baker in 1942 (44), Mueller in 1942 (31), and Monrad and Pelton (30) in 1942. The work of these investigators has been critically analyzed and summarized by Davis (5) in 1943. Work of McMillen and Larson in 1943 (29) was discussed by Colburn and Gunter (3) in 1944. Wiegand in 1945 (45) discussed and compared most of the equations which had been proposed to that date. Carpenter, Colburn, Schoenborn, and Wurster (2) made investigations in 1946. These have been discussed by Jakob (21).

Many of these investigators have proposed correlating equations for the heat transfer coefficients in terms of the fluid properties, the flow rate, and the geometry of the system. The equations differ in form of presentation and also in other more important aspects including the values of numerical constants, the proper measure of the "equivalent diameter" of the annulus, the influence of the diameter ratio of the annulus, etc. Wiegand (45) points out, however, that all the equations may be expressed in the form:

$$J = \frac{h}{CG}\phi\left(\frac{C\mu}{K}\right) = K\psi\left(\frac{D_1}{D_2}\right)\left(\frac{D'G}{\mu}\right)^{-0.2} \qquad (7)$$

where h = convection heat transfer coefficient, Btu/hr.°F.ft.^{2}

C = specific heat of fluid, Btu/lb.°F.

G = mass flow velocity, lbs./hr.ft.^{2}

μ = viscosity of fluid, lbs./ft.hr.

K = thermal conductivity of fluid, Btu-ft./hr.°F.ft.^{2}

$(C\mu/K)$ = Prandtl number

$(D'G/\mu)$ = Reynolds number

D_1 = diameter at inner wall of the annulus, ft.

D_2 = diameter at outer wall of the annulus, ft.

D' = equivalent diameter, $D_2 - D_1$, ft.

and ϕ and ψ denote functions.

The function of the Prandtl number, $\phi\,(C\mu/K)$, which accounts for the difference in fluid properties, is given the following expression by the various proponents of equations:

Dittus-Boelter* (7): $(C\mu/K)^{1-m}$ (8)

where m = 0.4 for heating
m = 0.3 for cooling.

Colburn* (4): $(C\mu/K)^{2/3}\,(\mu/\mu_f)^{0.2}$ (9)

Norris-Sims*(28): $(C\mu/K)^{0.8}\,(\mu_w/\mu)^{0.14}$ (10)

Davis: $(C\mu/K)^{2/3}\,(\mu_w/\mu)^{0.14}$ (11)

where μ_f = viscosity evaluated at the film temperature, lbs./ft.hr.

μ_w = viscosity evaluated at the wall temperature, lbs./ft.hr.

For the heat transfer coefficient at the inner wall the value of $K\,\psi\,(D_1/D_2)$ is given as:

---

*Equations for circular pipes.

$$0.020\ (D_2/D_1)^{0.53} \qquad \text{by Monrad and Pelton} \qquad (12)$$

$$0.031\ (D_2/D_1)^{0.15}\ (D_2-D_1)^{0.2}\ D_1^{-0.2} \qquad \text{by Davis} \qquad (13)$$

$$0.0305\ (D_2-D_1)^{0.2}\ D_1^{-0.2} \qquad \text{by McMillen and Larson} \qquad (14)$$

and as $$0.077\ (D_2/D_1)^{0.2}\ (D_2-D_1)^{0.5}\ D_1^{-0.5} \qquad \text{by Mueller} \qquad (15)$$

The more complicated expressions, Equations (13), (14), and (15), arise from the fact that the Davis, McMillen, and Mueller equations all contained different "equivalent diameters" in the Reynolds number than does the "form" Equation (7).

For the heat transfer coefficient at the outer wall Davis gives:

$$K \not\phi\ (D_1/D_2) = 0.023\ (D_2-D_1)^q\ D_1^{-q} \qquad (16)$$

where q lies between 0.05 and 0.15.

Wiegand after a critical study of each of the proposed equations for heat transfer at the inner wall of an annulus, recommends the equation:

$$j = \frac{h}{CG}\left(\frac{C\mu}{K}\right)^{1-m} = 0.023\left(\frac{D_2}{D_1}\right)^{0.45}\left(\frac{D'G}{\mu}\right)^{-0.2} \qquad (17)$$

This equation may be transformed to the "Dittus-Boelter" form by multiplying each side by $D'G/\mu$ to obtain:

$$\frac{hD'}{K} = 0.023\left(\frac{D_2}{D_1}\right)^{0.45}\left(\frac{C\mu}{K}\right)^{m}\left(\frac{D'G}{\mu}\right)^{0.8} \qquad (18)$$

or $$h = 0.023\,\frac{K}{D'}\left(\frac{D_2}{D_1}\right)^{0.45}\left(\frac{C\mu}{K}\right)^{m}\left(\frac{D'G}{\mu}\right)^{0.8} \qquad (19)$$

For heat transfer at the outer annular wall, Wiegand recommends the "circular pipe" equation:

$$h = 0.023 \frac{K}{D'} \left(\frac{C\mu}{K}\right)^m \left(\frac{D'G}{\mu}\right)^{0.8} \qquad (20)$$

Carpenter, et. al. (2), investigating an annulus having a diameter ratio of 1.334, found their turbulent heat transfer data at the inner wall to satisfy the equation for circular pipes, i.e.,

$$h = 0.023 \frac{K}{D'} \left(\frac{C\mu}{K}\right)^m \left(\frac{D'G}{\mu}\right)^{0.8} \qquad (20)$$

better than that proposed by Wiegand.

Martinelli, Weinberg, Morrin, and Boelter (27) in 1942 conducted experiments under conditions in which q_{RTW} (radiation from the inner tube to the outer wall) was significant. These workers after making allowance for the radiation found their data to satisfy the Colburn analogy (4). The equation proposed by Colburn in his analogy between heat and momentum transfer is (4);

$$\frac{h}{CG} \left(\frac{C\mu}{K}\right)^{2/3} = \frac{f}{8} \qquad (21)$$

where f = friction factor.

The Nikuradse equation (32) for Reynolds numbers between 10,000 and 100,000 is closely approximated (27) by:

$$f = 0.176 \ (D'G/\mu)^{-0.2} \qquad (22)$$

By combining these, Martinelli obtained the equivalent of:

$$h = 0.021 \frac{K}{D'} \left(\frac{C\mu}{K}\right)^{1/3} \left(\frac{D'G}{\mu}\right)^{0.8} \qquad (23)$$

which was closely satisfied by their data. It should be mentioned, however, that the diameter ratio for their annulus was only 1.12 and that this does not constitute a sensitive test for the effect of this ratio.

Discussion of the theory of the radiation allowance as made by Martinelli, et.al., and of radiant heat transfer in general is deferred to a later section.

Regarding convection heat transfer at the inner wall of plain annuli, therefore, it must be concluded that while the Wiegand Equation (19) perhaps represents the bulk of the data reasonably well, the exact influence of annulus diameter ratio is still not known. So far as heat transfer to the outer wall is concerned, the regular Dittus-Boelter equation for circular pipes (with D' replacing D) appears to correlate the available data in a satisfactory manner.

Many of the investigators of annular heat transfer have also investigated annular pressure drop. The data are correlated in terms of f, the friction factor, and the Reynolds number. The friction factor is defined (44) as:

$$f = \frac{2F\beta D'}{V^2 L} \qquad (24)$$

where F = energy dissipated due to friction, feet of flowing fluid.

β = dimensional constant

= 32.1740 (mass lbs.) ft/(force lbs.) $sec.^2$

$D' = D_2 - D_1$ = equivalent diameter, ft.

V = lineal velocity, ft./sec.

L = length, ft.

(This friction factor is not to be confused with the other friction factor also in common use, $f' = f/4$).

The friction factor-Reynolds number correlations indicate pipe roughness to be an important parameter, but not diameter ratio (35,44).

Modified Annuli: Both heat transfer and pressure drop data have been obtained by Gunter and Shaw (12) in 1942 and DeLorenzo and Anderson (6) in 1944 for fluids flowing in the modified annulus formed between longitudinally finned tubes and circular shells. These data, however, are mainly in the streamline flow region and therefore not of particular interest to the problem at hand.

In 1946, Katz, Hope, and Datsko (16) presented turbulent pressure drop and heat transfer data for freon vapor flowing in the modified annuli formed between helically finned tubes and circular shells. Interpretation of these data in terms of fluid properties, flow rate, and geometrical parameters is difficult, however, because of the proportionately large "end effect". (The tubes employed were 12 inches, 24 inches, and 36 inches long.)

Summarizing, it may be stated that convection heat transfer coefficients for the inner tubes of plain annuli may be correlated by an equation of the Dittus-Boelter type, i.e.,

$$h = 0.023 \frac{K}{D'} \psi\left(\frac{D_1}{D_2}\right) \left(\frac{C\mu}{K}\right)^m \left(\frac{D'G}{\mu}\right)^{0.8} \qquad (25)$$

where $m = 0.3$ for cooling, and 0.4 for heating; in which, however, the term $\psi (D_1/D_2)$ is not definitely known. No equations are available for the corresponding cases of modified annuli. By analogy, however, one might expect correlations with equations of the form:

$$h = N \frac{K}{D'} \left(\frac{C\mu}{K}\right)^m \left(\frac{D'G}{\mu}\right)^n \qquad (26)$$

where N and n are constants dependent upon the geometry of the system. Equation (26) for modified annuli introduces the question of what constitutes the equivalent diameter for modified annuli of the type considered in this investigation. Details of those annuli are given in Figure 2 and in Table I, which follows in a later section. From Figure 2 it will be seen that the ordinary definition of equivalent diameter, i.e., 4 x cross sectional area/wetted perimeter, is inadequate in the cases of the annuli of "star" and helical fins. This is because the ratio of the cross sectional area to the wetted perimeter is not constant along these annuli, but alternates from its maximum value at the base of the fins to its minimum at the tip of the fins.

It is possible to define four different types of equivalent diameters for such annuli. First, the equivalent diameter might be defined at the point of maximum free cross section and secondly, at the point of minimum free cross section. A third possibility is to define the equivalent diameter in terms of the free volume for flow per unit of length and the "rubbing surface" per unit of length, i.e., the surface parallel to the axis of the annulus. Finally, the equivalent diameter might be defined in terms of the free volume for flow per unit of length and the total wetted surface per unit of length. Of these four possibilities the last one is believed to have more physical significance for the case of modified annuli in which the fin height-fin spacing ratio is relatively small, say 2 to 2-1/2 or less.

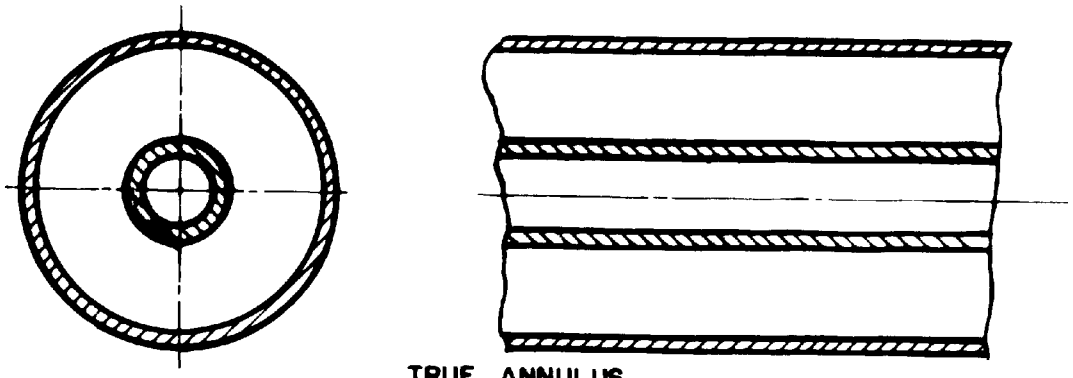

TRUE ANNULUS

a. BARE 1.500" x 1.000" TUBE IN 4.500" x 4.026" SHELL

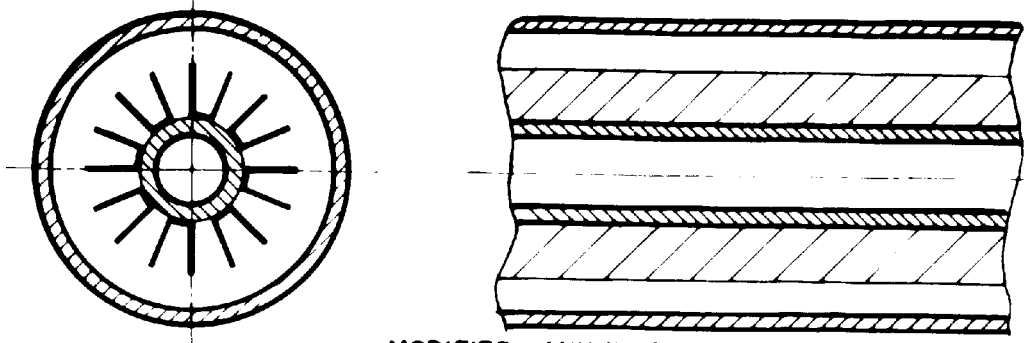

MODIFIED ANNULUS

b. LONGITUDIONALLY FINNED ($\frac{3}{4}$" HIGH) 1.500" x 1.000" TUBE IN 4.500" x 4.026" SHELL

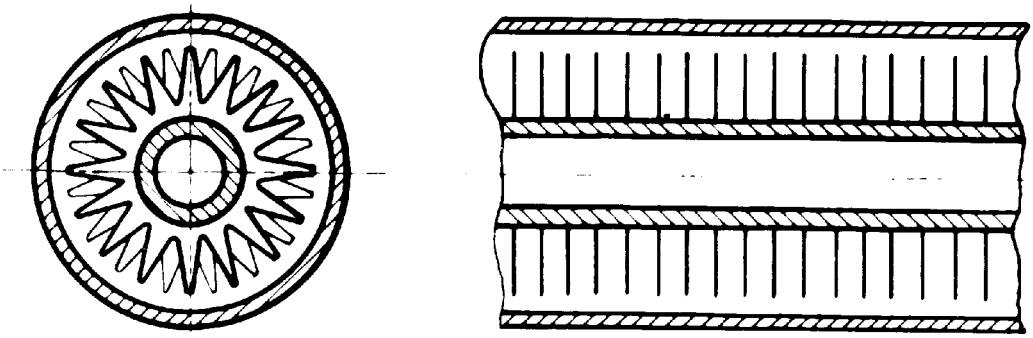

MODIFIED ANNULUS

c "STAR" FINNED (1" HIGH) 1.500" x 1.000" TUBE IN 4.500" x 4.026" SHELL

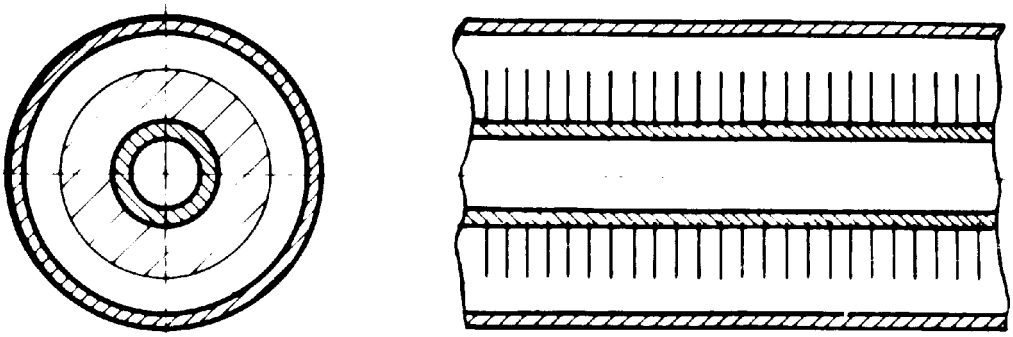

MODIFIED ANNULUS

d. HELICALLY FINNED ($\frac{3}{4}$" HIGH) 1.500" x 1.000" TUBE IN 4.500" x 4.026" SHELL

FIGURE 2

DETAILS OF THE TUBES AND THEIR ANNULI

III. EXPERIMENTAL EQUIPMENT

General

The experimental unit is designed to permit circulation of superheated steam through the annulus of a double tube heat exchanger, the inner tube of which is heated by circulating molten "heat transfer salt" (17). A schematic flow diagram is shown in Figure 3. This figure indicates the separate steam and salt circuits, the main pieces of equipment, and the important control devices.

The steam circuit includes the spray chamber, the circulating blower, the annulus of the heat exchanger, and the connecting piping. The steam is circulated by the blower and travels through a short connecting pipe to the heat exchanger, through the exchanger, and back to the spray chamber. A flow-regulating valve and an orifice plate installation are contained in the return line to the spray chamber.

The salt system consists of an electrically heated salt reservoir, a submerged-type vertical centrifugal pump, and the connecting lines to the inner tube of the heat exchanger. Molten salt is circulated through the exchanger by the pump. The salt piping contains a by-pass line and valve, an automatic flow control valve (not used in this work), an orifice plate installation, and a manual flow regulation valve.

The main control devices are for the control of the steam pressure, the steam temperature, and the salt temperature. Steam pressure is controlled through a small constant make-up of steam and automatic venting of the equipment whenever the pressure exceeds the desired value.

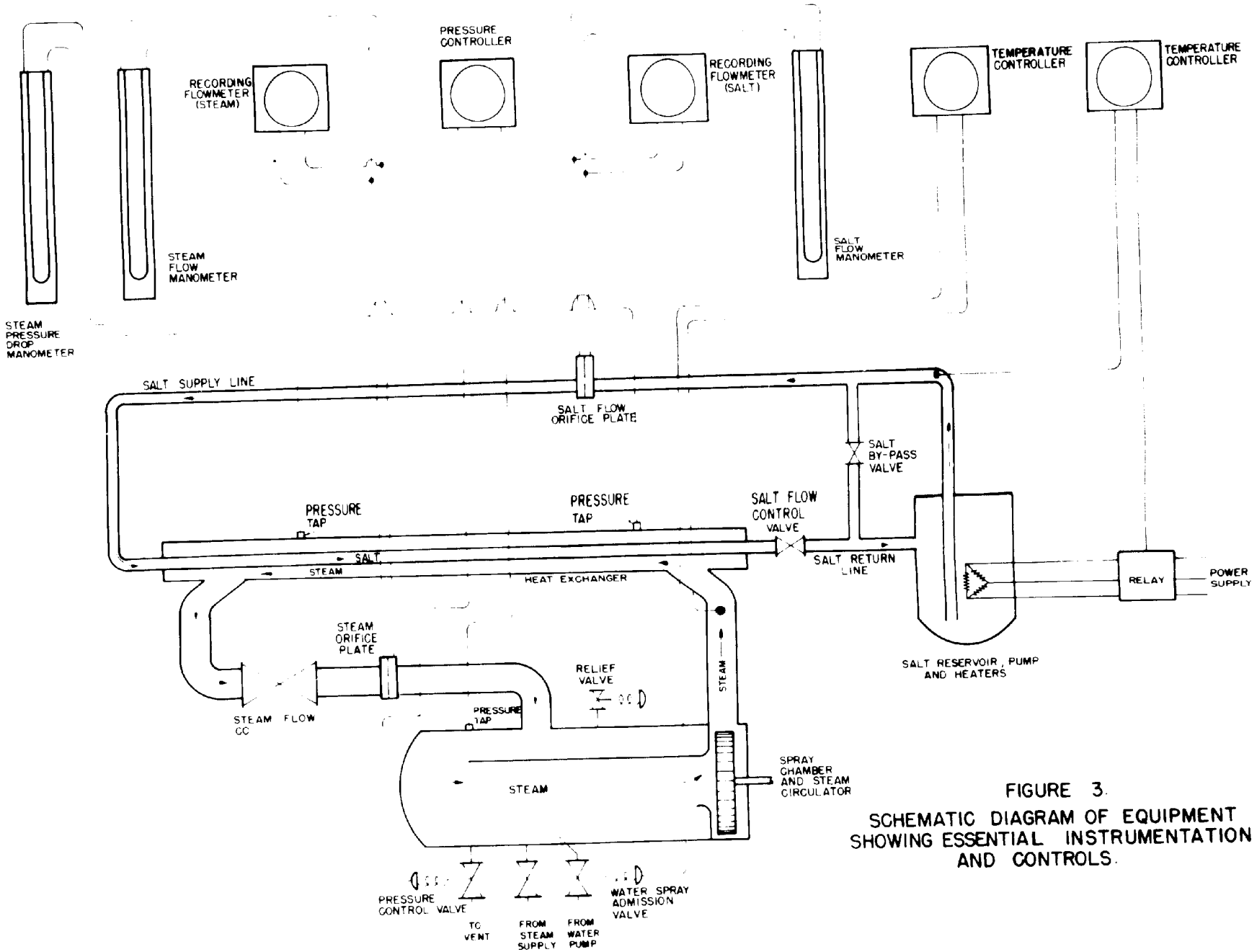

FIGURE 3.

SCHEMATIC DIAGRAM OF EQUIPMENT SHOWING ESSENTIAL INSTRUMENTATION AND CONTROLS.

Steam temperature is controlled by an automatic spray of cold water into the spray chamber. Salt temperature control is achieved by automatic regulation of the electric heaters to maintain the salt at the desired point. The flow diagram also indicates flow-measuring devices for both the steam and salt circuits.

Figures 4, 5, and 6 are photographic views of the equipment. Details of the equipment and instrumentation are described below.

Spray Chamber

The spray chamber was designed to permit its use in other work as well, and for this reason it is larger and more complex than really required for the present studies. The chamber consists of a horizontal cylindrical pressure vessel, closed at one end by a quick-opening door, and at the other end by the blower assembly which is connected by a flanged union seating on a Crane asbestos and graphite gasket, and closed by twelve 1-1/4-inch studs. The cylindrical shell from the quick-opening door to the blower-assembly flange is 71-11/16 inches long while the distance from flange face to the blower impeller housing is 11-7/16 inches.

The chamber shell is made from 18-inch, sched.40 seamless steel pipe, and is constructed for a working pressure of 300 psi and tested at 450°F. and 600 psi.

A horizontal baffle made from 10-gauge mild steel plate extends from the blower impeller housing to within 8 inches from the gasket of the quick-opening door. This baffle is 14-1/4 inches wide and is supported between two plates welded to the blower impeller housing and by the chamber shell. Steam enters the chamber under this baffle through an opening centered 18 inches from the blower impeller housing. This entrance duct

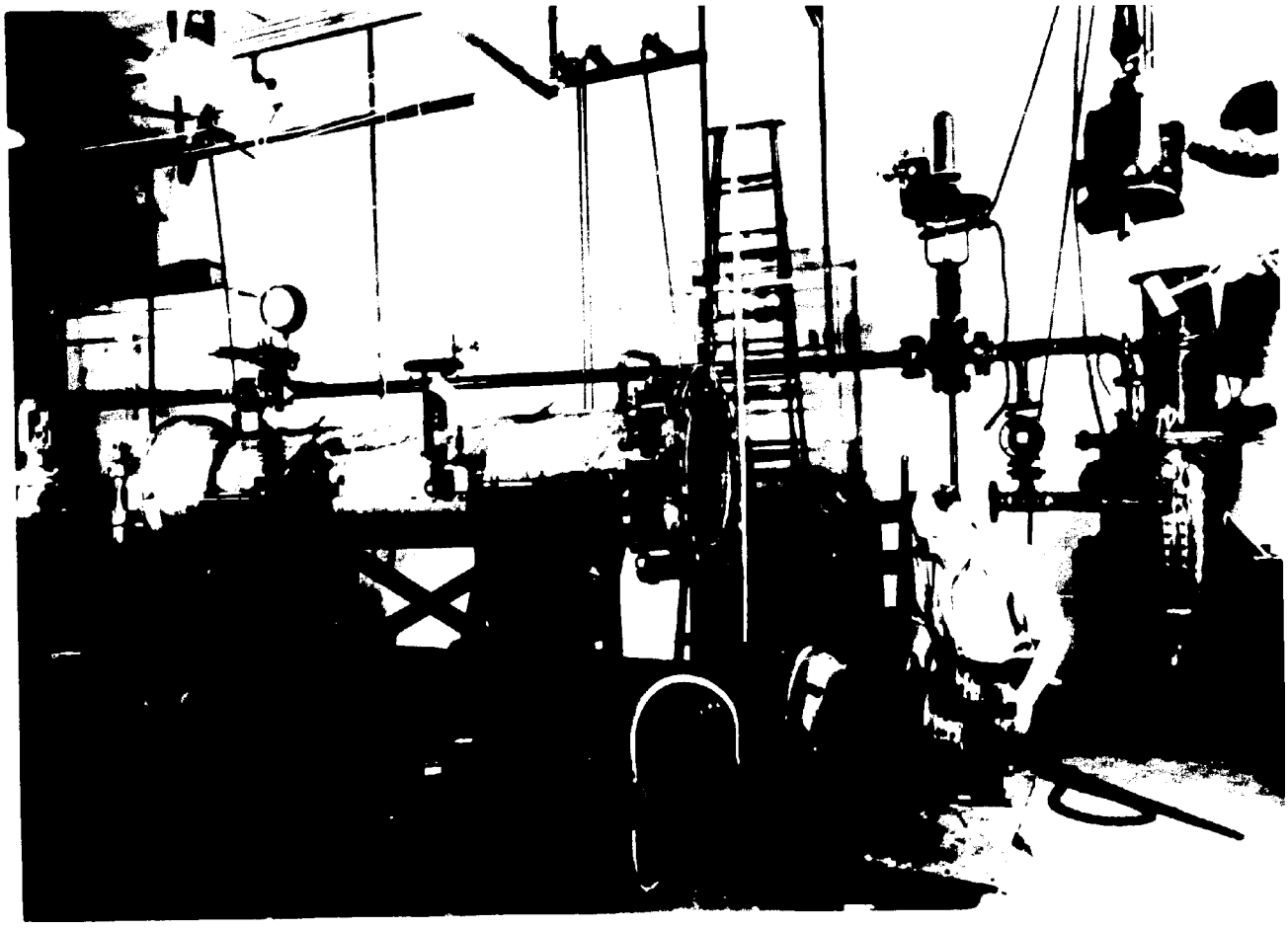

FIGURE 4

EXPERIMENTAL EQUIPMENT UNDER CONSTRUCTION

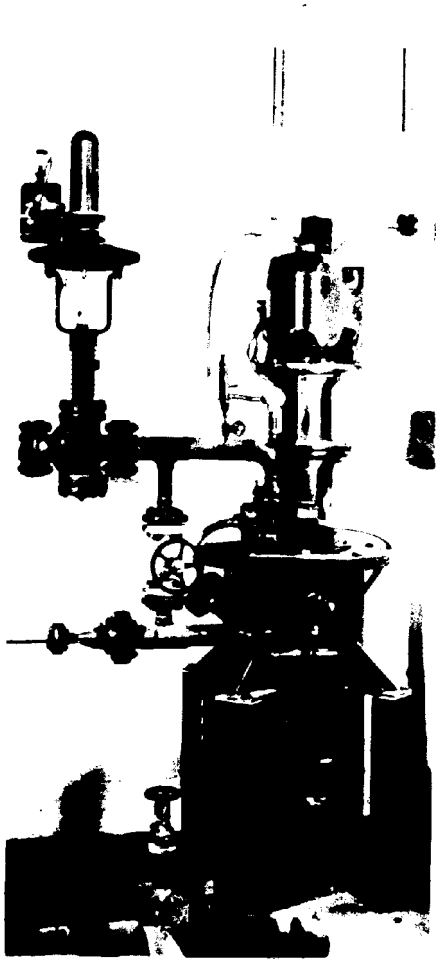

FIGURE 5

SALT RESERVOIR, PUMP, AND CONNECTIONS

BEFORE INSULATION

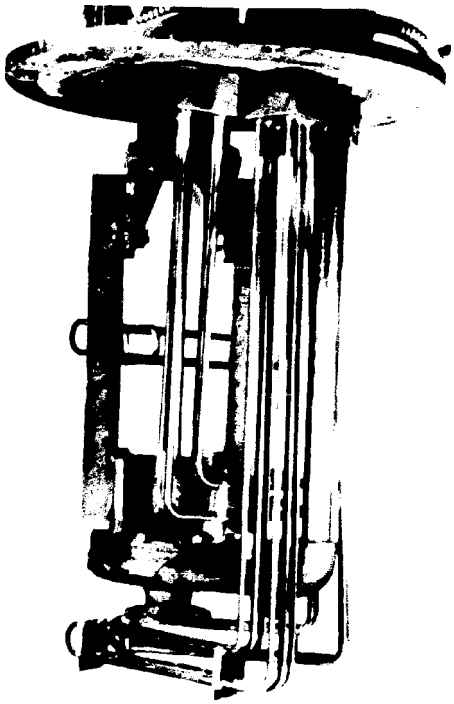

FIGURE 6

SALT PUMP AND HEATER ELEMENTS

is made from 4-inch sched.40 pipe welded tangent to the bottom of the chamber. From there, the steam travels underneath the horizontal baffle to the quick-opening door, then up past the baffle and back along it to the entrance duct of the blower impeller. The exit duct, also tangent to the bottom of the chamber, is rectangular, flaring into a length of 4-inch sched.40 pipe to which a 300-pound flange is welded.

Along the top of the spray chamber, openings are cut for two spray nozzles, a 150-pound U. S. Supergauge, a Taylor mercury thermometer, two 200-pound Kunkle relief valves, and a bleed valve. These openings are at the following distances from the quick-opening door: Taylor 50-750°F. thermometer, 10 inches; Kunkle relief valve and 150-pound gauge, 16 inches; spray nozzles, 29 inches and 69 inches; Kunkle relief valve and bleed line, 77 inches. On the side opposite the entrance port, openings are cut for the 125 psi. gauge, make-up steam which enters below the baffle 77 inches from the quick-opening door, and for the vent line on which the pressure control valve operates. The pressure tap leading to the (Foxboro) pressure controller is located on the opposite side of the chamber 28 inches from the quick-opening door.

Just behind the quick-opening door on the bottom of the chamber is a 3/4-inch drain line leading to a steam trap. This drain is used to remove the condensate that accumulates on first starting up the equipment. The 18-inch, 300-psi. quick-opening door was manufactured by the National Erie Corporation. This door consists of a blind flange in the shape of a spherical segment with the surface curving on an 18-inch radius. The edge of this plate is serrated with a tooth occupying every other five degrees. This plate rotates on a center shaft which swings on hinges attached to

the chamber. To close the door, the plate is swung into place against a rubber gasket. The door is then turned through five degrees so that the teeth on the door lock behind similar teeth on the door flange which is welded to the chamber shell. The gasket against which this door seals is made to fit in a slot in the door flange and is removed with the aid of an air jet which enters the bottom of the slot.

The chamber is insulated with 2-inch thick fiberglas board cut into strips and placed horizontally along the shell. A metal cover provided with handles and partially filled with fiberglas is used to insulate the quick-opening door.

The spray chamber is supported on a framework formed by four upright 10-inch x 1-1/2-inch channel irons braced with 2-inch x 2-inch x 1/4-inch angle iron.

Steam Blower

Impeller: Steam circulation is achieved by means of a turbo-blower mounted inside the spray chamber head and powered by a 10-horsepower motor. The blower impeller which was designed and fabricated by the American Blower Corporation is 12 inches in diameter, 1.72 inches wide, and fashioned of 18-8 stainless steel. The sides of the impeller are of No. 10 gauge steel, while the 10 blades are of 12 gauge steel. It weighs approximately 17 pounds and is welded throughout. The hub of the impeller is 2 inches in diameter with a 1-inch hole for mounting upon the drive shaft. It is designed to be run up to a maximum of 5000 rpm.

The impeller was warped somewhat during construction and machined almost paper thin on one face to eliminate the warping, so that an end plate 1/8-inch thick and 8 inches in diameter was riveted and welded to it

as reinforcement. It has been carefully balanced statically and dynamically by the Engineering Mechanics Department of the University of Michigan.

Scroll Case: The impeller is encased within a scroll case which has an outside diameter of 17-1/16 inches and fits snugly inside the head of the spray chamber. This is also fashioned of 10 gauge stainless steel, completely welded. It is 2-1/4 inches deep so that when the impeller, which with the reinforced plate is 1.86 inches wide, is centered in the space between the end plate of the chamber and the scroll case, there is 3/16-inch clearance on either side. The scroll case serves to enclose completely the impeller except near the center where the intake port, 4-3/8 inches in diameter, directs the steam flow into the impeller. The double-wall construction on the inside of the scroll case directs the steam from the impeller out of the 4-inch opening in the side of the spray chamber.

The closed face of the scroll case is reinforced on the outside by eight stainless steel angles 3/4-inch x 3/4-inch x 1/8-inch welded to it. Also welded perpendicular to this face are two stainless steel plates, 10-1/4 inches wide and 14-1/2 inches long, spaced 6-3/16 inches apart to form a groove into which is inserted the longitudinal baffle.

Blower Drive: The blower is driven by a motor, 10 horsepower, running at 1750 rpm. The power is transmitted through an Allis-Chalmers Vari-speed drive unit to a counter shaft on which is mounted a 7.4-inch pitch diameter Texdrive sheave with four grooves. Four belts, No. 6-B, run from the driver sheave to another Texdrive shaft with 4.6-inch pitch diameter, which is located on the blower shaft 27 inches directly above the counter shaft.

The pitch diameter of the Vari-pitch sheaves, one mounted on the motor and one on the countershaft, can be varied to drive the impeller at speeds ranging between 1470 and 5400 rpm. In the present work, however, the blower operates at approximately 3000 rpm to minimize the possibility of any breakdown in equipment. The bearings for the countershaft are two Fafnir ball-bearing self-aligning units mounted on steel supports so that the countershaft is located 10 inches off the motor base. The Vari-pitch sheave is between the two bearings while the Texdrive sheave is located on the 3-1/2-inch overhang.

The countershaft, the Vari-speed units, and the 10-horsepower motor are all located on a motor base, a plate of mild steel 38 inches x 36 inches x 1/2 inch. Five inches of cork board placed under this base reduces the vibration transmitted to the concrete floor. Belt guards fashioned of 10 gauge steel are fastened to this motor base and cover all belts.

Four V-belts, No. 6-B, run from 7.4-inch driver sheave to a 4.6-inch Texdrive sheave on the 1-7/16-inch blower shaft. This sheave is located between two Fafnir bearings of the self-aligning type, which in turn are mounted on a steel bracket securely bolted to the head of the autoclave (see illustration). Both Fafnir bearings are faced out to reduce the amount of overhang of the impeller as much as possible, but this overhang is still 11 inches from the face of the inboard bearing.

Stuffing Box: A stuffing box is provided where the 1-7/16-inch blower shaft passes through the spray chamber head. The stuffing box is 4-7/8 inches deep and receives 11 to 12 packing rings of alternate plastic and semi-metallic construction supplied by the Durametallic Corporation.

A lantern ring 3/4 inch wide is inserted as the sixth ring for lubrication purposes.

Part (1-7/8 inches) of the depth of the stuffing box is formed by a hole 2 inches in diameter bored into the chamber head so that the thickness of the head at the bottom of the stuffing box is only 1/2 inch. The stuffing box proper is fashioned out of mild steel 4 inches in diameter and 2-7/8 inches high. It is firmly bolted to the chamber head by means of six 1/2-inch cap screws. The 2-1/8-inch holes for the shaft and packing rings in the wall of the head and through the stuffing box are in perfect alignment since the hole was bored with the stuffing box in place. Taper pins are set to relocate the box if it should be necessary to unfasten it at any time.

A large nut 5 inches in diameter with a hole 1-1/2 inches for the shaft is screwed on over the stuffing box to tighten down on the follower and the packing rings. An Alemite connection for greasing and an air jacket for cooling are also provided on the stuffing box for smoother operation. This stuffing box performs very well with only a small amount of steam escaping.

The drive shaft, which is 1.436 inches in diameter, passes through the stuffing box and then through a hole 1.446 inches in diameter in the end plate of the spray chamber. Because of the small clearance between the shaft and the end plate at this point it is essential that the shaft be perfectly centered in the hole and then maintained in that position. Taper pins are inserted in key positions throughout the external bracket and pillow blocks to help relocate the shaft after dismantling operations.

Heat Exchanger

From the blower the steam passes to the annulus of the heat exchanger. The heat exchanger consists of a fixed shell in which various inner tubes may be installed.

The characteristics of the tubes are shown in Figure 2 and listed in Table I. Figure 9 is a photograph of the tubes to a larger scale than the photographs of Table I. The tubes all have a base O. D. of 1.500 inches and three of them carry extended surfaces:

(1) Tube, bare.

(2) Longitudinal fins, 3/4 inch high, 13 feet long, 16 fins equally spaced, and spot welded. Manufactured by the Brown FinTube Company.

(3) Star-shaped fins, 16 fins on a ring that slips on the tube, each fin 1/8 inch wide at the top, 3/8 inch wide at the base, and 13/16 inch high, rings spaced 3/8 inch apart and all fins staggered. Manufactured by the Foster-Wheeler Corporation.

(4) Transverse spiral fins, 3/4 inch high, 3 fins per inch, for length of 13 feet, crimped into slots in the tube wall. Manufactured by the Griscom-Russell Corporation.

The last two finned surfaces are intended by their manufacturers for heat transfer in transverse flow.

The selection of 1.500-inch O. D. tubing with 1/4-inch thick walls was quite arbitrary, although the heavy wall was chosen partly to give the tubes sufficient rigidity so that little or no sagging is encountered in the 14 feet of unsupported tube in the heat exchanger. This removes the necessity for using supports of any sort inside the heat exchanger that would disturb the flow pattern within the test section.

TABLE I

PROPERTIES OF EXCHANGER TUBES AND THEIR "ANNULI" IN A 4.026 I.D. SHELL

1	2	3	4	5	6	7	8	9	10	11		12	13	14	15	16	17
Type of Inner Tube (All Steel)	Photograph	Fin Height	Number of Fins per Lineal Inch	Number of Fins Around	Thickness of Fins	Active or Finned Length	Total Heat Transfer Length	Total Outside Surface Area per Lineal Finned Foot	Ratio of Surface of Finned Tube to Bare Tube	Total Outside Surface Area per 15.0 Feet		Equivalent Diameter of "Annulus" at Minimum Cross Section	Equivalent Diameter of "Annulus" at Maximum Cross Section	Equivalent Diameter of "Annulus" Volumetric Basis	Equivalent Diameter of "Annulus" Rubbing Surface Basis	Maximum Clear Cross Section in "Annulus"	Minimum Clear Cross Section in "Annulus"
Symbol, Units		w, Inches	per Inch		2y, Inch	Feet	Feet	Square Feet		Square Feet		D_e', Feet	D_e'', Feet	D_v, Feet	D_r, Feet	S_{max}, Sq. Ft.	S_{min}, Sq. Ft.
BARE		0	0	0		15.0	15.0	0.392	1.000	Unfinned portion: Finned portion: Total:	5.890 0.000 5.890	0.2105	0.2105	0.2105	0.2105	0.0760	0.0760
LONGI-TUDINAL FIN		0.750		16	0.0375 (20 ga.)	13.0	15.0	2.392	6.10	Unfinned portion (2.0 ft.) Finned portion (13.0 ft.) Bare tube, A_o: 4.45 Extended surface, A_f: 26.65 Total:	0.79 31.10 31.89	0.0849	0.0849	0.0849	0.0849	0.0730	0.0730
"STAR" FIN		1.000	2.49		0.062 (16 ga.)	13.0	15.0	2.332	5.94	Unfinned portion (2.0 ft.) Finned portion (13.0 ft.) Bare tube, A_o: 4.69 Extended surface, A_f: 25.61 Total:	0.79 30.30 31.09	0.0553	0.2001	0.0788	0.370	0.0740	0.0470
HELICAL FIN		0.750	3.00		0.0188 (26 ga.)	13.0	15.0	3.059	7.74	Unfinned portion (2.0 ft.) Finned portion (13.0 ft.) Bare tube, A_o: 4.81 Extended surface, A_f: 34.96 Total:	0.79 32.77 40.56	0.0855	0.2105	0.0720	0.714	0.0760	0.0393

The heat exchanger shell is symmetrically made by welding to a straight 13-foot section of 4-inch sched.40 pipe, two 4-inch sched.40 welding laterals. Complete details of this are shown in Figure 7. The inner tube, which can be removed and changed, enters through stuffing box assemblies bolted to 4-inch 300-pound welding neck flanges which are welded to the straight arm of the 4-inch laterals.

Figure 8 shows the details of the heat exchanger test section with the location of all measuring points. At the two ends of the central 10-foot section of the heat exchanger shell, 1/4-inch pressure taps are drilled through the 4-inch pipe and 1/4-inch nipples welded in the holes. Also, at these positions, thermocouples are placed in contact (by spot welding) with the outside of the 4-inch pipe, just under the surface of the insulation. Thermocouples are also located after the 45 degree bends formed by the welding laterals. In the downstream lateral, just beyond the thermocouple well, a bundle of ten 3-inch pieces of 3/4-inch sched.40 pipe is placed to serve as straightening vanes to help even out the temperature of the stream. A similar bundle of pipe lengths is placed in the welding neck flange opposite that welded to the downstream welding laterals. It was thought that these two short bundles of pipe length would even out the temperature so that the thermocouple immediately downstream from them would give a reliable average value for the steam temperature.

The heat exchanger, and the pressure taps leading from it, are completely insulated with 2-inch thick fiberglas PF pipe insulation. This insulation is covered with light canvas and painted white.

Connecting Piping: The spray chamber and heat exchanger are connected by two steam lines, each of 4-inch, sched.40 pipe. One line running from the blower outlet to the exchanger is 20-3/4 inches long and

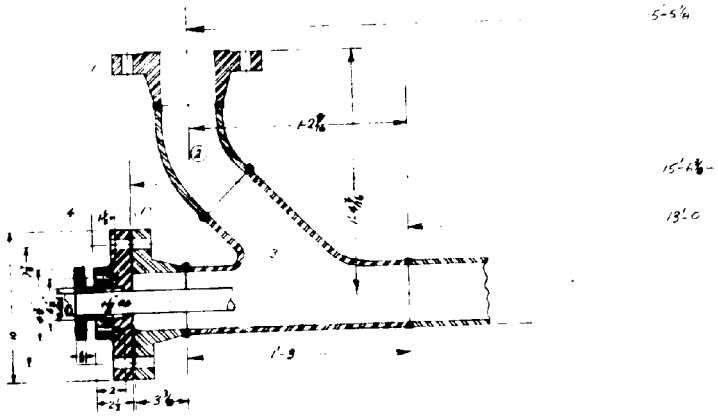

MARK NO.	UNITS	DESCRIPTION
	4	3" SCH. 40 WELDING NECK FLANGE
		3" SCH. 40 45° WELDING ELBOW
	2	4" SCH. 40 "TUBE TURN" WELDING LATERAL
	2	SLEEVING BOX ASSEMBLY FOR 2½" I.P.S.
	2	" " " " 1" I.P.S.
	2	" " " " 1½" I.P.S.
	L.C.	4" SCHEDULE NO. 40 PIPE - PERFECTLY STRAIGHT

NOTE

MAINTAIN BEST POSSIBLE ACCURACY IN ALIGNMENT.

FIGURE 7
CONSTRUCTION DRAWING
HEAT EXCHANGER SHELL
300 LB. W.P. STEAM 600°F

consists of two 300-pound welding flanges welded to a piece of 4-inch, sched.40 pipe. Inside of this spool are stacked seven 13-inch lengths of 1-inch pipe to remove any trace of water from the steam. The return line running from the heat exchanger to the chamber is joined to the exchanger by a flanged connection which is welded at a 45-degree angle to the main body of the exchanger. A flanged elbow completes the U-bend and the return pipe runs parallel to, but 28 inches closer to the chamber than, the heat exchanger. Eleven feet of straight 4-inch pipe plus a welded elbow with flange for bolting to the spray chamber constitute the remainder of the return system.

Two steel stands spaced 8 feet apart support both the exchanger and return pipe at a height of approximately 3 feet off the floor. These stands have adjustable members of 1/4-inch steel plate which gives the heat exchanger and connecting piping a slope of 1/4-inch per foot up from the spray chamber, thus permitting condensate to drain down into the trap into the chamber. A second Armstrong steam trap is located in the spool at the blower outlet for draining the heat exchanger.

Just after the U-bend at the outlet of the heat exchanger, is located a 4-inch flanged gate valve which is used for varying steam flow. The adjustments of this valve give all the range of steam flow desired in this work.

Nine and one-half feet downstream from the valve in the straight portion of the return pipe are located the orifice flanges,10 inches in diameter and 1-1/2 inches thick. These flanges are made to receive stainless steel orifice plates 7 inches in diameter with orifice sizes of 5/8 inch, 7/8 inch, 1-1/4 inches and 1-3/4 inches. Two jack screws 7/8 inch

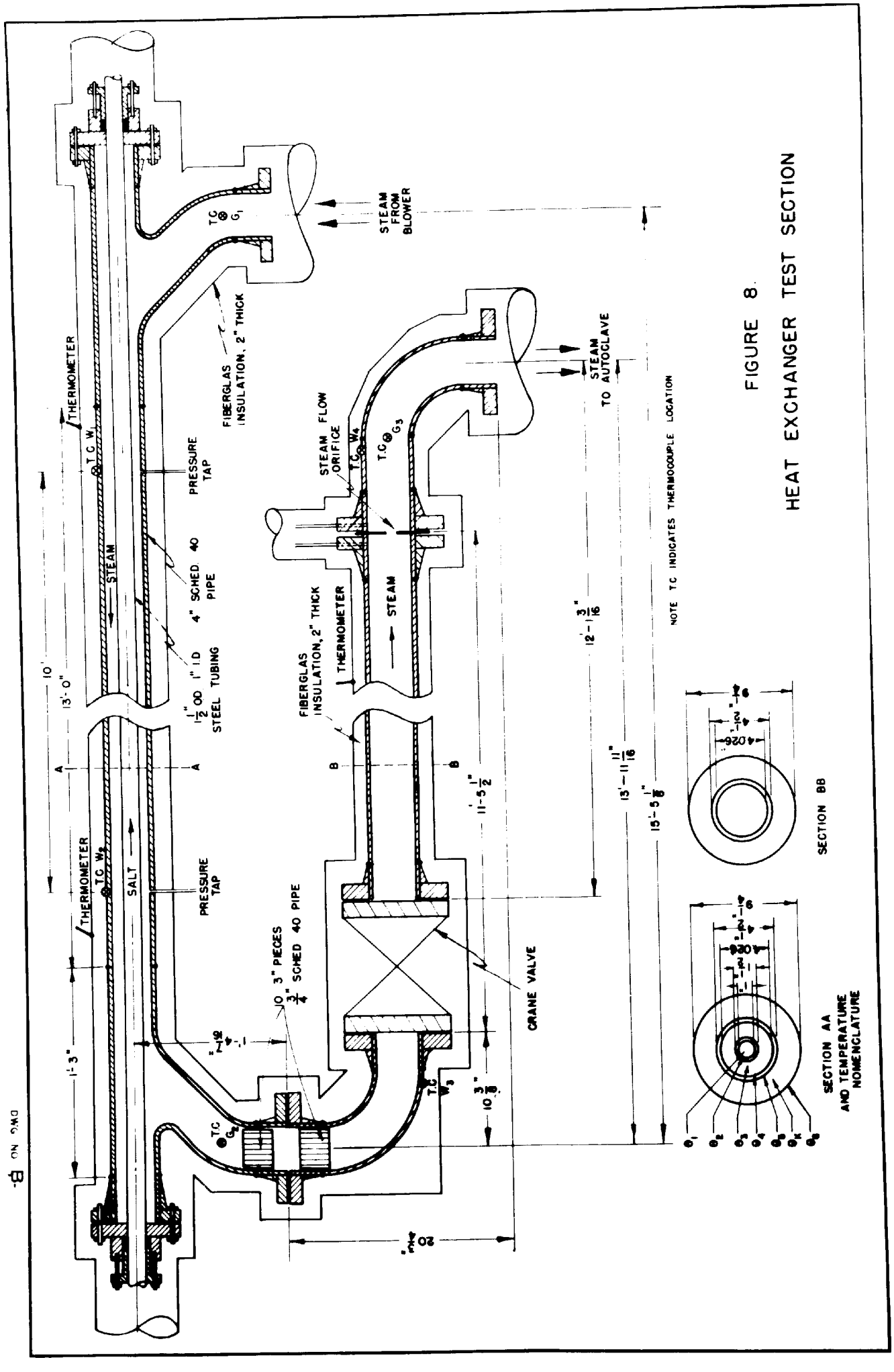

FIGURE 8.

HEAT EXCHANGER TEST SECTION

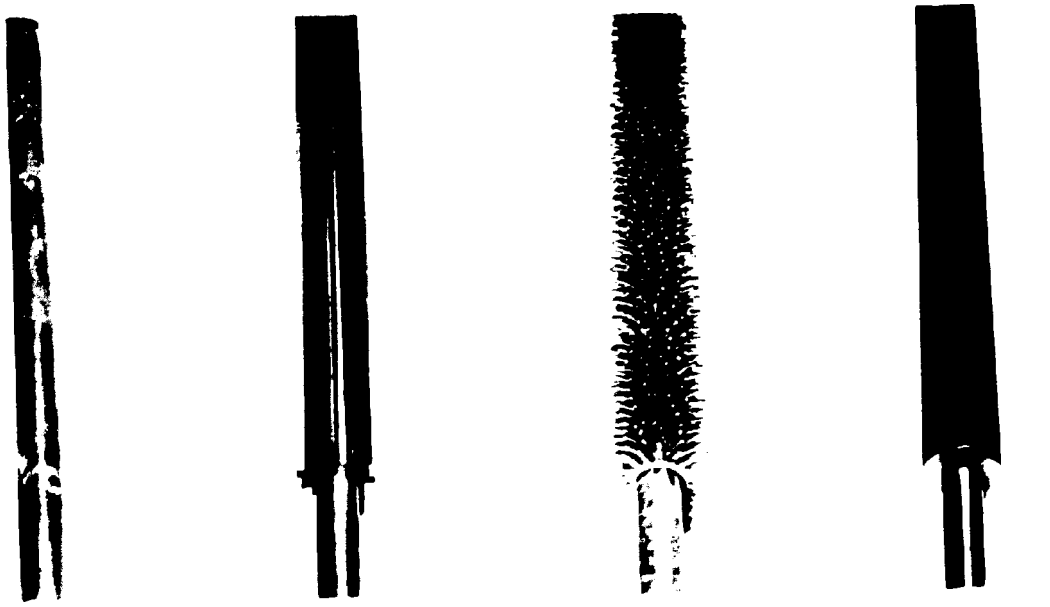

BARE TUBE

LONGITUDINAL FIN TUBE

"STAR" FIN TUBE

HELICAL FIN TUBE

FIGURE 9

HEAT EXCHANGER TUBES

in diameter aid in separating the orifice flanges when changing plates.

Spray System

The spray chamber is fitted with two water spray nozzles to be used to control the steam temperature. These nozzles are Spraying Systems Company nozzles type 1/4-LN-1 and 1/4-LN-1.5. Both have orifice diameters of 0.020 inch. These nozzles are screwed by means of a 1/4-inch coupling and nipple into a special steel fitting in the form of an elongated coupling which is welded diagonally into the top of the chamber so that the water spray is directed toward the quick-opening door. Outside the chamber each nozzle has its own valve and external filter. The supply lines then run to a tee, which is connected to the 1/4-inch Foxboro control valve and to the discharge side of a Milton Roy pump.

The 1/4-inch Foxboro control valve is pneumatically operated and designed to open when air pressure of 17 psi. gauge is applied. It is actuated by the Foxboro Dynalog temperature controller described under "Instruments."

The pump used to pump the water to the spray nozzles is a Milton Roy Simplex positive displacement pump. It is fitted with a 7/16-inch diameter stainless steel piston making 99 strokes per minute with a 3-inch maximum stroke which may be reduced by means of a screw adjustment. The pump has a capacity of 8.5 gallons per hour against a pressure of 500 psi. The step valve is made of cast iron with stainless steel valve seats and checks. The inlet port is 3/8-inch pipe tap, while the outlet is 1/4-inch pipe tap. The pump is driven by a General Electric 1/3-horsepower, single-phase, 60-cycle, 115-volt motor.

City water passes through a 1/4-inch line to a check valve, to a strainer, and then to the Milton Roy pump. The discharge side of the pump goes to a tee. One arm of the tee leads to a 300-pound Crosby gauge, then to the Foxboro control valve and to the spray nozzles. The other arm of the tee leads to a Kunkle 1/2-inch, 200 psi., relief valve which discharges into the drain. In operation the by-pass is closed and the relief valve manually set to control the pressure on the spray nozzles.

Salt System

The heat transfer medium employed in this experimental setup is the Dupont heat transfer salt known as "Hi-tec" (17). This is a mixture of sodium nitrite, sodium nitrate, and potassium nitrate with a melting point of 288°F. This salt is heated and kept in a molten state at about 500°F. by electrical immersion heaters located in a steel pot which also serves as a storage vessel for the salt when the unit is not operating. A submerged centrifugal pump, which is also located in the salt pot, pumps the molten salt from the bottom of the pot through a long loop, the upper half of which consists of approximately 22 feet of 2-1/2-inch pipe. In this section of the salt piping are located the Stabiflo control valve (not used in this work) and the orifice plate for measuring the rate of flow. The lower half of the loop, or the return portion of the system, is the inner tube of the heat exchanger.

Salt Pot: The salt pot is of a welded construction employing mild steel 1/2-inch thick. It has an internal diameter of 20 inches, straight sides 30 inches high, and a dished bottom 8 inches deep, giving it a capacity of 3 cubic feet of liquid. A heavy flange 1 inch thick with 20 inches I. D. internal diameter and 28 inches O. D. is welded to the top

of the pot and to this is bolted the pot cover which bears the salt pump and motor. The pot is supported on four I-beams 6 inches x 3-1/4 inches x 1/4 inch and 27 inches long so that the bottom of the pot is 6 inches off the floor.

A 2-1/2-inch welding neck flange located 10 inches below the top is used for charging the salt pot with Hi-tec salt and for adding occasional make-up salt. At approximately the same height, a short length of 2-1/2-inch pipe has been welded tangentially into the pot to serve as the return connection for the salt being circulated. Since the salt line is made to drain by gravity back into the pot when the pump is stopped, the pot can be filled only to the bottom of this opening. When the pump is operating, however, the salt level in the pot will drop approximately 7 inches below the original level, as the salt lines have a capacity of 0.66 cubic feet.

A Jerguson gauge is located on one side of the salt pot to show the salt level in the pot. It is connected to the pot by 3/4-inch pipe fittings screwed into couplings which were welded into the side of the pot. At a point 2 inches below the lower connection for the Jerguson gauge and in the dished bottom of the pot is welded a 1/4-inch pipe coupling into which is screwed an iron-constantan thermocouple for indication of the salt temperature near the entrance to the pump. At the same level and diametrically opposite from the thermocouple opening is an opening for a Fenwal thermoswitch which serves as a secondary control for the salt temperature. A packing gland and follower is used to tighten the thermoswitch into position. Since the tube of the thermoswitch is 8 inches long, it extends well into the salt pot and in between the loops of the lowest

electrical heater so that the thermoswitch is inserted only after the centrifugal pump and heaters have been lowered into position. Similarly, if the pump and heaters are to be removed from the pot, it is imperative that the thermoswitch be withdrawn first.

The salt pot was originally charged by making a mixture of Hi-tec and water, and then pouring this slush into the pot. As the water was evaporated, more of the mixture was added until 3 cubic feet of salt had been charged. In the case where the molten salt has been allowed to solidify in the shallow drainage pans, it is expected that the salt will simply be broken into pieces small enough to be fed through the 2-1/2-inch charging port, and then water will be added to immerse the heaters before starting heating. It is estimated that from 48 to 60 hours of heating will be required to evaporate all of the water completely and bring the salt temperature up to 500°F.

At the bottom of the pot is welded a 1-inch pipe connection with a Crane gate valve to be used for draining purposes. Since this pipe is located only 4 inches above the floor level, two pans 6 feet long, 30 inches wide, and 4 inches high are required to hold the entire contents of the pot. Due to the high temperature of the molten salt, these pans are intended to be filled to a depth of 2 inches so as to minimize the danger of injury from splashing and spilling of the hot liquid.

The salt pot is insulated completely with a 4-inch thickness of fiberglass, metal mesh blanket securely fastened to the sides, bottom and top. The heat loss from the pot to the surroundings is thus reduced to approximately 5700 Btu per hour so that when the pump is not in operation only one electric heater in Y circuit is sufficient to maintain the salt temperature at around 500°F.

Salt Pump: The salt pump is a Taber centrifugal pump of the submerged type, Model No. CL-3 with a rated capacity of 100 gpm against a 40-foot head. The pump is mounted to the 1-inch thick steel pot cover. The intermediate and lower bearing bushing and the pump casing are bolted to the under side of the pot cover, while the cast iron frame which supports the thrust bearing and motor is bolted to the top of the cover. The pump is powered by a 7-1/2-horsepower motor mounted on the cast iron frame 26 inches above the pot cover. It is connected to the 1-1/2 CR steel shaft by an American Flexible motor coupling.

The pump shaft is supported by 2 bearings including the Fafnir cartridge tube ball thrust and radial bearing which is fastened to the cast iron support 14 inches above the pot cover. Two lock nuts on this bearing permit the shaft to be raised or lowered for centering purposes. A steel bearing, cast iron bushed and located just above the pump casing, serves to hold the shaft in alignment. Since no lubrication can be used in this bearing, proper alignment of the shaft is very important. A water-jacketed stuffing box is located at the point where the 1-1/2-inch shaft passes through the 1-inch pot cover.

The entire pump assembly is offset 2-3/4 inches from the center of the pot to leave sufficient space for the 1-1/2-inch discharge pipe to pass through the cover. A stuffing box on the cover plate seals the pot, but allows for vertical expansion of the pipe. This pump operates very well.

Salt Heaters: Four Chromalox immersion heaters of the tubular heavy-duty type are mounted in the salt pot for heating the Hi-tec. These are shown in Figure 6. Three of the heaters, the two L-shaped heaters

located at the bottom of the pot and the semicircular type located 8 inches higher, are rated at 5 kilowatts each; while the fourth heater, which is located at present 6 inches above the middle heater, is rated at 3 kilowatts. Each heater is composed of three elements, porcelain insulated, and sheathed in 1/2-inch diameter steel tubes. The bottom two heaters are L-shaped, having a heated height of 13-3/4 inches, while the middle semicircular heater has a heated height of 4 inches. However, since the middle heater is situated approximately 8 inches above the bottom heater, the tops of the heated length of all three heaters are located at approximately the same level. Due to the limited space available in the salt pot, all of these heaters are specially designed.

To insure uniform distribution of heat in the salt pot, the 3- to 5-kilowatt heaters are interconnected so that each heater contributes one element to a three-phase circuit. In this way two heater elements near the bottom of the pot and one element 8 inches higher are in use when one circuit is turned on, thus distributing the heat. Three circuits, all connected in this fashion, are available for heating when the salt system is in operation.

The fourth heater,which is rated at 3 kilowatts, is located near the surface of the molten salt when the pump is not operating, but is completely exposed when the salt is being circulated. The purpose of this heater is to serve as a crust-breaker whenever the salt is being melted. At such times there is the possibility of gases being formed due to the decomposition of the salt from the local overheating,and gases trapped beneath a hard crust may lead to an explosion. However, in actual operation the salt has been kept molten constantly because of the time consumed to melt the salt, as well as the danger of overheating the electrical heaters

in the process.

In addition to the heater connection mentioned above, two of the heater circuits are also arranged so that the elements may be connected in either Δ or Y circuits by means of a double-pole throw switch. This arrangement allows the heat input to the pot to be reduced to as low as 1-2/3 kilowatts when only one heater circuit of three elements is operating on Y. For overnight shutdowns, this amount of heat is sufficient to maintain the salt temperature at 500°F. Turning on two circuits, each connected in Y and maintaining a heat input of 3-1/3 kilowatts, which is more than the heat loss from the pot, raises the salt temperature to around 580°F., at which point it is controlled by the Fenwal thermoswitch previously mentioned. Decreasing the load on the heater by means of the Y circuit connection was taken as a precautionary measure to reduce the possibility of overheating the heater elements when the liquid is stagnant during overnight shutdown, etc.

To insure that none of the heater circuits are inadvertently left on the Δ connection when the salt circulation is stopped, an amber light has been placed on the panel board to show as a warning if either of the Circuits 1 or 2 are left on in Δ. Circuit No. 3 is always turned off when the salt pump is stopped.

Salt Piping: The salt is circulated from the pot through a piping system which is essentially a long loop approximately 22 feet long and 2 feet across. The pipe has been welded wherever possible to reduce possibility of leakage. At places where connections have to be broken, steel flanges with Armco iron gaskets are employed. With the flanges tightened both at room temperature and again at operating temperature,

very little leakage has occurred. The upper leg of the loop, which is approximately 5 feet above the floor, is composed of standard 2-1/2-inch pipe. The lower half of the loop is composed of a short length of 2-1/2-inch pipe plus 17 feet, 9 inches of 1-1/2-inch O. D. tubing which constitutes the inner tube of the heat exchanger. Standard 1-inch pipe thread on both ends of the tubing facilitates installing and removing this section.

For installation of the heat exchanger tubes, a section of the 2-1/2-inch line located at the U-bend of the loop consisting of an elbow and a welded reducing coupling is unbolted and removed to allow sufficient room for the tube to be slipped into or out of the exchanger.

A Foxboro Stabiflo pneumatically-operated valve for controlling the salt flow is located on the upper 2-1/2-inch pipe line 21 inches from the elbow which connects to the 1-1/2-inch pump discharge. This valve is for other uses of the equipment and has been left wide open throughout the tests reported here.

Between the Stabiflo valve and pump discharge line and 5 inches upstream from the valve is the 1-1/2-inch by-pass line with a Crane flanged gate valve. This line connects the upper and lower salt lines at a point just outside the salt pot. It is intended for use in conjunction with the Foxboro Stabiflo valve mentioned above to control the salt flow during drying tests. It is kept closed during the normal course of operation in heat transfer study, being opened only to aid in the draining of the upper 2-1/2-inch line.

The 1-inch Edwards Globe valve is located just after the 1-1/2-inch O. D. tube test section and is intended for use in manual control of

the salt flow rate.

Twelve feet downstream from the flanged Stabiflo valve and on the upper 2-1/2-inch line are located the set of orifice flanges for measuring the rate of salt flow. These flanges, 7-1/2 inches in diameter and 1-1/2 inches thick, are both welded to the 2-1/2-inch pipe. Two 3/4-inch jackscrews are provided with flanges to aid in separating them while the orifice plates are being changed. Four orifice plates, 5 inches in diameter, 1/8 inch thick and of stainless steel, are available with hole sizes of 3/4 inch, 1-1/4 inches, 1-3/4 inches, and 2-1/4 inches.

The salt temperature during experimental runs is controlled through a "Thermohm" (platinum resistance thermometer) which is connected to a temperature controller. The opening for the Thermohm is located in the 2-1/2-inch welded elbow and allows the Thermohm to extend vertically into the 1-1/2-inch line which forms the outlet from the salt pump.

Along the upper line of 2-1/2-inch pipe and wired to it are six Chromalox strip heaters 3/4 inch x 36 inches, rated at 600 watts each. They are used to preheat the line before starting the salt flow. Four of these strip heaters are located between the Foxboro control valve and the orifice flanges, while the other two are between the orifice flanges and the far end of the loop. These strip heaters are able to raise the temperature of the pipe from room temperature to 600°F. in half an hour or less and have operated very satisfactorily at all times. Steam from the main supply is admitted to the double heat exchanger to preheat the portion of the salt line which is within the exchanger.

To allow proper drainage of the salt line when the salt pump is stopped, all the salt piping is constructed with a slope of approximately

1/8-inch per foot so that salt will flow by gravity back to the pot. To insure complete drainage, an air valve is located at the highest point in the system which is at the opposite end of the loop from the salt pot, and air at 90 pounds per square inch is used to blow the salt back into the pot. Care must be taken, however, that the air is not turned on too strongly or some of the molten salt will be blown out of the charging port, as well as up around the junction box of the electric heaters.

The entire length of the salt system has been very carefully insulated. The upper line of 2-1/2-inch pipe is covered with a layer of high-temperature asbestos pipe covering and another layer of fibreglas pipe covering 2 inches thick. That portion of the lower layer which is outside the heat exchanger shell is insulated by a 2-inch layer of fibreglas pipe covering with the irregular spaces filled by bats of fibre wool also 2 inches thick. Irregular spaces such as valves and elbows have also been carefully insulated in the above manner.

A general photographic view of the equipment is shown in Figure 10.

Instrumentation and Control

The experimental unit is well equipped with instruments both for the control of its operation and the indication and recording of data. All the instruments are centrally located on a panel board shown in the photograph, Figure 11.

Steam Temperature: The steam temperature at the point of the blower outlet is controlled by a thermocouple-actuated, recording, temperature controller, a Foxboro "Dynalog" instrument. This controller positions the Foxboro pneumatic valve in the spray system to admit an

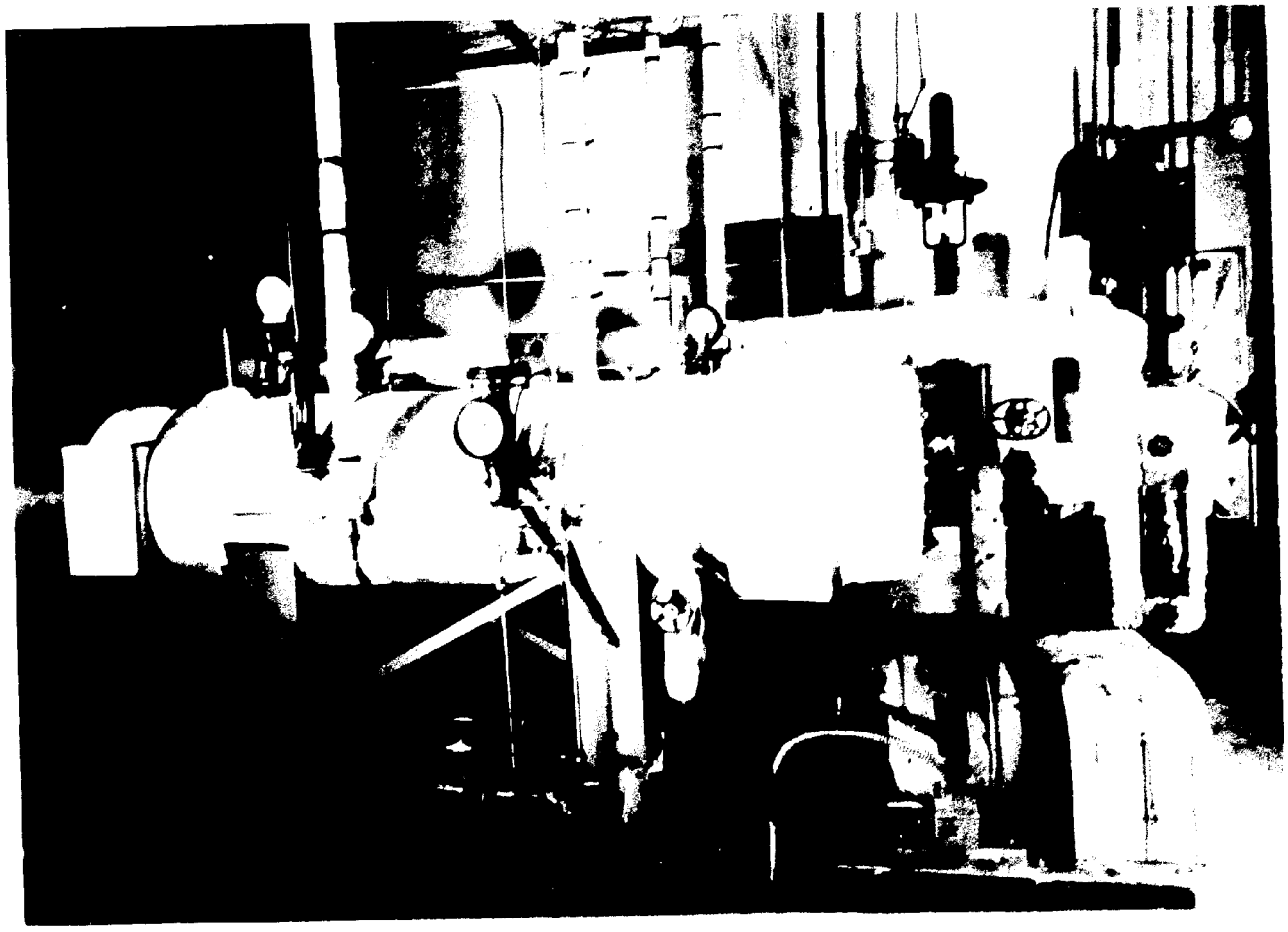

FIGURE 10

GENERAL VIEW OF EQUIPMENT

(STEAM SPRAY CHAMBER IN FOREGROUND)

amount of spray water just sufficient to hold the temperature of the steam at the desired point. The Dynalog controller gives excellent stable control to within less than 1°F. of the desired point.

Steam Pressure: The steam pressure is maintained under control with the aid of an indicating Foxboro "M41" pressure controller. A constant amount of make-up steam is admitted to the system through a manual valve. This tends to build up the system pressure and causes the M41 controller to open the pneumatic vent valve, bleeding off the pressure to the desired point. Control is of the on-off type with a cyclical variation of less than ± 1 psi. The control is completely satisfactory, the deviation from the average being insignificant.

Salt Temperature: The salt temperature is controlled by means of a Leeds and Northrup Electromax controller. This controller is acuated by a Thermohm, or platinum resistance thermometer, placed in the salt stream leaving the Taber salt-circulating pump. The controller, in turn, operates a relay controlling the power input to the three 5-kilowatt Chromalox heaters located in the salt pot. The percent of the total time that the heaters are on is proportioned to the temperature difference between the control point and the salt temperature, with the average time on proportioned to keep the temperature at the control point. With this controller the temperature may be controlled to ± 0.5°F.

A Fenwal A3100 Thermoswitch is used as a safety device in the salt pot. This bimetallic strip thermostat switch is placed in the relay circuit and opens the main power circuit when the salt temperature goes above 580°F.

FIGURE II

INSTRUMENT PANEL BOARD

(STEAM FLOW CONTROL VALVE IN LEFT FOREGROUND)

Steam Flow Rate: The steam flow rate is indicated by a differential reading on a Meriam U-tube manometer and also recorded on a Taylor Aneroid-type flowmeter. The primary element is the orifice plate set in the orifice flanges of the steam piping. Upstream and downstream taps lead from this installation through seal pots to the Meriam manometer and the Taylor flowmeter, which are connected in parallel. The manometer is in the inverted position and operates with water under air as the fluid system. The purpose of the two instruments is convenience in the case of the Taylor recorder, and high accuracy in the case of the U-tube manometer.

Steam Pressure Drop: The steam pressure drop is indicated on a similar Meriam U-tube manometer. Pressure taps from the two ends of the 10-foot pressure drop test length of the heat exchanger lead through seal pots to the two limbs of the manometer. The manometer is installed in the inverted-U position to permit the use of light organic liquids over water, and so obtain high sensitivity.

Salt Flow Rate: A companion system to that installed for obtaining the steam flow rate is available for salt flow determination. The seal pot system, however, is much more complex. The system involves, on both the upstream and downstream sides, a lower steam-heated pot with Dow-Corning silicone fluid (DC 200) over molten salt, and an upper pot with silicone over water. The two pots are joined at their tops by a silicone-filled line. The instrument lead line, for each limb, extends from the bottom of the upper pot.

Considerable trouble has been encountered in the operation of this system due to freezing of the salt in the connecting lines and frothing of the silicone fluid. For the present work, since only one rate of

salt flow is used, and this is the maximum output of the pump; the flow rate is inferred from a test in which the flow rate of water was determined.

Temperature Measurements: A 16-point recording Brown "Electronik" potentiometer, 200-800°F. range, is employed for recording the temperature at most of the important points of the unit. This instrument indicates and records as many as 16 temperatures at 30-second intervals.

Thermocouples located at the following points are connected to the potentiometer (see Figure 8 for identification by symbol):

--: Salt, in pot.

L_1: Salt, inlet to heat exchanger.

L_2: Salt, outlet from heat exchanger.

G_1: Steam, inlet to heat exchanger.

G_2: Steam, outlet from heat exchanger.

G_3: Steam, downstream from orifice installation.

W_1: Heat exchanger shell, outsdie wall near steam inlet.

W_2: Heat exchanger shell, outside wall near steam outlet.

W_3: Downstream steam piping, outside wall, location near exchanger.

W_4: Downstream steam piping, outside wall, location near steam spray chamber.

--: Stuffing box.

Of these, the thermocouples at points L_1, L_2, G_1, G_2, and G_3 are each connected to two points on the instrument in order to give a more nearly continuous record at these important locations. The salt

pot and stuffing box temperatures are used merely for operational guides; the others, to give data on the performance of the heat exchanger.

Thermocouples were also installed temporarily at other points during the preliminary testing of the equipment and particularly during the checking of the temperature indication at G_2, the steam outlet.

Calibrated iron-constantan thermocouples are employed throughout. Those which are inserted into the salt or steam are constructed as follows. The two wires are threaded through a two-hole porcelain insulation and this unit is then inserted into a 6-to 8-inch length of 1/4-inch or 1/8-inch O. D. thin wall stainless steel tubing until the two ends of the thermocouple wires barely protrude. The wires are then joined together and the end of the tube sealed closed by silver solder. A suitable bushing carrying 1/4-inch pipe threads is silver-soldered to the tube to permit it to be screwed into the pipe line fitting. Figure 12 is a photograph showing typical thermocouples of this type.

The Brown instrument is graduated in 2°F. divisions and estimation to 1/5 of a division is readily possible. Tests on the instrument indicate it to be completely reproducible to 0.2°F. Photographs of sample charts from actual tests are shown in Figure 13.

Other temperatures, i.e., those of the surface of the insulation and at the instrument panel board, are obtained with ordinary glass thermometers having a range of 20°F. to 220°F.

Pressure Measurement: The pressure of the steam is indicated by the Foxboro Model 41 pressure controller, but an accurate U. S. Supergauge, 0 to 150 psi. range, is used to obtain the pressure to within 0.1 psi. This gauge has been calibrated against a dead weight tester.

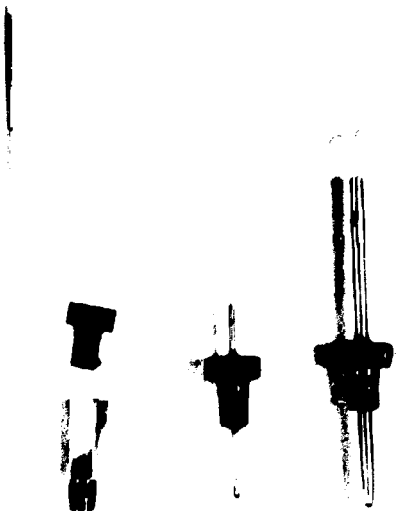

FIGURE 12

THERMOCOUPLE ASSEMBLIES.

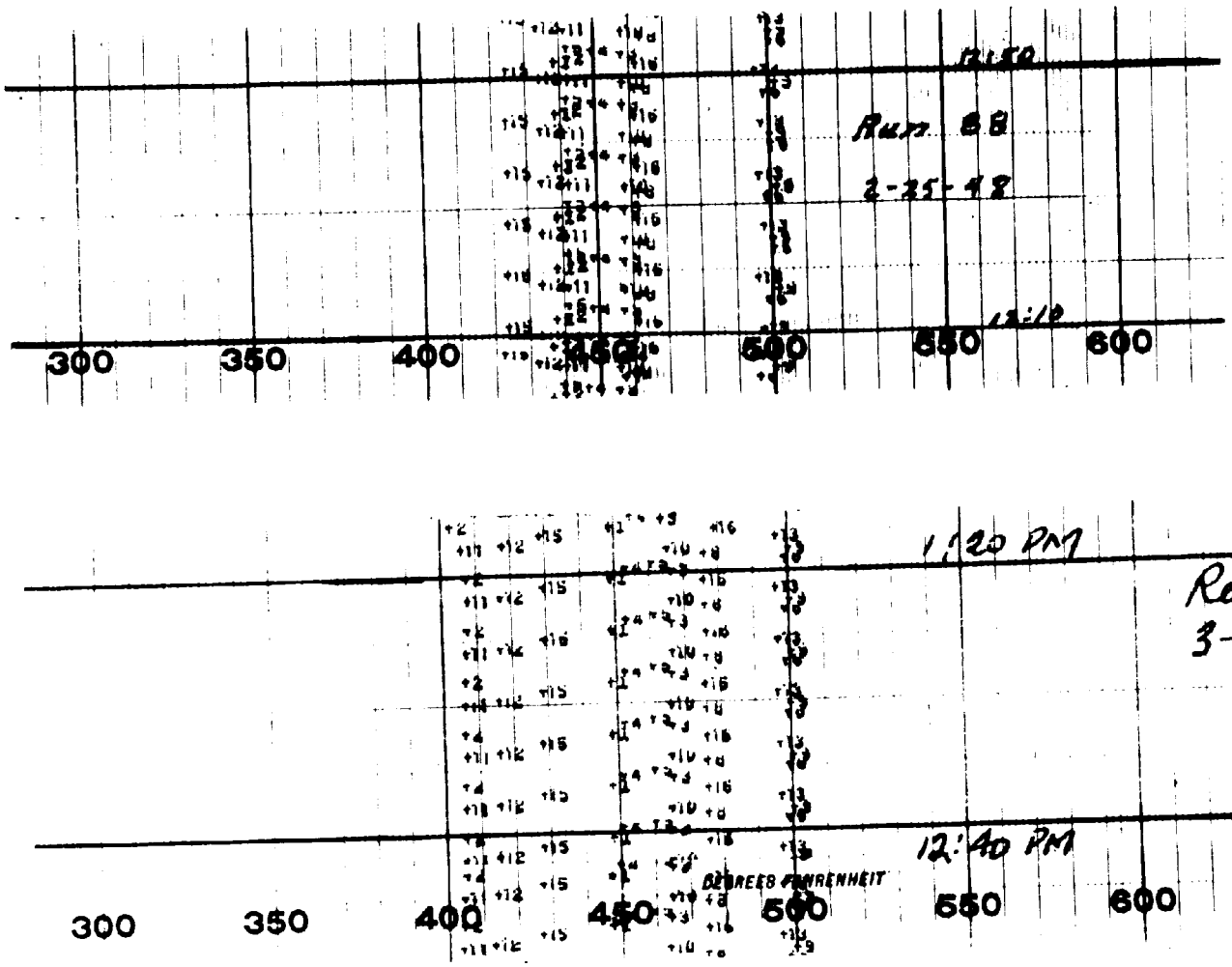

FIGURE 13

SAMPLE CHARTS FROM BROWN POTENTIOMETER

IV. EXPERIMENTAL PROCEDURES

The procedures for starting, operating, and shutting down the equipment are outlined below.

General Procedure for Starting Up the Equipment

It is assumed that the salt heaters will have been left on in Y circuit during the time before the unit is to be started and that the temperature of the salt pot will be approximately 560°F. The starting up procedure is as follows:

1. The strip heaters are turned on to preheat the 2-1/2-inch salt discharge line.
2. If the equipment has been idle for some time, the manometer and flowmeter lead lines are checked to be sure that they are solidly filled with water.
3. Air is admitted to the upper part of the Meriam manometer used to indicate the steam flow.
4. The four-inch circulating valve and the valves to the steam traps are opened.
5. The manual vent on the spray chamber is opened and steam is admitted to bring the unit to the desired operating pressure.
6. The Foxboro pressure controller is set to control at the desired pressure and the make-up steam roughly adjusted to hold the system at this pressure. The quantity of make-up steam required to maintain the desired pressure diminishes considerably as the equipment heats up.
7. After the unit has been at operating pressure for a few minutes and the initial rush of condensate is over, the four-inch circulating valve is closed.
8. The blower drive is now turned over two or three times by hand to make sure that everything is all right, and then the circulating blower is started.
9. The four-inch circulating valve is opened slowly until the desired flow is indicated on the Taylor flowmeter or the Meriam manometer.

10. Approximately one hour after the strip heaters have been turned on, the salt pump is started, but only after the following precautions have been observed.

    (a) Make certain that salt in the pot is above 500°F.

    (b) Make sure that the air admission valve to the salt line is closed.

    (c) Make sure that the by-pass valve is closed.

    (d) Make sure that the 2-1/2-inch Foxboro control valve and the Edwards discharge valve are open.

    (e) Turn the pump over by hand a few times.

    (f) Wait until the Brown instrument is about to print the outlet salt temperature from the heat exchanger and then start the salt pump.

    (g) The temperature should respond within a matter of four or five seconds if salt circulation is obtained.

    (h) If there is no such response, it may be assumed that the salt has frozen in the circuit and it will then be necessary to shut off the salt pump and thaw out the lines with the aid of the upper strip heaters, steam from the spray chamber, an oxy-acetylene torch, etc.

11. The heater circuits are switched to Δ and the Electromax controller is set to maintain the desired salt temperature. The strip heaters are turned off.

12. The Dynalog temperature controller is set to control the steam outlet temperature at the desired level. Note that the control point must be below the temperature which would be reached after a long time by equilibrium between the heat supply to the system and the heat loss from the system. The water spray system is started as follows:

    (a) The water supply valve to the pump is opened and the by-pass valve is closed.

    (b) The pump is started.

    (c) The pressure relief valve is set to a pressure about 200 psi. greater than the steam operating pressure.

    (d) The spray nozzle valves are opened.

13. The unit is now in operation.

General Procedure for Routine Operation of Equipment

After the equipment has been started up according to the procedure outlined above, it requires one and a half to two hours for the system to heat up and come to equilibrium. The system is assumed to be at equilibrium when all the thermocouple readings given by the Brown instrument have reached constant values.

After equilibrium has been reached the following data are taken and recorded at ten-minute intervals:

1. Steam pressure.
2. Meniscus heights in steam pressure drop and steam flow manometers are read both at the maximum and minimum of the steam pressure control cycle.
3. Readings of thermometers located on the panel board and just under the skin of the insulation on the heat exchanger and on the steam line leading from the heat exchanger to the spray chamber.

These data are taken over a forty-minute period during which all process variables must remain substantially constant. Meanwhile, the Brown instrument maintains a record of all thermocouple readings.

After the required data have been collected the conditions of steam flow rate and pressure are readjusted to those desired for the next test. The steam flow rate is adjusted by the manually-operated valve located in the line running from the heat exchanger to the spray chamber. The steam pressure is adjusted by resetting the Foxboro pressure controller and the make-up steam. After the conditions are reset it is again necessary to wait for equilibrium to be established.

Procedure for Shutting Down the Equipment

The following procedure is followed when shutting down the equipment:

1. The water spray pump is stopped and the associated valves are closed.

2. The steam blower is stopped.

3. One salt heater is turned off and the other two are switched to Y circuit.

4. The salt pump is stopped and the salt by-pass valve is opened.

5. Air is admitted to the salt line by opening the high pressure air valve. This valve is left about one-half open to insure proper drainage of the lines into the salt pot. After the lines are drained the salt by-pass valve is closed.

6. If it is desired to hold the unit under pressure overnight the necessary adjustments are made to the Foxboro pressure controller and the steam make-up.

7. In the event that the pressure of the system is reduced or brought to atmospheric, the manometer shutoff valves are first closed.

8. The Brown instrument is switched to its indicating position when the temperature of the salt in the salt pot is being indicated.

9. The chart drives on the other instruments are turned off.

V. EXPERIMENTAL DATA

The experimental data are presented in detail in Table II, with supplementary data in Figures 18 and 19 and in Table IA of Appendix A and Table IB of Appendix B.

Table II indicates in Columns 1 and 2 the test number and type of inner tube being tested. Column 3 gives the operating pressure in psi. abs. corrected for pressure gauge calibration.

Columns 4 to 13 inclusive present the basic temperature data as follows:

Column 4 - the temperature of the salt entering the heat exchanger; L_1, °F.

Column 5 - the temperature of the salt leaving the heat exchanger; L_2, °F.

Column 6 - the temperature of the steam entering the heat exchanger; G_1, °F.

Column 7 - the temperature of the steam leaving the heat exchanger as calculated from the downstream measurement reported in Column 12; G_2^*, °F. The necessity for this calculation, supplementary data taken, and complete calculations of G_2^* are presented in full detail in Appendix B.

Column 8 - the temperature of the outside wall of the heat exchanger at its contact with the insulation near the steam inlet end; W_1, °F.

Column 9 - as Column 8 but near the steam outlet end of the unit; W_2, °F.

Column 10 - the temperature of the outside of the insulation below the cloth covering and near the steam inlet end of the unit; S_1, °F.

Column 11 - as Column 9 but near the steam outlet end of the unit; S_2, °F.

TABLE II

EXPERIMENTAL DATA

1	2	3	4	5	6	7	8	9	10	11	12	13	14	15	16	17	18	1
			TEMPERATURE										FLOW RATE			PRESSURE DROP		
Test Number	Type of Inner Tube	Steam Pressure	Salt Inlet	Salt Outlet	Steam Inlet	Steam Outlet*	Outside of Outer Pipe Wall		Outside Surface of Insulation		Steam After Orifice Plate	Room at Instrument Panel	Diameter of Orifice Plate	Differential Across Orifice	Manometer Fluid	Manometer Differential	Manometer Fluid	Test Number
Symbols, Units →		P, psi abs.	L_1, °F	L_2, °F	G_1, °F	G_2, °F	W_1, °F	W_2, °F	S_1, °F	S_2, °F	G_3, °F	S_p, °F	Inches	h_p, cm.		h_p, cm.		
Column Reference →		Data	Data	Data	Data	Table IA,15	Data	Data	Data	Data	Data	Data	Data	Data	Data	Data		
58	BARE	100	496	494	338.1	371.0	---	---	103	96	363.3	79.0	0.875	59.11	A"	--	-	58
58A	"	100	495	495	335.5	373.4	345.8	364.7	105	97	365.4	82.0	0.875	59.06	A"	--	-	58A
59	"	100	496	495	338.5	373.3	---	---	103	97	363.9	80.0	0.875	39.65	A"	--	-	59
59A	"	100	495	496	334.8	375.3	346.6	370.2	105	98	365.6	82.2	0.875	38.71	A"	--	-	59A
60	"	100	495	495	333.6	378.8	---	---	104	98	358.9	80.0	0.875	8.61	A"	--	-	60
60A	"	100	498	499	327.8	384.0	350.0	381.1	106	100	364.0	83.0	0.875	9.39	A"	--	-	60A
61	"	50	494	494	326.1	377.8	---	---	104	98	360.7	80.0	0.875	28.82	A'	--	-	61
61A	"	50	498	499	304.8	372.1	331.4	370.4	105	98	354.9	83.5	0.875	30.05	A'	--	-	61A
62	"	50	497	496	315.1	373.9	---	---	104	98	352.4	81.0	0.875	16.87	A'	--	-	62
62A	"	50	498	500	294.4	370.0	328.2	365.6	104	99	347.9	83.5	0.875	16.27	A'	--	-	62A
63	"	50	496	496	302.5	379.9	---	---	104	98	347.1	81.0	0.875	7.18	A'	--	-	63
63A	"	50	499	500	287.9	378.3	331.5	375.8	104	99	345.8	83.5	0.875	7.44	A'	--	-	63A
64	"	100	499	498	378.0	397.7	---	---	109	98	395.4	83.0	1.750	55.04	A"	22.0	B	64
65	"	100	498	497	377.7	398.4	---	---	110	99	395.4	84.0	1.750	30.22	A"	12.5	"	65
66	"	100	498	497	371.8	397.0	---	---	109	101	391.6	84.0	1.750	8.95	A"	3.2	"	66
67	"	50	499	498	378.6	402.5	---	---	109	99	397.7	83.5	1.750	29.39	A'	8.8	"	67
68	"	50	498	497	372.1	400.1	375.5	390.6	108	100	393.0	83.0	1.750	12.50	A'	4.2	"	68
69	"	50	499	498	357.8	394.7	364.4	385.6	107	100	383.8	83.0	1.750	4.89	A'	0.5	"	69
70	"	100	497	497	369.1	392.7	369.4	381.7	109	100	388.5	85.5	1.250	61.4	A"	4.4	"	70
71	"	100	498	498	367.8	393.6	368.8	383.3	109	103	388.3	86.0	1.250	37.8	A"	4.1	"	71
72	"	100	498	498	351.2	388.3	356.0	380.2	108	102	378.8	85.5	1.250	10.3	A"	3.6	"	72
73	"	50	498	497	353.1	388.6	358.4	378.1	107	101	379.9	85.2	1.250	30.0	A'	3.65	"	73
74	"	50	498	497	348.3	386.8	356.1	378.1	107	101	376.1	85.0	1.250	19.4	A'	1.6	"	74
75	"	50	498	498	338.9	386.8	350.7	379.4	107	101	371.6	85.0	1.250	9.30	A'	1.3	"	75
76	LONGI-TUDINAL FIN	100	500	498	405.5	446.7	403.5	429.1	108	100	440.8	81.0	1.250	56.2	A"	21.0	"	76
77	"	100	500	498	400.6	447.1	399.4	429.2	108	100	439.9	81.0	1.250	35.8	A"	14.8	"	77
78	"	100	500	498	388.7	445.2	389.2	426.6	107	100	435.7	81.0	1.250	19.5	A"	9.15	"	78
79	"	50	499	496	390.2	449.5	392.7	431.8	106	100	437.0	78.5	1.250	27.0	A'	8.46	"	79
80	"	50	498	492	377.8	448.4	385.3	432.2	104	99	431.2	78.0	1.250	13.0	A'	5.16	"	80
81	"	50	498	496	351.1	445.4	371.6	430.4	103	99	418.0	77.0	1.250	4.93	A'	1.26	"	81
82	"	100	501	499	343.7	428.2	352.6	405.6	106	101	417.8	81.0	0.875	57.6	A"	4.86	"	82
83	"	100	500	496	357.7	435.0	365.9	418.1	106	100	421.3	81.7	0.875	34.2	A"	3.72	"	83
84	"	100	498	497	354.3	442.3	368.6	428.8	106	101	419.2	82.0	0.875	12.2	A"	3.51	"	84
85	"	50	496	495	317.8	427.5	346.5	416.1	106	103	406.3	84.2	0.875	28.9	A'	1.21	"	85
86	"	50	496	496	318.0	431.4	357.7	427.7	108	105	400.4	85.5	0.875	13.1	A'	0.72	"	86
87	"	50	496	496	308.8	440.2	361.1	439.4	108	105	394.4	85.0	0.875	5.85	A'	--	-	87
88	"	100	499	497	441.6	460.9	437.3	449.7	110	97	457.6	82.5	1.750	50.6	A"	--	-	88
89	"	100	498	496	442.1	462.5	436.0	450.8	112	100	458.0	83.8	1.750	27.1	A"	--	-	89
90	"	100	500	497	434.7	460.4	429.7	447.4	111	102	455.0	83.5	1.750	18.7	A"	--	-	90
91	"	50	497	496	397.6	442.7	396.8	425.3	111	104	436.5	85.4	1.750	26.2	A'	39.5	B	91
92	"	50	495	494	396.0	445.7	396.7	429.4	111	104	437.0	85.0	1.750	13.6	A'	18.3	"	92
93	"	50	496	495	393.7	448.5	395.9	433.5	110	102	436.1	84.5	1.750	6.57	A'	--	-	93

TABLE II, CONTINUED

EXPERIMENTAL DATA

1	2	3	4	5	6	7	8	9	10	11	12	13	14	15	16	17	18	1
			TEMPERATURE										FLOW RATE			PRESSURE DROP		
Test Number	Type of Inner Tube	Steam Pressure	Salt Inlet	Salt Outlet	Steam Inlet	Steam Outlet*	Outside of Outer Pipe Wall		Outside Surface of Insulation		Steam After Orifice Plate	Room at Instrument Panel	Diameter of Orifice Plate	Differential Across Orifice	Manometer Fluid	Manometer Differential	Manometer Fluid	Test Number
Symbols, Units →		P, psi abs	t_1, °F	t_2, °F	T_1, °F	T_2*, °F	W_1, °F	W_2, °F	S_1, °F	S_2, °F	T_3, °F	T_p, °F	Inches	h_f, cm.		h_p, cm.		
Column Reference →		Data	Data	Data	Data	Table IA,15	Data	Data	Data	Data	Data	Data	Data	Data	Data	Data		
94	"STAR" FIN	100	498	498	393.3	477.6	414.9	473.6	110	106	462.7	86.0	0.875	45.86	A"	---	--	94
95	"	100	496	496	387.2	477.9	415.3	475.6	110	106	457.6	85.0	0.875	21.78	A"	---	--	95
96	"	100	497	496	350.6	476.3	402.6	476.6	108	102	454.9	83.2	0.875	8.44	A"	---	--	96
97	"	50	497	495	324.1	474.2	384.6	464.3	107	105	446.1	80.0	0.875	24.13	A'	11.50	C	97
98	"	50	496	495	311.1	472.4	407.6	476.9	106	104	434.2	79.6	0.875	12.90	A'	5.80	"	98
99	"	50	498	496	292.3	467.9	398.2	479.2	107	103	408.1	78.0	0.875	4.00	A'	1.74	"	99
100	"	100	500	497	406.5	474.7	419.3	469.0	112	105	466.0	83.8	1.250	30.75	A"	62.1	"	100
101	"	100	498	496	391.8	475.8	411.3	470.8	112	106	463.6	84.0	1.250	15.28	A"	31.35	"	101
102	"	100	499	497	367.9	478.4	402.8	476.6	112	107	455.3	84.6	1.250	3.93	A"	9.07	"	102
103	"	50	506	504	393.1	484.8	418.6	483.9	101	100	465.2	79.5	1.250	14.65	A'	30.25	"	103
104	"	50	505	502	387.4	478.4	417.4	484.1	102	101	454.2	79.9	1.250	9.14	A'	18.45	"	104
105	"	50	505	502	371.3	478.8	414.3	484.9	101	100	446.0	80.1	1.250	4.47	A'	8.89	"	105
106	"	50	503	500	412.1	482.6	427.3	477.7	107	106	467.7	80.5	1.750	21.57	A'	52.45	"	106
107	"	50	505	501	397.7	480.9	421.1	483.0	109	109	460.2	83.2	1.750	3.07	A'	26.85	"	107
108	"	100	505	502	443.1	483.0	450.9	480.9	114	109	476.1	83.0	1.750	12.95	A"	27.24	A"	108
109	"	100	506	503	443.1	484.8	451.7	483.0	114	109	476.7	83.2	1.750	9.41	A"	17.44	"	109
110	"	100	506	504	430.5	487.1	445.5	485.1	115	110	473.7	84.1	1.750	3.86	A"	6.84	"	110
111	"	50	506	503	299.2	477.5	404.5	486.3	112	109	427.0	84.2	0.625	27.31	A'	4.18	C	111
112	"	50	505	504	291.4	468.1	415.2	486.8	111	108	402.0	84.0	0.625	13.70	A'	2.33	"	112
113	HELICAL FIN	100	500	499	412.9	465.7	420.8	457.1	111	105	457.5	82.8	1.750	8.95	A"	24.22	"	113
114	"	100	500	499	421.8	466.4	428.0	459.0	112	105	460.0	83.5	1.750	14.64	A"	36.62	"	114
115	"	100	500	499	426.7	466.9	432.1	459.2	113	106	461.2	84.0	1.750	18.85	A"	50.2	"	115
116	"	100	500	499	430.0	466.8	434.5	459.2	114	107	461.8	84.0	1.750	25.12	A"	67.6	"	116
117	"	100	500	499	419.9	468.7	424.6	460.2	114	108	460.3	83.5	1.750	8.78	A"	24.4	"	117
118	"	50	501	500	382.0	461.8	396.1	499.9	109	106	452.0	83.4	1.750	14.47	A'	40.9	"	118
119	"	50	501	500	373.9	461.7	392.0	451.3	110	107	450.3	84.1	1.750	9.65	A'	27.6	"	119
120	"	50	501	500	369.3	467.5	392.2	406.7	111	109	451.2	84.7	1.750	5.18	A'	16.3	"	120
121	"	50	500	499	355.5	460.7	380.0	451.3	107	105	446.3	82.6	1.250	23.18	A'	17.70	"	121
122	"	50	500	501	350.6	461.0	379.2	453.3	108	106	444.6	82.5	1.250	17.76	A'	13.68	"	122
123	"	50	500	499	347.1	465.5	379.7	456.4	109	108	445.5	84.2	1.250	12.02	A'	9.85	"	123
124	"	50	500	501	341.4	467.0	378.2	457.7	110	108	444.1	85.0	1.250	9.00	A'	7.30	"	124
125	"	50	500	500.	336.0	469.2	378.5	459.1	110	109	441.3	85.1	1.250	6.00	A'	5.34	"	125
126	"	100	500	498	388.0	457.2	399.4	444.7	111	106	450.5	85.9	1.250	46.70	A"	33.10	"	126
127	"	100	500	499	387.4	461.3	401.0	451.2	110	105	451.6	85.1	1.250	23.80	A"	17.22	"	127
128	"	100	500	499	380.1	467.7	400.7	459.1	110	106	451.5	84.3	1.250	8.57	A"	6.07	"	128

Column 12 - the temperature of the outlet steam measured downstream of the steam flow control valve and immediately downstream of the flowmeter orifice plates; G_3, °F.

Column 13 - room temperature at the instrument panel board; S_p, °F.

Column 14 records in inches the diameter of the orifice plate used in the measurement of the steam flow. The differential across the steam flow manometer, corrected for zero reading, is reported in Column 15 as centimeters of manometer fluid. The manometer fluid system employed is indicated in Column 16 by the letters A' or A". A' refers to a manometer fluid system embodying water-saturated air at 50 psi. abs. trapped over water, while A" refers to a similar system with water-saturated air at 100 psi.abs. The effective specific gravities of these two systems are shown as functions of temperature in Figure 18, which is based upon data from the literature.

Pressure drop data are presented in Columns 17 and 18. Column 17 shows the manometer differential, corrected for zero reading and in centimeters of manometer fluid. The manometer fluid system is indicated by letter in Column 18. Here B refers to a fluid system of turpentine with dissolved carbon tetrachloride trapped over water and C refers to a system with gasoline trapped over water. The effective specific gravities of these fluid systems are reported as functions of temperature in Figure 19, which is based upon measured densities of the organic mixtures and literature values for water.

Additional flow rate and pressure drop data for the bare tube and for tests in which unsatisfactory heat transfer data were obtained are reported and analyzed in Appendix A.

VI. CALCULATED RESULTS

This section dealing with the results calculated from the experimental data is subdivided as follows: 1. Properties of Superheated Steam, 2. Flow Rate and Pressure Drop Calculations, and 3. Calculation of the Composite Heat Transfer Coefficients.

1. Properties of Superheated Steam

A detailed and reliable knowledge of the physical properties of superheated steam is essential to the intelligent interpretation of the experimental data reported in the previous section. The physical properties of importance include the following: viscosity, thermal conductivity, specific heat, and density. These properties are reported by Keenan and Keyes (23) in their "Thermodynamic Properties of Steam." Unfortunately, however, in the cases of viscosity and thermal conductivity the reported data do not cover the pressure-temperature range of interest. Moreover, the specific heat is not available as such, but only in the form of enthalpy. For these reasons, it is apparent that a detailed analysis of the available data on these properties is required.

The established empirical correlations of heat transfer data, in terms of the physical properties of the fluid and other important variables, require also the use of the Prandtl Number, (specific heat)(viscosity)/(thermal conductivity). It has generally been assumed (28) that the Prandtl Number for steam is independent of both pressure and temperature. In the light, however, of fairly complete data on its

contributing factors, it is believed that the possible influence of pressure and temperature on the Prandtl Number warrants investigation.

Following, for the pressure-temperature range of interest, are the best available data on the above-mentioned physical properties and calculated values of the Prandtl Number.

Viscosity

The viscosity data on superheated steam available in Keenan and Keyes (23), Table VI, does not cover the range of pressure and temperature of interest. For this reason it was necessary to consult the original literature on the measurements of this property. During the past twenty years several investigations (13, 14, 36, 38, 39, 42) have been conducted on the viscosity of superheated steam. Results to date are conflicting and inconclusive. The degree of conflict is shown by the data of Table III, which indicates the viscosities reported in the five different investigations considered most reliable (13, 36, 38, 39, 42).

It is of interest to note that all of the investigators except Schiller (36) employed the capillary method in one modification or another. Schiller's investigation was carried out with a calibrated nozzle. The investigators, Sigwart (38), Timroth (42), and Hawkins, et. al. (13, 14), conducted their experiments chiefly in the very high temperature and pressure region and their data on the viscosity of steam below 200 psi.abs. and 600°F. was obtained by extrapolation and cross-plotting. Speyerer (39) and Schiller (36) investigated the viscosity primarily in the region below 200 psi. and 600°F. Their results, however, are not in agreement.

TABLE III

COMPARISON OF VISCOSITY OF STEAM AS REPORTED BY DIFFERENT INVESTIGATORS

Viscosity in Lbs./Ft. Hr.

T°F	Sigwart (11)	Timroth (13)	Hawkins (3)	Speyerer (12)	Schiller (10)
			14.7 psi., abs.		
212	.0324	.0297	.0304	.0316	.0314
250	.0343	.0306	.0324	---	---
300	.0369	.0332	.0348	.0361	---
350	.0396	.0357	.0373	.0387	.0387
400	.0421	.0382	.0398	.0412	.0416
450	.0445	.0409	.0422	.0439	.0441
500	.0471	.0433	.0447	.0463	.0467
550	.0496	.0460	.0471	.0491	.0494
600	.0520	.0486	.0496	.0516	.0520
			100 psi., abs.		
400	.0421	.0386	.0448	.0440	.0475
450	.0445	.0412	.0467	.0463	.0491
500	.0471	.0437	.0484	.0489	.0513
550	.0497	.0462	.0504	.0515	.0537
600	.0521	.0489	.0523	.0540	.0563
			200 psi., abs.		
400	.0421	.0390	.0489		.0582
450	.0445	.0416	.0499		.0489
500	.0471	.0440	.0513		.0598
550	.0499	.0466	.0530		.0610
600	.0524	.0493	.0547		.0617

It has been concluded by Sigwart, Timroth, and Hawkins that the values obtained by Schiller are too high. On the other hand, the values obtained by Sigwart are considered by both Timroth and Hawkins to be too low. It seems probably, but by no means certain, that the correct viscosity for superheated steam lies somewhere in the range reported by Timroth, Hawkins in 1940, and Speyerer. The choice of values within this range is entirely arbitrary; however, the data of Timroth are recommended as being the most reliable by both Professor F. G. Keyes (24A) of Massachusetts Institute of Technology and Mr. G. H. Van Hengel (43) of the Detroit Edison Company. Values of Timroth's viscosity data were obtained from his article (42) and also from the still unpublished review of the viscosity of steam by Hawkins, Sibbitt, and Solberg (15).

These values by Timroth are tabulated in Table IV over the range 14.7 to 200 psi.abs. and saturation temperature to 600°F. For convenience in later use the values have also been plotted to large scale in Figure 14.

Thermal Conductivity

The thermal conductivity data reported by Keenan and Keyes (23) in their Table VII does not cover the range of pressure and temperature of interest. The original literature on the subject, consisting only of the work of Timroth and Vargaftik (41) was consulted. In the absence of other corroborative data the values of thermal conductivity reported in this reference are assumed to be correct. This assumption seems reasonably justified in view of the fact that Timroth and

TABLE IV

VISCOSITY OF SUPERHEATED STEAM

Lbs./Ft. Hr.

Pressure psi. abs.		14.7	50	100	150	200
Saturation Temp. °F		212	281	328	358	382
Saturation		.02970	.03460	.03795	.03990	.04130
Superheat Temperature	250	.03055	----	----	----	----
	300	.03315	.03347	----	----	----
	350	.03573	.03597	.03625	----	----
	400	.03820	.03835	.03855	.03875	.03900
	450	.04090	.04100	.04120	.04137	.04155
	500	.04330	.04347	.04367	.04385	.04400
	550	.04600	.04610	.04622	.04640	.04660
	600	.04860	.04871	.04885	.04900	.04913

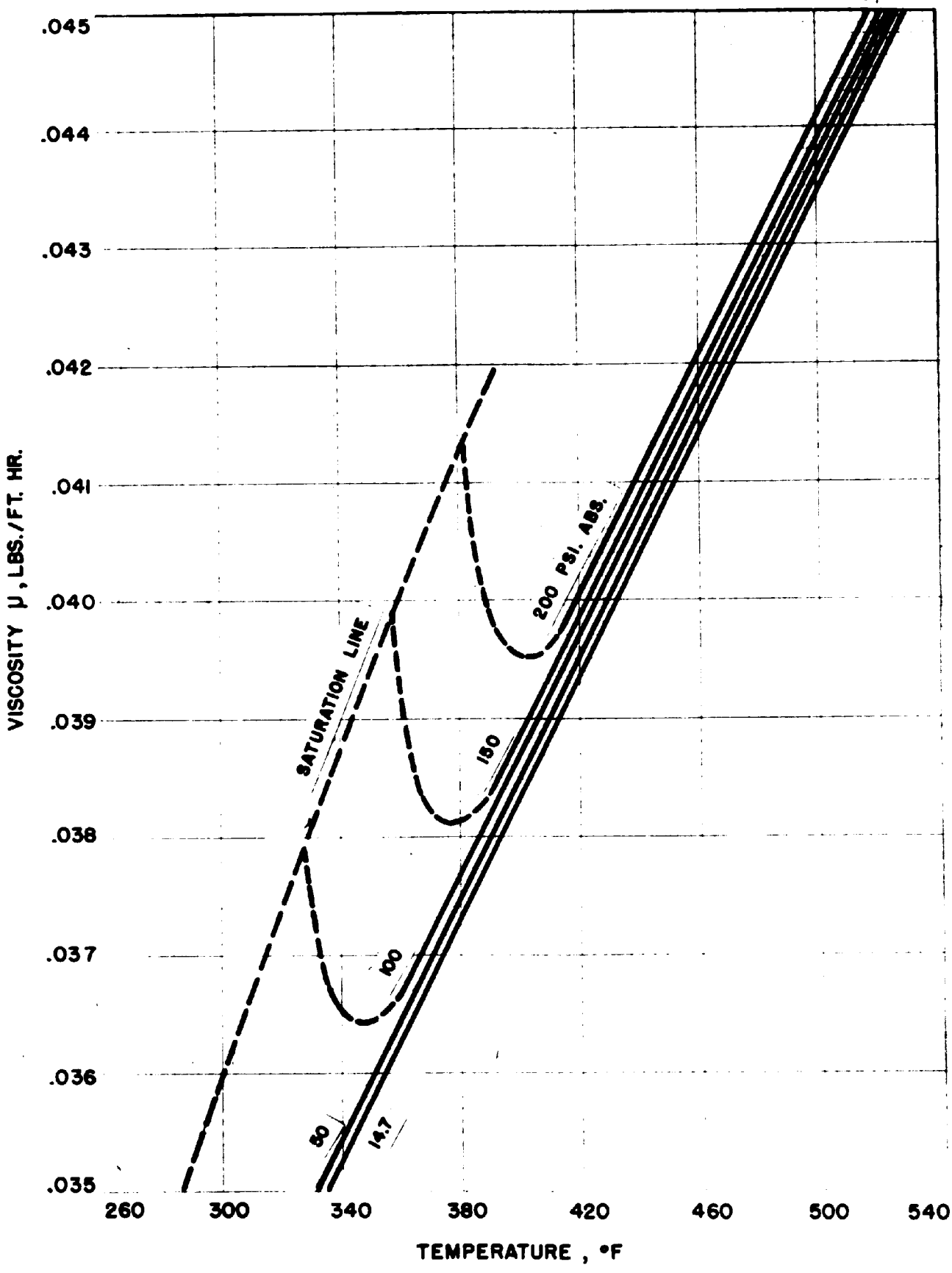

FIGURE 14

VISCOSITY OF SUPERHEATED STEAM

Vargaftik made a six-year study of thermal conductivity of steam prior to the final publication in 1940 of their results.

Values of the thermal conductivity taken from this reference are presented in Table V, which covers the range 14.7 to 200 psi. abs. and saturation temperature to 600°F. These values have also been plotted in Figure 15.

Specific Heat

Specific heat data on superheated steam were calculated by using the reliable empirical equations of Keyes, Smith, and Gerry (24B).

$$C_p^\bullet = 1.47198 + 7.5566 \times 10^{-4} T + \frac{47.8365}{T}$$

$C_p^\bullet$ in Int. Joules

T in °K.

$$C_p = C_p^\bullet + Ap + Bp^2 + Cp^4 - Dp^{13}$$

p in kg./cm.^{2}

C_p in Int. Joules

Constants for the latter equation are given by Keyes, Smith, and Gerry.

The calculated values for specific heat are listed in Table VI and plotted in Figure 16.

Values of specific heat at atmospheric pressure were read from an alignment chart in McAdams (28) "Heat Transmission", page 337. The

TABLE V

THERMAL CONDUCTIVITY OF SUPERHEATED STEAM

Btu Ft./Hr. °F Ft.^{2}

Pressure psi. abs.		14.7	50	100	150	200
Saturation Temp. °F		212	281	328	358	382
Saturation		.01335	.01790	.02098	.02285	.02448
Superheat Temperature	250	.01488	----	----	----	----
	300	.01613	.01810	----	----	----
	350	.01760	.01888	.02106	----	----
	400	.01925	.02008	.02158	.02305	.02450
	450	.02088	.02150	.02255	.02362	.02470
	500	.02248	.02300	.02365	.02445	.02530
	550	.02415	.02455	.02515	.02558	.02615
	600	.02585	.02613	.02660	.02695	.02730

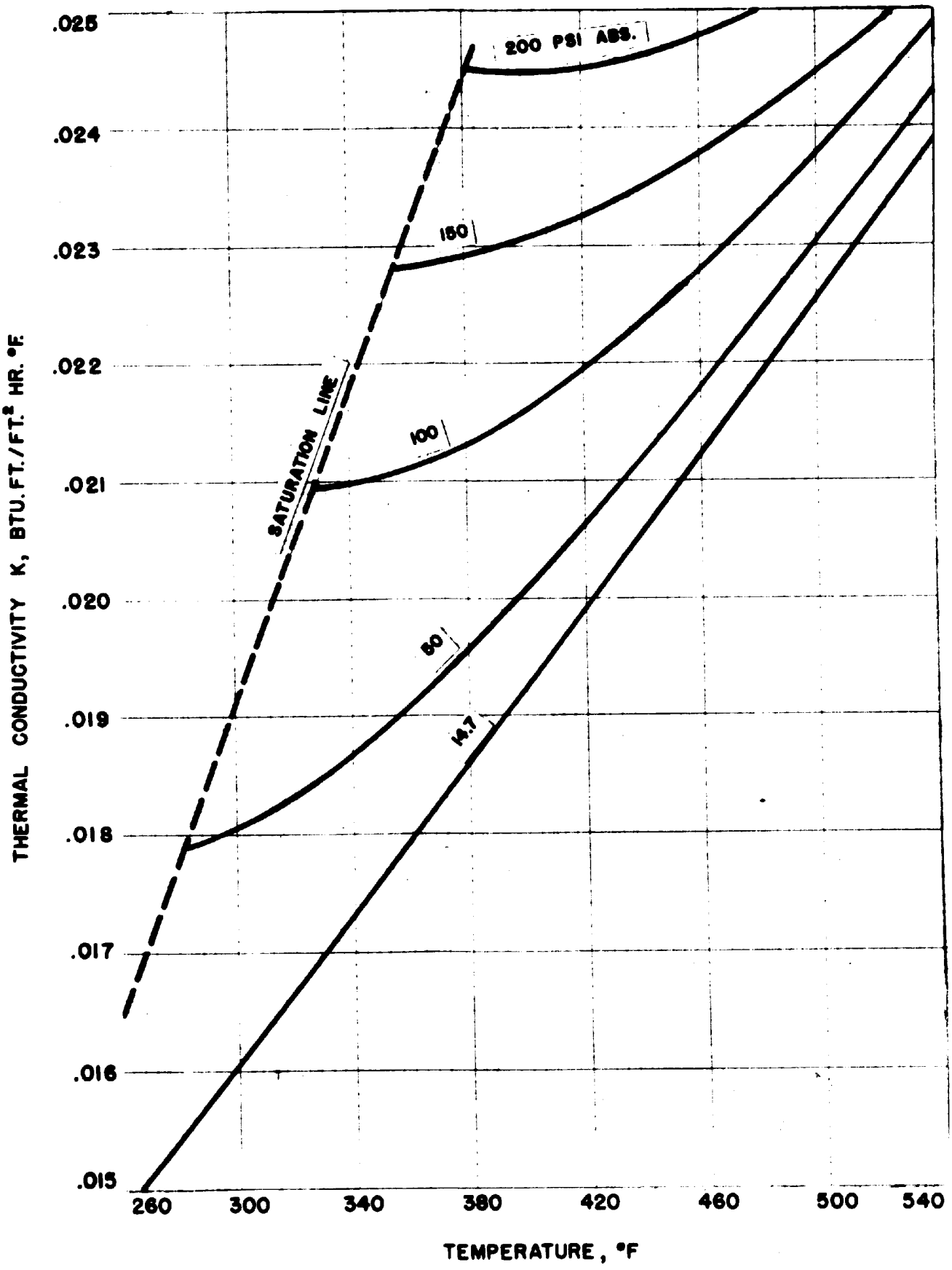

FIGURE 15.

THERMAL CONDUCTIVITY OF SUPERHEATED STEAM

TABLE VI

SPECIFIC HEAT OF SUPERHEATED STEAM

Btu/Lb. °F

Pressure psi, abs.		14.7	50	100	150	200
Saturation Temp. °F		212.0	281	328	358	382
Saturation		.4967	.5460	.5980	.6405	.6760
Temperature, °F	250	.4825	---	---	---	---
	300	.4740	.5310	---	---	---
	350	.4707	.5055	.5705	---	---
	400	.4000	.4930	.5345	.5825	.6427
	450	.4713	.4877	.5161	.5440	.5810
	500	.4738	.4857	.5045	.5225	.5491
	550	.4767	.4855	.4993	.5145	.5308
	600	.4796	.4870	.4980	.5085	.5201

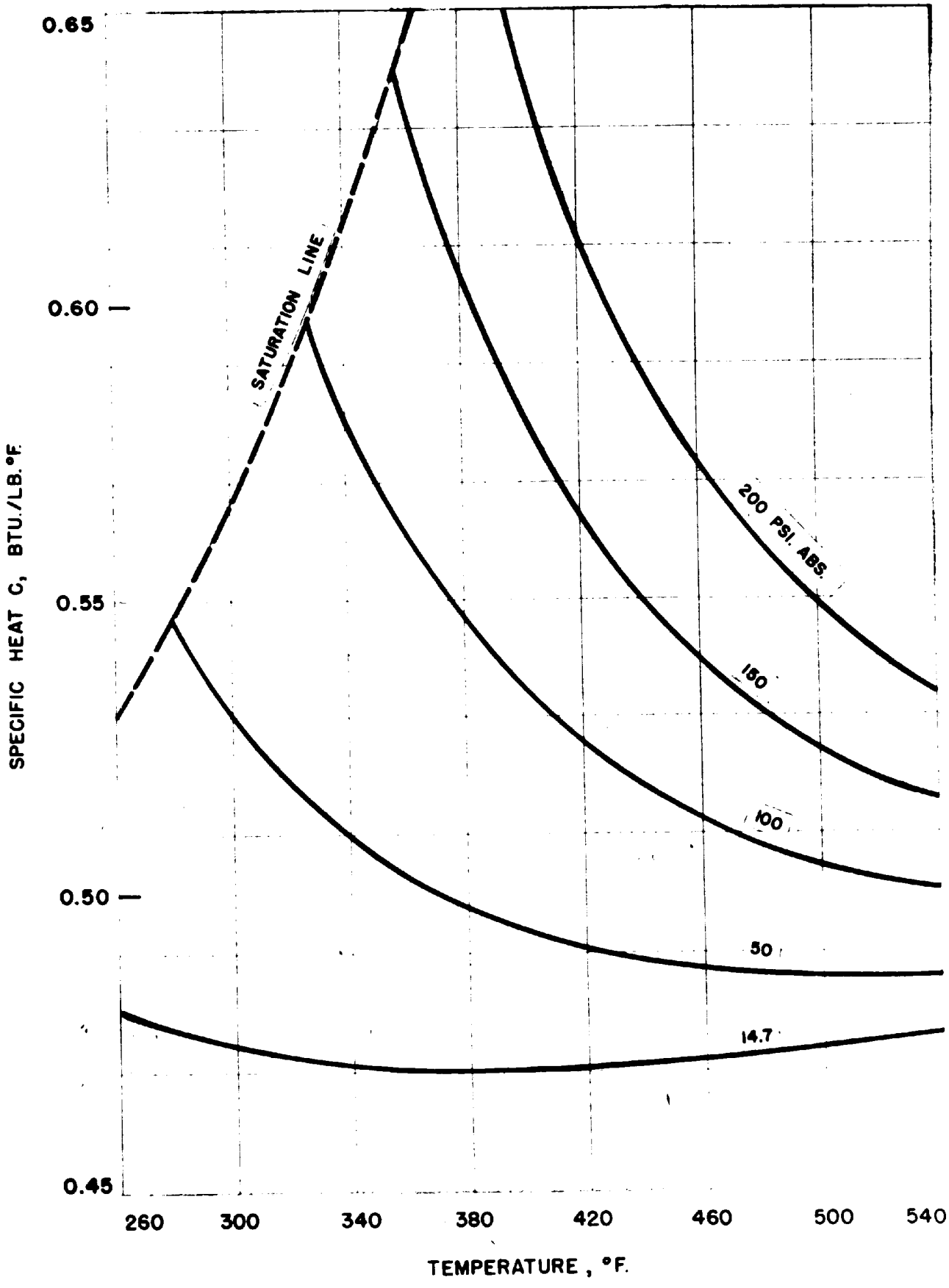

FIGURE 16

SPECIFIC HEAT OF SUPERHEATED STEAM.

following table indicates the disagreement between the values reported by McAdams and those calculated from the above equations.

SPECIFIC HEAT OF STEAM AT ONE ATMOSPHERE

T, °F.	McAdams Values	Keyes, Smith and Gerry
212	.466	.496
250	.469	.483
300	.472	.474
400	.478	.400
500	.485	.474
600	.492	.480

Density

In view of the extensive data on specific volume of superheated steam which is available in steam tables (23), it was unnecessary to make any special study of the density of superheated steam.

Prandtl Number

From the data of Figures 14, 15, and 16 the Prandtl Number has been calculated, and values are presented in Table VII. These values are also plotted over the range 14.7 to 200 psi.abs. and saturation temperature to 600°F. in Figure 17.

It is to be noted in connection with these values of the Prandtl Number that there is considerable discrepancy between the value of 1.055 at 212°F. and 14.7 psi.abs., as read from Figure 17, and the value of 0.78 reported by McAdams (28). The low value of the Prandtl Number given by McAdams is due primarily to his low value for the specific

TABLE VII

PRANDTL NUMBER FOR SUPERHEATED STEAM

Dimensionless

Pressure psi, abs.		14.7	50	100	150	200
Saturation Temp. °F		212	281	328	358	382
Saturation		1.0550	1.0554	1.0817	1.1184	1.1405
Temperature, °F	250	0.9935	---	---	---	---
	300	0.9742	0.9819	---	---	---
	350	0.9556	0.9631	0.9820	---	---
	400	0.9327	0.9416	0.9548	0.9793	1.0231
	450	0.9232	0.9300	0.9429	0.9528	0.9767
	500	0.9126	0.9180	0.9316	0.9425	0.9505
	550	0.9080	0.9117	0.9176	0.9333	0.9490
	600	0.9017	0.9078	0.9146	0.9245	0.9392

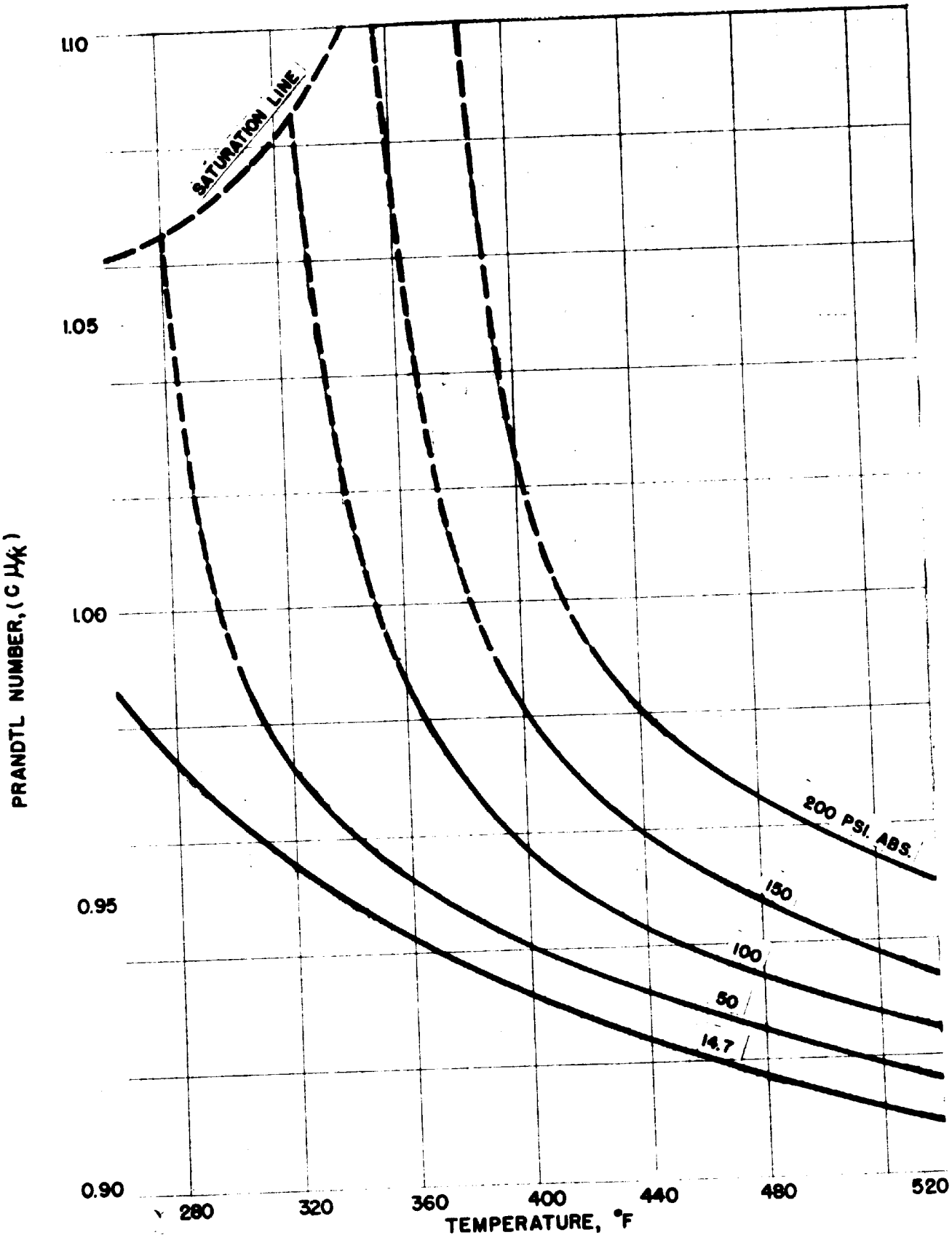

FIGURE 17

PRANDTL NUMBER FOR SUPERHEATED STEAM

heat of steam at 212°F. Since the Keyes, Smith, and Gerry specific heat data may be considered reliable, the higher value of 1.055 is believed the more accurate.

Moreover, McAdams states that to the best of present knowledge, the Prandtl Number must be assumed independent of both pressure and temperature. In the case of superheated steam, however, the knowledge of properties, while by no means perfect, certainly appears sufficient to justify taking into account the variation of the Prandtl Number with pressure and temperature.

2. Flow Rate and Pressure Drop Calculations

The calculations of the steam flow rate and the pressure drop due to flow are presented in Table VIII.

The flow rate calculation is based upon the equation for gas flow through an orifice, given as follows by A. D. MacLean (25):

$$Q_s = 359.15\ E\ d^2 \sqrt{h_w v} \qquad (27)$$

where Q_s = rate of flow of steam in cubic feet per hour.

E = orifice efficiency factor.

d = orifice diameter in inches.

h_w = head in inches of water.

v = specific volume of gas under flowing conditions.

This equation may be rewritten:

$$W = \frac{359.15}{345.65} F_e R_f F_b' \sqrt{h_w/v} \qquad (28)$$

where W = rate of flow in pounds per hour.

F_b' = $345.92\ E\ d^2 \simeq 345.65\ E\ d^2$ = basic orifice flow factor.

F_e = factor for expansion of the orifice plate with temperature.

R_f = Reynolds number factor.

For the conditions of the tests it may be shown that both F_e and R_f are sufficiently close to 1 to be neglected. The equation therefore becomes:

$$W = 1.04\ F_b' \sqrt{h_w/v} \qquad (29)$$

i.e., $$W = F_b \sqrt{h_w/v} \qquad (30)$$

where $F_b = 1.04\ F_b'$

For standard flange taps MacLean gives the following values of F_b' for orifice plates inserted in a standard 4-inch pipe.

Orifice Diameter, d, inches	F_b'	$1.04\ F_b' = F_b$
0.625	80.22	83.4
0.875	157.8	164
1.250	324.7	338
1.750	648.9	675

The steam flow rates are calculated according to Equation (30) employing the values of F_b appropriate to the orifice plate. The factors for this calculation are given in Columns 3, 4, 5, and 6 of Table VIII. Column 3 indicates the value of F_b; Column 4, the effective specific gravity of the manometer fluid as obtained from Table II and Figure 18; Column 5 presents the product of Column 15 of Table II and Column 4 of Table VIII

TABLE VIII

FLOW RATE AND PRESSURE DROP CALCULATIONS

1	2	3	4	5	6	7	8	9	10	11	12	13	14	1
		FLOW RATE								PRESSURE DROP				
Test Number	Type of Tube	Orifice Factor	Effective Specific Gravity Manometer Fluid	Effective Manometer Differential	Specific Volume of Steam at θ_5	Steam Flow Rate	Specific Volume of Steam at θ_3	Linear Velocity of Steam at S_{min}	Effective Specific Gravity Manometer Fluid	Pressure Drop over 10-Foot Length	Viscosity of Steam at θ_5	Friction Factor	Reynolds Number	Test Number
Symbols, Units →		F_b, ---	ρ_m, ---	h_w, in. H_2O	v, ft^3/lb	w, lbs/hr	v, ft^3/lb	V, ft/min	ρ_m, ---	Δp, in. H_2O	μ, lbs/ft-hr	f, ----	$(D_i V \rho / \mu)_{min}$	
Column Reference →		Table II, 14	Table II, 13,16 Figure 20	Table II, 15 Table VIII, 4	Table II, 3, 12 Steam Tables	Table VIII, 3,4,5,6	Table II, 3,6 Steam Tables	Table I, 17 Table VIII, 7,8	Table II, 13,18 Figure 21	Table II, 17 Table VIII, 10	Table IX, 3,6 Figure 14	Table VIII, 7, 11 Table I, 14,17	Table I, 14,17 Table VIII, 7, 12	
58	BARE	164	0.989	23.0	4.68	364	4.76	380	---	---	0.0365	---	27,600	58
58A	"	"	"	23.0	4.70	362	4.76	378	---	---	.0365	---	27,500	58A
59	"	"	"	15.4	4.69	298	4.77	312	---	---	.0365	---	22,600	59
59A	"	"	"	15.1	4.70	293	4.76	306	---	---	.0365	---	22,200	59A
60	"	"	"	3.35	4.65	139	4.77	145	---	---	.0365	---	10,600	60
60A	"	"	"	3.66	4.69	144	4.77	151	---	---	.0365	---	10,900	60A
61	"	"	0.994	11.5	9.57	178	9.45	368	---	---	.0361	---	13,700	61
61A	"	"	"	11.9	9.49	182	9.29	370	---	---	.0352	---	14,300	61A
62	"	"	"	6.60	9.46	137	9.37	281	---	---	.0355	---	10,700	62
62A	"	"	"	6.36	9.40	135	9.20	272	---	---	.0348	---	10,700	62A
63	"	"	"	2.81	9.39	89.6	9.32	183	---	---	.0353	---	7,040	63
63A	"	"	"	2.91	9.38	91.4	9.19	184	---	---	.0348	---	7,270	63A
64	"	675	0.989	21.4	4.90	1410	4.85	1500	0.0437	0.378	.0381	0.0206	102,000	64
65	"	"	"	11.8	4.90	1045	4.85	1111	.0441	.217	.0381	.0216	76,000	65
66	"	"	"	3.48	4.80	570	4.83	604	.0441	.056	.0379	.0188	41,600	66
67	"	"	0.994	11.5	10.04	721	9.95	1572	.0440	.152	.0380	.0154	52,600	67
68	"	"	"	4.89	9.98	473	9.89	1023	.0440	.073	.0378	.0172	34,600	68
69	"	"	"	1.91	9.86	297	9.76	636	.0440	.009	.0373	.0096	22,100	69
70	"	338	0.989	23.9	4.85	749	4.81	790	.0446	.077	.0377	.0150	55,000	70
71	"	"	"	14.7	4.85	590	4.81	625	.0450	.073	.0377	.0228	43,400	71
72	"	"	"	4.00	4.79	309	4.73	320	---	---	---	---	23,400	72
73	"	"	0.994	11.7	9.80	370	9.70	787	.0446	.054	.0370	.0252	27,700	73
74	"	"	"	7.59	9.75	299	9.66	634	.0446	.028	.0369	.0172	22,500	74
75	"	"	"	3.64	9.68	207	9.59	435	.0446	.023	.0366	.0292	15,700	75
76	LONGITUDINAL FIN	338	0.989	21.9	5.19	695	5.09	807	.0426	.347	.0399	.0279	20,300	76
77	"	"	"	13.9	5.18	555	5.08	644	.0427	.246	.0398	.0311	16,300	77
78	"	"	"	7.56	5.15	410	5.05	470	.0427	.155	.0394	.0363	12,100	78
79	"	"	0.994	10.5	10.50	338	10.27	791	.0417	.134	.0394	.0227	9,950	79
80	"	"	"	5.16	10.43	238	10.19	554	.0415	.0804	.0390	.0273	7,100	80
81	"	"	"	1.93	10.27	146	9.98	333	.0410	---	.0381	---	4,460	81
82	"	164	0.989	22.4	5.04	346	4.83	382	.0425	.0795	.0379	.0272	10,600	82
83	"	"	"	13.4	5.07	266	4.90	298	.0451	.0632	.0383	.0362	8,080	83
84	"	"	"	4.72	5.05	158	4.90	177	.0432	---	.0384	---	4,800	84
85	"	"	0.993	11.3	10.13	173	9.67	382	.0442	---	.0369	---	5,460	85
86	"	"	"	5.11	10.05	117	9.69	258	.0448	---	.0370	---	3,670	86
87	"	"	"	2.29	9.98	78.5	9.66	173	.0446	---	.0369	---	2,470	87
88	"	675	0.989	19.7	5.30	1300	5.26	1560	---	---	.0413	---	36,600	88
89	"	"	"	10.6	5.30	950	5.27	1141	---	---	.0413	---	26,700	89
90	"	"	"	7.28	5.25	795	5.22	945	---	---	.0411	---	22,400	90
91	"	"	0.993	11.3	10.50	666	10.29	1566	.0448	.696	.0395	.0302	19,600	91
92	"	"	"	5.33	10.50	480	10.30	1129	.0445	.325	.0395	.0269	14,200	92
93	"	"	"	2.97	10.50	333	10.30	785	.0442	---	.0395	---	9,880	93

TABLE VIII, CONTINUED

FLOW RATE AND PRESSURE DROP CALCULATIONS

1	2	3	4	5	6	7	8	9	10	11	12	13	14	1
			FLOW RATE							PRESSURE DROP				
Test Number	Type of Tube	Orifice Factor	Effective Specific Gravity Manometer Fluid	Effective Manometer Differential	Specific Volume of Steam at G_3	Steam Flow Rate	Specific Volume of Steam at θ_3	Lineal Velocity of Steam at S_{min}	Effective Specific Gravity Manometer Fluid	Pressure Drop over 10-Foot Length	Viscosity of Steam at θ_3	Friction Factor	Reynolds Number	Test Number
Symbols, Units →		F_b, ---	ρ_m, ---	h_w, in. H_2O	v, ft^3/lb	w, lbs/hr	v, ft^3/lb	V, ft/min	ρ_m, ---	Δp, in. H_2O	μ, lbs/ft-hr	f, ---	$(D_v W/\mu S_{min})$	
Column Reference →		Table II, 14	Table II, 13,16 Figure 20	Table II, 15 Table VIII, 4	Table II, 3, 12 Steam Tables	Table VIII, 3,4,5,6	Table IX, 3,6 Steam Tables	Table I, 17 Table VIII, 7,8	Table II, 13,18 Figure 21	Table II, 17 Table VIII, 10	Table IX 3,6 Figure 14	Table VIII, 7, 11 Table I, 14,17	Table I, 14,17 Table VIII, 7, 12	
94	"STAR" FIN	164	0.989	17.8	5.34	290	5.17	532	---	---	.0405	---	12,000	94
95	"	"	"	8.48	5.31	208	5.15	380	---	---	.0403	---	8,650	95
96	"	"	"	3.28	5.29	130	5.02	232	---	---	.0396	---	5,500	96
97	"	"	0.993	9.45	10.63	154	10.05	549	0.281	1.275	.0385	0.401	6,700	97
98	"	"	"	5.05	10.48	114	9.965	403	0.281	0.646	.0381	.374	5,010	98
99	"	"	"	1.56	10.16	64.5	9.81	224	.281	0.193	.0375	.355	2,880	99
100	"	338	0.989	11.9	5.36	505	5.20	931	.283	6.92	.0407	.392	20,800	100
101	"	"	"	5.95	5.35	356	5.15	650	.283	3.50	.0403	.403	14,800	101
102	"	"	"	1.53	5.29	182	5.08	326	.283	1.01	.0398	.451	7,650	102
103	"	"	0.994	5.77	10.86	246	10.54	920	.281	3.34	.0405	.393	10,200	103
104	"	"	"	3.60	10.77	196	10.47	728	.281	2.04	.0401	.381	8,190	104
105	"	"	"	1.77	10.63	138	10.37	507	.281	0.996	.0398	.379	5,820	105
106	"	675	0.993	2.56	10.88	329	10.64	1240	.281	5.82	.0409	.379	13,500	106
107	"	"	"	1.23	10.80	228	10.55	853	.283	2.99	.0405	.409	9,430	107
108	"	"	0.989	5.05	5.43	651	5.34	1233	.989	10.60	.0419	.468	26,000	108
109	"	"	"	3.66	5.44	554	5.35	1051	.989	6.79	.0419	.310	22,100	109
110	"	"	"	1.50	5.42	355	5.32	670	.989	2.66	.0416	.298	14,300	110
111	"	83.4	0.993	10.69	10.40	84.5	9.91	237	.283	0.466	.0379	.495	3,730	111
112	"	"	"	5.56	10.09	60.7	9.81	211	.283	0.233	.0375	.485	2,710	112
113	HELICAL FIN	675	0.989	3.48	5.31	546	5.19	1006	.282	2.69	.0406	.0836	24,500	113
114	"	"	"	5.70	5.33	697	5.20	1285	.283	4.08	.0407	.0775	31,200	114
115	"	"	"	7.33	5.33	791	5.24	1469	.283	5.60	.0410	.0820	35,400	115
116	"	"	"	9.78	5.34	912	5.25	1700	.283	7.53	.0411	.0828	40,500	116
117	"	"	"	3.42	5.33	533	5.22	987	.283	2.72	.0409	.0880	23,900	117
118	"	"	0.993	5.66	10.71	490	10.34	1800	.283	4.55	.0396	.0880	22,600	118
119	"	"	"	3.77	10.68	400	10.29	1460	.283	3.08	.0394	.0899	18,600	119
120	"	"	"	2.02	10.70	294	10.29	1072	.283	1.82	.0394	.0982	13,600	120
121	"	338	"	3.04	10.63	311	10.16	1121	.282	1.97	.0389	.0962	14,600	121
122	"	"	"	6.92	10.62	272	10.14	980	.283	1.52	.0388	.0972	12,800	122
123	"	"	"	4.70	10.63	225	10.14	810	.283	1.10	.0388	.1026	10,600	123
124	"	"	"	3.52	10.61	195	10.11	700	.283	0.814	.0387	.1013	9,220	124
125	"	"	"	2.34	10.57	159	10.10	570	.283	0.594	.0387	.1112	7,520	125
126	"	"	0.989	18.18	5.27	636	5.08	1146	.284	3.70	.0398	.0865	29,200	126
127	"	"	"	9.25	5.27	448	5.09	809	.283	1.92	.0399	.0902	20,500	127
128	"	"	"	3.33	5.27	269	5.09	486	.283	0.676	.0399	.0880	12,300	128

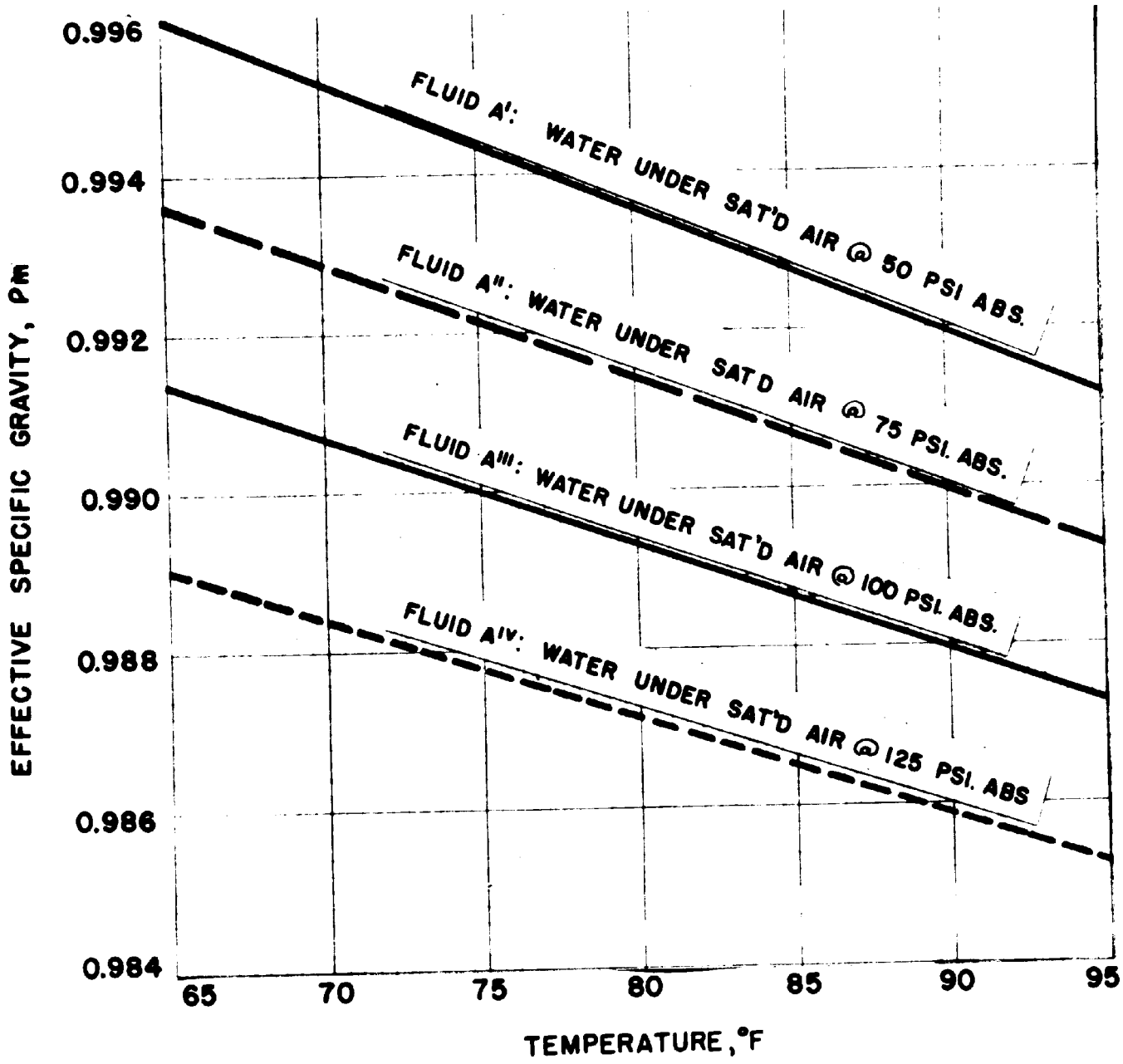

FIGURE 18

EFFECTIVE SPECIFIC GRAVITY OF MANOMETER FLUIDS A^{I}, A^{II}, A^{III}, A^{IV}

and gives the manometer differential in inches of water. The specific volume of the steam is given in Column 6. This value is obtained from steam tables at a pressure and temperature corresponding with conditions at the orifice plate and recorded in Table II Columns 3 and 12. Column 7 gives the steam flow rate as computed by Equation (30) from Columns 3, 5, and 6.

The lineal velocity through the heat exchanger is presented in Column 9 and is computed from the relation:

$$V_{max} = \frac{Wv}{S_{min}(60)} \qquad (31)$$

where V_{max} = lineal velocity through minimum cross section in ft/min.

W = flow rate in lbs/hr.

v = specific volume of steam at average exchanger conditions.

S_{min} = minimum free cross section of heat exchanger available for flow as indicated in Table I, Column 17.

The required specific volume at average heat exchanger conditions is evaluated at the temperature θ_3 presented in Table IX, Column 6.

The results of the pressure drop calculations are also presented in Table VIII.

The pressure drop over the 10.0-foot test section is presented in Column 11. This value is obtained from the observed manometer differential, as reported in Column 17 of Table II, by multiplying by the effective specific gravity of the appropriate manometer fluid (see Columns 13 and 18 in Table II and Figure 19) reported in Column 10 of Table VIII.

The friction factor is evaluated and presented in Column 13. The friction factor, f, has been defined by the equation:

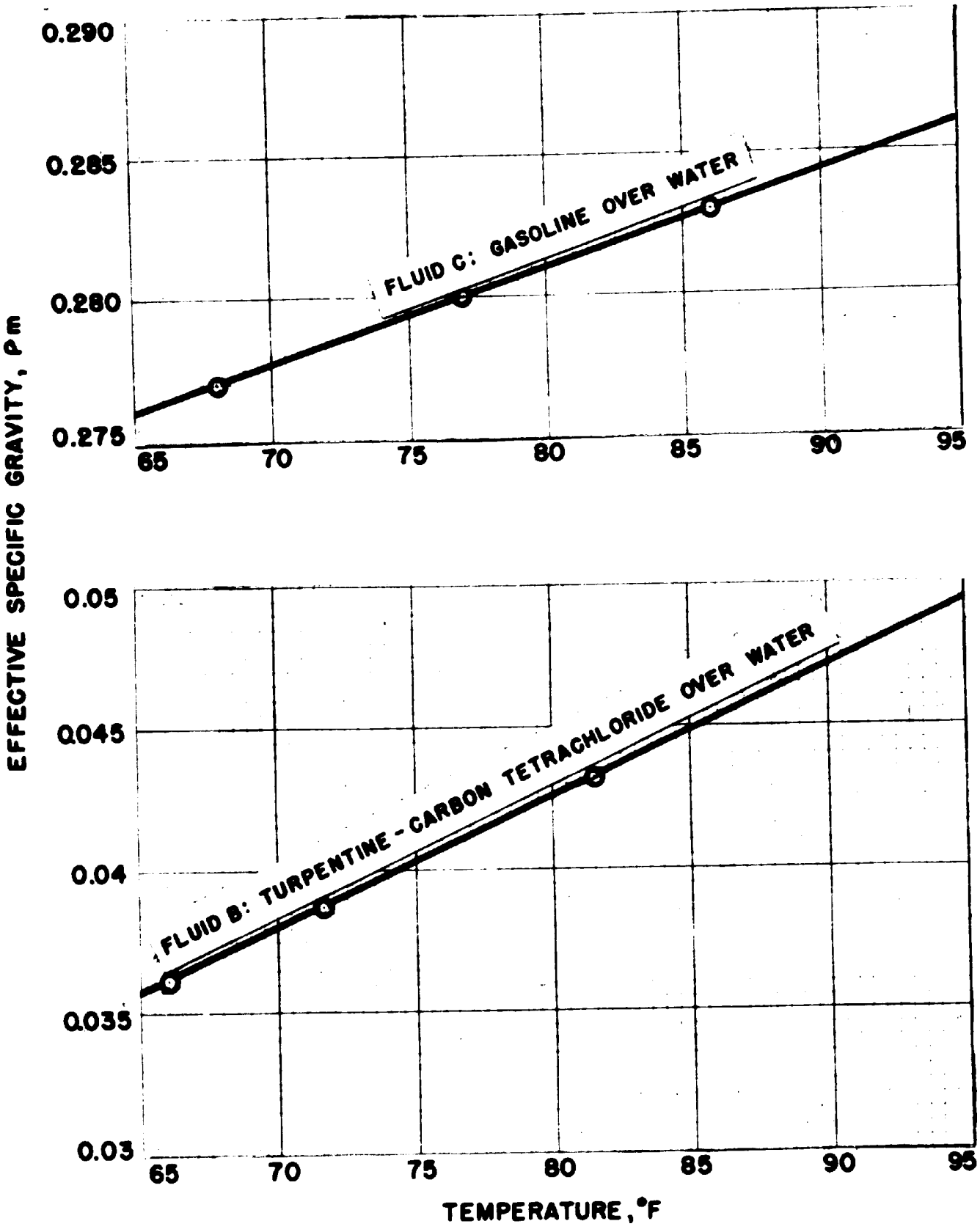

FIGURE 19

EFFECTIVE SPECIFIC GRAVITIES OF MANOMETER FLUIDS B AND C

$$f = \frac{2F\beta D'}{V^2 L} \qquad (24)$$

previously given. Introducing D_v, the "volumetric" equivalent diameter, ΔP, and ρ_w and rearranging, the equation becomes:

$$f = S_{min}^2 \; D_v \; (2\beta/12) \; \rho_w \; (\Delta P/W^2 v) \; (1/L) \qquad (32)$$

where ρ_w = density of water at 60°F., lbs/ft.^{3}

ΔP = pressure drop corresponding to F but expressed in inches of water. at 60°F. and given in Table VIII, Column 11.

L = 10.0 feet.

The constant $(1/L)(2\beta/12)(\rho_w)$ may be evaluated as 6.95×10^5, permitting the equation to be written as:

$$f = 6.95 \times 10^5 \; S_{min}^2 \; D_v \; (\Delta P/W^2 v) \qquad (33)$$

Friction factors reported in Column 13 of Table VIII are computed from Equation (33) using values obtained from Columns 14 and 17 of Table I and Columns 7, 8, and 11 of Table VIII.

The Reynolds number, defined as $(D_v W/\mu S_{min})$, where μ = viscosity of the steam at average heat exchanger conditions in lbs/ft.hr., is tabulated in Column 14 of Table VIII. This value is computed from values obtained from Columns 14 and 17 of Table I and Columns 7 and 12 of Table VIII. The viscosity listed in Column 12 of Table VIII is evaluated at the temperature θ_3 (Column 6 of Table IX), and the operating pressure as given in Column 3 of Table II.

3. Calculation of the Composite Heat Transfer Coefficients

It has been shown previously that the total heat transfer from the inner tube of the exchanger may be written as the sum of two terms, one representing the convection heat transfer and the other the radiation heat transfer.

$$\text{i.e.,} \quad q = q_{CTG} + q_{RT} \tag{2}$$

The convection term for the plain annulus may be expressed (28) as

$$q_{CTG} = h A (\theta_2 - \theta_3)_{lm} \tag{34}$$

where h = the convection heat transfer coefficient, Btu/hr.ft.^{2}°F.

A = heat transfer surface of the bare tube, ft.^{2}

$(\theta_2 - \theta_3)_{lm}$ = logarithmic mean temperature difference between the surface of the inner tube and the steam, °F.

For the modified annuli where the inner tube carries extended surface, the expression for the convection heat transfer is (28):

$$q_{CTG} = h (A_o + \phi A_f) (\theta_2 - \theta_3)_{lm} \tag{35}$$

where A_o = area of the bare tube exposed between fins, ft.^{2}

ϕ = fin efficiency, defined (28) as the ratio of the average temperature difference between the extended surface and the steam, to the temperature difference at the base of the fin; i.e., at the tube wall.

A_f = area of finned surface, ft.^{2}

Equation (35) may in fact be used for either the plain or the modified annuli; in the case of its use with the plain annulus A_o becomes equivalent

to A, and A_f becomes zero.

A detailed discussion of radiation has been deferred, but if at this time a "radiation coefficient," h_R, be defined (28) so that

$$q_{RT} = h_R (A_o + \phi A_f) (\theta_2 - \theta_3)_{lm} \qquad (36)$$

then the total heat transfer from the inner tubes of the annuli may be represented by the equation:

$$q = (h + h_R) (A_o + \phi A_f) (\theta_2 - \theta_3)_{lm} \qquad (37)$$

or

$$q = h' (A_o + \phi A_f) (\theta_2 - \theta_3)_{lm} \qquad (38)$$

The coefficient h' is referred to as the "composite" heat transfer coefficient, since it accounts for both the convection and the radiation transfer.

The calculations of the composite heat transfer coefficients are presented in Table IX. In this table Columns 1 and 2 give the test number and the type of inner tube. Column 3 indicates the steam pressure as reported in Table II. Columns 4, 5, 6, 7, and 8 indicate temperatures averaged over the length of the equipment as follows:

Column 4 - θ_1, the average between the inlet and the outlet salt temperatures, i.e., the average of Columns 4 and 5 of Table II.

Column 5 - θ_2, the average temperature of the outside surface of the inner tube as calculated from θ_1 and the total heat transfer. This is discussed in detail in a later paragraph.

Column 6 - θ_3, the average between the steam inlet and outlet temperatures, i.e., the average of Columns 6 and 7 of Table II.

TABLE II

CALCULATION OF THE COMPOSITE HEAT TRANSFER COEFFICIENTS

1	2	3	4	5	6	7	8	9	10	11	12	13	14	15	16	17	18	19	20	21	22	23	1
			AVERAGE TEMPERATURES						TEMPERATURE DIFFERENCES, °F														
Test Number	Type of Inner Tube	Steam Pressure	Average Salt	Average Outside Inner Tube	Average Steam	Average Outer Wall	Average Surface	Average Mid Insulation	Tube to Steam	Pipe to Surface	Steam Gain	Specific Heat of Steam at θ_3	Steam Flow Rate	Heat Gained by Steam	Heat Loss	Total Heat Transferred	Correction for Transfer Through Nonfinned Portion	Total Heat Transferred Over Finned Portion	Heat Transferred per Foot Length per Degree	Fin Efficiency	Total Effective Heat Transfer Surface	Composite Coefficient	Test Number
Symbols, Units →		P, psi abs	θ_1, °F	θ_2, °F	θ_3, °F	$\theta_4-\theta_5$ °F	θ_6, °F	θ_7, °F	$(\theta_2-\theta_3)_{lm}$	$\theta_5-\theta_6$	$\theta_2-\theta_1$	c_3, Btu/lb °F	w, lbs/hr	WAH Btu/hr	q_L, Btu/hr	Σq, Btu/lb	q', Btu/hr	q_t, Btu/hr	q/LA Btu/hr	ϕ, --	A_w sq ft	h'	
Column Reference →		Table II, 3	Table II, 4,5	Table IX, 4, 19 Figure 19	Table II, 6,7	Table II, 8,9	Table II, 10,11	Table IX, 7,8	Table IX, 5,6,12	Table IX, 7,8	Table II, 6,7	Table IX, 3,6 Figure 16	Table VIII, 7	Table IX, 12, 13,14	Table IX, 9, 11 Figure 18	Table IX, 15,16	Table X,5	Table IX, 17,18	Table IX,19 Table I,7,9	Table IX,23 Figure 25	Table I, 11 Table IX,21	Table IX,10, 19,22	
58	BARE	100	495	493	354.6	355.2	100	228	137	255	33.1	0.566	364	6,810	1180	7,990	Nil	7,990	3.89	1.000	5.89	9.98	58
58A	"	"	496	494	354.4	355.2	101	228	138	254	37.3	.567	362	7,770	1180	8,950	"	8,950	4.32	"	"	11.00	58A
59	"	"	496	494	355.9	358.4	100	229	137	258	34.8	.565	248	5,860	1190	7,050	"	7,050	3.44	"	"	8.74	59
59A	"	"	496	493	355.1	358.4	102	230	137	256	40.5	.566	293	6,720	1180	7,900	"	7,900	3.84	"	"	9.80	59A
60	"	"	495	494	356.2	365.6	101	234	137	265	45.2	.565	139	3,550	1230	4,780	"	4,780	2.32	"	"	5.93	60
60A	"	"	4 9	497	355.9	365.6	103	234	139	263	56.2	.565	144	4,590	1220	5,810	"	5,810	2.79	"	"	7.11	60A
61	"	50	494	492	352.0	351.3	101	226	138	250	51.7	.505	178	4,650	1160	5,810	"	5,810	2.80	"	"	7.15	61
61A	"	"	4 7	497	358.5	351.3	102	226	156	249	67.3	.510	182	6,250	1150	7,400	"	7,400	3.16	"	"	8.06	61A
62	"	"	496	495	344.5	346.9	101	224	148	246	58.8	.507	137	4,080	1140	5,220	"	5,220	2.35	"	"	6.00	62
62A	"	"	4 9	497	352.2	346.9	102	224	162	245	75.6	.513	135	5,240	1140	6,380	"	6,380	2.62	"	"	6.68	62A
63	"	"	496	495	341.2	353.6	101	228	151	253	77.4	.509	87.6	3,530	1170	4,700	"	4,700	2.07	"	"	5.29	63
63A	"	"	499	498	351.0	353.6	102	228	161	252	90.4	.513	91.4	4,230	1170	5,400	"	5,400	2.23	"	"	5.69	63A
64	"	100	499	494	388.0	384.0	104	244	106	280	19.7	.541	1410	15,000	1330	16,330	"	16,330	10.25	"	"	26.17	64
65	"	"	498	494	388.1	385.0	104	244	106	281	20.7	.541	1045	11,700	1340	13,040	"	13,040	8.18	"	"	20.86	65
66	"	"	498	495	384.4	382.0	105	244	111	277	25.2	.544	570	7,800	1320	9,120	"	9,120	5.46	"	"	13.93	66
67	"	50	499	496	390.6	388.0	104	246	105	284	23.3	.495	721	8,540	1350	9,890	"	9,890	6.26	"	"	15.97	67
68	"	"	498	496	386.1	383.1	104	244	108	279	28.0	.496	473	6,570	1330	7,900	"	7,900	4.86	"	"	12.40	68
69	"	"	499	497	376.0	375.0	104	239	119	272	36.3	.498	247	5,460	1280	6,740	"	6,740	3.77	"	"	9.62	69
70	"	100	497	494	380.9	375.6	104	240	114	271	23.6	.546	749	9,650	1280	10,930	"	10,930	6.38	"	"	16.28	70
71	"	"	498	495	380.7	376.1	106	241	115	270	25.8	.546	590	8,300	1370	9,670	"	9,670	6.00	"	"	15.31	71
72	"	"	498	496	369.8	368.1	105	237	125	263	37.1	.554	309	6,350	1230	7,580	"	7,580	4.04	"	"	10.30	72
73	"	50	497	495	370.9	368.3	104	236	124	264	35.5	.499	370	6,550	1230	7,780	"	7,780	4.18	"	"	10.66	73
74	"	"	498	496	367.6	367.1	104	236	127	263	38.5	.500	299	5,760	1230	6,990	"	6,990	3.66	"	"	9.35	74
75	"	"	498	496	362.9	365.1	104	235	132	261	47.9	.501	207	4,970	1220	6,190	"	6,190	3.12	"	"	7.97	75
76	LONGITUDINAL FIN	100	499	494	426.1	416.2	104	260	69.6	312	41.2	.523	695	14,900	1520	16,400	820	15,600	18.30	0.782	25.25	9.39	76
77	"	"	499	496	423.9	414.3	104	259	69.6	310	46.5	.522	555	13,400	1510	14,900	760	14,100	15.58	.810	26.05	7.78	77
78	"	"	499	495	417.0	407.9	103	256	74.0	309	57.5	.527	410	12,400	1470	13,900	670	13,200	13.72	.830	26.55	6.70	78
79	"	50	497	494	419.9	412.3	103	258	69.7	309	59.3	.491	338	8,840	1500	11,340	550	10,800	11.91	.851	27.10	5.71	79
80	"	"	497	494	413.1	408.8	102	256	75.7	307	70.6	.492	238	8,260	1480	9,740	490	9,250	9.39	.882	27.95	4.35	80
81	"	"	497	495	398.3	401.0	101	251	88.9	300	94.3	.494	146	6,800	1430	8,230	460	7,770	6.74	.915	28.85	3.02	81
82	"	100	500	495	386.0	379.1	103	241	103.5	276	84.5	.543	346	15,900	1300	17,200	860	16,300	12.11	.848	27.05	5.82	82
83	"	"	498	494	396.4	392.0	103	248	92.1	289	77.3	.537	266	11,000	1390	12,400	660	11,700	9.77	.879	27.85	4.52	83
84	"	"	497	494	398.4	398.7	104	251	88.9	295	88.0	.536	158	7,450	1420	8,870	500	8,370	7.24	.908	28.65	3.28	84
85	"	50	495	492	372.7	381.3	105	243	110.2	276	109.7	.499	173	9,480	1310	10,790	610	10,200	7.10	.909	28.65	3.20	85
86	"	"	496	493	374.7	392.7	106	250	109.2	287	113.4	.499	117	6,620	1380	8,000	520	7,480	5.26	.933	29.30	2.31	86
87	"	"	496	494	374.5	400.3	106	253	105.9	294	131.4	.499	78.5	5,150	1410	6,560	450	6,110	4.44	.942	29.55	1.93	87
88	"	100	498	494	451.3	443.5	104	274	41.8	340	19.3	.515	1300	12,900	1680	14,600	790	13,800	25.39	.711	23.45	14.12	88
89	"	"	497	494	452.3	443.4	106	275	40.5	337	20.4	.515	950	9,970	1670	11,640	620	11,000	20.89	.756	24.60	11.00	89
90	"	"	498	495	447.6	438.6	106	273	46.0	332	25.7	.516	793	10,500	1640	12,100	360	11,500	19.24	.773	25.05	9.98	90
91	"	50	496	491	420.2	411.1	108	259	68.8	303	45.1	.491	666	14,700	1470	16,200	800	15,400	17.22	.794	25.60	8.71	91
92	"	"	494	490	420.9	413.1	107	260	66.5	306	49.7	.491	480	11,700	1490	13,200	630	12,600	14.59	.822	26.35	7.17	92
93	"	"	495	492	421.1	414.7	106	260	67.4	309	54.8	.491	333	8,950	1500	10,450	520	9,930	11.33	.857	27.30	5.40	93

TABLE IX, CONTINUED

CALCULATION OF THE COMPOSITE HEAT TRANSFER COEFFICIENTS

1	2	3	4	5	6	7	8	9	10	11	12	13	14	15	16	17	18	19	20	21	22	23	1
			AVERAGE TEMPERATURES						TEMPERATURE DIFFERENCES, °F														
Test Number	Type of Inner Tube	Steam Pressure	Average Salt	Average Outside Inner Tube	Average Steam	Average Outer Wall	Average Surface	Average Mid Insulation	Tube to Steam	Pipe to Surface	Steam Gain	Specific Heat of Steam at θ_3	Steam Flow Rate	Heat Gained by Steam	Heat Loss	Total Heat Transferred	Correction for Transfer Through Non-Finned Portion	Total Heat Transferred over Finned Portion	Heat Transferred per Foot Length per Degree	Fin Efficiency	Total Effective Heat Transfer Surface	Composite Coefficient	Test Number
Symbols, Units	→	P, psi abs	θ_1, °F	θ_2, °F	θ_3, °F	$\theta_{k_T}=\theta_5$	θ_6, °F	θ_k, °F	$(\theta_2-\theta_y)_{lm}$	$\theta_5-\theta_6$	$G_2^*-G_1$	C_3, $\frac{Btu}{lb\,°F}$	w, $\frac{lbs}{hr}$	WAH Btu/hr	q_L, Btu/hr	Σq, Btu/lb	q', Btu/hr	q, Btu/hr	q/LA Btu/hr	ϕ --	A_e sq ft	h'	
Column Reference	→	Table II, 3	Table II, 4,5	Table IX, 4, 19 Figure 19	Table II, 6,7	Table II, 8,9	Table II, 10,11	Table IX, 7,8	Table IX, 5, 6, 12	Table IX, 7,8	Table II, 6,7	Table IX, 3,6 Figure 16	Table VIII, 7	Table IX,12, 13,14	Table IX, 9,11 Figure 18	Table IX, 15,16	Table X,5	Table IX, 17,18	Table IX,19 Table I,7,9	Table IX,23 Figure 25	Table I, 11 Table IX,21	Table IX,10, 19,22	
94	"STAR" FIN	100	498	493	435.5	444.3	108	276	45.2	336	84.3	.520	299	13,100	1680	14,800	340	14,500	24.66	0.748	23.80	13.48	94
95	"	"	496	492	432.6	445.5	108	277	45.4	338	20.7	.521	208	9,820	1690	11,500	290	11,200	18.98	.800	25.15	9.81	95
96	"	"	497	492.7	413.4	439.6	105	272	58.2	335	125.7	.526	130	8,600	1660	10,260	300	9,960	13.18	.853	26.55	6.48	96
97	"	50	496	491	393.2	424.5	106	265	65.6	319	150.1	.494	154	11,400	1570	13,000	350	12,600	14.77	.838	26.15	7.38	97
98	"	"	496	492	391.8	442.3	105	274	74.0	337	161.3	.495	114	9,100	1680	10,800	350	10,400	10.80	.880	27.20	5.16	98
99	"	"	497	494	380.1	438.7	105	272	86.1	334	175.6	.498	64.5	5,640	1660	7,300	340	6,960	6.22	.945	28.90	2.85	99
100	"	100	498	491	440.6	444.2	109	276	41.3	336	68.2	.519	505	17,900	1680	19,600	500	19,100	35.58	.644	21.20	21.90	100
101	"	"	497	491	433.8	441.1	109	275	46.5	332	84.0	.521	356	15,600	1660	17,300	450	16,800	28.60	.712	23.10	15.63	101
102	"	"	498	494	423.2	439.7	109	275	52.7	330	110.5	.525	182	10,600	1640	12,200	310	11,900	17.36	.814	25.50	8.85	102
103	"	50	505	501	439.0	451.3	101	276	48.1	351	91.7	.489	246	11,000	1760	12,800	320	12,500	19.98	.790	24.90	10.44	103
104	"	"	504	500	432.7	450.8	102	276	55.5	349	91.0	.489	196	8,740	1750	10,500	330	10,200	13.90	.846	26.35	7.02	104
105	"	"	503	500	425.1	449.6	101	275	59.8	349	107.5	.490	138	7,270	1750	9,020	300	8,720	11.21	.876	27.10	5.38	105
106	"	"	502	497	447.4	452.5	107	280	39.6	346	70.5	.488	329	11,300	1740	13,000	310	12,700	24.67	.748	23.85	13.50	106
107	"	"	503	499	439.3	452.1	109	280	48.8	343	83.2	.489	228	7,270	1730	11,000	310	10,700	16.88	.819	25.65	8.56	107
108	"	100	504	499	463.0	465.9	112	289	31.4	354	39.9	.512	651	13,300	1820	15,100	370	14,700	36.04	.640	21.09	22.28	108
109	"	"	504	499	464.0	467.3	112	290	30.6	355	41.7	.512	554	11,800	1820	13,600	330	13,300	33.42	.666	21.72	20.00	109
110	"	"	505	501	458.8	465.3	112	288	34.4	353	56.6	.513	355	10,300	1810	12,100	290	11,800	26.39	.733	23.46	14.64	110
111	"	50	505	501	388.4	445.4	110	278	83.1	335	178.3	.496	84.5	7,480	1690	9,170	360	8,810	8.15	.913	28.05	3.79	111
112	"	"	504	502	379.8	451.0	110	280	96.6	331	176.7	.498	60.7	5,340	1670	7,010	380	6,630	5.28	.956	29.16	2.38	112
113	HELICAL FIN	100	500	495	439.3	438.9	108	274	50.6	331	92.8	.519	546	14,940	1650	16,590	540	16,100	24.42	.472	21.30	14.35	113
114	"	"	499	494	441.1	443.5	108	276	49.5	336	44.6	.518	697	16,090	1680	17,770	610	17,200	26.71	.440	20.20	17.75	114
115	"	"	499	494	446.8	445.2	110	278	44.0	335	40.2	.517	791	16,440	1680	18,120	600	17,500	30.62	.375	17.90	22.30	115
116	"	"	499	493	448.4	446.4	110	278	42.4	336	36.8	.516	912	17,310	1680	18,990	630	18,400	33.36	.348	16.95	25.50	116
117	"	"	500	495	444.3	442.4	111	276	46.4	331	48.8	.517	533	13,430	1650	15,080	490	14,600	24.20	.460	20.85	15.10	117
118	"	50	501	494	421.9	448.0	108	278	64.1	340	79.8	.491	490	19,200	1700	20,900	610	20,300	24.36	.457	20.75	15.25	118
119	"	"	500	495	417.8	421.6	108	265	67.6	314	87.8	.491	400	17,230	1540	18,770	580	18,200	20.71	.520	23.00	11.75	119
120	"	"	500	496	418.4	399.4	110	254	65.5	289	98.2	.491	294	14,180	1390	15,570	470	15,100	17.75	.570	24.70	9.32	120
121	"	"	500	4 4	408.1	415.6	106	261	74.1	310	105.2	.493	311	16,140	1510	17,650	550	17,100	17.75	.570	24.70	9.32	121
122	"	"	501	496	405.8	416.2	107	262	77.2	309	110.4	.493	272	14,800	1510	16,310	540	15,800	15.74	.608	26.00	7.88	122
123	"	"	500	495	406.3	418.0	108	263	73.5	310	118.4	.493	225	13,120	1520	14,640	470	14,200	14.88	.625	26.60	7.30	123
124	"	"	500	496	404.2	418.0	109	264	75.8	309	125.6	.493	195	12,070	1520	13,590	450	13,100	13.30	.653	27.60	6.29	124
125	"	"	500	496	402.6	418.8	110	288	74.6	337	133.2	.493	159	10,440	1880	12,270	400	11,900	12.26	.676	28.50	5.64	125
126	"	100	499	491	422.6	422.0	108	265	62.3	314	69.2	.525	636	23,100	1540	24,640	740	23,900	29.72	.387	18.30	21.15	126
127	"	"	499	494	424.4	426.1	108	267	62.0	318	73.9	.524	448	17,310	1570	18,880	590	18,300	22.68	.487	21.80	13.56	127
128	"	"	499	495	423.9	430.0	108	269	60.9	322	87.6	.524	269	12,350	1590	13,940	430	13,500	17.09	.584	25.20	8.81	128

Column 7 - $\theta_4 = \theta_5$, the average between the temperatures of the outside of the exchanger shell at the two ends of the central 10-foot portion, equal to the average temperature of the inside of the exchanger shell, i.e., the average of Columns 8 and 9 of Table II.

Column 8 - θ_6, the average temperature of the surface of the insulation, i.e., the average of Columns 10 and 11 of Table II.

Column 9 - θ_k, the average temperature of the insulation, obtained by averaging Columns 7 and 8.

The important temperature differentials are indicated in Columns 10, 11, and 12.

Column 10 - $(\theta_2 - \theta_3)_{lm}$, the logarithmic mean temperature differential between the tube wall (Column 5) and the steam (Column 6). This value is computed from Columns 5, 6, and 12 of the table.

Column 11 - $(\theta_5 - \theta_6)$, the average temperature differential across the insulation, computed from Columns 7 and 8. Column 12 gives the increase in temperature of the steam on passing through the exchanger and is obtained from Columns 6 and 7 of Table II.

In Columns 13, 14, and 15, the net energy gain of the steam is computed. This is the term $W\Delta H$ discussed earlier and contained in Equation (6a), $q = q_{CTG} + q_{RT} = W\Delta H + q_L$. The heat gained by the steam is the product of the average specific heat of the steam, its temperature increase, and the flow rate. The specific heat in Column 13 is obtained from Figure 16 at the pressure and temperature of Columns 3 and 6. Column 14 repeats the flow rate as calculated in Table II; and Column 15 gives the heat gained by the steam, calculated from Columns 12, 13, and 14.

The heat loss from the exchanger is given in Column 16. This quantity requires fairly detailed explanation.

The heat loss, q_L, may be approximated (28) from the equation

$$q_L' = \frac{kA_{lm}}{L} (\theta_5 - \theta_6) \qquad (39)$$

which represents the conductive heat transfer rate from the outside wall of the exchanger shell to the surface "skin" of the insulation. In this equation:

q_L' = approximation to the heat loss from the heat exchanger, Btu/hr.
k = mean thermal conductivity of the insulation, Btu-in./ft.^{2}hr.°F.
L = thickness of insulation, in.
A_{lm} = logarithmic mean area normal to the direction of heat flow, ft.^{2}
$(\theta_5 - \theta_6)$ = temperature difference across the insulation, °F.

This equation, however, does not take into account heat loss through the supporting stands of the equipment and through the piping leading to the pressure drop seal pots. These latter losses may be estimated as equivalent to the loss through three rectangular steel supports of cross section A_s and length L_s, i.e.,

$$q_L'' = \frac{3k_sA_s}{L_s} (\theta_5 - \theta_6) \qquad (40)$$

where q_L'' = heat loss from stands and connecting pipes, Btu/hr.
k_s = thermal conductivity of steel, Btu-ft./ft.^{2} hr.°F.
A_s = cross-sectional area normal to heat flow, ft.^{2}
L_s = length of travel to a point where the metal temperature is equal to θ_6, ft.

Combination of Equations (39) and (40) leads to:

$$q_L = q_L' + q_L'' = \left(\frac{kA_{lm}}{L} + \frac{3k_sA_s}{L_s}\right) (\theta_5 - \theta_6) \qquad (41)$$

where q_L = calculated heat loss from the heat exchanger section.

Numerical values may be substituted into Equation (41) as follows:

$$A_{lm} = \frac{6.62}{12} (\pi)\ 17.5 = 30.3 \text{ ft.}^2$$

where 6.62 = logarithmic mean diameter of insulation, in.
17.5 = effective length of unit, ft.

L = 2.375 in.
k_s = 26.0 Btu-ft./hr.ft.^{2}°F.
L_s = 1.50 ft. (estimated)
A_s = 1.25 in.^{2} = 0.0087 ft.^{2} (estimated)

This leads to $q_L = (12.75k + 0.451)(\theta_5 - \theta_6)$ (42)

The thermal conductivity of the insulation is dependent upon its average temperature, θ_k, in accordance with the relationship shown in Figure 20 (a), which represents the manufacturer's data.

Equation (36), along with Figure 20(a), gives a procedure whereby the heat loss may be calculated. Examination of the various terms in this equation indicates an uncertainty of ten or fifteen percent. Because of this uncertainty it was decided to make a blank test in which no heat would be transferred from the inner tube and the drop in temperature of the steam in flowing through the exchanger circuit would be a measure of the heat loss. This test gave the following results:

q_L (observed) = 1020 Btu/hr.

$\theta_5 - \theta_6$ = 195°F.

θ_k = 200°F. = average temperature of the insulation

It is believed that the value of q_L obtained from this test is within about ten percent of the true value. Calculating q_L from Equation (42) and Figure 20(a) for the conditions of the test,

$$q_L = \left[12.75(0.31) + 0.451\right] 195$$

$$= 860 \text{ Btu/hr.}$$

which differs from the measured value by sixteen percent. The average of the two values, i.e., $q_L = 940$, is, however, well within ten percent of both the measured and the computed values and is probably within about five percent of the true value. Equation (42) may be modified therefore to give:

$$q_L = \frac{940}{860}(12.75k + 0.451)(\theta_5 - \theta_6) \qquad (43)$$

The relationship of Equation (43) is presented in chart form for easy use in Figure 20(b). The quantity q_L, reported in Column 16 of Table IX, is obtained from this chart using values of θ_k and $(\theta_5 - \theta_6)$ from Columns 9 and 11.

Addition of Columns 15 and 16 (representing the heat gained by the steam and the heat loss from the unit) gives Column 17, the total heat transferred from the inner tube. This is in accord with Equation (6a):

$$q = q_{CTG} + q_{RT} = W\Delta H + q_L$$

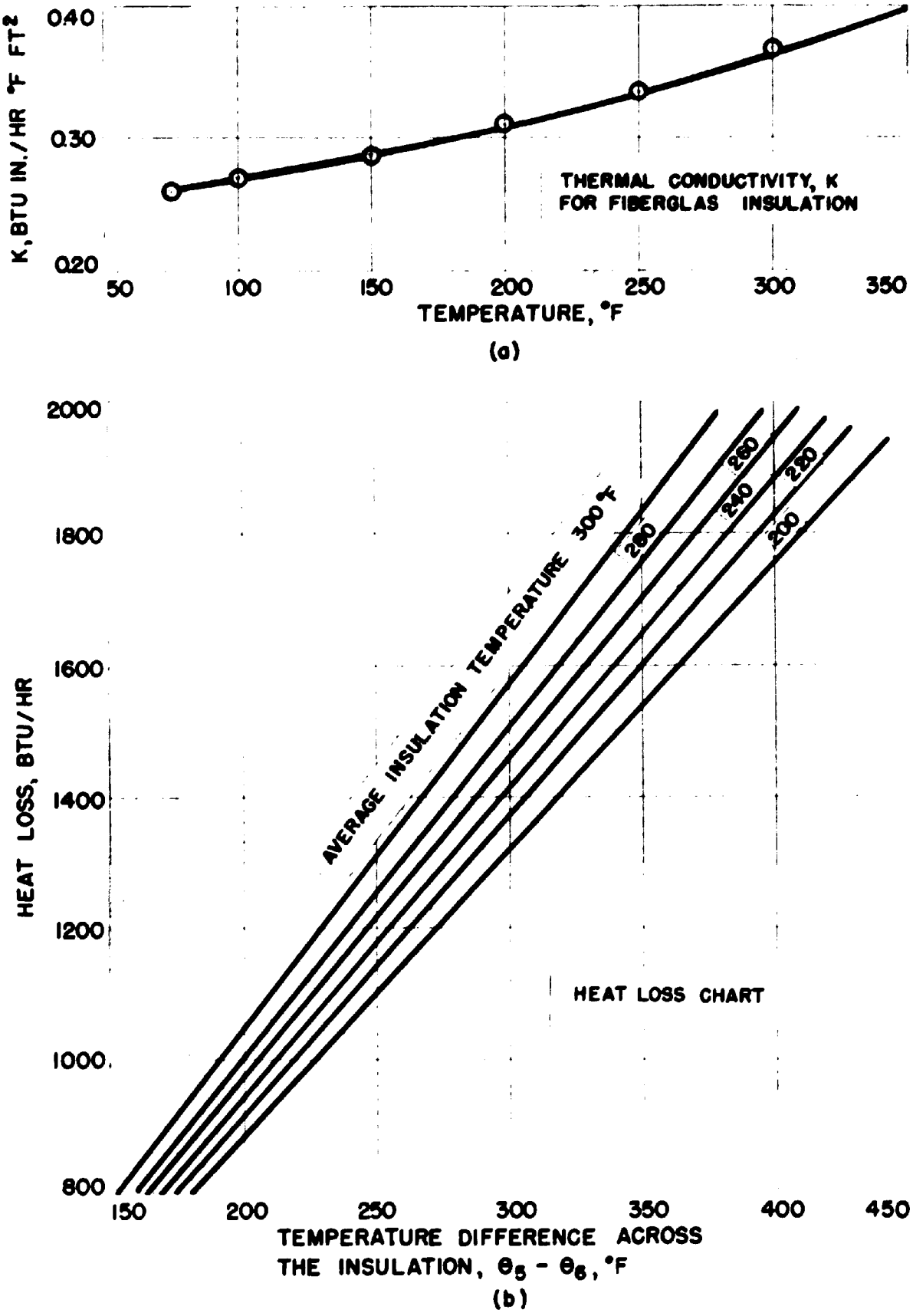

FIGURE 20

(a) THERMAL CONDUCTIVITY OF FIBERGLAS

(b) HEAT LOSS CHART FOR HEAT EXCHANGER

It is to be noted at this point that the conventional method of checking heat transfer measurements by application of an over-all heat balance, i.e., of Equation (5), $w\Delta h = W\Delta H + q_L$, is inapplicable in this work since the experimental error in the determination of Δh is of the order of 200 or 300 percent. This is because of the high rate of salt flow (w) and the extremely small change in salt temperature and enthalpy (Δh).

For all of the fin tubes Column 18 gives a correction, representing the heat transfer over the non-finned portion of these tubes, which is subtracted from the total heat transferred (Column 17) to give the heat transferred over the finned length. Details of this correction are discussed at the end of this section after the remaining calculations leading to the composite coefficient.

Applying the correction of Column 18, Column 19 is obtained to represent the total heat transfer over a 15.0-foot length in the case of the plain annulus and a 13.0-foot length in the case of the modified annuli (See Table I).

Before proceeding further, the procedure for obtaining Column 5, i.e., Θ_2, the average temperature of the outside surface of the inner tube, will be discussed. The calculation of Θ_2 from Θ_1, the average salt temperature, and q, the total heat transferred, is based upon the equation for the transfer of heat from the salt by convection to the inside of the inner tube and by conduction through to the outside surface.

This equation may be written (28) as:

$$q = \frac{A}{\left(\frac{D_o}{h_s D_i} + \frac{t\, D_o}{k_s D_m}\right)} (\Theta_1 - \Theta_2) \qquad (44)$$

where A = outside surface area of the inner tube, ft.^{2}

D_o = O. D. of inner tube, in.

D_i = I. D. of inner tube, in.

D_m = average diameter of inner tube, in.

$= 1/2\ (D_o + D_i)$

h_s = salt heat transfer coefficient, Btu/ft.^{2} hr.°F.

k_s = thermal conductivity of steel, Btu-ft./ft.^{2} hr.°F.

t = thickness of inner tube wall, ft.

$= 1/24\ (D_o - D_i)$

Substituting numerical values for the case of the bare tube (having a heat transfer length of 15.0 feet) and rearranging,

$$\theta_1 - \theta_2 = \frac{q}{5.89}\left(\frac{1.5}{h_s} + 0.000961\right) \qquad (45)$$

Equation (45) indicates that θ_2 may be calculated from θ_1 and q provided that h_s, the salt heat transfer coefficient, is known. This quantity may be estimated from data of Kirst, Nagle, and Castner (17) with the help of the Dittus-Boelter equation (28) for heat transfer coefficients inside circular pipes.

First, however, it is necessary to know the rate of flow of the salt in the tube. It will be recalled that this rate is maintained constant at the maximum output of the pump during all tests, but also that the salt rate itself was not observed due to difficulties in the operation of the seal pot system. Appendix C presents the details of a calculation of the salt flow rate from the results of a test of the flow characteristics of the salt system with water. This calculation leads to the conclusion that the rate of flow of the salt, in all tests, is 19.5 ft./sec. The calculation requires no assumptions and this result is believed reliable to at least five percent.

Kirst, Nagle, and Castner present data on the viscosity and specific gravity of molten salt as a function of temperature, and also a plot of $(h_s D/\mu_s^{0.4})$ vs. Reynolds number, $(DV_s\rho_s/\mu_s)$. Here,

h_s = salt heat transfer coefficient, Btu/hr.ft.^{2}°F.

D = inside diameter of tube, ft.

μ_s = viscosity of salt, lbs./ft.hr.

ρ_s = density of salt, lbs./ft.^{3}

V_s = velocity of salt, ft./hr.

Assuming an average salt temperature of 500°F. (see Column 4, Table IX), the viscosity and density are obtained (17) as:

μ_s = 10.16 lbs./ft.hr.

ρ_s = 118.9 lbs./ft.^{3}

Taking V_s = 19.5 (3600) and D = 1/12 foot, the Reynolds number may be computed as:

$$DV_s\rho_s/\mu_s = 68,000$$

This is slightly beyond the range of reliable data on the Kirst plot of $h_sD/\mu_s^{0.4}$.

The Dittus-Boelter equation for circular pipes, which is well established (28), is

$$h_sD/K_s = 0.023\ (C_s\mu_s/K_s)^{0.4}\ (DV_s\rho_s/\mu_s)^{0.8} \qquad (46)$$

where K_s = thermal conductivity of the salt, Btu/ft.^{2} hr.°F.
C_s = specific heat of the salt, Btu/lb.°F.

Rearranging this equation:

$$h_sD/\mu_s^{0.4} = 0.023\ C_s^{0.4}\ K_s^{0.6}\ (DV_s\rho_s/\mu_s)^{0.8} \qquad (47)$$

If it now be assumed that K_s is approximately constant with temperature (Kirst shows that C_s is constant at 0.373), the equation becomes:

$$h_sD/\mu_s^{0.4} = \gamma\ (DV_s\rho_s/\mu_s)^{0.8} \qquad (48)$$

where γ is a constant. This equation is used to extrapolate the Kirst data (from a Reynolds number of 10,000) and indicates a value of $h_sD/\mu_s^{0.4}$ = 74.0 for a Reynolds number of 68,000. Substition of the values of D and μ_s into the expression $h_sD/\mu_s^{0.4}$ = 74.0 yields the final result, h_s = 2240 Btu/hr. ft.^{2} °F.

This is the computed value of the salt coefficient which is realized in all tests. The value is considered reliable to about fifteen percent. This accuracy is more than adequate, since the differences between Θ_1 and Θ_2 are small.

Returning to Equation (45) and inserting the value h_s = 2240, it is found that

$$\Theta_1 - \Theta_2 = 0.000277\ q \qquad (49)$$

This relationship for the bare tube is plotted in Figure 21 along with similar relations for the other tubes.

The temperature Θ_2 may now be obtained from Θ_1 (Column 4, Table IX), q (Column 19, Table IX), and Figure 21. Strictly speaking, a trial and error calculation is required, since q is not known until Θ_2 is determined. Actually, however, a sufficiently close estimate of q for use with Figure 21 may be obtained by substituting Θ_1 for Θ_2 in the calculations

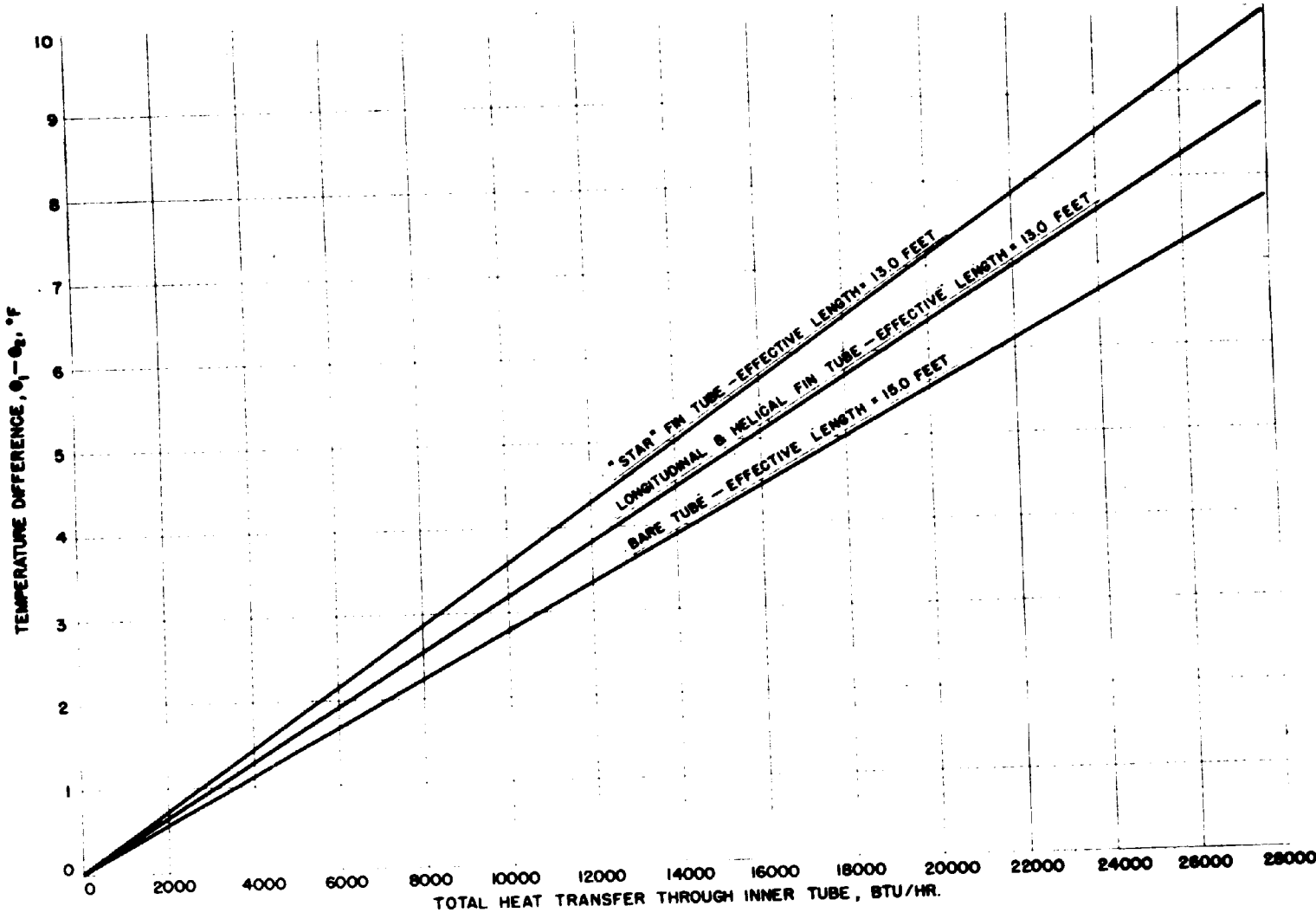

FIGURE 21

ESTIMATION OF OUTSIDE TEMPERATURE OF INNER TUBE

leading to q. The temperature θ_2 is therefore determined, and then the final value of q, which is inserted in Column 19.

Column 20 reports the total heat transferred per foot of effective length and per unit temperature differential. This value is obtained by dividing Column 19 by Column 10 and by the length of the transfer section (15.0 feet for the bare tube and 13.0 feet for the fin tubes). This quantity is a measure of the over-all ability of the surface to transfer heat and is plotted against the lineal velocity of the steam (Table VIII, Column 9) in Figures 22 and 23.

Figures 22 and 23, which represent the variation in the over-all heat transfer ability of the various tubes with lineal velocity, may be considered to summarize the results of the heat transfer tests without reference to the details of the mechanisms.

To complete the summary, Figure 24 is presented to show the relationship between the pressure drop per foot of length and the lineal velocity of the steam. Figure 24 is constructed by plotting Column 11 of Table VIII, divided by 10, against Column 9 of Table VIII.

Column 21 of Table IX presents the fin efficiencies for the various surfaces. These are calculated by the methods of Gardner (11) and are plotted against the composite heat transfer coefficient in Figure 25. The calculations are straightforward in the case of the longitudinal and helical fins. In the case of the "star" fin, however, because of the complexity of the geometry, it is necessary to consider the "star" as equivalent to a disc of slightly less diameter. It is believed that this estimation of the "equivalent diameter" of the star is made to quite satisfactory accuracy.

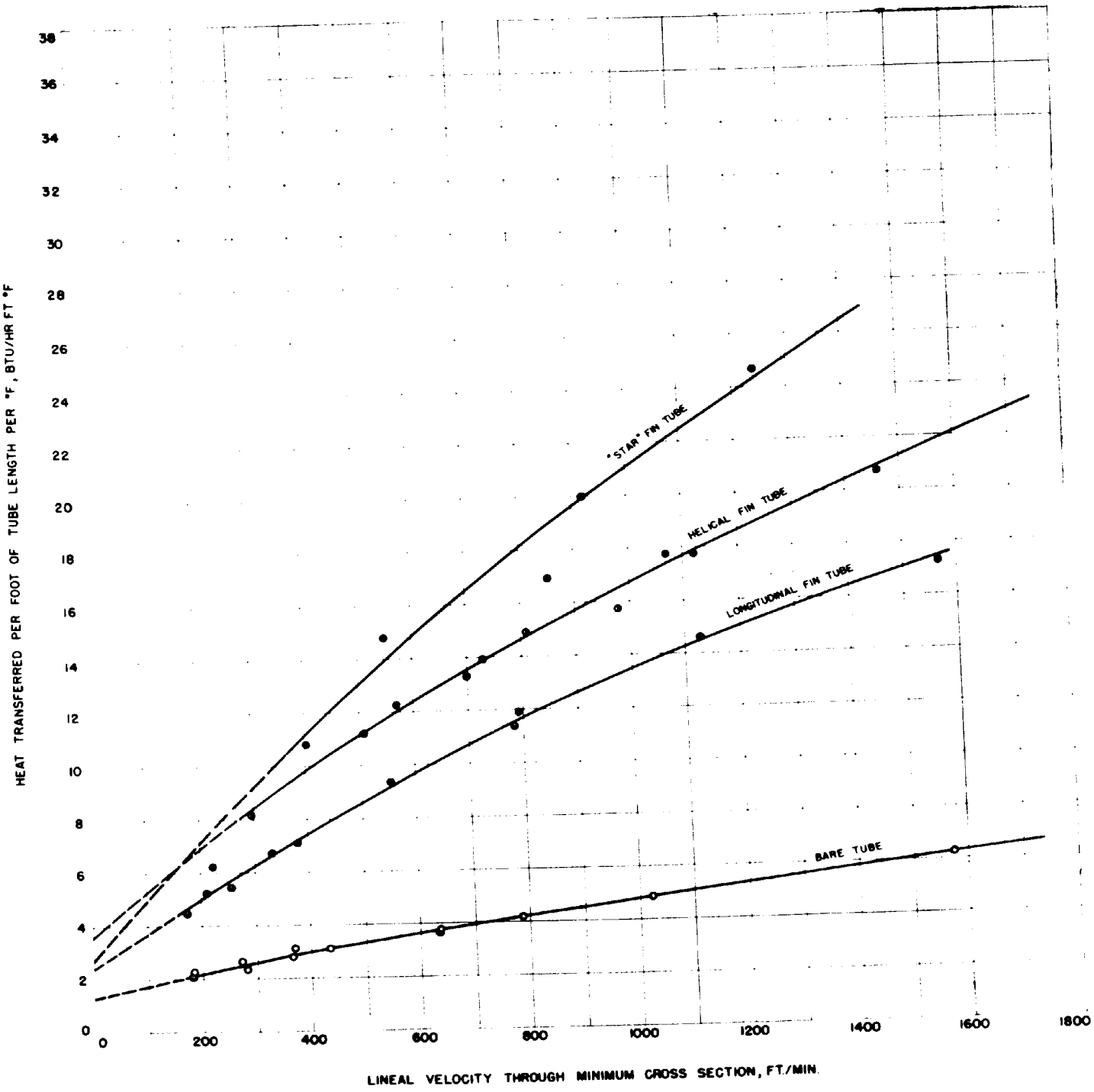

FIGURE 22

HEAT TRANSFERRED PER FOOT OF TUBE LENGTH TO SUPERHEATED STEAM AT 50 PSI. ABS.

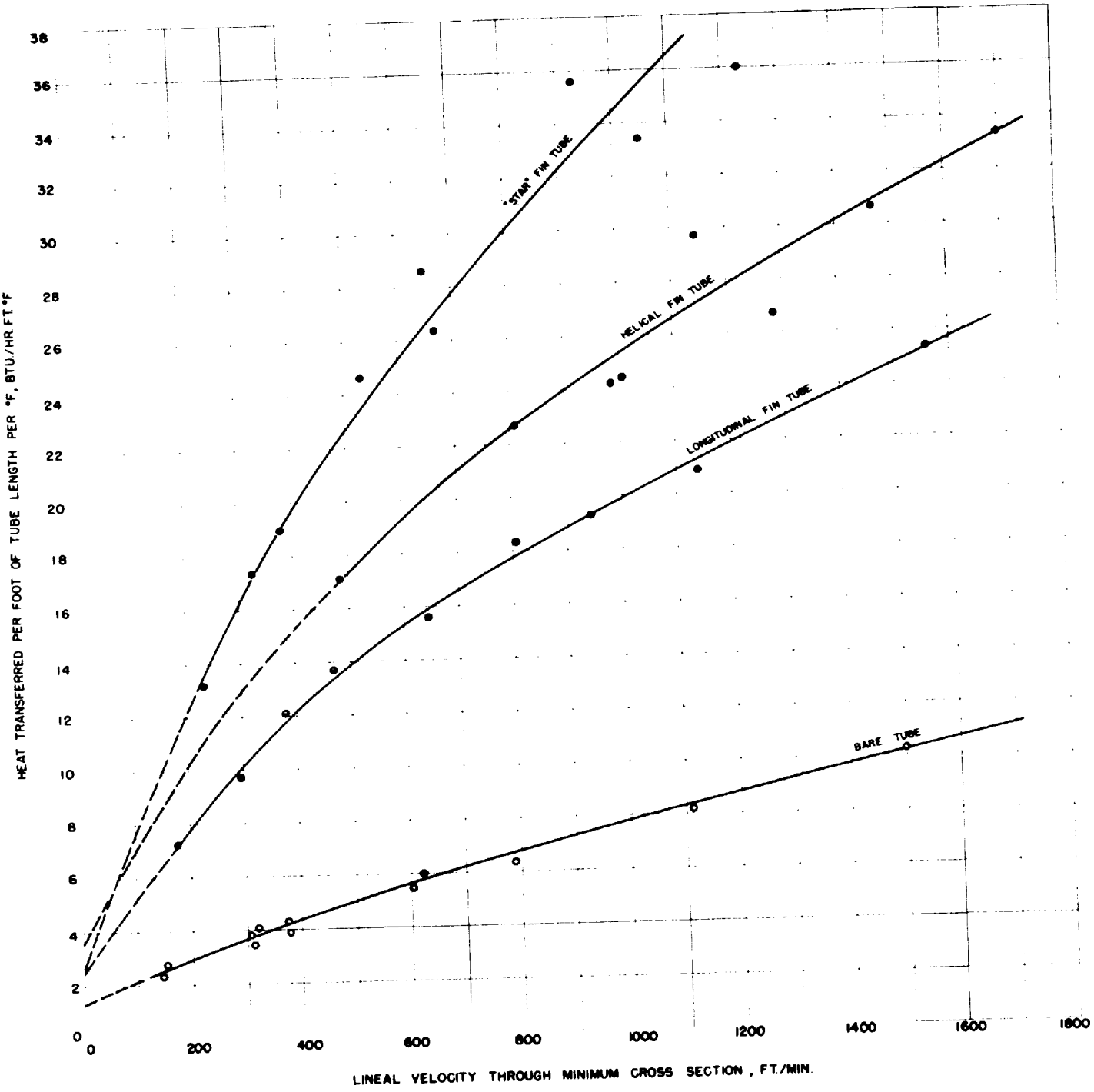

FIGURE 23

HEAT TRANSFERRED PER FOOT OF TUBE LENGTH TO SUPERHEATED STEAM AT 100 PSI. ABS.

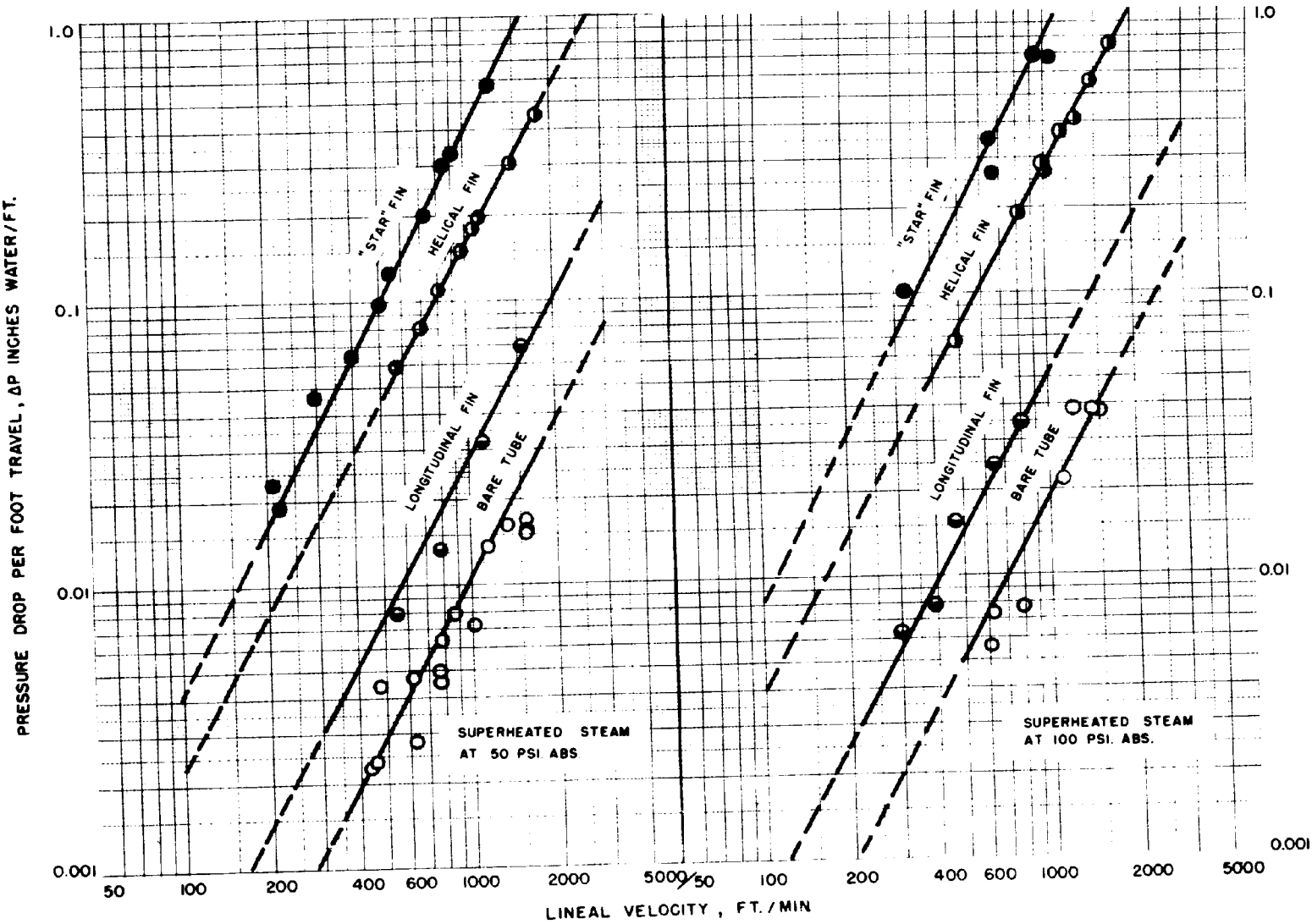

FIGURE 24

PRESSURE DROP — LINEAL VELOCITY RELATIONS

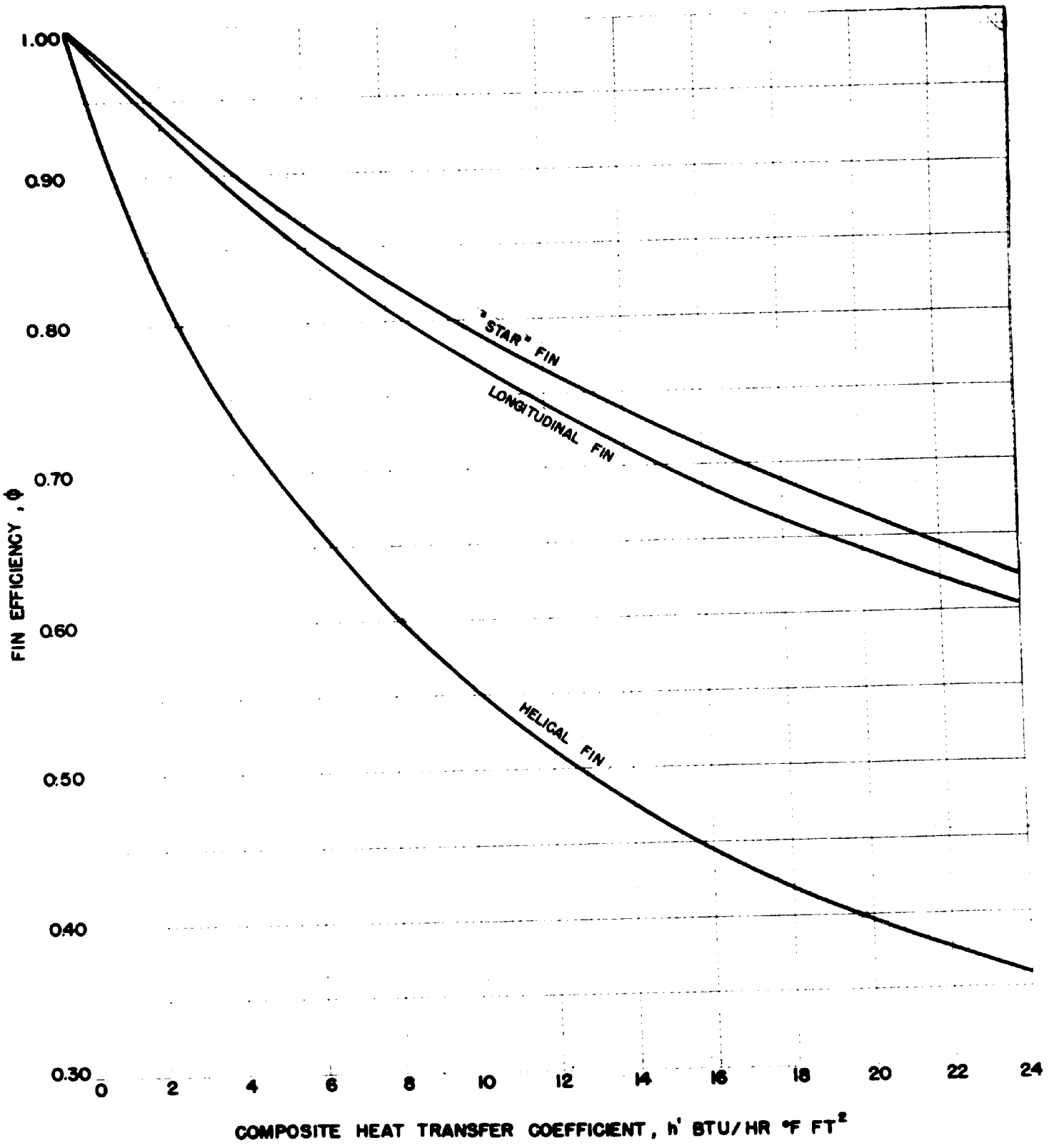

FIGURE 25

FIN EFFICIENCIES

The fin efficiencies and the composite heat transfer coefficients are interdependent, and it might be suspected therefore that trial and error calculation would be required for the final step in calculating the composite coefficient. The coefficient is defined by Equation (38), which, rearranged, is:

$$h' = \frac{q}{(A_o + \phi A_f)(\theta_2 - \theta_3)_{lm}}$$

The trial and error work may be avoided by constructing a plot of $h'(A_o + \phi A_f)$ vs. h' and making use of the relationship, from Equation (38), that

$$h'(A_o + \phi A_f) = \frac{q}{(\theta_2 - \theta_3)_{lm}}$$

The quantity $q/(\theta_2 - \theta_3)_{lm}$ is obtained from Columns 10 and 19 of Table IX, and h' from this with the aid of the plot of $h'(A_o + \phi A_f)$ vs. h'. This latter plot is not presented, since it represents a mere device of calculation.

The composite coefficient h' is reported in Column 23; the values of ϕ, the fin efficiency, and $(A_o + \phi A_f)$, the effective transfer area, are tabulated in Columns 21 and 22.

This completes the discussion of the calculation of the composite heat transfer coefficients, and of Table IX, with the exception of the item of Column 18, the correction for the heat transferred over the nonfinned portion of the finned tubes. This quantity is computed by application of Equation (38) to the nonfinned portion of the finned tubes. The composite coefficient required for use in this equation is best obtained by anticipating the correlation of the bare tube coefficients which is

presented in Figure 26. The correlation gives a linear relationship between h', the composite coefficient, and $K/D_v(C\mu/K)^{0.4}(D_vW/\mu S_{min})^{0.8}$. (These symbols are defined in an earlier section and again in the Table of Nomenclature.)

To obtain the heat transfer over the nonfinned length of the fin tubes, it is only necessary, therefore, to compute $K/D_v(C\mu/K)^{0.4}(D_vW/\mu S_{min})^{0.8}$ for the bare portion of the tube, obtain h' from Figure 26, and make the substitution into Equation (38).

The details of this calculation are presented in Table X. Column 1 of this table indicates the test number; Column 2, the value of $K/D_v\ (C\mu/K)^{0.4}\ (D_vW/\mu S_{min})^{0.8}$ for the nonfinned portion of the tube. Column 3 gives the composite coefficient h', as obtained from Figure 26, and Column 4 repeats the value of $(\Theta_2 - \Theta_3)_{lm}$ from Table IX, Column 10. The heat transfer through the nonfinned portion of the tube is calculated from Equation (38) and reported in Column 5. This is the correction quantity in Column 18 of Table IX.

TABLE X

CORRECTION FOR HEAT TRANSFER OVER NON-FINNED PORTIONS OF THE EXCHANGER TUBES

1	2	3	4	5	1	2	3	4	5	1	2	3	4	5
	LONGITUDINAL FIN					"STAR" FIN					HELICAL FIN			
Test Number	$\frac{K}{D}\left(\frac{C\mu}{K}\right)^{0.4}\left(\frac{D_v M}{\mu S_{min}}\right)^{0.8}$ for non-finned portion	h' for non-finned portion	$(\theta_2-\theta_3)_{lm}$ °F.	Heat Transferred Through Non-Finned Portion q', Btu/hr	Test Number	$\frac{K}{D}\left(\frac{C\mu}{K}\right)^{0.4}\left(\frac{D_v M}{\mu S_{min}}\right)^{0.8}$ for non-finned portion	h' for non-finned portion	$(\theta_2-\theta_3)_{lm}$ °F.	Heat Transferred Through Non-Finned Portion q', Btu/hr	Test Number	$\frac{K}{D}\left(\frac{C\mu}{K}\right)^{0.4}\left(\frac{D_v M}{\mu S_{min}}\right)^{0.8}$ for non-finned portion	h' for non-finned portion	$(\theta_2-\theta_3)_{lm}$ °F.	Heat Transferred Through Non-Finned Portion q', Btu/hr
Column Reference →	Table I, 14 Table VIII,14 Table IX, 3,6 Figures 15,17	Figure 26	Table IX, 10	Table I, 11 Table X, 3,4		Table I, 14 Table VIII,14 Table IX, 3,6 Figures 15,17	Figure 26	Table IX, 10	Table I, 11 Table X, 3,4		Table I, 14 Table VIII,14 Table IX, 3,6 Figures 15,17	Figure 26	Table IX, 10	Table I, 11 Table X, 3,4
76	372	16.0	65.6	820	94	286	9.6	45.2	340	113	467	13.6	50.6	540
77	477	13.9	69.6	760	95	218	8.1	45.4	290	114	565	15.8	49.5	610
78	376	11.6	74.0	670	96	150	6.6	58.2	300	115	650	17.3	44.0	600
79	302	10.0	69.7	550	97	160	6.8	65.6	350	116	707	19.0	42.4	630
80	230	8.3	75.7	490	98	125	6.0	74.0	350	117	461	13.5	46.4	490
81	152	6.6	88.9	460	99	75.0	5.0	86.1	340	118	402	12.2	64.1	610
82	333	10.6	103.5	860	100	550	15.5	41.3	500	119	344	10.9	67.6	580
83	268	9.2	92.1	660	101	418	12.6	45.2	450	120	268	9.2	65.5	470
84	176	7.1	88.9	500	102	195	7.6	52.7	310	121	279	9.4	74.1	550
85	176	7.1	110.2	610	103	233	8.4	48.1	320	122	251	8.85	77.2	540
86	128	6.1	109.2	520	104	195	7.6	55.9	330	123	216	8.10	73.5	470
87	94.0	5.4	105.9	450	105	147	6.5	59.8	300	124	192	7.51	75.8	450
88	933	24.0	41.8	790	106	298	9.9	39.6	310	125	165	6.90	74.6	400
89	729	19.5	40.5	620	107	221	8.2	48.8	310	126	533	15.1	62.3	740
90	554	15.6	46.0	560	108	541	15.3	31.4	370	127	401	12.15	62.0	590
91	518	14.8	68.8	800	109	475	13.8	30.6	330	128	266	9.10	60.9	430
92	400	12.1	66.5	630	110	333	10.6	34.4	290					
93	299	9.9	67.4	520	111	99.0	5.5	83.1	360					
					112	76.0	5.0	96.6	380					

VII. INTERPRETATION AND CORRELATION OF RESULTS

This section, which deals with the interpretation and correlation of the results, is subdivided as follows: 1. Interpretation of the Heat Transfer Data without Detailed Analysis of the Radiation Transfer; 2. Interpretation of the Heat Transfer Data Through Detailed Analysis of the Radiation Transfer; and 3. Interpretation of Pressure Drop Data.

1. Interpretation of the Heat Transfer Data Without Detailed Analysis of the Radiation Transfer

The composite heat transfer coefficient, h', presented in Table IX represents the rate of total heat transfer from the inner tube per unit of effective surface and per unit temperature differential. The coefficient is defined by Equation (38):

$$q = q_{CTG} + q_{RT} = h' (A_o + \phi A_f) (\theta_2 - \theta_3)_{lm}$$

and is a composite of the convection coefficient h and the "radiation coefficient" h_R defined earlier; i.e., $h' = h + h_R$.

The study of previous work and the equations proposed for correlating convection coefficients indicate that convection coefficients for heat transfer from the inner tube of plain or modified annuli might be correlated by the "Dittus-Boelter" type equation

$$h = N \frac{K}{D_v} \left(\frac{C\mu}{K}\right)^m \left(\frac{D_v W}{\mu S_{min}}\right)^n \qquad (26)$$

where N and n are constants dependent upon geometrical factors and m = 0.3 for heat being transferred to the inner tube and 0.4 for heat being

transferred from the inner tube.

Without, at the moment, inquiring too deeply into the nature of the radiation, the following behavior might be expected: that

(a) the radiation transfer rate is independent of the steam flow rate,

(b) the radiation transfer rate is dependent upon the differences of the fourth powers of the temperatures involved (28), and

(c) for any comparatively narrow range of temperatures, the fourth-power differences of (b) are approximately proportional to the first power difference, $(\theta_2 - \theta_3)_{lm}$.

On the basis of these observations, the radiation heat transfer coefficient h_R might be expected to remain approximately constant for a given inner tube and over a reasonable range of temperature differences.

If this assumption, i.e., of constant h_R, be made, then

$$h' = h_R' + N \frac{K}{D_v} \left(\frac{C\mu}{K}\right)^{0.4} \left(\frac{D_v W}{\mu S_{min}}\right)^n \qquad (50)$$

where h_R' designates, for any inner tube, the value of h_R if h_R be assumed constant, or h_R' is the average value of h_R. Equation (50) indicates a linear relationship between h', the composite coefficient, and $(K/D_v)(C\mu/K)^{0.4}\ (D_v W/\mu S_{min})^n$.

This suggests the following as a procedure for separating the composite coefficient into its components:

(a) the trial and error selection of values of "n" to yield a linear relationship when h' is plotted against $(K/D_v)(C\mu/K)^{0.4}\ (D_v W/\mu S_{min})^n$

(b) the interpretation of the slope of the resulting straight line as N, the multiplying constant of Equation (26) for the convection coefficient.

(c) the interpretation of the intercept at $(K/D_v)(C\mu/K)^{0.4}\ (D_v W/\mu S_{min})^n = 0$ as h_R', the "constant" or average value of the radiation coefficient, h_R.

In the case of the plain annulus, previous work indicates that the exponent n of the Reynolds number is 0.80. Accepting this value, the quantity $(K/D_v)(C\mu/K)^{0.4}\ (D_vW/\mu S_{min})^{0.80}$ is computed for each test. Results of this calculation are presented in Table XXII along with other calculations to be discussed later. Column 1 of Table XXII indicates the test number; Column 3, the composite coefficient as obtained from Table IX; and Column 10, the values of $(K/D_v)(C\mu/K)^{0.4}\ (D_vW/\mu S_{min})^{0.80}$.

Figure 26 is a plot of h', the composite coefficient, vs. $(K/D_v)(C\mu/K)^{0.4}\ (D_vW/\mu S_{min})^{0.80}$. It is to be noticed that the data fall well along a straight line, confirming the procedure and the value of $n = 0.80$. The intercept value is 3.3, which is interpreted as the average value of h_R, the radiation coefficient. The slope of the straight line is determined as 0.022 and this is the multiplying constant of Equation (26).

Summarizing for the bare tube, the straight-line plot of Figure 26 confirms the method of interpretation and indicates

$$h_R' = 3.3 \text{ Btu/hr.ft.}^2 \text{°F.}$$

$$h = 0.022 \frac{K}{D_v} \left(\frac{C\mu}{K}\right)^{0.4} \left(\frac{D_vW}{\mu S_{min}}\right)^{0.8} \qquad (51)$$

Considering now the case of the longitudinal fin tube, it might also be expected that the exponent of the Reynolds number would be 0.80, since the type of flow is similar to that in the plain annulus. Table XXII presents, in Columns 1, 3, and 10, the results of calculations on the assumption of $n = 0.80$. The data of Columns 3 and 10 are plotted in Figure 27, where they are seen to be well represented by a straight line.

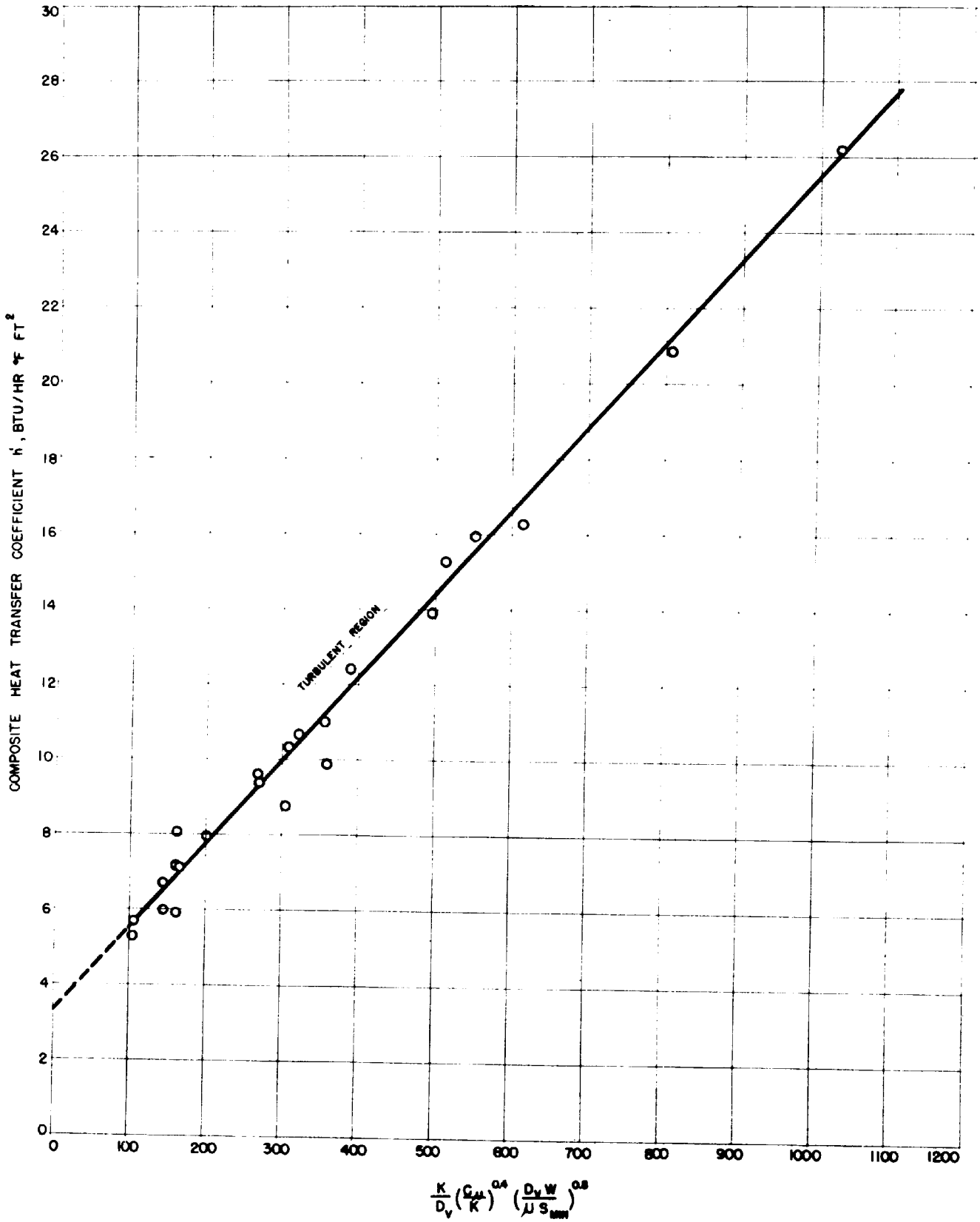

FIGURE 26

COMPOSITE HEAT TRANSFER COEFFICIENTS FOR THE BARE TUBE.

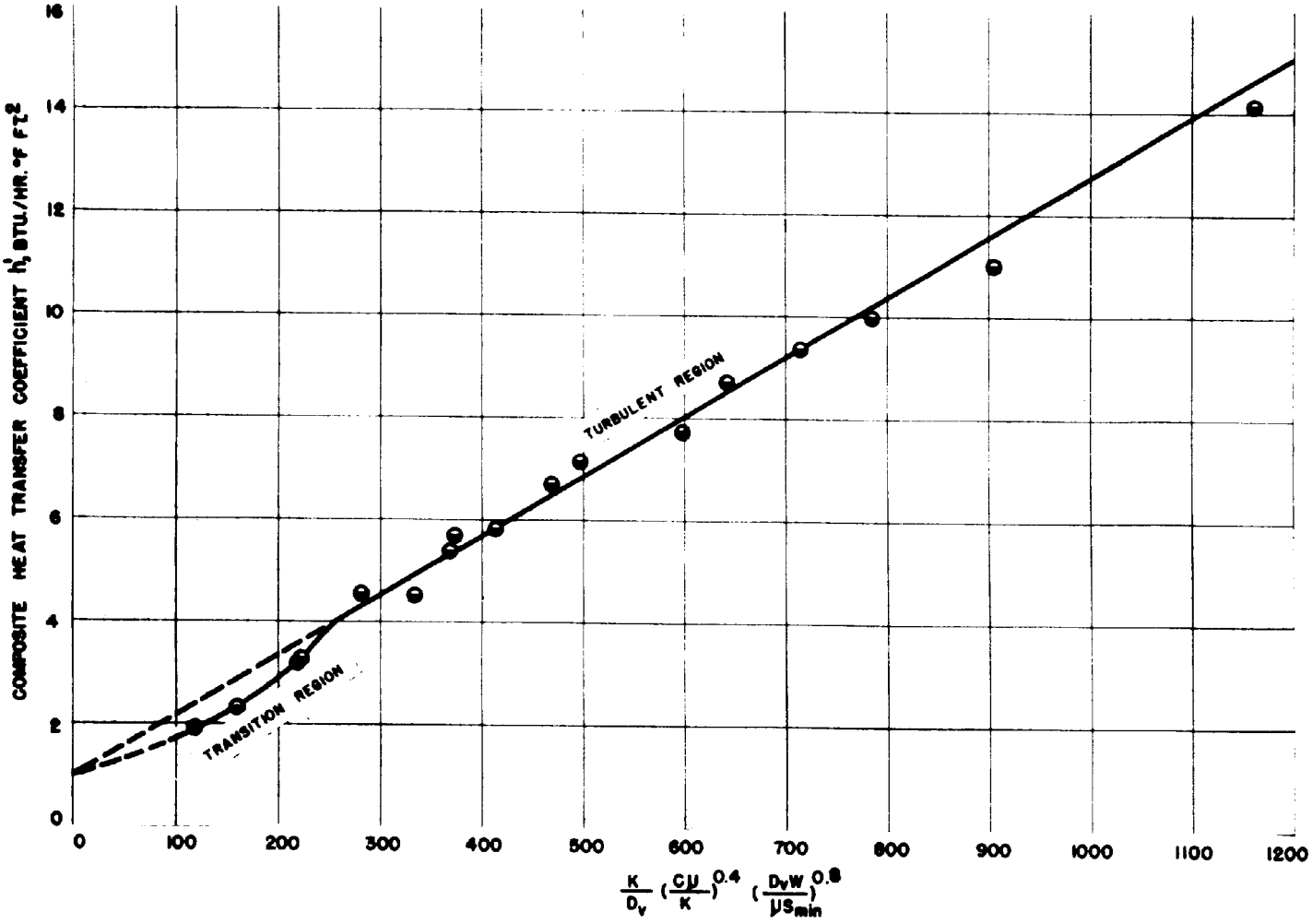

FIGURE 27

COMPOSITE HEAT TRANSFER COEFFICIENTS FOR THE LONGITUDINAL FIN TUBE.

The satisfactory straight-line relationship of Figure 27 is interpreted as confirmation of the procedure and indicates for this tube:

$$h_R' = 1.0 \text{ Btu/ft.}^2 \text{ °F.hr.}$$

$$h = 0.0117 \frac{K}{D_v} \left(\frac{C\mu}{K}\right)^{0.4} \left(\frac{D_v W}{\mu S_{min}}\right)^{0.80} \qquad (52)$$

For the remaining fin tubes, Table XXII presents in Columns 1, 3, and 10 the results of calculations using an n value of 0.91. The data are plotted in Figures 28 and 29 and show satisfactory straight lines, which confirm the choice of exponents. (It should be mentioned that although the exponent values of 0.91 could be obtained by trial and error for the "best straight line," they were in this case first determined by the method to be discussed later in this section. This, however, does not obviate the argument confirming their choice.)

Figure 28 for the "star" fin tube indicates:

$$h_R' = 1.0 \text{ Btu/ft.}^2 \text{ °F.hr.}$$

$$h = 0.00795 \frac{K}{D_v} \left(\frac{C\mu}{K}\right)^{0.4} \left(\frac{D_v W}{\mu S_{min}}\right)^{0.91} \qquad (53)$$

Figure 29 for the helical fin tube indicates:

$$h_R' = 0.8 \text{ Btu/ft.}^2 \text{ hr.°F.}$$

$$h = 0.00514 \frac{K}{D_v} \left(\frac{C\mu}{K}\right)^{0.4} \left(\frac{D_v W}{\mu S_{min}}\right)^{0.91} \qquad (54)$$

It is of interest to reduce the four values of h_R' to a common basis, i.e., to the basis of a unit area of bare tube. Calling the reduced value of h_R', h_{Rb}', this yields:

For the bare tube: $h_{Rb}' = 3.3$ (unchanged from h_R')

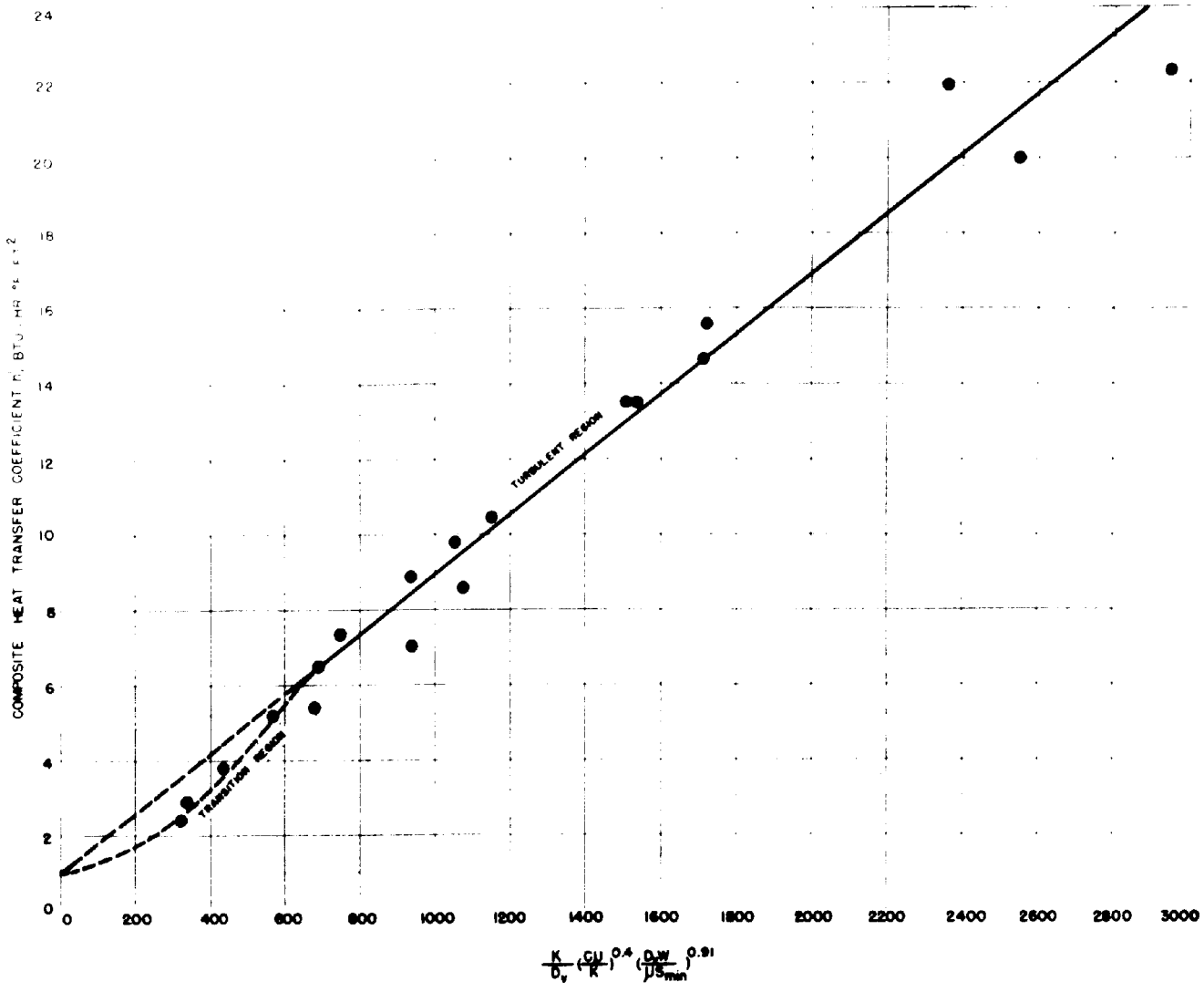

FIGURE 28

· COMPOSITE HEAT TRANSFER COEFFICIENTS FOR THE "STAR" FIN TUBE

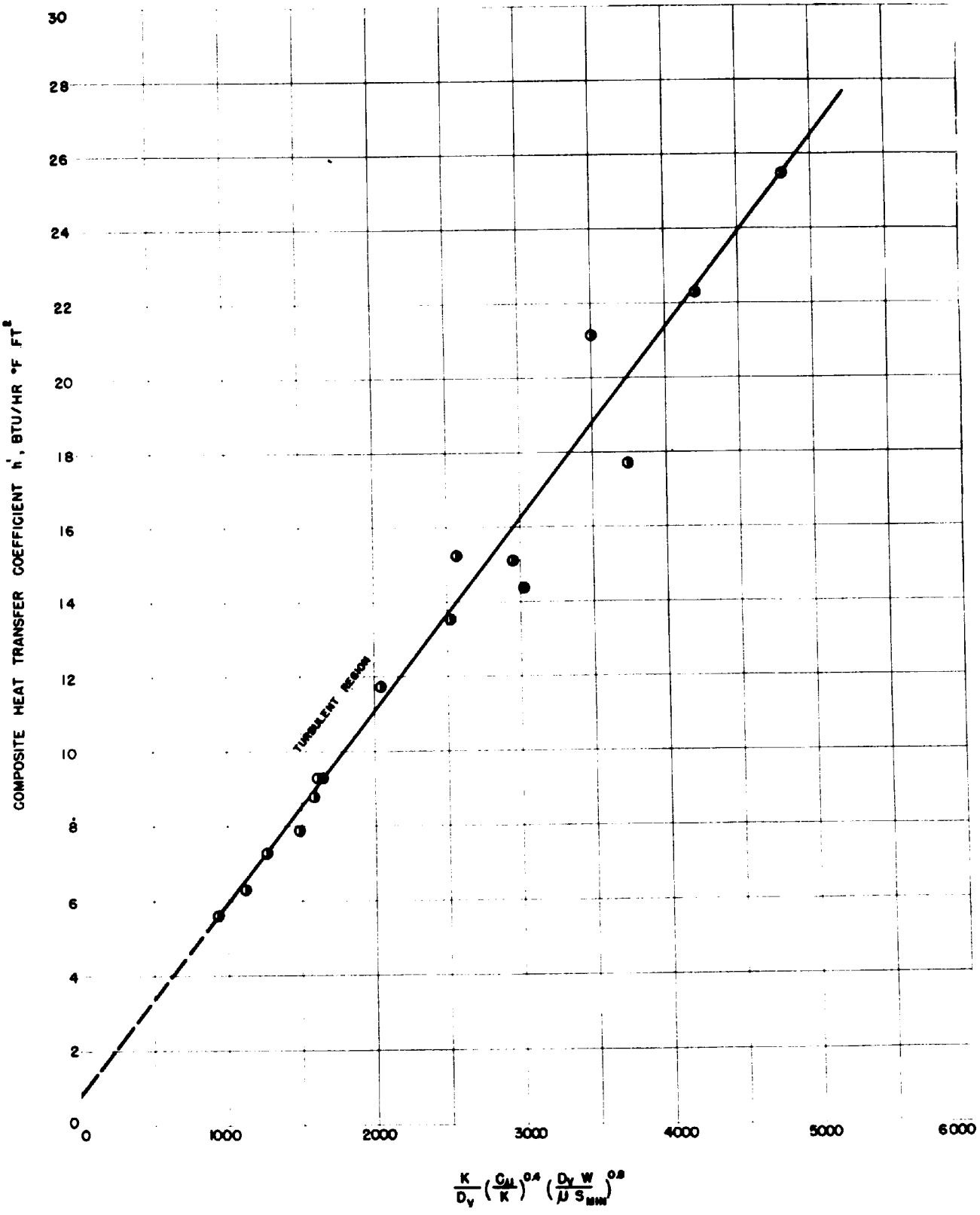

FIGURE 29

COMPOSITE HEAT TRANSFER COEFFICIENTS FOR THE HELICAL FIN TUBE.

For the longitudinal fin tube: $h_{Rb}' = 1.0 \left(\frac{30.30}{5.10}\right)$

$= 5.94$

where 30.30 represents the effective area of 13.0 feet of the longitudinal fin tube at an h_R' value of 1.0 (see Table I and Figure 25) and 5.10 represents the area of 13.0 feet of bare tube.

For the "star" fin tube: $h_{Rb}' = 1.0 \left(\frac{29.94}{5.10}\right)$

$= 5.86$

where 29.94 represents the effective area of 13.0 feet of the "star" fin tube at an h_R' value of 1.0.

For the helical fin tube: $h_{Rb}' = 0.8 \left(\frac{37.21}{5.10}\right)$

$= 5.85$

where 37.21 represents the effective area of 13.0 feet of helical fin tube at an h_R' value of 0.80.

The indication here is that the average radiation coefficient is the same for all the fin tubes when expressed on the basis of the bare tube area. Moreover, the average coefficient is 5.88/3.3 = 1.78 times the average coefficient for the bare tube. This figure may be taken as a measure of the relative radiation performance of the fin tubes compared to the bare tube.

2. Interpretation of the Heat Transfer Data Through Detailed Analysis of the Radiation Transfer

Another approach to the separation of the composite heat transfer coefficients of Table IX into their radiation and convection components is through a detailed analysis of the radiation mechanism. This

section is subdivided as follows:

(a)* Radiation Analysis

i. Theory

ii. Emissivity of Steam

iii. Beam Lengths and Angle Factors

iv. Interrelations Between Steam Absorptivities and Emissivities

v. Approximate Evaluation of the Radiation Equations

vi. Emissivity of the Steel Walls of the Plain Annulus

vii. Final Radiation Equations

viii. Evaluation of the Radiant Heat Transfer

(b) Convection Analysis.

(a) Radiation Analysis - i. Theory

The set of relationships which describes the transfer of radiant energy between the bounding walls of an annulus and an absorbing gaseous medium may be developed through a detailed consideration of typical "rays" of energy originating at different points in the annulus.

In order, however, to give precise definition to each of these quantities of energy, it is necessary first to review the underlying concepts of the transfer of energy by radiation.

The Nature of Radiant Energy, Its Transmission and Reception

Radiant energy is believed to consist of transverse vibrations

---

*Items i. to vi. of Topic 2(a) may be omitted for a brief reading.

of electric and magnetic fields which are propagated as waves by the acceleration of electric charges, as for example, the acceleration of the electrons of matter. All matter above the absolute zero of temperature is believed to emit radiant energy by virtue of its electron motion. This radiant energy is distributed over a band or several bands of wave lengths; the distribution is dependent upon the temperature and nature of the radiating material.

Radiant energy is transmitted from each differential source area in straight lines which radiate in all directions to the surrounding hemisphere. The energy is transmitted at the velocity of light (indeed, light is a form of radiant energy). Radiant energy may be transmitted any distance through a vacuum without diminution in total amount. The amount of energy per unit of area, however, decreases rapidly with increasing distance of transmission.

When radiant energy impinges on matter of any kind it is more or less absorbed, more or less transmitted through the material, and more or less reflected from it. Radiant energy which is absorbed is quantitatively converted into thermal energy and increases the internal energy of the absorbing substance by an equivalent amount. Transmitted energy proceeds, usually with slight change in direction, but otherwise as though it had not been intercepted. Reflected radiation may be regular (specular), diffuse, or intermediate. Regular, or specular, reflection is realized from polished surfaces and is characterized by an angle of reflection equal to that of incidence. Diffuse reflection, which is more common, is obtained from rough surfaces and results approximately in equal reflection in all directions to the surrounding hemisphere.

Certain quantitative ideas have developed concerning the emission, transfer, and reception of radiant energy. The ideas are, for the most part, dependent upon two fundamental laws of experience: the second law of thermodynamics and the "square-of-the-distance" law of physics. The second law of thermodynamics finds its application in the emission phenomenon and in the relationship between the emission and the various reception phenomena (absorption, transmission, and reflection). The square-of-the-distance law operates to give the relation between the intensities of the radiant energy emitted by one substance and that received by another from the first. These quantitative ideas and certain definitions are reviewed below.

The Emission of Radiant Energy: The quantity of energy radiated from a surface of unit area per unit time to a surrounding hemisphere is called the emissive power of the surface. It has been found both experimentally and by thermodynamic analysis using the second law (28) that the maximum emissive power E_B of any surface is proportional to the fourth power of the absolute temperature of the surface, i.e.,

$$\frac{dq_B}{dA} = E_B = \sigma T^4 \qquad (55)$$

where σ = a proportionality constant of numerical value 0.173×10^{-8} Btu/hr.$(°R)^4$

q = radiant energy emission, Btu/hr. from a given area A.

T = the absolute temperature of the radiating surface, °R.

This equation is commonly known as the Stefan-Boltzmann Equation.

A substance, or area, which radiates this maximum amount of energy is called a "black body." Most substances, or exposed areas, do not emit the maximum amount of energy. The ratio between the actual emissive power of the substance and that of the ideal "black body" is termed the emissivity of the substance.

Several types of emissivities may be identified, referring, for example, to energy of specific wave length (monochromatic emissivity); energy associated with rays which leave the emitter normal to its surface (normal emissivity); energy associated with total radiation (total or hemispherical emissivity); etc. Further reference in this discussion is to total or hemispherical emissivity.

The Stefan-Boltzmann Equation for black body radiation may be modified to represent radiation from any material, or surface, by the inclusion of the emissivity term. With the inclusion of the total or hemispherical emissivity, the equation indicates the total emissive power of the substance:

$$\frac{dq}{dA} = E = \sigma T^4 \varepsilon \qquad (56)$$

Emissivities of all substances are dependent upon the temperature of the substance. In the case of solid materials the emissivity appears also to be dependent upon the nature of the surface, this being particularly true in the case of oxidized surfaces. Emissivities of gases are dependent upon gas density and depth of gas layer as well as upon temperature. Many gases, e.g., oxygen, nitrogen, emit radiation in an almost negligible amount or have extremely low emissivities. Others such as carbon dioxide, water vapor, and sulphur dioxide emit strongly in certain wave length bands and have finite emissivities. In mixtures of emitting and non-emitting gases, the emitting gas appears to behave

approximately as though it were alone in the same volume (i.e., present alone at its partial pressure). Experimental gas emissivity data are usually correlated vs. temperature at constant values of the so-called "PL" product. The PL product is the product of the partial pressure of the radiating constituent of the gas in atmospheres and the "beam length" in feet. The beam length is the distance traversed by the "ray" in the gas. For gas masses other than those of hemispherical shape, it is necessary to define an appropriate average, or effective, beam length. The term "mean effective beam length" is widely used in such common cases.

Interception of Radiant Energy: Since radiant energy is emitted in all directions to a hemisphere surrounding its source, only bodies which subtend the complete hemispherical solid angle will intercept all the emitted energy; i.e., only "enclosing" bodies will intercept energy at the rate given by

$$dq = \sigma T^4 \epsilon_{dA} \qquad (56)$$

Bodies subtending a fraction of the hemispherical angle will intercept a part of the emitted energy. The amount of energy actually intercepted is indicated by application of the familiar square-of-the-distance law.

(a) For the case of interception of radiation from one body by another separated from the first by a non-absorbing gas, McAdams (28)

gives the following:

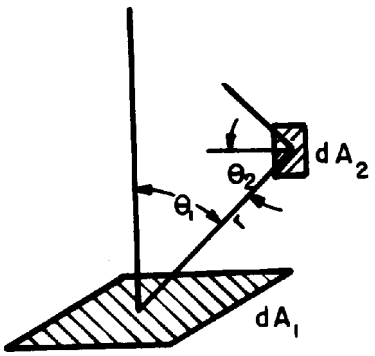

SKETCH (a)

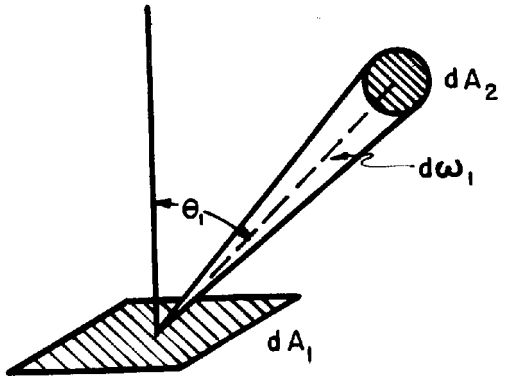

SKETCH (b)

Visualize a small surface element dA_1 radiating in all directions from one side. The problem is to determine what portion of its radiation is intercepted by some other small surface of element dA_2. Sketch (a) presents the details of this problem. The radiation per unit time, dq_{1-2} from dA_1 intercepted by dA_2 is proportional to the apparent area dA_1' as viewed from dA_2. Furthermore, the interception of the emitted beam is proportional to the apparent area dA_2' of dA_2 taken normal to the beam. Also the radiation received at dA_2 will vary inversely as the square of the distance or radius r separating dA_1 and dA_2. These relations give the equation:

$$dq_{1-2} = I(dA_1')\,(dA_2')/r^2 \qquad (57)$$

where I is a proportionality constant. (This is the "square-of-the-distance" law familiar from physics experiments on illumination.) Since $dA_1' = dA_1 \cos \theta_1$ and $dA_2' = dA_2 \cos \theta_2$, Equation (57) may be written:

$$dq_{1-2} = I \frac{(dA_1 \cos \theta_1)\,(dA_2 \cos \theta_2)}{r^2} \qquad (58)$$

This relation is sometimes expressed in an alternate form. Let the small solid angle subtended by dA_2 at dA_1 be called $d\omega_1$ (see Sketch (b). By definition of a solid angle

$$d\omega_1 = \frac{dA_2'}{r^2} = \frac{dA_2 \cos \Theta_2}{r^2} \tag{59}$$

Hence,

$$dq_{1-2} = I_1 dA_1 \cos \Theta_1 \, d\omega_1 \tag{60}$$

a relationship commonly known as the "cosine law."

The proportionality constant I_1 may now be evaluated by recalling that the total radiant emission from dA_1 is given by the Stefan-Boltzmann Equation as

$$dq_1 = \sigma T_1^4 \varepsilon_1 \, dA_1 \tag{56}$$

and this same quantity may be obtained by integration of Equation (60) over the total hemispherical angle $\omega = 2\pi$, i.e.,

$$dq_1 = I_1 \int_0^{2\pi} dA_1 \cos \Theta_1 \, d\omega_1 \tag{61}$$

This integration results in (28)

$$dq_1 = \pi I_1 \, dA_1 \tag{62}$$

Comparing Equations (56) and (62) indicates that

$$I_1 = \frac{\sigma T_1^4 \varepsilon_1}{\pi} \tag{63}$$

and insertion of this value for I_1 in Equation (60) results in

$$dq_{1-2} = \sigma T_1^4 \varepsilon_1 \, dA_1 \frac{\cos \Theta_1 \, d\omega_1}{\pi} \tag{64}$$

which represents the energy interception by the elemental area dA_2 from the elemental emitter dA_1.

For the energy interception by a finite area from an elemental emitter, it is necessary to perform the integration to obtain, for example,

$$dq_{1-2'} = \sigma T_1^4 \varepsilon_1 \, dA_1 \int_0^{\omega'} \frac{\cos \theta_1 \, d\omega_1}{\pi} \qquad (65)$$

where ω' represents the total solid angle subtended at the finite surface A_2'. It is to be noted that this equation is the Stefan-Boltzmann Equation with an additional multiplying quantity, $\int_0^{\omega'} \cos \theta_1 \, d\omega_1/\pi$, on the right-hand side. This quantity represents the fraction of the total emitted energy intercepted and is called the "angle factor" and designated F_{12}, the subscripts indicating the direction of its evaluation.

(b) A similar analysis may be made for the case of interception of energy from an emitting gas mass by an object which does not wholly enclose the mass. Here, as before, the total hemispherical radiation from the gas mass is given by

$$dq_G = \sigma T_G^4 \varepsilon_{eff} \, dA_G \qquad (66)$$

where ε_{eff} is the effective emissivity of the gas mass.

The problem is complicated by the fact that in general the radiation beams from the boundaries of the gas to the intercepter of their energy are not of equal length. Consequently, different parts of the gas will have different emissivities (since emissivity depends upon beam length). This necessitates the use of an effective emissivity.

The significance of the effective emissivity and the key to its evaluation are evident from a comparison of the Stefan-Boltzmann law and the cosine law integrated for the total hemispherical angle. The cosine law indicates

$$dq_{G-2} = I_G \, dA_G \cos \theta \, d\omega \tag{67}$$

substituting $I_G = \sigma T_G^4 \varepsilon / \pi$, (63)

$$dq_{G-2} = \sigma T_G^4 \, dA_G \frac{(\varepsilon \cos \theta \, d\omega)}{\pi} \tag{68}$$

where ε now depends upon ω, since ε is different for the different beam lengths associated with various values of ω. Integration over the total hemispherical angle yields

$$dq_G = \sigma T_G^4 \, dA_G \int_0^{2\pi} \frac{\varepsilon \cos \theta \, d\omega}{\pi} \tag{69}$$

which, by comparison with Equation (66), leads to

$$\varepsilon_{eff} = \int_0^{2\pi} \frac{\varepsilon \cos \theta \, d\omega}{\pi} \tag{70}$$

The effective emissivity leads to the definition of another quantity, previously mentioned, the mean effective beam length. This is defined as that beam length which, at the pressure and temperature involved, indicates an emissivity equal to the effective emissivity as defined above.

By extension of this method of analysis, the case of the interception of energy from an emitting gas mass by an object, A_2', which subtends

only the fractional hemispherical angle, ω', is found to be represented by

$$dq_{1-2}' = \sigma T_G^4 \, dA_G \left(\frac{\int_0^{\omega'} \varepsilon \cos\theta \, d\omega}{\int_0^{\omega'} \cos\theta \, d\omega} \right) \left(\frac{\int_0^{\omega'} \varepsilon \cos\theta \, d\omega}{\int_0^{2\pi} \varepsilon \cos\theta \, d\omega} \right) \qquad (71)$$

where the quantity in the first set of parentheses is the effective emissivity of the subtended gas mass, and the quantity in the second set of parentheses is the angle factor, F_{G1}. The equation is more simply written

$$dq_{1-2}' = \sigma T_G^4 \, \varepsilon_G \, F_{G1} \, dA_G \qquad (72)$$

with the implication that ε_G is evaluated at the proper mean effective beam length, i.e., one which would give

$$\varepsilon_G = \int_0^{\omega'} \varepsilon \cos\theta \, d\omega \Big/ \int_0^{\omega'} \cos\theta \, d\omega \qquad (73)$$

and with F_{G1} defined by the equation

$$F_{G1} = \int_0^{\omega'} \varepsilon \cos\theta \, d\omega \Big/ \int_0^{2\pi} \varepsilon \cos\theta \, d\omega \qquad (74)$$

The Reception and Interchange of Radiant Energy: It has been stated that intercepted or impinging radiant energy may be absorbed, transmitted, or reflected. The fractions of the incident energy which are absorbed, transmitted, and reflected are defined as the

absorptivity, the transmissivity, and the reflectivity, respectively. For any substance, at a given condition, the sum of these three quantities is equal to unity; this represents the energy balance on the substance. Certain substances, e.g., the metals, are substantially opaque, and for these the reflectivity is equal to one minus the absorptivity. Other substances, e.g., most gases, reflect little or no energy, and for these the transmissivity is equal to one minus the absorptivity. Commonly then,

For metals: α_s = absorptivity

$1 - \alpha_s$ = reflectivity

For gases: α_G = absorptivity

$1 - \alpha_G$ = transmissivity

As in the case of emissivity, several different kinds of absorptivity (and reflectivity and transmissivity) may be identified. It is commonly assumed for metals that the various absorptivities are approximately equal, and one value, "the" absorptivity, is employed. Gases, on the other hand, exhibit striking variation in their absorption of radiation of different wave length bands, or of different "quality." It is imperative, therefore, in the case of gases, to distinguish between the absorptivities for different kinds of radiation.

Absorptivities for both solids and gases are found to depend upon temperature in much the same way as do the emissivities. For gases the absorptivities, as well as being dependent upon "quality" of incident radiation and temperature, depend (again as do the emissivities) upon the

partial pressure of the absorbing constituent and the beam length.

Reception of radiant energy is almost always an indication of interchange of radiant energy. This follows because

(1) all substances above the absolute zero of temperature emit radiation, and

(2) a material intercepts energy emitted from another because it is within view of the other, and if it is in view of the other then the other is in view of it and will intercept its radiation.

The amount of the energy interchange between substances is the question of primary importance in the analysis of radiant heat transfer. The amount of interchange between two substances A and B is given as the difference between

(1) the total amount of energy received and absorbed at B from A, and

(2) the total amount of energy received and absorbed at A from B.

The mathematical expression of the energy interchange between two black bodies (which "see one another" over the total hemispherical angle) serves, with the second law of thermodynamics to prove that the absorptivity of a "black body" is unity (28). Other useful concepts which arise from the application of the second law to the interchange of radiant energy are (28):

(1) Kirchhoff's Law which states that at thermal equilibrium (radiating and absorbing substances at the same temperature) the emissivity and the absorptivity of any substance are the same. This is necessary, for otherwise there could be a net flux of energy between two bodies at the same temperature, in violation of experience. For metals in which the change of both emissivity and absorptivity with temperature is small, it is common and usually justifiable to assume that the emissivity and the absorptivity are equal over considerable ranges of temperature, i.e., for metals, approximately,

$$\varepsilon_s = \alpha_s \qquad (75)$$

(2) The product of the angle factor from a surface A to a surface B and the area of surface A must equal the product of the angle factor from the surface B to the surface A and the area of surface B; i.e.,

$$F_{AB} A_A = F_{BA} A_B \qquad (76)$$

This follows also because of the idea that no flux can exist without a temperature difference.

The foregoing brief treatment of general radiation theory will serve as an introduction to the analysis of the radiant transmission in an annulus, which follows.

Detailed Consideration of Typical "Rays" of Radiant Energy Originating in an Annulus Filled with an Emitting Gas

The typical rays of radiant energy which are involved in the annular situation are shown in Figures 30 and 31. These rays include those originating (a) at the surface of the inner tube,

(b) in the gas, directed toward the inner tube,

(c) in the gas, directed toward the outer tube, and

(d) at the surface of the outer wall.

The method of analysis is to trace each typical ray through its various partial absorptions and reflections until the residual is negligibly small. When a ray of radiant energy passes through a gas, the fraction α_G is absorbed, and the remainder $(1 - \alpha_G)$ passes through. Similarly, when the ray strikes a metal surface, a fraction α_s (assumed equal to ε_s by application of Kirchhoff's Law) is absorbed, and the remainder $(1 - \varepsilon_s)$ is reflected back.

Ray (a), Figures 30 and 31, originates from a typical differential area, dA_1, on the surface of the inner tube. The quantity of radiant energy emitted from a differential area dA_1 on the inner tube is

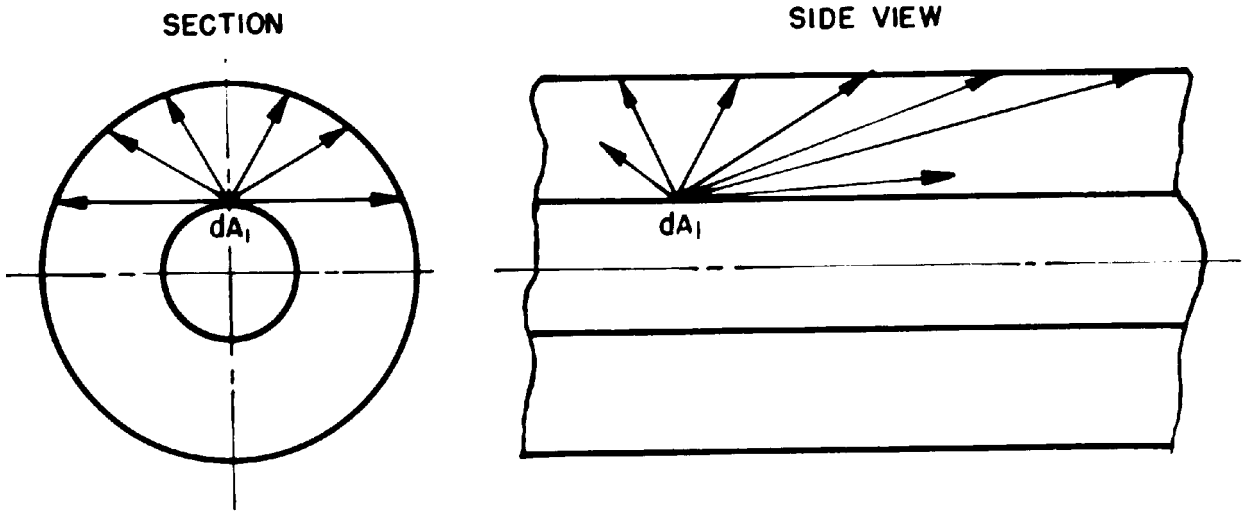

RAY(A)- RADIANT ENERGY ORIGINATING FROM A TYPICAL DIFFERENTIAL AREA ON THE SURFACE OF THE INNER TUBE

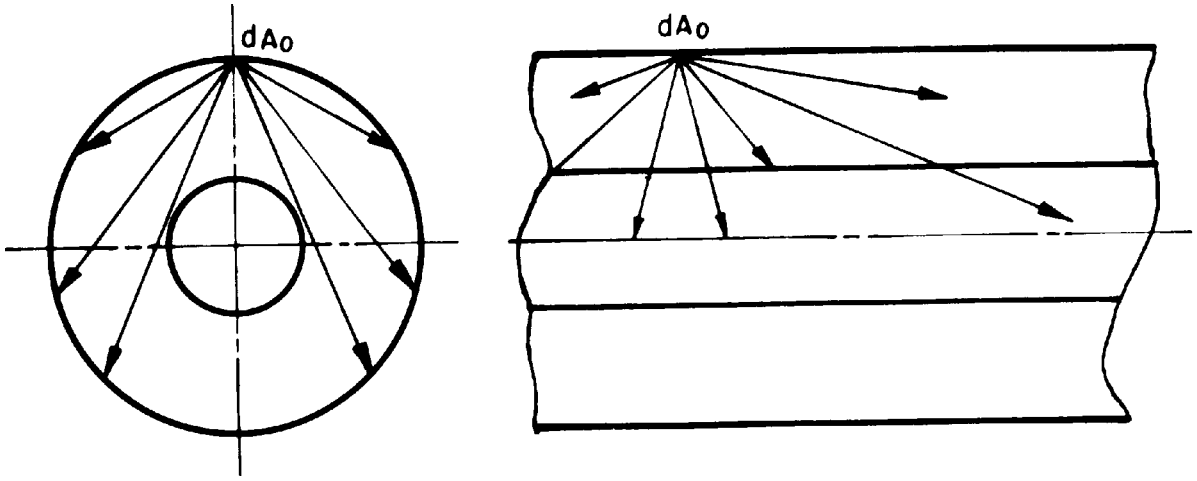

RAY(d)- RADIANT ENERGY ORIGINATING FROM A TYPICAL DIFFERENTIAL AREA ON THE SURFACE OF THE OUTER TUBE

FIGURE 30

"RAYS" OF RADIANT ENERGY FROM TWO DIFFERENT SOURCE POINTS IN AN ANNULUS

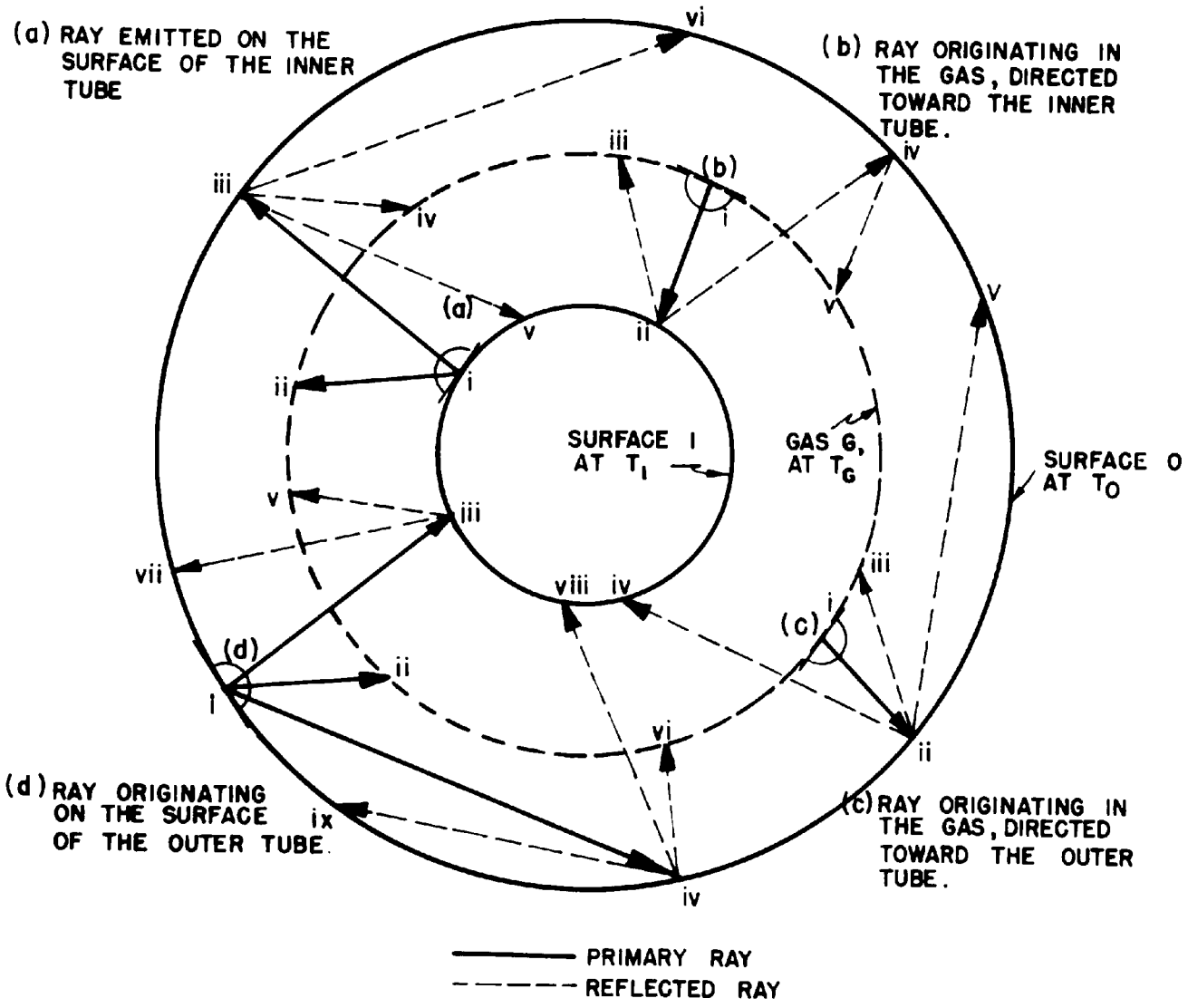

FIGURE 31

RADIANT ENERGY INTERCHANGE IN AN ANNULUS CONTAINING AN ABSORBING GAS. (CONSIDERATION OF TYPICAL "RAY" OF ENERGY)

$$dq = \sigma \varepsilon_1 (dA_1) T_1^4 \qquad (56)$$

in which ε_1 is the emissivity of the steel surface of the inner tube of area dA_1 and temperature T_1. Since each point on the inner tube is geometrically similar with respect to the entire system, Equation (56) may be written for the entire tube as

$$q = \sigma \varepsilon_1 A_1 T_1^4 \qquad (77)$$

where A_1 is the total area of the inner tube.

Ray (b) is emitted from a typical spot in the gas directed toward the inner tube. It will be shown later than a small mass of gas at any location in the annulus is made exactly as "typical" as any other by a geometrical shift of viewing position, involving the relation

$$F_{G1} A_G = F_{1G} A_1 \qquad (76)$$

For an unsophisticated picture of the situation, the gas may be imagined to be all concentrated in a thin cylinder near the center of the annulus, which permits identification of an area A_G and an angle factor F_{G1}. Ray (b) is typical of the beams which see the inner tube from this position. Its magnitude may be represented as $\sigma \varepsilon_{G1} T_G^4 A_G F_{G1}$, where ε_{G1} is the emissivity of gas at T_G and P_G and at a mean effective beam length equal to L_1; A_G is the area of the emitting spot of gas; and F_{G1} equals the angle factor with which the spot views the surface A_1. By the introduction of the concept of Equation (76) the term $A_G F_{G1}$ may be replaced by the term $A_1 F_{1G}$ where F_{1G} now refers to the angle factor with which the surface of the inner tube views the surrounding gas. This angle factor F_{1G} is

equal to unity because the gas completely encloses the inner tube. The expression for the magnitude of Ray (b) therefore becomes:

$$q_b = \sigma \varepsilon_{G1} T_G^4 A_1 \qquad (78)$$

Ray (c) is typical of all beams which view the outer tube from a position in the gas. The simple picture mentioned above has now led to apparent contradiction, as Ray (c) is able to "see" the outer tube over a solid angle larger than a hemisphere. It is necessary now to recall the strict definition of gas emissivity, which employs the concept of a hemispherical gas mass, and to observe that the shift in position from the gas to the outer tube (to be explained below) uses this definition strictly. This arbitrary division of the direction of radiation originating from the gas is a delicate point, necessary to the present analysis, and dependent on careful definition of the terms used. The magnitude of Ray (c) is $\sigma \varepsilon_{GO} T_G^4 A_G F_{GO}$. As before, $A_G F_{GO} = A_O F_{OG}$ and $F_{OG} = 1$, since a spot on the wall sees gas in all directions, being surrounded with it. Hence, the magnitude of the ray originating in the gas directed toward the outer wall is

$$q_c = \sigma \varepsilon_{GO} A_O T_G^4 \qquad (79)$$

in which ε_{GO} is the emissivity of the gas at T_G and P_G and at a mean effective beam length equal to L_O.

Ray (d), Figure 31, originates from a typical differential area, dA_O, on the surface of the outer tube. Here, as with Ray (a), each point has the same geometrical position as all others, and is equally typical. Ray (d) is, however, immediately broken into the two fractions: those

which see the inner tube and the outer tube, respectively. The magnitude of Ray (d) is therefore:

$$dq_d = \sigma \varepsilon_0 (dA_0) T_0^4 (F_{01} + F_{00}) \quad (80)$$

or

$$q_d = \sigma \varepsilon_0 A_0 T_0^4 (F_{01} + F_{00}) \quad (81)$$

$$(F_{01} + F_{00}) = 1 \quad (82)$$

Disposition of the Typical "Rays" - Ray (a): The fractions into which the Ray (a) of magnitude $\sigma \varepsilon_1 A_1 T_1^4$ is divided are shown in Figure 31 and may be listed as follows:

i. Fraction absorbed by the surface

- 1.000 (Fraction emitted = 1.000)

ii. Fraction absorbed by the absorbing gas

$\alpha_{G1,S1}$

where $\alpha_{G1,S1}$ refers to the absorptivity of the absorbing gas at a temperature T_G, a pressure P_G, and a "mean effective beam length" of L_1 for radiation emitted from the surface A_1 at a temperature T_1.

iii. Fraction absorbed by outer wall A_0 after passing through the gas

$(1 - \alpha_{G1,S1}) \varepsilon_0$

where ε_0 refers to the absorptivity of the outer wall, assumed equal to its emissivity.

iv. Fraction absorbed by gas, after passing through the gas, striking the outer wall, and being reflected back toward the gas

$(1 - \alpha_{G1,S1})(1 - \varepsilon_0)(\alpha_{G0,S1(G1)})$

where $\alpha_{GO,S1(G1)}$ refers to the absorptivity of a gas at T_G and P_G and at a mean effective beam length of L_O for radiant energy originating from the surface A_1 at T_1; this radiant energy having passed through a layer of gas at temperature T_G and P_G and of mean effective beam length equal to L_1.

v. Fraction absorbed by surface A_1 after passing through the gas, having been reflected by surface A_O, and having passed through the gas a second time and having struck surface A_1

$$(1 - \alpha_{G1,S1})\ (1 - \varepsilon_O)\ (1 - \alpha_{GO,S1(G1)})\ F_{O1}\varepsilon_1$$

where F_{O1} refers to the "angle factor" with which a representative spot on surface A_O views the inner tube (this angle factor concept will be discussed in detail later in this report).

vi. Fraction absorbed by a surface A_O after having passed through the gas, having been reflected from the surface A_O, having passed through the gas a second time, and having struck the surface A_O

$$(1 - \alpha_{G1,S1})\ (1 - \varepsilon_O)\ (1 - \alpha_{GO,S1(G1)})\ F_{OO}\varepsilon_O$$

where F_{OO} refers to the "angle factor" with which a representative spot of the surface A_O views the surface A_O itself.

This procedure, i.e., tracing the original ray emitted from a representative area, dA_1, on the surface A_1, may be followed indefinitely, giving rise to an infinite series of terms. It should be clear, however, that the terms of this series soon become insignificantly small, as they arise from continuously taking fractions of the original ray.

It is convenient in further treatment of the energy in the annulus to treat together the quantities which are absorbed by the same medium; that is, the gas, the surface A_O, and the surface A_1. The series

of terms is accordingly broken up arbitrarily into three infinite series, depending on the absorbing medium. These infinite series are complicated by the fact that their coefficients, the terms involving various special absorptivities of the gas, are not constant, and must be separately computed in each case. As mentioned above, these series converge rather rapidly, and ordinarily between two and four terms in each series will suffice to determine its magnitude to within one or two percent. (This fact is demonstrated by approximate numerical computations of Table XVII, to be presented later.) It is convenient, therefore, to stop the evaluation of the fractions absorbed at this point and later, when numerical values are introduced, to make small adjustments in order that the algebraic sum of all terms equal zero. (The necessity for the algebraic sum to equal zero follows from the over-all heat balance applied to the typical ray of radiant energy. This heat balance requires that the fraction of the emitted ray total 1.000.)

It is well to notice here that two separate methods of summation of the radiant energy in the annulus may be applied. First, the radiant energy emission may be studied by consideration of the four typical emitted rays. Secondly, the absorption of these rays may be considered by reference to the absorbing medium, giving rise to three series of terms involving energy absorbed by the gas, by the surface A_1, and by the surface A_0. Each emitted ray is broken up into fractions which are absorbed by the three different media. The disposition of each of the rays is presented in summary form in Table XI.

Disposition of the Typical Rays - Ray (b): Ray (b), see Figure 31, may be traced through its various absorptions as in the case of Ray

(a) above by itemizing the fractions of the original ray absorbed by the gas, the surface A_1, and the surface A_0. Its magnitude is $\sigma T_G^4 A_1 \varepsilon_{G1}$.

i. Fraction absorbed by the gas

- 1.000

ii. Fraction absorbed by the surface A_1

ε_1

iii. Fraction absorbed by the gas after striking the surface A_1 and being reflected back into the gas

$(1 - \varepsilon_1)\ (\alpha_{G1,G1})$

where $\alpha_{G1,G1}$ refers to the absorptivity of gas at T_G and P_G and a mean effective beam length equal to L_1 for radiation originating in a gas at T_G and P_G and a mean effective beam length equal to L_1.

iv. Fraction absorbed by the surface A_0 after having struck the surface A_1, having been reflected from this surface, and having passed through the gas

$(1 - \varepsilon_1)\ (1 - \alpha_{G1,G1})\ \varepsilon_0$

v. Fraction absorbed by gas after having struck the surface A_1, having been reflected from this surface, having passed through the gas, having struck the surface A_0, and having been reflected from this surface

$(1 - \varepsilon_1)\ (1 - \alpha_{G1,G1})\ (1 - \varepsilon_0)\ (\alpha_{G0,G(2L1)})$

where $\alpha_{G0,G(2L1)}$ refers to the absorptivity of a gas at T_G and P_G and a mean effective beam length equal to L_0 for radiation originating in a gas at T_G and P_G and a mean effective beam length equal to L_1, this radiation, however, having passed through an additional layer of gas at T_G and P_G and of mean effective beam length equal to L_1.

The above series of terms may be divided, as before, into three series, depending on whether the energy is absorbed by the surface A_1, the

surface A_0, or the gas. As before, these infinite series are rapidly converging, and may safely be stopped at this point. The assignment of each term listed above into one of these three series is made in Table XI.

Disposition of the Typical Rays - Ray (c): The magnitude of Ray (c) of radiant energy emitted from a typical spot in the gas in the direction of A_0 is $\sigma T_G^4 A_0 \varepsilon_{GO}$. This ray is traced through its absorptions as before (see Figure 31).

i. Fraction absorbed by the gas

- 1.000

ii. Fraction absorbed by the surface A_0

ε_0

iii. Fraction absorbed by the gas after striking the surface A_0 and being reflected back into the gas

$(1 - \varepsilon_0)\ (\alpha_{GO,GO})$

where $\alpha_{GO,GO}$ refers to the absorptivity of the gas at T_G and P_G and a mean effective beam length equal to L_O for radiation originating in a gas at T_G and P_G and a mean effective beam length equal to L_O.

iv. Fraction absorbed by the surface A_1 after having struck the surface A_0, having been reflected from this surface, and having passed through the gas

$(1 - \varepsilon_0)\ (1 - \alpha_{GO,GO})\ F_{01}\ \varepsilon_1$

where F_{01} is the angle factor by which a representative spot on the surface A_0 "sees" the surface A_1.

v. Fraction absorbed by the surface A_0, after having struck the surface A_0, having been reflected from this surface,

and having passed through the gas

$$(1 - \varepsilon_0)\,(1 - \alpha_{GO,GO})\,F_{OO}\,\varepsilon_1$$

where F_{OO} is the angle factor by which a spot on the surface A_O "sees" the surface A_O. Note that the representative spot on the surface A_O sees either surface A_1 or surface A_O; hence, $F_{O1} + F_{OO} = 1$.

The evaluation of this infinite series of terms is stopped here. The above terms may each be assigned to one of the three absorption series. See Table XI.

Disposition of the Typical Rays - Ray (d): The magnitude of Ray (d) of radiant energy emitted by a typical point on the surface A_O is $\sigma T_O^4 \varepsilon_O A_O$, which is broken up into the following fractions (see Figure 31):

i. Fraction absorbed by the surface A_O

- 1.000

ii. Fraction absorbed by the gas on the first passage of the ray through it

$$\alpha_{GO,SO}\,(F_{O1} + F_{OO})$$

where $\alpha_{GO,SO}$ refers to the absorptivity of the absorbing gas at a temperature T_G, a pressure P_G, and a mean effective beam length of L_O for radiation emitted from the surface A_O at a temperature T_O. Note that $(F_{O1} + F_{OO}) = 1$.

iii. Fraction absorbed by the inner tube after having passed through the gas

$$(1 - \alpha_{GO,SO})\,F_{O1}\,\varepsilon_1$$

where F_{O1} is the angle factor by which a representative spot on the surface A_O sees the surface A_1.

iv. Fraction absorbed by the outer tube after having passed through the gas once

$$(1 - \alpha_{GO,SO})\ F_{OO}\ \varepsilon_O$$

where F_{OO} is the angle factor by which the surface A_O sees itself.

v. Fraction absorbed by the gas of the fractional ray which has passed through the gas and been reflected from the surface A_1

$$(1 - \alpha_{GO,SO})\ F_{O1}\ (1 - \varepsilon_1)\ (\alpha_{G1,SO(GO)})$$

where $\alpha_{G1,SO(GO)}$ refers to the absorptivity of the gas at T_G and P_G and a mean effective beam length of L_1 for radiant energy originating from the surface A_O at T_O; this radiant energy has previously passed through a layer of gas at temperature T_G and pressure P_G and of mean effective beam length of L_O.

vi. Fraction absorbed by the gas of the fractional ray which has passed through the gas and been reflected from the surface A_O

$$(1 - \alpha_{GO,SO})\ F_{OO}\ (1 - \varepsilon_O)\ \alpha_{GO,SO(GO)}$$

where $\alpha_{GO,SO(GO)}$ refers to the absorptivity of the gas at T_G and P_G and a mean effective beam length of L_O for radiant energy originating from the surface A_O at T_O, this radiant energy having previously passed through a layer of gas at temperature T_G and pressure P_G and a mean effective beam length of L_O.

vii. Fraction absorbed by the outer tube of the fractional ray which has originated from the surface A_O, passed through the gas once, been reflected by the surface A_1, and passed again through the gas

$$(1 - \alpha_{GO,SO})\ F_{O1}\ (1 - \varepsilon_1)\ (1 - \alpha_{G1,SO(GO)})\ \varepsilon_O$$

viii. Fraction absorbed by the inner tube of the fractional ray which has passed through the gas and been reflected from the surface A_O, and passed again through the gas

$$(1 - \alpha_{GO,SO})\ F_{OO}\ (1 - \varepsilon_O)\ (1 - \alpha_{GO,SO(GO)})\ \varepsilon_1\ F_{O1}$$

ix. Fraction absorbed by the outer tube of the fractional ray which has passed through the gas and been reflected from the surface A_0, and passed again through the gas

$$(1 - \alpha_{GO,SO})\, F_{OO}\, (1 - \varepsilon_0)\, (1 - \alpha_{GO,SO(GO)})\, \varepsilon_0\, F_{OO}$$

The infinite series of fractions into which Ray (d) is broken is stopped at this point. The terms listed above may each be assigned to one of the three "absorption series" mentioned previously by consideration of the medium absorbing the particular fraction. As before, this is done in Table XI.

The numerical evaluation of the first few terms of these series is dependent upon a knowledge of the various emissivities and absorptivities of steam and upon the angle factors. The emissivities and absorptivities in turn are interrelated and dependent upon the mean effective beam lengths of the system. The next three divisions of this section are concerned, therefore, with the evaluation of the emissivity of steam as a function of pressure, temperature, and beam length; with the determination of the mean effective beam lengths and the angle factors; and finally, with the interrelations between the various emissivities and absorptivities.

(a) Radiation Analysis - ii. Emissivity of Superheated Steam

Literature on the emissivity of superheated steam in the general region of pressure from 25 to 150 psi. abs. is completely missing. The

TABLE XI

FRACTIONAL DISPOSITION OF TYPICAL RADIATION RAYS IN AN ANNULUS

(The first few terms of the infinite series)

RAY (a), TYPICAL OF THE RADIATION ORIGINATING ON THE SURFACE OF THE INNER TUBE AND EQUAL IN TOTAL AMOUNT TO $\sigma\mathcal{E}_1 A_1 (T_1/100)^4$

Symbol in Figure 31	FRACTION OF ORIGINAL RAY ABSORBED BY INNER TUBE (A_1)	BY GAS	BY OUTER WALL (A_o)
i	- 1.000	-------	-------
ii	-------	$\alpha_{G1,S1}$	-------
iii	-------	-------	$(1 - \alpha_{G1,S1})\mathcal{E}_0$
iv	-------	$(1-\alpha_{G1,S1})(1-\mathcal{E}_0)\alpha_{G0,S1(G1)}$	-------
v	$(1-\alpha_{G1,S1})(1-\mathcal{E}_0)(1-\alpha_{G0,S1(G1)})\mathbf{F}_{01}\mathcal{E}_1$	-------	-------
vi	-------	-------	$(1-\alpha_{G1,S1})(1-\mathcal{E}_0)(1-\alpha_{G0,S1(G1)})\mathbf{F}_{00}\mathcal{E}_0$

RAY (b), TYPICAL OF THE RADIATION ORIGINATING IN THE GAS, DIRECTED TOWARD THE INNER TUBE AND EQUAL IN AMOUNT TO $\sigma\mathcal{E}_{G1}A_1(T_0/100)^4$

i	-------	- 1.000	-------
ii	$\mathcal{E}_1$	-------	-------
iii	-------	$(1-\mathcal{E}_1)\,\alpha_{G1,G1}$	-------
iv	-------	-------	$(1-\mathcal{E}_1)(1-\alpha_{G1,G1})\,\mathcal{E}_0$
v	-------	$(1-\mathcal{E}_1)(1-\alpha_{G1,G1})(1-\mathcal{E}_0)\alpha_{G0,G(2L1)}$	-------

RAY (c), TYPICAL OF THE RADIATION ORIGINATING IN THE GAS, DIRECTED TOWARD THE OUTER WALL AND EQUAL IN AMOUNT TO $\sigma\mathcal{E}_{G0}A_0(T_0/100)^4$

i	-------	- 1.000	-------
ii	-------	-------	$\mathcal{E}_0$
iii	-------	$(1-\mathcal{E}_0)(\alpha_{G0,G0})$	-------
iv	$(1-\mathcal{E}_0)(1-\alpha_{G0,G0})\mathbf{F}_{01}\mathcal{E}_1$	-------	-------
v	-------	-------	$(1-\mathcal{E}_0)(1-\alpha_{G0,G0})\mathbf{F}_{00}\mathcal{E}_1$

RAY (d), TYPICAL OF THE RADIATION ORIGINATING ON THE SURFACE OF THE OUTER WALL AND EQUAL IN AMOUNT TO $\sigma\mathcal{E}_0 A_0(T_0/100)^4$

i	-------	-------	- 1.000
ii	-------	$\alpha_{G0,S0}\,(\mathbf{F}_{01} + \mathbf{F}_{00})$	-------
iii	$(1-\alpha_{G0,S0})\,\mathbf{F}_{01}\mathcal{E}_1$	-------	-------
iv	-------	-------	$(1-\alpha_{G0,S0})\,\mathbf{F}_{00}\mathcal{E}_0$
v	-------	$(1-\alpha_{G0,S0})\mathbf{F}_{01}(1-\mathcal{E}_1)\alpha_{G1,S0(G0)}$	-------
vi	-------	$(1-\alpha_{G0,S0})\mathbf{F}_{00}(1-\mathcal{E}_0)\alpha_{G0,S0(G0)}$	-------
vii	-------	-------	$(1-\alpha_{G0,S0})\mathbf{F}_{01}(1-\mathcal{E}_1)(1-\alpha_{G1,S0(G0)})\mathcal{E}_0$
viii	$(1-\alpha_{G0,S0})\mathbf{F}_{00}(1-\mathcal{E}_0)(1-\alpha_{G0,S0(G0)})\mathcal{E}_1\mathbf{F}_{01}$	-------	-------
ix	-------	-------	$(1-\alpha_{G0,S0})\mathbf{F}_{00}(1-\mathcal{E}_0)(1-\alpha_{G0,S0(G0)})\mathcal{E}_0\mathbf{F}_{00}$

only related data available are data of Hottel and others (19) on the emissivity of water vapor in the presence of air at a total pressure of 14.7 psi. abs. The data are correlated in terms of temperature and PL product referring to the product of the mean effective beam length, in feet, and the partial pressure of water vapor, in atmospheres. The range of PL products covered in the most recent correlation by Hottel is from 0.005 to 20 foot-atmospheres. This correlation also covers a range of temperature from 0 to 3600°F.

With the absence of data on the emissivity of superheated steam, it became necessary to develop a procedure for extrapolating the nearest related data, those of water vapor in air.

A reasonable theoretical basis for such an extrapolation may be arrived at through the following analysis taken in part from "Heat Transfer Notes' by L. M. K. Boelter, et. al. (1)

Assume radiant energy in a band of wave lengths of width $d\lambda$ to fall upon the exposed area dA of a layer of gas at a temperature T and containing water vapor at a partial pressure P, which may or may not be equal to the total pressure of the gas. If P is not equal to the total pressure of the gas, assume the other constituents present to be completely transparent to radiant energy. (Dry air approximates this latter condition.)

Let the quantity of radiation per unit time within the wave length band $d\lambda$ be designated as $dq_{d\lambda}$. An absorption coefficient B_λ may now be defined, so that the quantity of energy absorbed due to its passage a distance dL through the gas is given by the equation:

$$d(dq_{d\lambda}) = - B_\lambda \, dq_{d\lambda} \, dL \qquad (83)$$

Assuming that the coefficient B_λ is constant with L, integration gives the energy rate after the radiant energy has passed through a finite layer of thickness L.

$$(dq_{d\lambda})_L = (dq_{d\lambda})_{L=0} e^{-B_\lambda L} \qquad (84)$$

(e is the basis of natural logarithms) and the amount of energy absorbed in the distance L may be represented by

$$(dq_{d\lambda})_{L=0} - (dq_{d\lambda})_L = \Delta(dq_{d\lambda})_L = (dq_{d\lambda})_{L=0} (1-e^{-B_\lambda L}) \qquad (85)$$

The fraction of the incident energy absorbed which, by definition, is the absorptivity of the absorbing medium, may be represented by:

$$\frac{\Delta(dq_{d\lambda})_L}{(dq_{d\lambda})_{L=0}} = \alpha_{d\lambda,L,T} = 1 - e^{-B_\lambda L} \qquad (86)$$

Now, if the incident radiation covers a finite band of wave lengths, $\Delta\lambda$, a similar analysis may be made if the additional assumption be made that an "effective absorption factor," B_m, exists which may then operate over the entire wave band. Thus,

$$\alpha_{\Delta\lambda,L,T} = 1 - e^{-B_m L} \qquad (87)$$

It is further to be expected that, at any given temperature, and in the absence of other than thermal excitation, the "effective absorption factor" B_m will be proportional to the number of encounters of the radiant "rays" with molecules of the absorbing constituent. This number of encounters is, in turn, proportional to the density of the absorbing medium evaluated at its partial pressure. Thus, the equation may be

written as

$$\alpha_{\Delta\lambda,L,T} = 1 - e^{-K\rho L} \qquad (88)$$

where ρ represents the density of the absorbing medium measured at its partial pressure (the total pressure in the absence of other constituents), and K is a proportionality factor.

Equation (88) has been developed, with certain assumptions, for the case of absorption of radiant energy (within the wave length band $\Delta\lambda$) by an absorbing gaseous medium, and results in an expression for the absorptivity of the medium for such radiation as a function of the density of the medium and the beam length. By Kirchhoff's Law, it now follows that at the same temperature and for energy within the same wave length band, the emissivity of the absorbing medium is identical with this absorptivity, i.e.,

$$\varepsilon_{\Delta\lambda,L,T} = \alpha_{\Delta\lambda,L,T} = 1 - e^{-K\rho L} \qquad (89)$$

In order to improve its generality the equation may be modified empirically to

$$\varepsilon_{\Delta\lambda,L,T} = \alpha_{\Delta\lambda,L,T} = 1 - e^{-K(\rho L)^n} \qquad (90)$$

where n is a constant, probably dependent on temperature. Equation (90) may also be written

$$-\ln (1 - \varepsilon_{\Delta\lambda,L,T}) = -\ln (1 - \alpha_{\Delta\lambda,L,T}) = K(\rho L)^n \qquad (91)$$

which indicates a linear relation on logarithmic paper between $-\ln(1-\varepsilon_{\Delta\lambda,L,T})$ or $-\ln(1-\alpha_{\Delta\lambda,L,T})$ and ρL.

Equations (90) and (91) are equivalent to the statement that the emissivity of an absorbing gas equals zero when its ρL (or PL) product is zero, and unity when its ρL (or PL) product is infinity. A point of issue is the question of the value of the emissivity (or the absorptivity) of a gas at a ρL product of infinity. There are two ways of looking at this question. One is to assume that gas at an infinite ρL product will emit with an emissivity equivalent to the ratio of the total energy associated with those wave length bands in which the gas is normally considered to be an emitter, divided by the total energy emitted by a black body at the same temperature. This concept assumes that even with a gas at infinite ρL product, no radiation will be emitted beyond the normal emitting bands. The other viewpoint is that with gas at an infinite ρL product, emission from all wave lengths may be expected, with total emission equivalent to that of a black body and resulting in an emissivity equal to unity. This question has been discussed with Professor Hottel (18), who favors the latter viewpoint. In any event, the equation developed seems to be a reasonable one for finite densities and it might certainly be expected to fit the existing data for water vapor which are available in the range of PL from .005 to 20 foot-atmospheres. Equation (91) may also be written as

$$- \log (1 - \mathcal{E}) = (K' L^n) \rho^n \qquad (92)$$

or, at constant beam length, as

$$- \log (1 - \mathcal{E}) = K_L' \rho^n \qquad (93)$$

This equation now indicates a linear relationship on logarithmic paper between the negative logarithm of $(1 - \mathcal{E})$ and density for data at constant

temperature and beam length.

Table XII presents a tabulation of data on the emissivity of water vapor at various temperatures and PL products from Hottel's most recent correlation which is available in McAdams (28). These data are interpreted as though at a series of constant beam lengths, L, and at varying pressure or density. Column 1 of the table gives the series of arbitrarily chosen constant beam lengths; Columns 2 and 3, the temperature and PL product, respectively. Column 4 indicates the pressure which corresponds to the PL product of Column 3 and the arbitrary beam length of Column 1. The density of water vapor at this pressure and at the temperature of Column 2 is reported in Column 5. Columns 6, 7, and 8 give respectively the emissivity of water vapor at the given temperature and PL product, but at a "reference water vapor partial pressure of zero" as read from an enlargement of Figure 29, page 66 of McAdams (28). Column 7 gives a correction factor C_1 by which the values of Column 6 must be multiplied to correct them to the water vapor partial pressure under consideration. The factor C_1 has been obtained from an enlargement of Figure 30, page 66 of the above reference. Column 8 presents the corrected water vapor emissivity at the temperature and PL product of Columns 2 and 3 and represents Hottel's smoothed experimental data. Column 9 indicates the value of the negative logarithm (to the base 10) of $(1-\varepsilon)$ as required for a test of Equation (93).

Values of the negative logarithm of $(1 - \varepsilon)$ are plotted against the corresponding water vapor densities at constant temperature and beam length in Figure 32. It is seen that excellent straight lines result over the range of the data. This is interpreted as confirmation of the

TABLE XII

TABULATION AND CALCULATIONS FOR THE EXTRAPOLATION OF WATER VAPOR EMISSIVITY DATA

1 Mean Effective Beam Length L, ft.	2 Temperature T, °F	3 PL Product PL, ft.atm.	4 Pressure P, atm.	5 Density of Water Vapor at P ρ, lbs/ft^3	6 Emissivity at P = 0 ε',--	7 Correction Multiplier C_1,--	8 Emissivity at P or ρ ε,--	9 -log(1-ε)
0.100	300	0.005	0.05	0.00164	0.0140	1.045	.01463	.01471
"	"	.007	.07	.00229	.0183	1.060	.0194	.01959
"	"	.010	.10	.00328	.0242	1.080	.0261	.02645
"	"	.020	.20	.00656	.0393	1.140	.0448	.0458
"	"	.040	.40	.0131	.0617	1.268	.0782	.08143
"	"	.060	.60	.01963	.0788	1.378	.1086	.1150
"	"	.080	.80	.0262	.0931	1.470	.1368	.1471
"	"	.100	1.00	.0328	.1055	1.553	.1638	.1789
"	500	0.005	.05	.00129	.0115	1.045	.01202	.01207
"	"	.007	.07	.00181	.0152	1.060	.01611	.01613
"	"	.010	.10	.00258	.0203	1.080	.0219	.02214
"	"	.020	.20	.00516	.0337	1.140	.0384	.03916
"	"	.040	.40	.0103	.0535	1.268	.0678	.0702
"	"	.060	.60	.0155	.0694	1.378	.0956	.10048
"	"	.080	.80	.0206	.0829	1.470	.1219	.1300
"	"	.100	1.00	.0258	.0945	1.553	.1467	.1586
0.150	300	0.005	.0333	.00109	.0140	1.028	.01439	.01450
"	"	.007	.0467	.00153	.0183	1.041	.01905	.01928
"	"	.010	.0667	.00218	.0242	1.057	.0256	.02593
"	"	.020	.1333	.00437	.0393	1.105	.0434	.0444
"	"	.040	.2666	.00875	.0617	1.190	.0734	.0762
"	"	.060	.400	.0131	.0788	1.266	.0998	.1051
"	"	.080	.533	.01742	.0931	1.339	.1247	.1332
"	"	.100	.667	.0218	.1055	1.400	.1477	.1598
"	"	.120	.800	.0262	.1148	1.457	.1673	.1831
"	"	.150	1.000	.0328	.1300	1.533	.1993	.2224
"	500	0.005	.0333	.000860	.0115	1.028	.01182	.01187
"	"	.007	.0467	.001205	.0152	1.041	.0158	.01593
"	"	.010	.0667	.00172	.0203	1.057	.0214	.02163
"	"	.020	.1333	.00344	.0337	1.105	.0372	.03791
"	"	.040	.2666	.00688	.0535	1.190	.0637	.06582
"	"	.060	.400	.0103	.0694	1.266	.0879	.09200
"	"	.080	.533	.01375	.0829	1.339	.1110	.1176
"	"	.100	.667	.0172	.0945	1.400	.1323	.1419
"	"	.120	.800	.0206	.1051	1.457	.1531	.1662
"	"	.150	1.000	.0258	.1195	1.533	.1832	.2024
0.200	300	0.005	.025	.00082	.0140	1.022	.0143	.01440
"	"	.007	.035	.001146	.0183	1.031	.0189	.01908
"	"	.010	.050	.001637	.0242	1.043	.0252	.02552
"	"	.020	.100	.00328	.0393	1.080	.0424	.04333
"	"	.040	.200	.00656	.0617	1.151	.0710	.0736
"	"	.060	.300	.00983	.0788	1.208	.0952	.1000
"	"	.080	.400	.0131	.0931	1.263	.1176	.1251
"	"	.100	.500	.01637	.1055	1.314	.1386	.1492
"	"	.120	.600	.01962	.1148	1.362	.1564	.1701
"	"	.150	.750	.0245	.1300	1.424	.1851	.2047
"	"	.200	1.00	.0328	.1502	1.517	.2278	.2583

TABLE XII, CONTINUED

TABULATION AND CALCULATIONS FOR THE EXTRAPOLATION OF WATER VAPOR EMISSIVITY DATA

1 Mean Effective Beam Length L, ft.	2 Temperature T, °F	3 PL Product PL, ft.atm.	4 Pressure P, atm.	5 Density of Water Vapor at P ρ, lbs/ft^3	6 Emissivity at P = 0 ε',--	7 Correction Multiplier C_1,--	8 Emissivity at P or ρ ε,--	9 $-\log(1-\varepsilon)$
0.200	500	0.005	0.025	0.00644	0.0115	1.022	0.0117	0.01177
"	"	.007	.035	.00903	.0152	1.031	.0157	.01582
"	"	.010	.050	.00129	.0203	1.043	.0212	.02143
"	"	.020	.100	.00258	.0337	1.080	.0364	.03708
"	"	.040	.200	.00516	.0535	1.151	.0616	.06358
"	"	.060	.300	.00773	.0694	1.208	.0838	.08752
"	"	.080	.400	.0103	.0829	1.263	.1047	.1106
"	"	.100	.500	.0129	.0945	1.314	.1242	.1326
"	"	.120	.600	.0155	.1051	1.362	.1431	.1544
"	"	.150	.750	.01935	.1195	1.424	.1702	.1866
"	"	.200	1.00	.0258	.1395	1.517	.2116	.2377
0.300	300	0.005	.01667	.000546	.0140	1.015	.0142	.01430
"	"	.007	.0233	.000765	.0183	1.021	.0187	.01888
"	"	.010	.0333	.00109	.0242	1.030	.0249	.02521
"	"	.020	.0667	.00218	.0393	1.056	.0415	.04239
"	"	.040	.1333	.00437	.0617	1.105	.0682	.07064
"	"	.060	.200	.00656	.0788	1.150	.0906	.09497
"	"	.100	.333	.0109	.1055	1.221	.1288	.1379
"	"	.120	.400	.0131	.1148	1.256	.1442	.1557
"	"	.150	.500	.01636	.1300	1.303	.1694	.1856
"	"	.200	.667	.0218	.1502	1.373	.2062	.2309
"	"	.250	.833	.0273	.1670	1.434	.2395	.2738
"	"	.300	1.00	.0328	.1810	1.487	.2691	.3135
"	500	0.005	.01667	.000430	.0115	1.015	.0117	.01177
"	"	.007	.0233	.000601	.0152	1.021	.0155	.01562
"	"	.010	.0333	.00086	.0203	1.030	.0209	.02112
"	"	.020	.0667	.00172	.0337	1.056	.0356	.03625
"	"	.040	.1333	.00344	.0535	1.1050	.0591	.06092
"	"	.060	.200	.00516	.0694	1.150	.0798	.08316
"	"	.100	.333	.00860	.0945	1.221	.1154	.1226
"	"	.120	.400	.0103	.1051	1.256	.1320	.1416
"	"	.150	.500	.0129	.1195	1.303	.1557	.1692
"	"	.200	.667	.0172	.1395	1.373	.1915	.2126
"	"	.250	.833	.0215	.1565	1.434	.2244	.2541
"	"	.300	1.00	.0258	.1690	1.487	.2513	.2894
1.00	500	0.02	.02	.000516	.0336	1.018	.0342	.03480
"	"	.1	.1	.00258	.0945	1.080	.1021	.1077
"	"	.3	.3	.00774	.1690	1.181	.1996	.2226
"	"	.5	.5	.0129	.2135	1.257	.2687	.3129
"	"	1.0	1.0	.0258	.2820	1.392	.3925	.4984

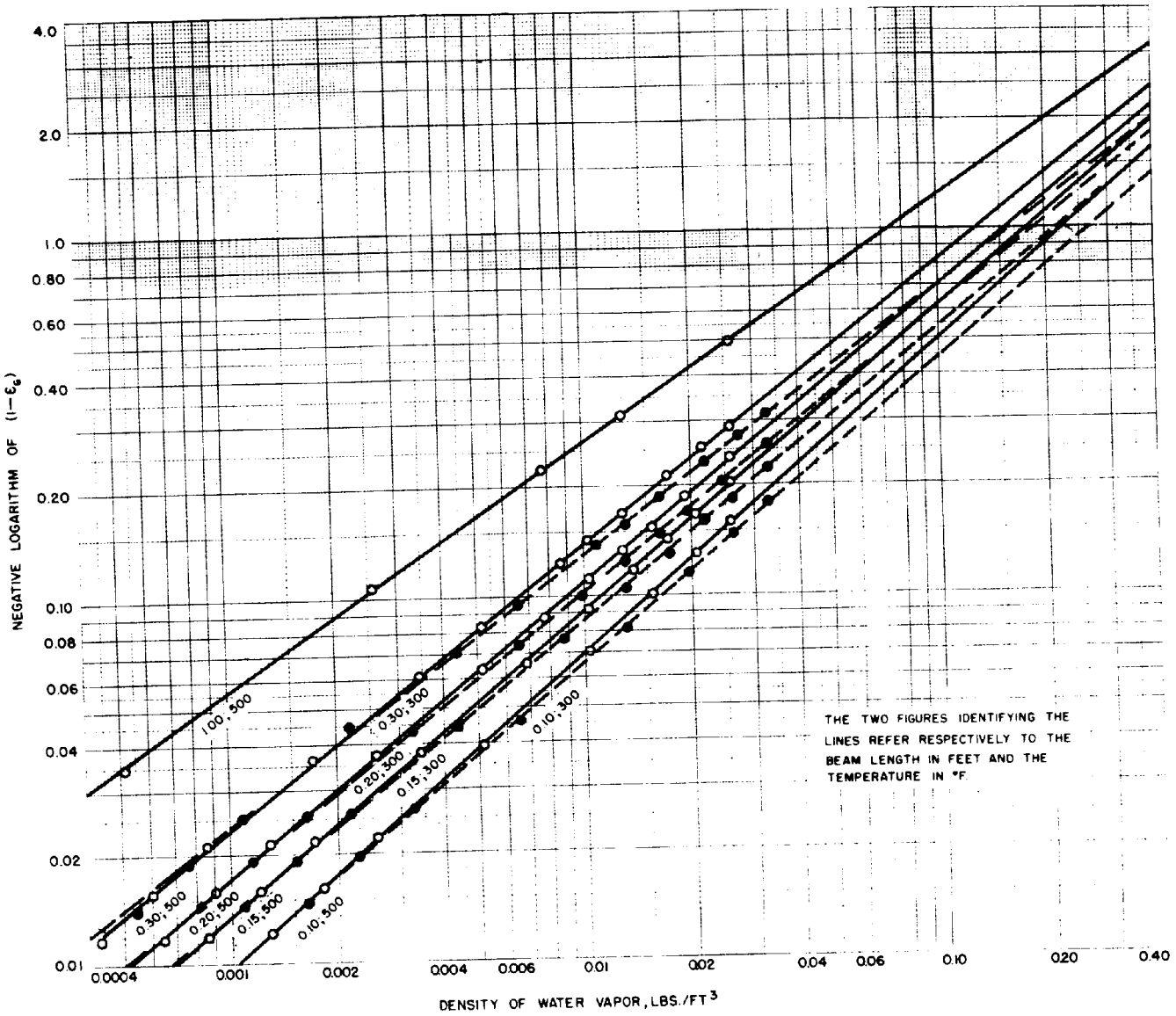

FIGURE 32

EXTRAPOLATION CHART FOR WATER VAPOR EMISSIVITY DATA

general form of Equation (93) for this range and suggests that the extension of the straight lines toward increasing densities offers an excellent method for extrapolating the data.

Quantities obtained from the extension of these lines are tabulated in Table XIII, which also shows the calculations of the corresponding pressures and emissivities. In this table, Columns 1 and 2 indicate the constant beam lengths and temperatures. Column 3 gives the density at which the value of the negative logarithm of $(1 - \epsilon)$, reported in Column 6, has been obtained from Figure 32. Column 4 presents the specific volume corresponding to Column 3; and Column 5, the pressure which corresponds to this specific volume and the temperature of Column 2. The pressure values were obtained from superheat steam tables. Column 7 reports the emissivity value which is calculated from Column 6.

For convenience in use, the data of Columns 1, 2, 5, and 6 are presented graphically in Figures 33 and 34. Figure 33 is a plot of the emissivity of steam as a function of pressure and shows lines of constant temperature and beam length. Figure 34 is a cross-plot of Figure 33, presenting the emissivity of steam as a function of beam length with lines of constant temperature and pressure. This latter method of presentation gives the data in a more convenient form for use in the analysis of experiments conducted at definite constant pressures, over a narrow range of temperatures, and under conditions where emissivities at various mean effective beam lengths are required.

It is difficult, if not impossible, to make a direct evaluation of the validity of the extrapolation process by means of which

TABLE XIII

EXTRAPOLATED EMISSIVITY DATA ON SUPERHEATED STEAM

1 Mean Effective Beam Length L, ft	2 Temperature T, °F	3 Density of Water Vapor ρ, lbs/ft^3	4 Specific Volume of Water Vapor v, ft^3/lb	5 Pressure P, psi.abs.	6 -log(1-ε)	7 ε
0.100	300	.0381	26.25	17.0	.2	.1813
"	"	.0498	20.10	22.15	.25	.2212
"	"	.0620	16.12	27.4	.3	.2592
"	"	.0741	13.5	32.8	.35	.2954
"	"	.0872	11.46	38.7	.4	.3297
"	"	.113	8.85	49.5	.5	.3935
"	"	.140	7.14	61.0	.6	.4512
"	"	.169	5.92	----	.7	.5035
"	500	.0339	29.5	19.3	.2	.1813
"	"	.0540	18.52	30.9	.3	.2592
"	"	.0752	13.3	42.6	.4	.3297
"	"	.0972	10.3	54.4	.5	.3935
"	"	.1201	8.33	67.6	.6	.4512
"	"	.1425	7.02	80.	.7	.5035
"	"	.1685	5.93	94.2	.8	.5507
"	"	.1910	5.23	106.1	.9	.5935
"	"	.217	4.61	120.3	1.0	.6322
"	"	.267	3.75	146.4	1.2	.6989
0.150	300	.0380	26.3	17.0	.25	.2212
"	"	.0479	20.9	21.4	.3	.2592
"	"	.0578	17.3	25.8	.35	.2954
"	"	.0682	14.67	30.3	.4	.3297
"	"	.0898	11.13	39.6	.5	.3935
"	"	.112	8.93	49.1	.6	.4512
"	"	.136	7.36	59.2	.7	.5035
"	500	.0332	30.1	18.5	.25	.2212
"	"	.0412	24.3	23.3	.3	.2592
"	"	.0581	17.2	33.0	.4	.3297
"	"	.0758	13.2	43.0	.5	.3935
"	"	.0942	10.61	53.2	.6	.4512
"	"	.113	8.86	63.8	.7	.5035
"	"	.133	7.52	74.7	.8	.5507
"	"	.172	5.81	96.1	1.0	.6322
"	"	.214	4.67	118.7	1.2	.6989
"	"	.259	3.86	143.5	1.4	.7535
0.200	300	.0402	24.9	18.0	.3	.2592
"	"	.0496	20.15	22.2	.35	.2954
"	"	.0582	17.15	26.0	.4	.3297
"	"	.0780	12.82	34.7	.5	.3935
"	"	.0982	10.20	43.1	.6	.4512
"	"	.120	8.33	52.6	.7	.5035
"	"	.141	7.09	62.1	.8	.5507
"	"	.163	6.13	----	.9	----

TABLE XIII, CONCLUDED

EXTRAPOLATED EMISSIVITY DATA ON SUPERHEATED STEAM

1 Mean Effective Beam Length	2 Temperature	3 Density of Water Vapor	4 Specific Volume of Water Vapor	5 Pressure	6 $-\log(1-\varepsilon)$	7 ε
L, ft	T, °F	ρ, lbs/ft^3	v, ft^3/lb	P, psi.abs.		
0.200	500	.0347	28.8	19.7	.3	.2598
"	"	.0498	20.1	28.1	.4	.3297
"	"	.0642	15.58	36.3	.5	.3935
"	"	.0802	12.48	45.3	.6	.4512
"	"	.0968	10.33	54.6	.7	.5035
"	"	.113	8.85	63.7	.8	.5507
"	"	.149	6.71	83.5	1.0	.6322
"	"	.187	5.35	104.1	1.2	.6989
"	"	.224	4.46	124.2	1.4	.7535
"	"	.264	3.79	146.0	1.6	.7981
0.300	300	.0378	26.5	16.9	.35	.2954
"	"	.0452	22.1	20.2	.4	.3297
"	"	.0604	16.56	26.8	.5	.3935
"	"	.0772	12.94	34.3	.6	.4512
"	"	.0945	10.6	41.6	.7	.5035
"	"	.113	8.84	49.7	.8	.5507
"	"	.132	7.58	57.6	.9	.5935
"	"	.151	6.62	65.5	1.0	.6322
"	500	.0322	31.05	18.1	.35	.2954
"	"	.0381	26.2	21.7	.4	.3297
"	"	.0502	19.94	28.4	.5	.3935
"	"	.0635	15.74	36.0	.6	.4512
"	"	.0770	13.0	43.5	.7	.5035
"	"	.0907	11.02	51.0	.8	.5507
"	"	.121	8.27	68.0	1.0	.6322
"	"	.152	6.57	85.3	1.2	.6989
"	"	.183	5.47	102.0	1.4	.7535
"	"	.218	4.59	120.5	1.6	.7981
"	"	.252	3.96	138.9	1.8	.8347
"	"	.288	3.47	158.2	2.0	.8647
1.000	500	.0340	29.4	19.3	.6	.4512
"	"	.0426	23.5	24.1	.7	.5035
"	"	.0520	19.2	29.7	.8	.5507
"	"	.0720	13.9	40.8	1.0	.6322
"	"	.0941	10.6	53.2	1.2	.6989
"	"	.1185	8.43	66.8	1.4	.7535
"	"	.143	7.00	80.1	1.6	.7981
"	"	.200	5.00	110.7	2.0	.8647
"	"	.260	3.85	143.8	2.4	.9093

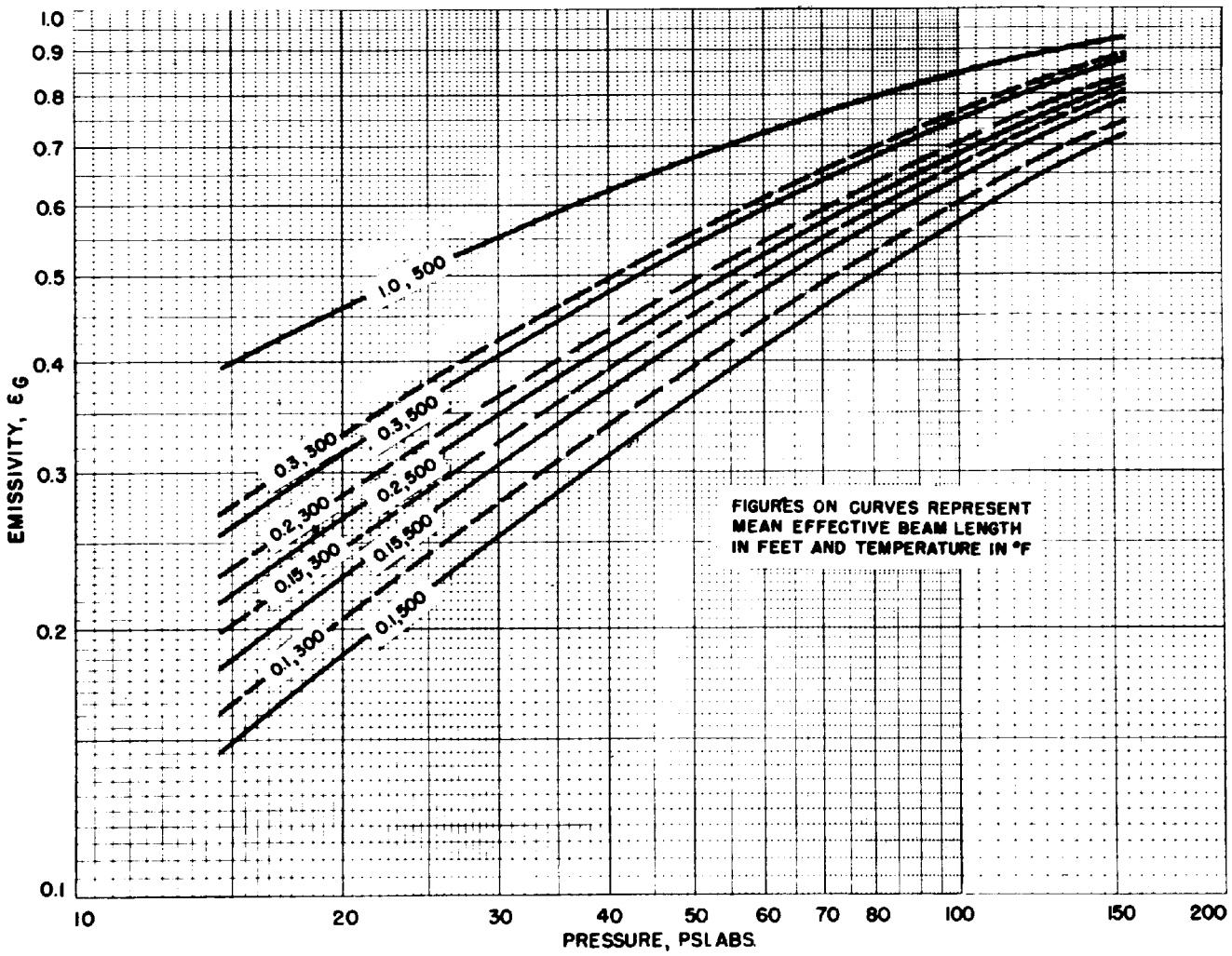

FIGURE 33
EMISSIVITY OF SUPERHEATED STEAM

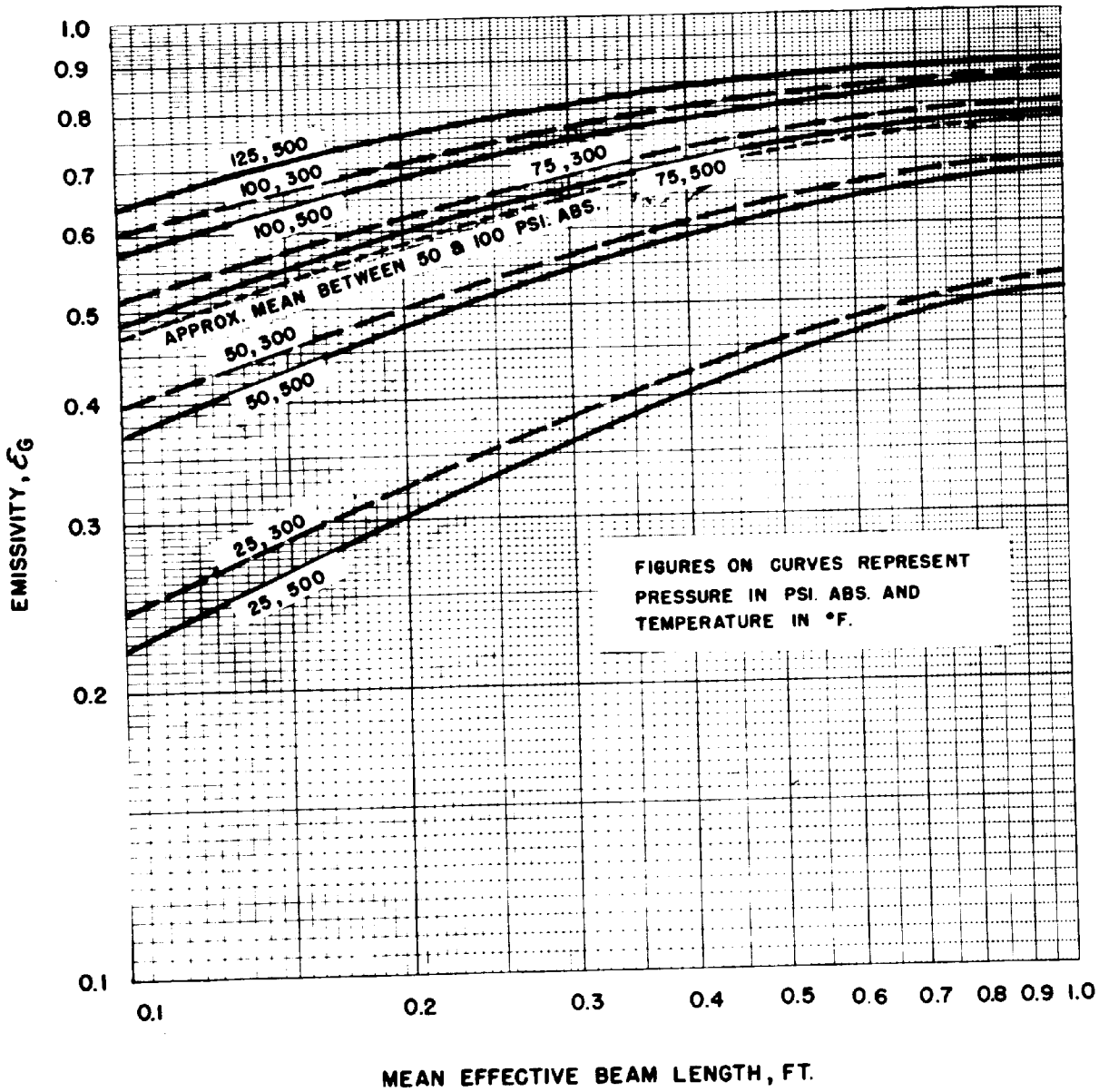

FIGURE 34
EMISSIVITY OF SUPERHEATED STEAM

these emissivity data are obtained. As has been indicated, this approach appears reasonable and seems to be the only one presently possible for obtaining emissivity values in the superheated steam region. Two opportunities exist, however, for checking the order of magnitude and the internal consistency of the extrapolated figures. Reference here is made to the use of these extrapolated emissivities in the analysis of experimental data to obtain values of the emissivity of steel. It will be shown later that the values of the emissivity of steel so determined lie nicely within the range of reported values. This may be considered as at least a partial check on the order of magnitude and the pressure consistency of the extrapolated steam emissivities. A further check of the extrapolated data may also be obtained by means of the results of the use of these data in analyzing experiments with steam flow in an annular space. This check again is not a direct one, but can only be inferred from the fact that the convection heat transfer coefficients, obtained by the correction of composite coefficients through the use of the extrapolated emissivity data, may be correlated along with other convection data represented in the literature.

The extrapolated emissivity data of Figures 33 and 34 may be utilized in the numerical evaluation of the terms in the basic equation for radiant heat transfer, provided the quantities T_G, the temperature; P, the pressure; F_{01} and F_{00}, the angle factors; and L, the mean effective beam length are known. Fortunately, the temperature and pressure of the radiating or absorbing superheated steam are known, since these quantities are subject to direct measurement. The situation is not quite so simple, however, in the case of the angle factors or the mean effective beam lengths, which are dependent not only upon the geometry of the

system, but also upon the emissivity itself.

(a) Radiation Analysis - iii. Beam Lengths and Angle Factors

From the Inner Tube to the Gas Mass

The basic relationship for the effective emissivity in this case has been presented earlier as

$$\varepsilon_{eff} = \int_0^{2\pi} \frac{\varepsilon \cos\theta \, d\omega}{\pi} \qquad (70)$$

Evaluation of this equation requires its integration over the entire hemispherical angle 2π. The geometrical relations involved for the particular annulus being considered are shown in detail in Figure 35. From this figure it may be seen that

$$\cos\theta = \frac{DS}{CS} = \frac{SB\cos\phi}{SB/\cos\psi} = \cos\phi\cos\psi \qquad (94)$$

Also that

$$d\omega = d\phi\, d\psi \frac{SB}{SC} = d\phi\, d\psi \cos\psi \qquad (95)$$

and that the beam length L may be represented by

$$L = SC = SB/\cos\psi \qquad (96)$$

Combining these terms into Equation (70)

$$\varepsilon_{1G} = \varepsilon_{eff} = \frac{1}{\pi}\int_0^{\pi}\int_0^{\pi} \varepsilon \cos\phi \cos^2\psi \, d\phi \, d\psi \qquad (97)$$

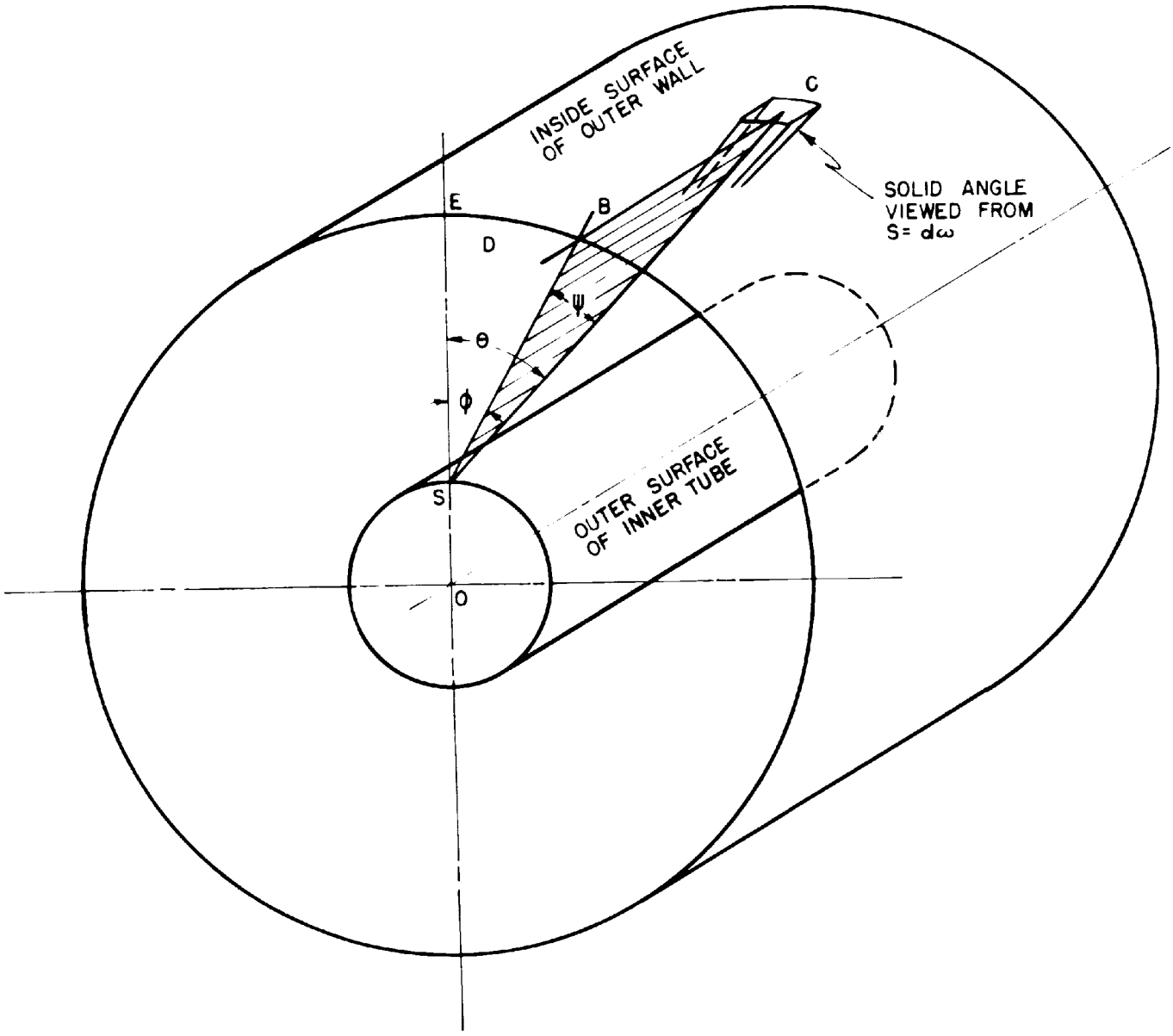

FIGURE 35

GEOMETRICAL RELATIONS IN THE EVALUATION OF THE MEAN BEAM LENGTHS FROM THE INNER SURFACE.

which may be rewritten as

$$\varepsilon_{1G} = \frac{4}{\pi} \int_0^{\pi/2} \int_0^{\pi/2} \varepsilon \cos \phi \, d\phi \cos^2 \psi \, d\psi \qquad (98)$$

and finally as

$$\varepsilon_{1G} = \int_0^{\pi/2} \int_0^{\pi/2} \varepsilon \, d(\sin \phi) \, d(2\psi + \sin 2\psi / \pi) \qquad (99)$$

In each of these equations ε refers to the emissivity evaluated at the appropriate pressure and temperature and at the beam length $L = SB/\cos \psi$. Since emissivities are available only as graphical functions of pressure, temperature, and beam length, it is most convenient to resort to graphical integration of Equation (99) in order to obtain ε_{1G}, and ultimately from this, the mean effective beam length.

It is necessary at this point to decide upon the pressure and temperature at which to evaluate the effective emissivity. It has been found by actual trial that the final value of beam length, or angle factor, is only very slightly dependent upon the pressure-temperature level employed in its evaluation. Since a value of beam length is desired for use over the pressure and temperature ranges of approximately 50 to 100 psi. abs. and 300 to 500°F., a pressure and a temperature are selected which will give emissivities about midway between the values for these extremes. A dotted line representing such a pressure and temperature condition has been drawn in Figure 34 and labelled "approximate mean between 50 and 100 psi. abs." Emissivities from this line are used for all beam length and angle factor calculations. The detailed calculations

of the mean effective beam length are presented in Table XIV and Figures 36 and 37. Table XIV lists the quantities required for the evaluation of

$$\int_0^{\pi/2} \varepsilon \; d(2\psi + \sin 2\psi / \pi) \quad \text{at five values of the angle } \phi.$$

Columns 1 and 2 show the values (in radians) of the angles ϕ and ψ at which the quantities indicated in the succeeding columns are evaluated. Columns 3, 4, and 7 are self-explanatory. Column 5 lists the values of beam length computed from the relation $L = SB/\cos \psi$, and Column 6 the corresponding emissivity as obtained from Figure 34.

The actual integration of the expression is performed graphically in Figure 36, which also includes a tabulation of the values of the integral for each of the five values of the angle ϕ.

The final determination of the effective emissivity is carried out in Figure 37, which represents the graphical performance of the second integration, i.e., of the evaluation of

$$\varepsilon_{1G} = \int_0^{\pi/2} \left[\varepsilon_d \left(\frac{2\psi + \sin 2\psi}{\pi} \right) \right] d \; (\sin \phi)$$

where the quantity in the square brackets is tabulated as a function of the angle ϕ in Figure 36. Figure 37 indicates the value resulting from the last integration to be $\varepsilon_{1G} = 0.520$. This represents the effective emissivity of the gas mass at the selected pressure-temperature level. The mean effective beam length is now the value of beam length which, at the same pressure-temperature level, yields an emissivity of 0.520. From Figure 34 this is obtained as $L_{1G} = 0.138$ feet. The mean effective beam

TABLE XIV

CALCULATIONS FOR THE EVALUATION OF THE MEAN EFFECTIVE BEAM LENGTHS FOR RADIATION FROM THE INNER TUBE OF THE PLAIN ANNULUS

1	2	3	4	5	6	7
ϕ	ψ	$\sin 2\psi$	$\cos \psi$	L	ε	$\frac{2\psi + \sin 2\psi}{\pi}$
0	0	0	1.000	0.1042	0.475	0
0	$\pi/8$	0.707	0.924	.1128	.488	0.475
0	$\pi/4$	1.000	0.707	.1474	.530	.818
0	$3\pi/8$	0.707	0.3825	.2723	.635	.975
0	$\pi/2$	0	0	∞	.800	1.000
$\pi/8$	0	0	1.000	0.1066	.478	0
$\pi/8$	$\pi/8$	0.707	0.924	.1155	.490	0.475
$\pi/8$	$\pi/4$	1.000	0.707	.1508	.533	.818
$\pi/8$	$3\pi/8$	0.707	0.3825	.2787	.639	.975
$\pi/8$	$\pi/2$	0	0	∞	.800	1.000
$\pi/4$	0	0	1.000	0.1158	.490	0
$\pi/4$	$\pi/8$	0.707	0.924	.1254	.502	0.475
$\pi/4$	$\pi/4$	1.000	0.707	.1637	.547	.818
$\pi/4$	$3\pi/8$	0.707	0.3825	.3027	.653	.975
$\pi/4$	$\pi/2$	0	0	∞	.800	1.000
$3\pi/8$	0	0	1.000	0.1320	.512	0
$3\pi/8$	$\pi/8$	0.707	0.924	.1429	.526	0.475
$3\pi/8$	$\pi/4$	1.000	0.707	.1867	.570	.818
$3\pi/8$	$3\pi/8$	0.707	0.3825	.3452	.670	.975
$3\pi/8$	$\pi/2$	0	0	∞	.800	1.000
$\pi/2$	0	0	1.000	0.1546	.538	0
$\pi/2$	$\pi/8$	0.707	0.924	.1674	.550	0.475
$\pi/2$	$\pi/4$	1.000	0.707	.2188	.600	.818
$\pi/2$	$3\pi/8$	0.707	0.3825	.4042	.690	.975
$\pi/2$	$\pi/2$	0	0	∞	.800	1.000

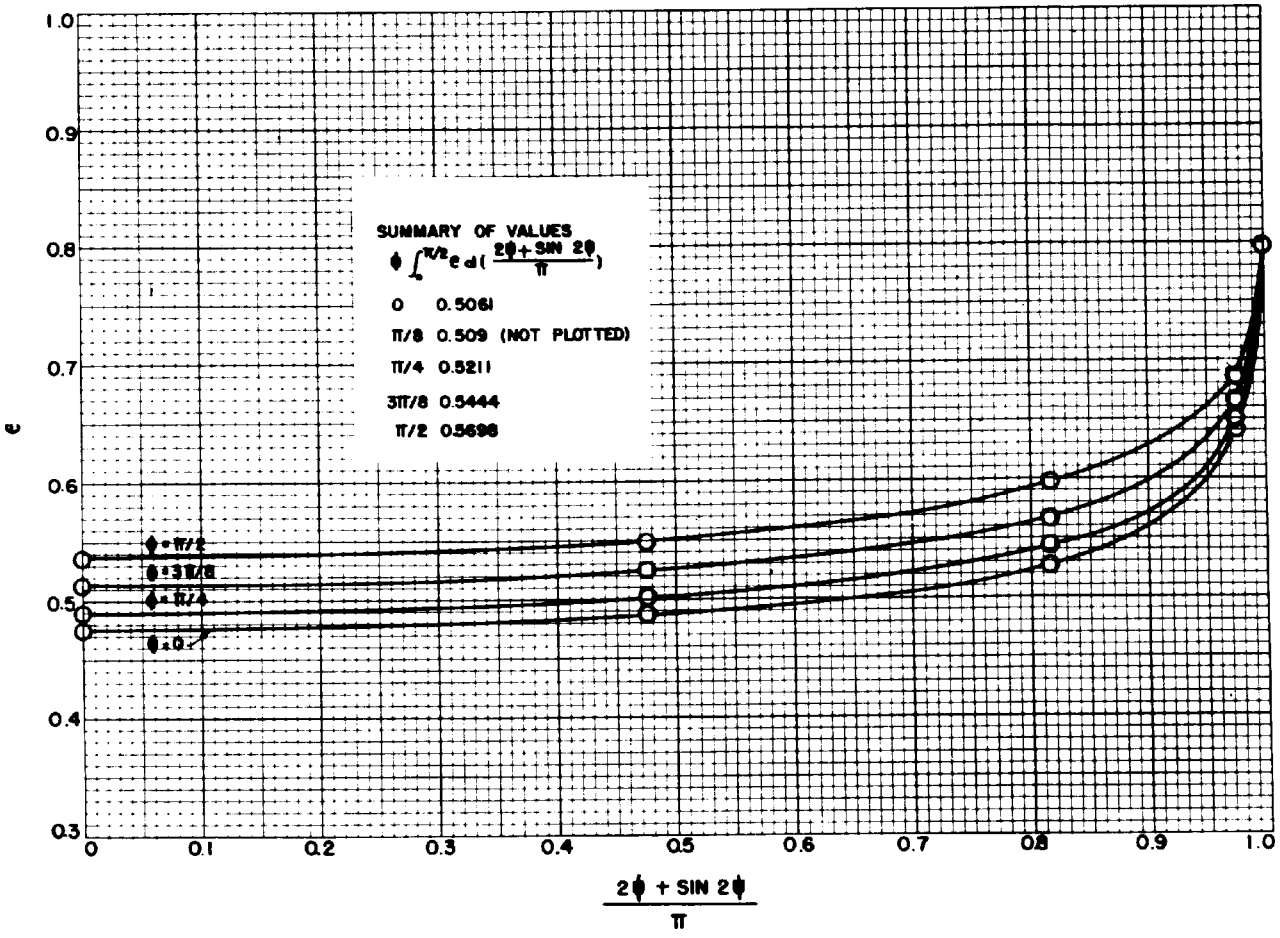

FIGURE 36.

EVALUATION OF $\int_0^{\pi/2} e\,d\left(\frac{2\phi+\sin 2\phi}{\pi}\right)$ FROM INNER SURFACE

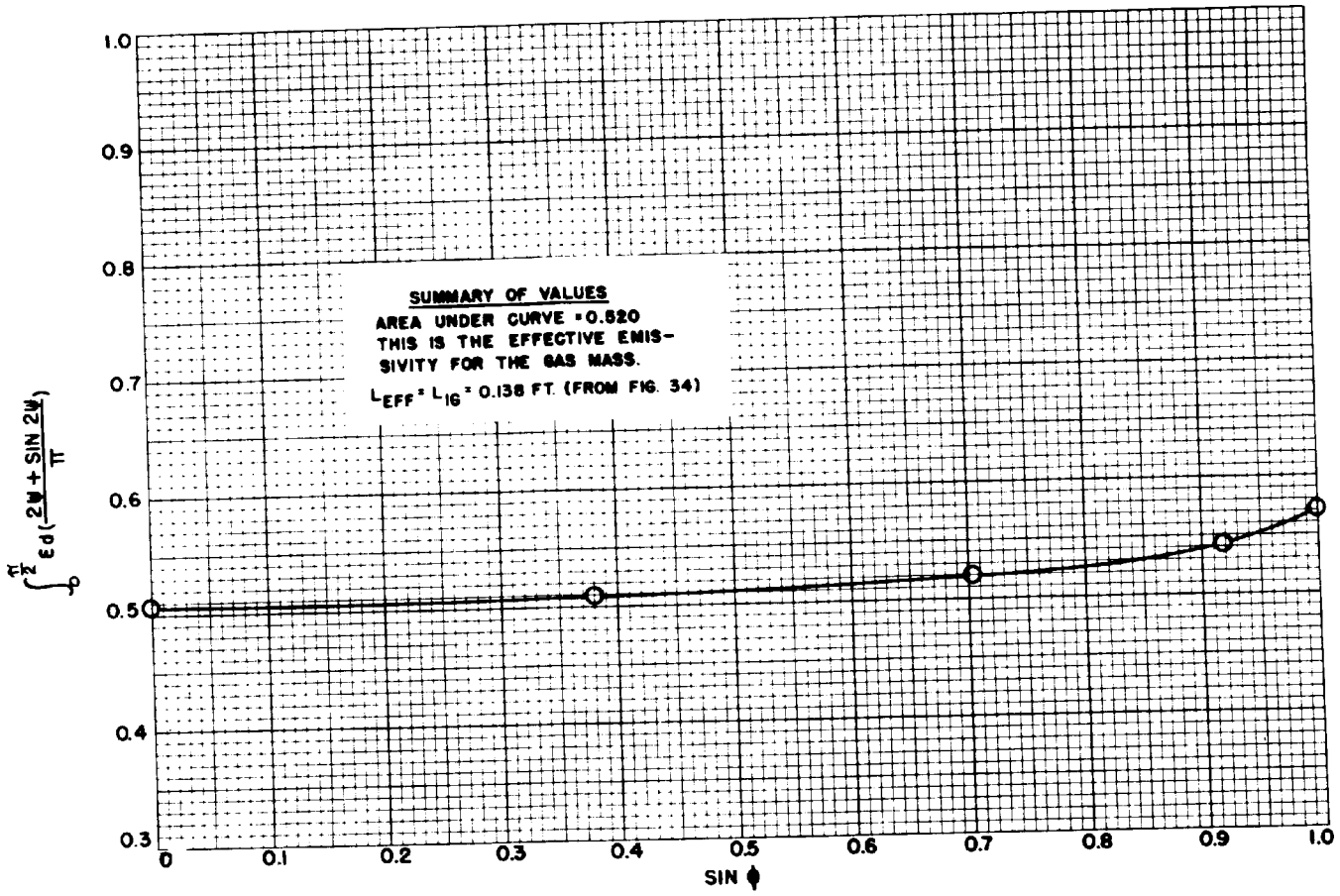

FIGURE 37

EVALUATION OF $\int_0^{\frac{\pi}{2}} d(\sin\phi)\left[\int_0^{\frac{\pi}{2}} \varepsilon d(\frac{2\psi + \sin 2\psi}{\pi})\right]$ FROM INNER TUBE

length for radiation from the inner tube to the gas, or vice versa, is therefore 0.138 feet.

From the Outer Tube to the Gas Mass

The geometrical relations for this case are shown in detail in Figure 38. Here,

$$\cos\theta = \frac{EF}{EC} = \frac{ED\cos\phi}{ED/\cos\psi} = \cos\phi\cos\psi \quad (100)$$

$$d\omega = d\phi\, d\psi \frac{ED}{EC} = d\phi\, d\psi \cos\psi \quad (101)$$

$$L = EC = ED/\cos\psi \quad (102)$$

Combining the terms into Equation (70) as before results in

$$\varepsilon_{OG} = \varepsilon_{eff} = \int_0^{\pi/2}\int_0^{\pi/2} \varepsilon\, d(\sin\phi)\, d\left(\frac{2\psi + \sin 2\psi}{\pi}\right) \quad (103)$$

The calculation of the mean beam lengths and angle factors for the two masses of gas which lie respectively within the solid angle subtended by the inner tube and within the remainder of the total hemispherical angle are presented in detail in Table XV and Figures 39, 40, and 41.

Table XV gives the quantities required for the evaluation of

$$\int_0^{\pi/2} \varepsilon\, d\left(\frac{2\psi + \sin 2\psi}{\pi}\right)$$ at five values of the angle ϕ.

Column 5, which indicates the beam length L, is obtained with the help of Figure 39 by dividing the distance ED by cos ψ. It is particularly to be noticed that the ray at $\phi = \pi/8$ radians (it is purely fortuitous

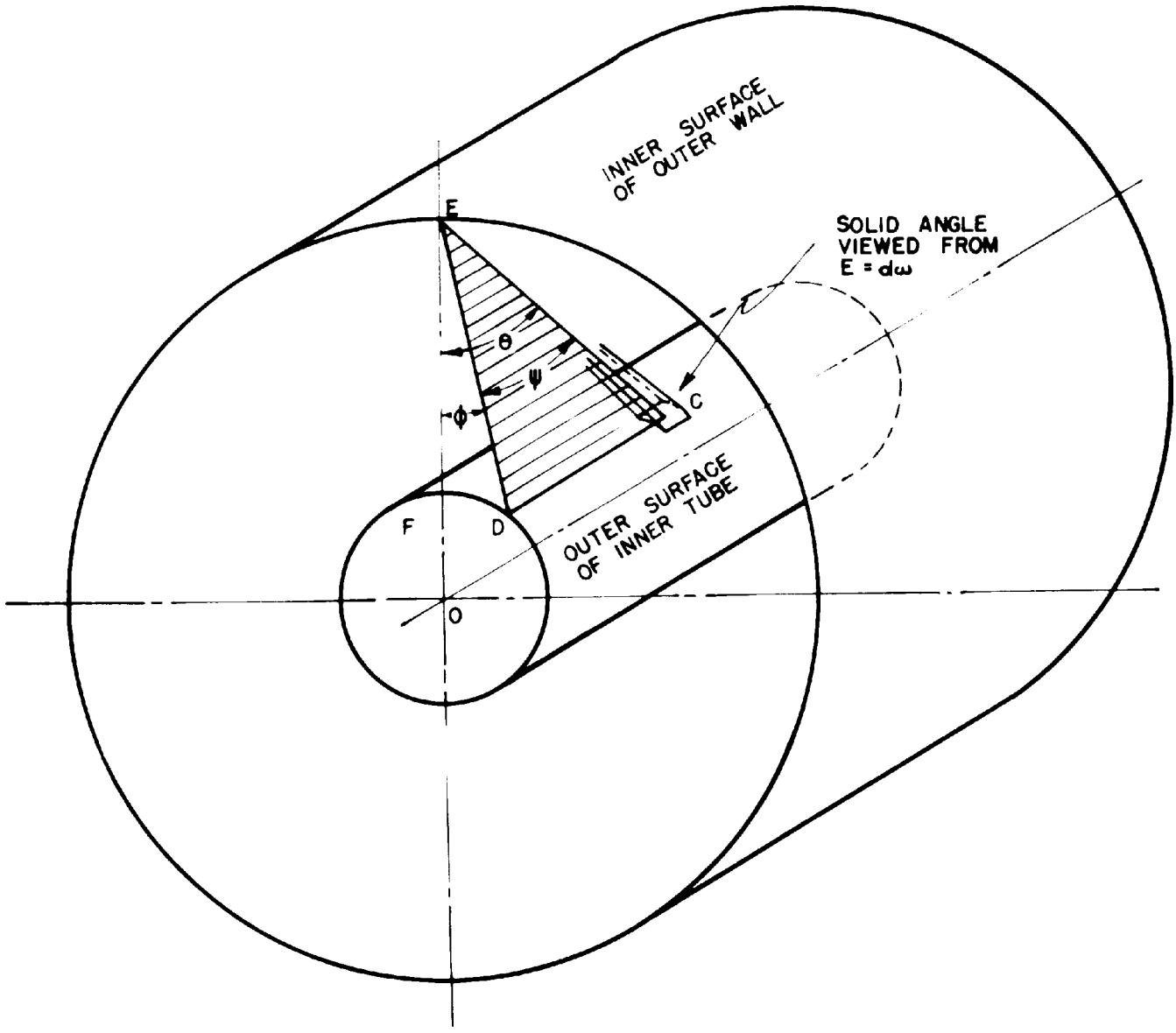

FIGURE 38

GEOMETRICAL RELATIONS IN THE EVALUATION OF THE MEAN BEAM LENGTHS FROM THE OUTER SURFACE.

THE BEAM SHOWN (EC), IS DIRECTED TOWARDS THE INNER TUBE, IN THE OTHER CASE (NOT SHOWN) THE BEAM IS DIRECTED TOWARDS THE OUTER WALL.

TABLE XV

CALCULATIONS FOR THE EVALUATION OF THE MEAN EFFECTIVE BEAM LENGTHS AND THE ANGLE FACTORS FOR RADIATION FROM THE OUTER WALL OF THE PLAIN ANNULUS

1	2	3	4	5	6	7
ϕ	ψ	$\sin 2\psi$	$\cos\psi$	L	ε	$\frac{2\psi + \sin 2\psi}{\pi}$
	0	0	1.000	0.104	0.475	0
	$\pi/8$	0.707	0.924	.113	.489	0.475
0	$\pi/4$	1.000	0.707	.147	.529	0.818
	$3\pi/8$	0.707	0.383	.272	.635	0.975
	$\pi/2$	0	0	∞	.800	1.000
	0	0	1.000	0.110	0.483	0
	$\pi/8$	0.707	0.924	.119	.496	0.475
$\pi/16$	$\pi/4$	1.000	0.707	.156	.540	0.818
	$3\pi/8$	0.707	0.383	.287	.643	0.975
	$\pi/2$	0	0	∞	.800	1.000
	0	0	1.000	0.154 .308	0.538 .655	0
	$\pi/8$	0.707	0.924	0.167 .334	0.552 .667	0.475
$\pi/8$	$\pi/4$	1.000	0.707	0.218 .436	0.600 .700	0.818
	$3\pi/8$	0.707	0.383	0.402 .805	0.690 .755	0.975
	$\pi/2$	0	0	∞	.800	1.000
	0	0	1.000	0.236	0.613	0
	$\pi/8$	0.707	0.924	.256	.625	0.475
$\pi/4$	$\pi/4$	1.000	0.707	.334	.668	0.818
	$3\pi/8$	0.707	0.383	.616	.738	0.975
	$\pi/2$	0	0	∞	.800	1.000
	0	0	1.000	0.128	0.508	0
	$\pi/8$	0.707	0.924	.139	.580	0.475
$3\pi/8$	$\pi/4$	1.000	0.707	.181	.565	0.818
	$3\pi/8$	0.707	0.383	.334	.667	0.975
	$\pi/2$	0	0	∞	.800	1.000
	0	0	1.000	0	0	0
	$\pi/8$	0.707	0.924	0	0	0.475
$\pi/2$	$\pi/4$	1.000	0.707	0	0	0.818
	$3\pi/8$	0.707	0.383	0	0	0.975
	$\pi/2$	0	0	--	--	1.000

that this value happens to be a simple fraction) which just grazes the inner tube has two possible lengths. The smaller value of these two is the value of the limiting ray which strikes the inner tube; the larger value is the value of the limiting ray which strikes the outer wall. It is important that both of these values be employed in the analysis.

The graphical integration of $\int_0^{\pi/2} \varepsilon \, d(2\psi + \sin 2\psi / \pi)$ is performed in Figure 40, which includes a tabulation of the values of the integral for each value of the angle ϕ.

The last step in the integration process, that of the evaluation of the integral

$$\int_0^{\pi/2} \left[\varepsilon_d \left(\frac{2\psi + \sin 2\psi}{\pi} \right) \right] d (\sin \phi)$$

is carried out in Figure 41 using the tabulated values from Figure 40. The point of discontinuity in this integral curve reflects the abrupt change in beam length from the limiting value at the inner tube to the limiting value at the outer wall. Figure 41 indicates the values of the above integrals to be $\varepsilon_{OG} = 0.5822$ from which a mean effective beam length of $L_{OG} = 0.201$ feet is obtained (Figure 34). This is the mean effective beam length of the gas mass as a whole, as viewed from the outer tube.

In this case, however, it is important to know, in addition, the mean effective beam lengths of the portions of the gas mass included and excluded in the solid angle subtended by the inner tube. It is also important to determine the corresponding two angle factors, F_{01} and F_{00}.

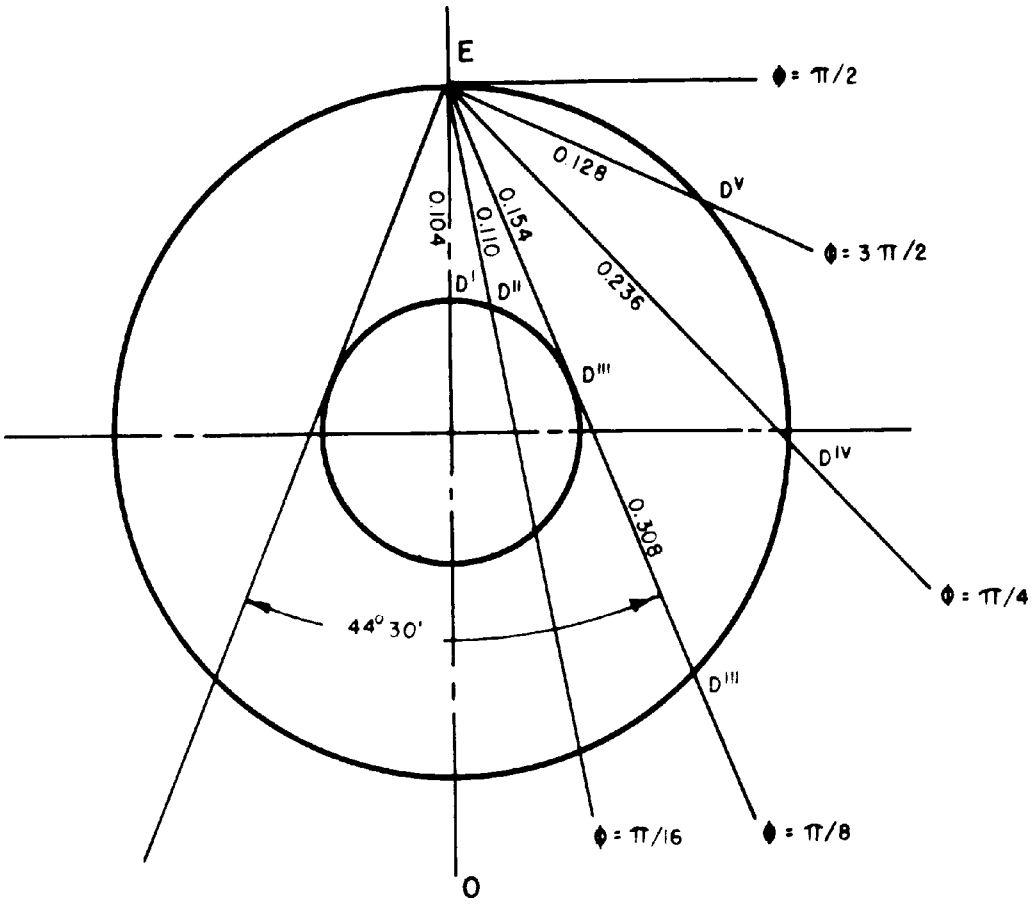

ED' = VALUE OF ED @ Φ = 0
ED'' = VALUE OF ED @ Φ = π/16, ETC.

FIGURE 39
SKETCH FOR EVALUATION OF BEAM LENGTHS

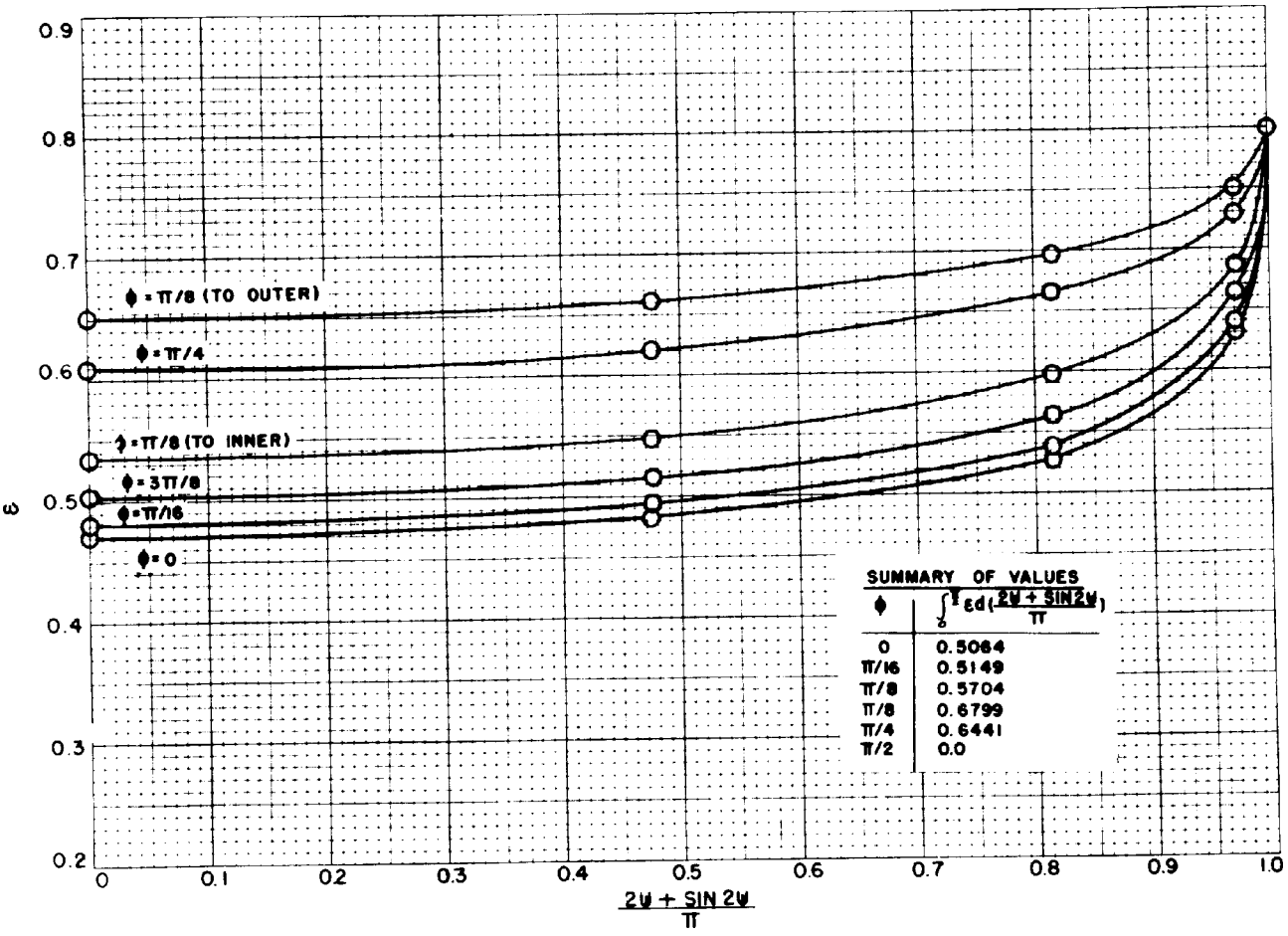

FIGURE 40

EVALUATION OF $\int_0^{\frac{\pi}{2}} \varepsilon d\left(\frac{2\psi + \sin 2\psi}{\pi}\right)$ FROM OUTER SURFACE

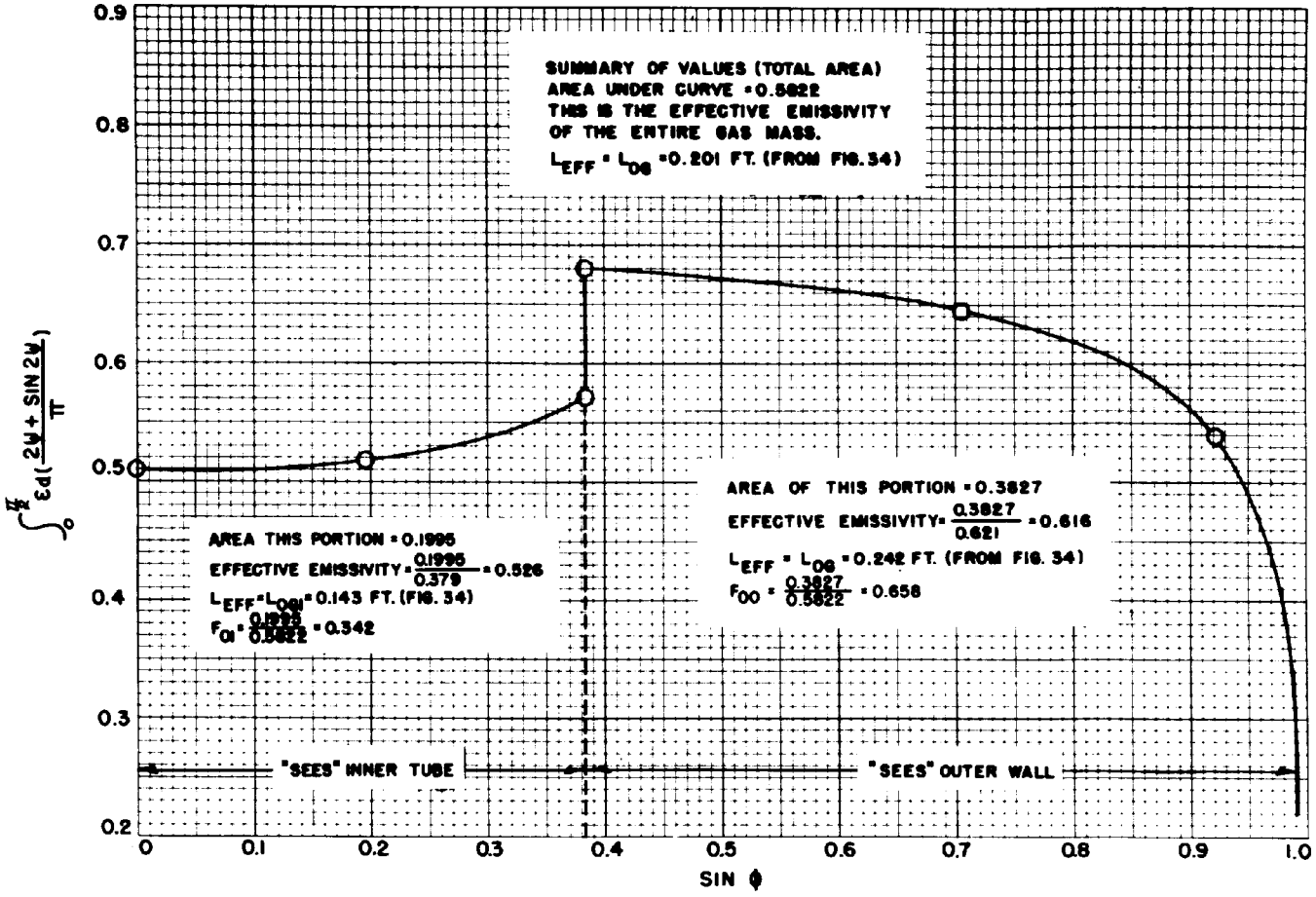

FIGURE 41

EVALUATION OF $\int d(\sin\phi)\left[\int_0^{\frac{\pi}{2}} \varepsilon d\left(\frac{2\psi + \sin 2\psi}{\pi}\right)\right]$ FROM OUTER WALL

From Equation (71) for such a case,

$$E_{eff.\omega'} = \frac{\int_0^{\omega'} \varepsilon \cos\theta \, d\omega}{\int_0^{\omega'} \cos\theta \, d\omega} \qquad (73)$$

and

$$F_{\omega'} = \frac{\int_0^{\omega'} \varepsilon \cos\theta \, d\omega}{\int_0^{2\pi} \varepsilon \cos\theta \, d\omega} \qquad (74)$$

The integral ratio represented by Equation (73) is given by Figure 41 by the ratio of 0.1995. (which represents the value of $\int_0^{\omega'} \varepsilon \cos\theta \, d\omega$) to 0.379 (which is obtained as the value of $\int_0^{\omega'} \cos\theta \, d\omega$). The effective emissivity for the gas mass subtended by the inner tube, ε_{0G1}, is therefore 0.526, which gives, from Figure 34, a value of L_{01} = 0.143 feet.

Similarly, the value of L_{00} is obtained from the effective emissivity ε_{0G0} given by 0.3827/0.621 = 0.616, from which L_{00} = 0.242 feet. The two angle factors are now obtained as

$$F_{01} = 0.1995/0.5822 = 0.342$$

$$F_{00} = 0.3827/0.5822 = 0.658$$

$$F_{01} + F_{00} = 1.000$$

The procedure for the outer tube is subject to a test for internal consistency, since

$$F_{01}\,\varepsilon_{0G1} + F_{00}\,\varepsilon_{0G0} = \varepsilon_{0G} \qquad (104)$$

$$(.342)(.526) + (.658)(.616) = ? \quad .582$$

$$.585 = ? \quad .582$$

This is a satisfactory check.

Summarizing, it has been found that

$$L_{1G} = 0.138 \text{ feet}$$

$$L_{0G} = 0.201 \text{ feet}$$

$$-L_{01} = 0.143 \text{ feet}$$

$$-L_{00} = 0.242 \text{ feet}$$

$$F_{01} = 0.342$$

$$F_{00} = 0.658$$

These quantities have been determined employing emissivity values intermediate between those at 50 and 100 psi. abs., but are considered reliable for any conditions within this range.

(a) Radiation Analysis - iv. Interrelations Between Steam Absorptivities and Emissivities

The evaluation of gas emissivities, with special reference to steam, has been explained in detail in a preceding section. There remain the details of the process for computing the absorptivities of gas masses for complicated beams involving partial absorptions and reflections. The various emissivities and absorptivities which are required for the evaluation of the relationships representing the radiation transfer in an annulus may be listed as follows.

1. ε_{G1}
2. ε_{G0}
3. $\alpha_{G1,G1}$

4. $\alpha_{GO,G(2L1)}$

5. $\alpha_{GO,GO}$

6. $\alpha_{G1,S1}$

7. $\alpha_{GO,SO}$

8. $\alpha_{GO,S1(G1)}$

9. $\alpha_{GO,SO(GO)}$

10. $\alpha_{G1,SO(GO)}$

where the significance of the subscripts is defined in the previous development.

The first two items, ϵ_{G1} and ϵ_{GO}, represent normal emissivities to be evaluated at the gas temperature and pressure and at L_{1G} and L_{OG} respectively.

Absorptivities of the type represented by Items 3, 4, and 5 of the above list may be defined precisely in terms of certain emissivities. The method of this calculation is indicated for the case of Item 1, $\alpha_{G1,G1}$, in Figure 42 which is self-explanatory, involving only the concept that the emissivity of a layer of gas is equal to the emissivities of any outer fraction of it, plus the emissivity of the remaining fraction multiplied by the transmissivity (one minus the absorptivity) of the outer layer. This same method may be applied to the evaluation of Items 4 and 5 with results as indicated in Table XVI, Columns 1, 2, and 3. Absorptivities of the type of Items 6 and 7 of the list are evaluated by an empirical rule due to Hottel (19). Hottel has found that a gas absorptivity for radiation from a metallic surface at another temperature may be related to the emissivity of the gas by the equation:

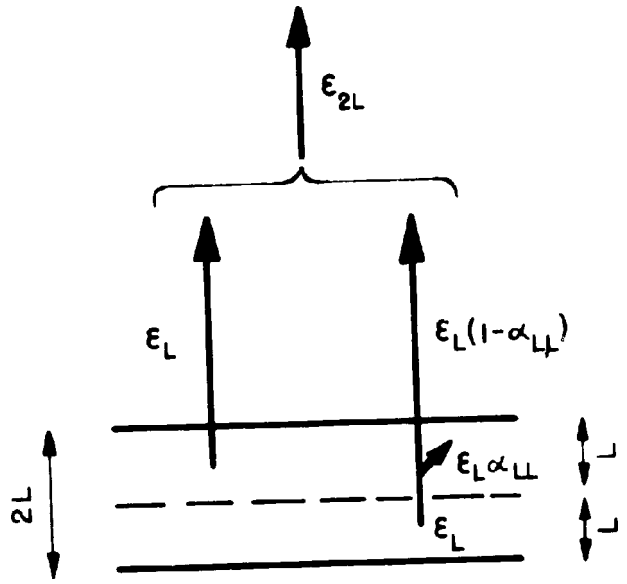

EMISSIVITY OF LAYER OF THICKNESS $2L = \varepsilon_{2L}$

FROM THE FIGURE $\varepsilon_{2L} = \varepsilon_L + \varepsilon_L(1-\alpha_{L,L})$

FROM WHICH $\alpha_{L,L} = 2 - \frac{\varepsilon_{2L}}{\varepsilon_L}$

FIGURE 42.

TYPICAL INTERRELATION BETWEEN EMISSIVITY AND ABSORPTIVITY.

RELATION BETWEEN $\alpha_{L,L}$ AND $\varepsilon_{2L}, \varepsilon_L$

$$\alpha_{GO,SO} = (\varepsilon_{G,TO,PL(TO/TG)}) (T_G/T_O)^{0.53} \qquad (105)$$

where $\varepsilon_{G,TO,PL(TO/TG)}$ = the emissivity of the gas evaluated at the surface temperature and at a PL product equal to $PL(T_O/T_G)$ where T_O/T_G is the ratio of the absolute temperatures of the surface and the absorbing gas. Application of this relationship to Items 6 and 7 gives the results indicated in Table XVI.

The remaining Items 8, 9, and 10 may be evaluated by the successive application of the concepts applied separately to Items 3, 4, and 5 and Items 6 and 7. The results are indicated in Table XVI in Columns 1, 2, and 3. Column 4 is discussed later.

(a) Radiation Analysis - v. Approximate Evaluation of the Radiation Equations

The first few terms of the infinite series representing the transfer of radiant energy in the bare annulus were developed in Division i. of this section. These first few terms do not, in themselves, constitute an expression of sufficient accuracy, but must be adjusted to compensate for the missing terms of the series.

Approximate numerical values for the various absorptivities and emissivities of steam may be computed for average conditions and these may be introduced into the series expressions to permit numerical evaluation and adjustment. Table XVI, discussed earlier, includes a set of numerical values for the various absorptivities and emissivities. These values are based upon the mean effective beam lengths determined in a previous section and upon the following assumed conditions: T_1 =

TABLE XVI

EXPRESSIONS AND APPROXIMATE MAGNITUDES FOR STEAM EMISSIVITIES AND ABSORPTIVITIES

THE APPROXIMATE MAGNITUDES ARE BASED ON:

$L_{1G} = 0.138$ ft. $\quad T_1 = 500°\ F = 960°\ R$
$L_{0G} = 0.201$ ft. $\quad T_G = 350°\ F = 810°\ R$
$L_{01} = 0.135$ ft. $\quad T_0 = 350°\ F = 810°\ R$
$L_{00} = 0.256$ ft. $\quad P = 75$ psi. abs.

1 Item	2 Emissivity or Absorptivity Factor	3 Expression for Factor	4 Approximate Numerical Value of Factor
1	ϵ_{G1}	$\epsilon_{G1} = \epsilon_{G,L1G}$	0.545
2	ϵ_{G0}	$\epsilon_{G0} = \epsilon_{G,L0G}$	0.608
3	$\alpha_{G1,G1}$	$\alpha_{G1,G1} = 2 - \dfrac{\epsilon_{G,2L1G}}{\epsilon_{G1}}$	0.800
4	$\alpha_{G0,G(2L1)}$	$\alpha_{G0,G(2L1)} = \dfrac{\epsilon_{G0} + \epsilon_{G,2L1G} - \epsilon_{G,(L0G + 2L1G)}}{\epsilon_{G,2L1G}}$	0.822
5	$\alpha_{G0,G0}$	$\alpha_{G0,G0} = 2 - \dfrac{\epsilon_{G,2L0G}}{\epsilon_{G0}}$	0.838
6	$\alpha_{G1,S1}$	$\alpha_{G1,S1} = \left[\epsilon_{G,T1,L1G(T1/TG)}\right](T_G/T_1)^{0.53}$	0.501
7	$\alpha_{G0,S0}$	$\alpha_{G0,S0} = \left[\epsilon_{G,T0,L0G(T1/TG)}\right](T_G/T_0)^{0.53}$	0.608
8	$\alpha_{G0,S1(G1)}$	$\alpha_{G0,S1(G1)} = \dfrac{\alpha_{G,(L1G + L0G),S1} - \alpha_{G1,S1}}{1 - \alpha_{G1,S1}}$	0.257
		where $\alpha_{G,(L1G + L0G),S1} = \left[\epsilon_{G,T1,(L1G + L0G)(T1/TG)}\right](T_G/T_1)^{0.53} = 0.630$	
9	$\alpha_{G0,S0(G0)}$	$\alpha_{G0,S0(G0)} = \dfrac{\alpha_{G,(L0G + L00),S0} - \alpha_{G,L00,S0}}{1 - \alpha_{G,L00,S0}}$	0.277
		where $\alpha_{G,(L0G + L00),S0} = \left[\epsilon_{G,T0,(L0G + L00)(T0/TG)}\right](T_G/T_0)^{0.53} = 0.717$	
		and $\alpha_{G,L00,S0} = \left[\epsilon_{G,T0,L00(T0/TG)}\right](T_G/T_0)^{0.53} = 0.642$	
10	$\alpha_{G1,S0(G0)}$	$\alpha_{G1,S0(G0)} = \dfrac{\alpha_{G,(L1G + L01),S0} - \alpha_{G,L01,S0}}{1 - \alpha_{G,L01,S0}}$	0.238
		where $\alpha_{G,(L1G + L01),S0} = \left[\epsilon_{G,T0,(L1G + L01)(T0/TG)}\right](T_G/T_0)^{0.53} = 0.658$	
		and $\alpha_{G,L01,S0} = \left[\epsilon_{G,T0,L01(T0/TG)}\right](T_G/T_0)^{0.53} = 0.551$	

960°R., T_G = 810°R., T_0 = 810°R., and pressure P = 75 psi. abs.

It is also necessary to introduce numerical values for the emissivities of the two steel surfaces. It will be assumed at this point that both surfaces have the same emissivity and this value will be taken, for the purposes of adjustment, as 0.75, i.e.,

$$\epsilon_0 = \epsilon_1 \simeq 0.75$$

The adjustment is conducted in Table XVII by a process which is almost self-explanatory. Table XVII is divided into four parts, one for each typical ray. In each part the ray fraction is identified in Column 1, the absorbing medium in Column 2. Column 3 gives the equation for the fraction and introduces the numerical values to give, in Column 4, an approximate value for the fraction.

A heat balance on the ray requires that the algebraic total of the values for the ray fractions equal zero when the emitting surface is considered, as here, to absorb a negative amount. Quantitative adjustments for the missing amount may therefore be made to the larger fractions. Also, certain fractions which are small may conveniently be deleted and their amounts added to the larger fractions. The final adjusted equations for the larger fractions are presented in the table. It is seen that the total of their numerical values is zero, as required.

The results of the adjustment process are summarized in Table XVIII, which gives the complete fractional disposition of the typical rays. Table XVIII represents the set of relationships, adjusted to account for missing terms, which in aggregate describe the radiant energy transfer in the plain annulus.

TABLE XVII

ADJUSTMENT OF THE FIRST FEW TERMS OF THE INFINITE SERIES TO COMPENSATE FOR THE MISSING TERMS

(Terms are adjusted to an algebraic total of zero to allow for the terms of the infinite series not considered. This adjustment is distributed among the larger terms.)

Ray (a), Originating on the Surface of the Inner Tube

1	2	3	4
Fraction	Absorbing Medium	Equation for Fraction	Approx. Value
(i)	A_1	-1.000	-1.000
(ii)	gas	$\alpha_{G1,S1}$	0.535
(iii)	A_0	$(1-\alpha_{G1,S1})\,\varepsilon_0 = (.465)(.750)$	0.349
(iv)	gas	$(1-\alpha_{G1,S1})^{.465}(1-\varepsilon_0)^{.25}(\alpha_{G0,S1(G1)})^{.257}$	0.0301*
(v)	A_1	$(1-\alpha_{G1,S1})^{.465}(1-\varepsilon_0)^{.25}(1-\alpha_{G0,S1(G1)})^{.743}F_{01}^{.342}\,\varepsilon_1^{.75}$	0.022*
(vi)	A_0	$(1-\alpha_{G1,S1})^{.465}(1-\varepsilon_0)^{.25}(1-\alpha_{G0,S1(G1)})^{.743}F_{00}^{.658}\,\varepsilon_0^{.75}$	0.042*
			0.978

1 - 0.978 = 0.022 to be adjusted. Also, *iv, v and vi are insignificantly small.

Adjustment:

(i) add 0.007 + item (v) = 0.029 $\quad -1 + 0.029/1.000 = -0.971$

(ii) add 0.004 + item (iv) = 0.034 $\quad 1 + 0.034/0.535 = 1.064$

(iii) add $\frac{0.011}{0.022}$ + item (vi) = 0.053 $\quad 1 + 0.053/0.349 = 1.152$

TABLE XVII, CONTINUED

Ray (a) After Adjustment

1 Fraction	2 Absorbing Medium	3 Equation for Fraction	4 Approx. Value
(i)	A_1	-1.000(0.971)	-0.971
(ii)	gas	$\alpha_{G1,S1}(1.064)$ = 0.535 x 1.064	0.569
(iii)	A_0	$(1-\alpha_{G1,S1})\ \varepsilon_0(1.152)$ = 0.465 x 0.750 x 1.152	0.402
		Sum	0.000

Ray (b), Originating in the Gas Directed Toward A_1

1 Fraction	2 Absorbing Medium	3 Equation for Fraction	4 Approx. Value
(i)	gas		-1.000
(ii)	A_1	ε_1 = 0.75	0.75
(iii)	gas	$(1-\varepsilon_1)\alpha_{G1,G1}$ = 0.25 x 0.800	0.200
(iv)	A_0	$(1-\varepsilon_1^{.25})(1-\alpha_{G1,G1}^{.2})\ \varepsilon_0$ = .05 x .75	0.0375
(v)	gas	$(1-\varepsilon_1^{.25})(1-\alpha_{G1,G1}^{.2})(1-\varepsilon_0^{.25})\alpha_{GO,G(2L1)}^{.822}$	0.0103*
			0.9978

1.000 - 0.9978 = 0.0022 to be adjusted. Also, (v) is insignificantly small.*
Adjustment:
(ii) add 0.0022 1 + .0022/.750 = 1.003
(iii) delete (v), add to (iii) 1 + .0103/.200 = 1.0501

TABLE XVII, CONTINUED

Ray (b) After Adjustment

1 Fraction	2 Absorbing Medium	3 Equation for Fraction	4 Approx. Value
(i)	gas	-1.000	-1.000
(ii)	A_1	$\varepsilon_1(1.003)$	0.7522
(iii)	gas	$(1-\varepsilon_1)\alpha_{G1,G1}(1.0501)$	0.2103
(iv)	A_0	$(0.05\ \varepsilon_0)$	0.0375
			0.000

Ray (c), Originating in the Gas, Directed Towards A_0

1 Fraction	2 Absorbing Medium	3 Equation for Fraction	4 Approx. Value
(i)	gas		-1.000
(ii)	A_0	$\varepsilon_0 = 0.75$	0.75
(iii)	gas	$(1-\varepsilon_0)(\alpha_{GO,GO}) = .25 \times .831$	0.2080
(iv)	A_1	$(1-\varepsilon_0)^{.25}(1-\alpha_{GO,GO})^{.169}F_{01}^{.342}\varepsilon_1^{.75}$	0.0108
(v)	A_0	$(1-\varepsilon_0)^{.25}(1-\alpha_{GO,GO})^{.169}F_{00}^{.658}\varepsilon_1^{.75}$	0.0208*
			0.9896

1.000 - .9896 = 0.0104 to be adjusted. Also, (v) will be combined with (ii)
Adjustment:

add 0.0104 to (iii) 1 + .0104/.2080 = 1.050
add (v) = .0208 to (ii) 1 + .0208/.75 = 1.028

TABLE XVII, CONTINUED

Ray (c) After Adjustment

1 Fraction	2 Absorbing Medium	3 Equation for Fraction	4 Approx. Value
(i)	gas	-1.000	-1.000
(ii)	A_0	$\varepsilon_0(1.028)$	0.7708
(iii)	gas	$(1-\varepsilon_0)(\alpha_{GO,GO})(1.050)$	0.2184
(iv)	A_1	$(1-\varepsilon_0)(1-\alpha_{GO,GO})F_{01}\,\varepsilon_1$	0.0108
		Sum	0.0000

Ray (d), Originating on the Surface A_0

1 Fraction	2 Absorbing Medium	3 Equation for Fraction	4 Approx. Value
(i)	A_0	-1.000	-1.000
(ii)	gas	$\alpha_{GO,SO}(F_{01} + F_{00}) = 0.599$	0.599
(iii)	A_1	$(1-\alpha_{GO,SO}^{.401})F_{01}^{.342}\,\varepsilon_1^{.75}$	0.103
(iv)	A_0	$(1-\alpha_{GO,SO}^{.401})F_{00}^{.658}\,\varepsilon_0^{.75}$	0.198
(v)	gas	$(1-\alpha_{GO,SO}^{.401})F_{01}^{.342}(1-\varepsilon_1^{.25})\alpha_{G1,SO(GO)}^{.238}$	0.008*
(vi)	gas	$(1-\alpha_{GO,SO}^{.401})F_{00}^{.658}(1-\varepsilon_0^{.25})\alpha_{GO,SO(GO)}^{.227}$	0.015*
(vii)	A_0	$(1-\alpha_{GO,SO}^{.401})F_{01}^{.342}(1-\varepsilon_1^{.25})(1-\alpha_{G1,SO(GO)}^{.762})^{.75}\,\varepsilon_0$	0.019*
(viii)	A_1	$(1-\alpha_{GO,SO}^{.401})F_{00}^{.658}(1-\varepsilon_0^{.25})(1-\alpha_{GO,SO(GO)}^{.773})^{.75}\,\varepsilon_1^{.342}F_{01}$	0.013*
(ix)	A_0	$(1-\alpha_{GO,SO}^{.401})F_{00}^{.658}(1-\varepsilon_0^{.25})(1-\alpha_{GO,SO(GO)}^{.773})^{.75}\,\varepsilon_0^{.658}F_{00}$	0.025*
			0.980

TABLE XVII, CONCLUDED

1.000 - .980 = .020 to be adjusted .008 to A_1(iii), .012 to A_0(iv)

(v) through (ix) to be deleted.

to A_0(iv):		to gas (ii):		to A_1(iii):	
	.019 (vii)		.008 (v)		.013 (viii)
	.025 (ix)		.015 (vi)		.008 adj.
	.012 adj.				
	(iv) .056		(ii) .023		(iii) .023

Ray (d) After Adjustment

1	2	3	4
Fraction	Absorbing Medium	Equation for Fraction	Approx. Value
(i)	A_0	-1.000	-1.000
(ii)	gas	$\alpha_{GO,SO}(1 + \frac{.023}{.599}) = \alpha_{GO,SO}(1.038)$	0.622
(iii)	A_1	$(1-\alpha_{GO,SO})F_{O1}\,\varepsilon_1(1 + \frac{.021}{.103}) = (1-\alpha_{GO,SO})$ x $F_{O1}\,\varepsilon_1(1.204)$	0.124
(iv)	A_0	$(1-\alpha_{GO,SO})F_{OO}\,\varepsilon_0(1 + \frac{.056}{.198}) =$ $(1-\alpha_{GO,SO})F_{OO}\,\varepsilon_0(1.283)$	0.254
		Sum	0.000

It is convenient to add together all those ray fractions which are absorbed at like surfaces. This is done in Table XVIII. Since the totals for the radiant energy absorption at each of the inner tube, the gas, and the outer wall involve all three temperatures to the fourth power, it is convenient to define the following three equations.

$$q_{RT} = GT_1^4 + HT_G^4 + JT_0^4 \qquad (106)$$

$$q_{RW} = AT_1^4 + BT_G^4 + CT_0^4 \qquad (107)$$

$$q_{RG} = DT_1^4 + ET_0^4 + FT_G^4 \qquad (108)$$

The quantities A, B, C, D, E, F, G, H, and J in the above equations represent the summation of the adjusted first few terms of infinite series involving the various absorptivities, emissivities, and angle factors. These quantities may be evaluated in terms of the absorptivities, etc., by introducing the numerical values of A_1, A_0, F_{01}, F_{00}, and σ. The values for the plain annulus are:

A_1 = 1.000 sq. ft. (basis)

A_0 = 2.69 sq. ft.

F_{01} = 0.342

F_{00} = 0.658

σ = 0.173 (when all temperatures are expressed in °R/100). With the introduction of the above values, and employing the symbol p for the emissivity of both surfaces (ε_1 and ε_0), the factors

TABLE XVIII

FRACTIONAL DISPOSITION OF TYPICAL RADIATION RAYS IN AN ANNULUS

(After Adjustment to Account for the Missing Terms of the Infinite Series)

1 Origin of Ray	2 Symbol in Figure 31	3 Fraction of Original Ray	4 FRACTION OF RAY ABSORBED BY INNER TUBE (A_1)	5 FRACTION OF RAY ABSORBED BY GAS	6 FRACTION OF RAY ABSORBED BY OUTER WALL (A_0)
Surface of Inner Tube	a	i	$-0.971\ \sigma A_1 T_1^4 p$	- - - - - - - - - - - - - - -	- - - - - - - - - - - - - - -
		ii	- - - - - - - - - - - - - - -	$1.064\ \sigma A_1 T_1^4 p\ \alpha_{G1,S1}$	- - - - - - - - - - - - - - -
		iii	- - - - - - - - - - - - - - -	- - - - - - - - - - - - - - -	$1.152\ \sigma A_1 T_1^4 p^2 (1-\alpha_{G1,S1})$
Gas Directed Toward Inner Tube)	b	i	- - - - - - - - - - - - - - -	$-1.000\ \sigma A_1 T_G^4\ \varepsilon_{G1}$	- - - - - - - - - - - - - - -
		ii	$1.003\ \sigma A_1 T_G^4\ \varepsilon_{G1}\ p$	- - - - - - - - - - - - - - -	- - - - - - - - - - - - - - -
		iii	- - - - - - - - - - - - - - -	$1.050\ \sigma A_1 T_G^4\ \varepsilon_{G1}(1-p)\ \alpha_{G1,G1}$	- - - - - - - - - - - - - - -
		iv	- - - - - - - - - - - - - - -	- - - - - - - - - - - - - - -	$0.050\ \sigma A_1 T_G^4\ \varepsilon_{G1}\ p$
Gas Directed Toward Outer Wall)	c	i	- - - - - - - - - - - - - - -	$-1.000\ \sigma A_0 T_G^4\ \varepsilon_{GO}$	- - - - - - - - - - - - - - -
		ii	- - - - - - - - - - - - - - -	- - - - - - - - - - - - - - -	$1.028\ \sigma A_0 T_G^4\ \varepsilon_{GO}\ p$
		iii	- - - - - - - - - - - - - - -	$1.050\ \sigma A_0 T_G^4\ \varepsilon_{GO}(1-p)\ \alpha_{GO,GO}$	- - - - - - - - - - - - - - -
		iv	$\sigma A_0 T_G^4\ \varepsilon_{GO}(1-p)(1-\alpha_{GO,GO})\ F_{O1} p$	- - - - - - - - - - - - - - -	- - - - - - - - - - - - - - -
Surface of Outer Wall	d	i	- - - - - - - - - - - - - - -	- - - - - - - - - - - - - - -	$-1.000\sigma A_0 T_0^4\ p$
		ii	- - - - - - - - - - - - - - -	$1.038\ \sigma A_0 T_0^4\ p\ \alpha_{GO,SO}$	- - - - - - - - - - - - - - -
		iii	$1.204\ \sigma A_0 T_0^4\ p^2 (1-\alpha_{GO,SO})\ F_{O1}$	- - - - - - - - - - - - - - -	- - - - - - - - - - - - - - -
		iv	- - - - - - - - - - - - - - -	- - - - - - - - - - - - - - -	$1.283\ \sigma A_0 T_0^4\ p^2 (1-\alpha_{GO,SO})\ F_{OO}$
Net Radiant Energy Absorbed By The Inner Tube, The Gas, and The Outer Tube			$q_{RT} = GT_1^4 + HT_G^4 + JT_0^4$ $G = -0.971\ \sigma A_1\ p$ $H = \sigma p\left[1.003\ A_1 \varepsilon_{G1} + A_0 \varepsilon_{GO}(1-p)(1-\alpha_{GO,GO}) F_{O1}\right]$ $J = 1.204\ \sigma A_0 p^2 (1-\alpha_{GO,SO})\ F_{O1}$	$q_{RG} = DT_1^4 + FT_G^4 + ET_0^4$ $D = 1.064\ \sigma A_1 p\ \alpha_{G1,S1}$ $E = 1.038\ \sigma A_0 p\ \alpha_{GO,SO}$ $F = \sigma\left[(A_1 \varepsilon_{G1})(1.050\alpha_{G1,G1}(1-p) - 1) + \ldots . \right.$ $\left. \ldots . + (A_0 \varepsilon_{GO})(1.050\alpha_{GO,GO}(1-p) - 1)\right]$	$q_{RW} = AT_1^4 + BT_G^4 + CT_0^4$ $A = 1.152\ \sigma A_1 p^2 (1-\alpha_{G1,S1})$ $B = \sigma p(0.050\ A_1 \varepsilon_{G1} + 1.028 A_0 \varepsilon_{GO})$ $C = -1.000\ \sigma A_0\ p$
Final Relations Incorporating Following Values $\sigma = 0.173 \times 10^{-8}$ $A_1 = 1.00\ ft^2$ (basis) $A_0 = 2.69\ ft^2$ $F_{O1} = 0.342$ $F_{OO} = 0.658$			$G = -0.168 \times 10^{-8}\ p$ $H = 0.173 \times 10^{-8} p\left[\varepsilon_{G1} + 0.920(1-p)(1-\alpha_{GO,GO})\varepsilon_{GO}\right]$ $J = 0.191 \times 10^{-8} p^2 (1-\alpha_{GO,SO})$	$D = 0.184 \times 10^{-8}\ p\ \alpha_{G1,S1}$ $E = 0.482 \times 10^{-8}\ p\ \alpha_{GO,SO}$ $F = -0.173 \times 10^{-8} \varepsilon_{G1} - 0.465 \times 10^{-8}\ \varepsilon_{GO}$ $+ 0.182 \times 10^{-8}(1-p)(\varepsilon_{G1}\alpha_{G1,G1} + \ldots .$ $+ \ldots . 2.69\ \varepsilon_{GO}\ \alpha_{GO,SO})$	$A = 0.199 \times 10^{-8} p^2 (1-\alpha_{G1,S1})$ $B = 0.173p(0.050\ \varepsilon_{G1} + 2.77\ \varepsilon_{GO})$ $C = -0.465 \times 10^{-8}\ p$ $+ 0.595 \times 10^{-8} p^2 (1-\alpha_{GO,SO})$

A, B, C, etc. become:

$$A = .199 \times 10^{-8} p^2 (1 - \alpha_{G1,S1}) \tag{109}$$

$$B = 0.173 \times 10^{-8} p (0.05 \varepsilon_{G1} + 2.77 \varepsilon_{GO}) \tag{110}$$

$$C = - .465 \times 10^{-8} p + .393 \times 10^{-8} p^2 (1 - \alpha_{GO,SO}) \tag{111}$$

$$D = 0.184 \times 10^{-8} p \alpha_{G1,S1} \tag{112}$$

$$E = .482 \times 10^{-8} p \alpha_{GO,SO} \tag{113}$$

$$F = - 0.173 \times 10^{-8} \varepsilon_{G1} - -.465 \times 10^{-8} \varepsilon_{GO} + 0.182 \times 10^{-8}(1-p)(\varepsilon_{G1}\alpha_{G1,G1} + 2.69 \varepsilon_{GO}\alpha_{GO,GO}) \tag{114}$$

$$G = - .168 \times 10^{-8} p \tag{115}$$

$$H = 0.173 \times 10^{-8} p \left[\varepsilon_{G1} + 0.920(1-p)(1-\alpha_{GO,GO}) \varepsilon_{GO}\right] \tag{116}$$

$$J = .191 \times 10^{-8} p^2 (1 - \alpha_{GO,SO}) \tag{117}$$

Equations (106), (107), and (108) above, together with the above expressions for the factors A, B, C, etc., constitute the relationships for the radiant heat transmission between an absorbing gas and the tube boundary walls of the particular illustrative annulus under the specified conditions. These relationships can be put to practical use provided a value for p, the emissivity of the metal surfaces, can be obtained. This problem is considered in the following section.

(a) Radiation Analysis - vi. Emissivity of the Steel Walls of the Plain Annulus

A procedure for interpreting certain of the tests on the bare tube in order to obtain values for the emissivity of the steel may be developed as follows:

A heat balance on the outer wall of the annulus yields the equation

$$q_{RW} = q_{CW} + q_L' \qquad (118)$$

(The equation is written for a length of equipment corresponding to that in which the inner tube exposes an area of one square foot.)

where q_{RW} = the total radiant heat received by the wall, Btu/hr.

q_{CW} = the total heat transferred from the wall by "back" convection to the steam, Btu/hr.

q_L' = the heat loss from the wall by conduction through the wall and insulation, Btu/hr.

The term q_{RW} has been expressed as

$$q_{RW} = AT_1^4 + BT_G^4 + CT_0^4 \qquad (107)$$

Substituting for T_1, T_G, and T_0 the mean values Θ_2, Θ_3, and Θ_4 as defined in Table IX, the equation becomes:

$$q_{RW} = A\Theta_2^4 + B\Theta_3^4 + C\Theta_4^4 \qquad (119)$$

The quantity q_{CW} may be expressed

$$q_{CW} = h_o (1.69) (\Theta_4 - \Theta_3) \qquad (120)$$

where h_o is a convection coefficient, Btu/hr.°F.ft.^{2},

1.69 is the ratio of surfaces of the outer and the inner wall,

and $(\theta_4 - \theta_3)$ is the average difference in temperature between the wall and the steam, °F.

The coefficient h_o may now be expressed in terms of a Dittus-Boelter type equation as

$$h_o = M \frac{K}{D_v} \left(\frac{C\mu}{K}\right)^{0.4} \left(\frac{D_v W}{\mu S_{min}}\right)^{0.8} \qquad (121)$$

where M is an unknown constant. Substitution of Equations (119), (120), and (121) in Equation (118) results in

$$q_{RW} = A\theta_2^4 + B\theta_3^4 + C\theta_4^4$$

$$= 1.69\, M \frac{K}{D_v} \left(\frac{C\mu}{K}\right)^{0.4} \left(\frac{D_v W}{\mu S_{min}}\right)^{0.8} (\theta_4 - \theta_3) + q_L' \qquad (122)$$

Rearranging,

$$\theta_4 - \theta_3 = \frac{A\theta_2^4 + B\theta_3^4 + C\theta_4^4 - q_L'}{1.69\, M(K/D_v)(C\mu/K)^{0.4}(D_v W/\mu S_{min})^{0.8}} \qquad (123)$$

This equation indicates two features of interest. First, when $\theta_4 - \theta_3 = 0$, q_L' becomes equal to q_{RW}. It will be recalled that q_L is a measured quantity and that

$$A = 0.199 \times 10^{-8}\, p^2\, (1 - \alpha_{G1,S1}) \qquad (109)$$

$$B = 0.0442 \times 10^{-8}\, p\, (0.196\, \varepsilon_{G1} + 10.9\, \varepsilon_{GO}) \qquad (110)$$

$$C = -0.465 \times 10^{-8} p + 0.391 \times 10^{-8} p^2 (1-\alpha_{GO,SO}) \quad (111)$$

in which the various absorptivities and emissivities are known as functions of temperature and pressure. Equation (123) indicates therefore that for tests in which $\Theta_4 - \Theta_3 = 0$, values for p, the emissivity of steel, may be computed from the equality between the radiation to the wall and the heat loss.

The second feature of interest of Equation (123) is that, if the numerator of the right hand side, i.e., $A\Theta_2^4 + B\Theta_3^4 + C\Theta_4^4 - q_L'$, should remain approximately constant, then $\Theta_4 - \Theta_3$ should indicate a linear relationship when plotted against the reciprocal of $(K/D_v)(C\mu/K)^{0.4}(D_vW/\mu S_{min})^{0.80}$.

There are, unfortunately, no tests in which the condition $\Theta_4 - \Theta_3 = 0$ is exactly satisfied, but several tests are available in which $\Theta_4 - \Theta_3$ is a relatively small positive or negative number. Making use of the second feature of Equation (123), $\Theta_4 - \Theta_3$ is plotted against the reciprocal of $(K/D_v)(C\mu/K)^{0.4}(D_vW/\mu S_{min})^{.8}$ in Figure 43 for all those bare tube tests in which the value of $\Theta_4 - \Theta_3$ is comparatively small. It is seen that two parallel straight lines represent the data, one line for each test pressure. This is as would be expected if the numerator of Equation (123) were approximately constant for tests at each pressure. Apparently such is the case.

Figure 43 now permits an accurate estimation for each pressure of the value of the reciprocal of $(K/D_v)(C\mu/K)^{0.4}(D_vW/\mu S_{min})^{0.8}$ corresponding to equality of Θ_4 and Θ_3. These two conditions correspond to the conditions in which $A\Theta_2^4 + B\Theta_3^4 + C\Theta_4^4 = q_L'$ at each pressure.

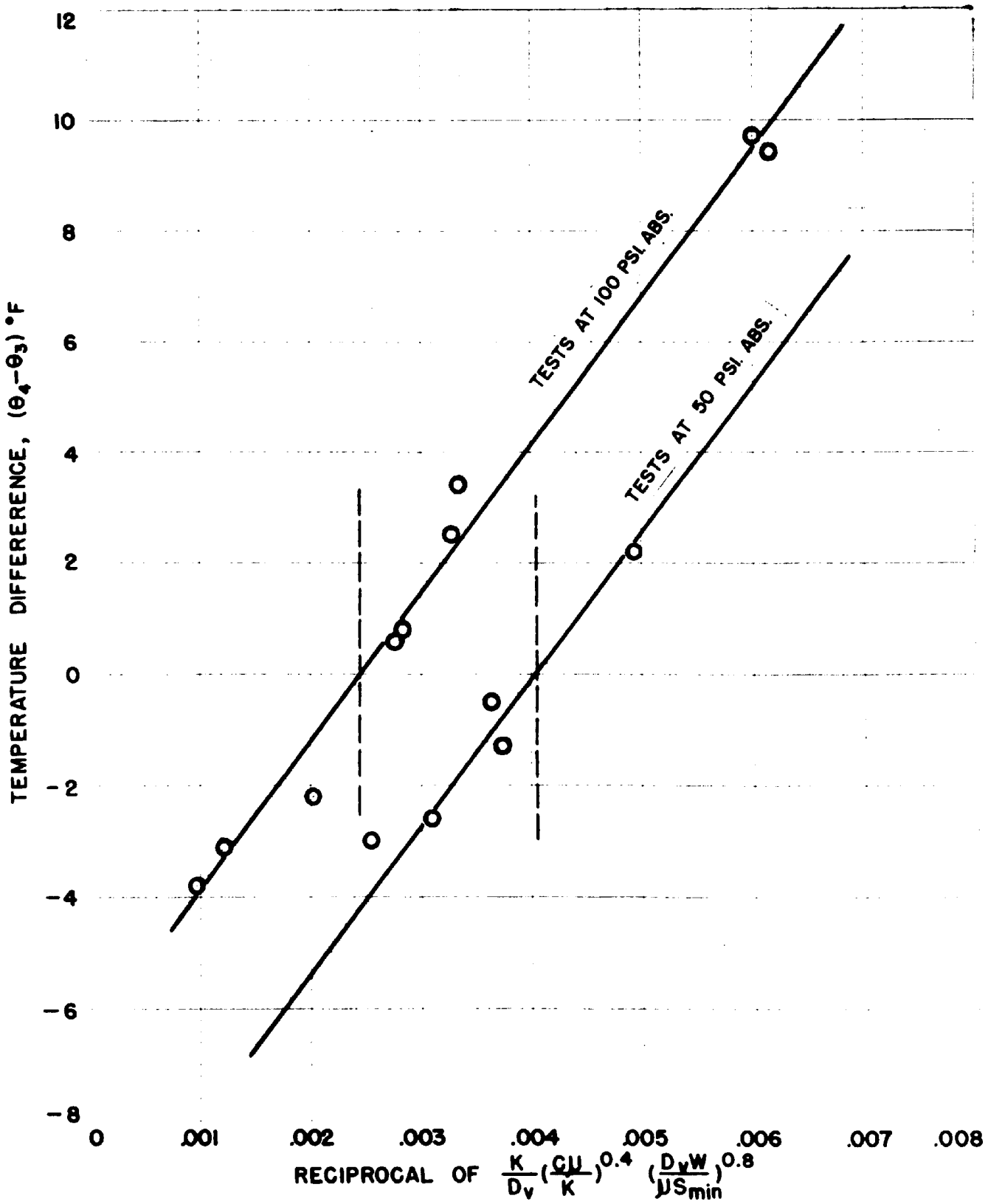

FIGURE 43

APPROACH OF WALL AND STEAM TEMPERATURES

The equality between $A\Theta_2^4 + B\Theta_3^4 + C\Theta_4^4$ and q_L' may be approximately satisfied at other values of the abscissa of Figure 43, but it is exactly satisfied, for the pressures of 50 and 100 psi. abs. at the indicated values of .00245 and .00405.

Values for the emissivity of steel may now be obtained by solving the equality between q_{RW} and q_L' for each test represented, and then plotting the resulting values of p vs. the reciprocal of $(K/D_v)(C\mu/K)^{0.4}(D_vW/\mu S_{min})^{0.8}$. The values of emissivity corresponding to an abscissa of .00245 at 50 psi. abs. and .00405 at 100 psi. abs. are the values which exactly satisfy the equality between q_{RW} and q'_L. These values should be identical.

Table XIX presents the details of the analysis of those tests (Numbers 58A, 59, 64, 65, 66 at 100 psi. abs. and 68, 69, 73, 74, and 75 at 50 psi. abs.) in which Θ_4 and Θ_3 are reasonably close.

Columns 1 and 2 present the test number and the pressure. Column 3 presents the reciprocal of $(K/D_v)(C\mu/K)^{0.8}(D_vW/\mu S_{min})^{0.8}$ which is computed from Column 10 of Table XXII. Columns 4 and 5 respectively show the surface temperature of the inner tube in °F. (obtained from Table IX, Column 5) and the fourth power of this temperature in °R. divided by 100.

Columns 6 and 7 give the mean steam temperature and the mean outside wall temperature in °F. These figures are from Table IX, Columns 6 and 7. The fourth power of the mean of the steam and the wall temperatures, in °R. and divided by 100, is presented in Column 8.

Columns 9, 11, 12, and 14 present $1-\alpha_{G1,S1}$, ε_{G1}, ε_{GO}, and $1-\alpha_{GO,SO}$, each evaluated for the corresponding values of the pressure

TABLE XIX

DETERMINATION OF THE EMISSIVITY OF THE STEEL WALLS OF THE PLAIN ANNULUS

1	2	3	4	5	6	7	8	9	10	11	12	13	14	15	16	17	18
Test Number	Pressure P, psi. abs.	Reciprocal of $\frac{K}{D_v}\left(\frac{C\mu}{K}\right)^{.4}$ times $\left(\frac{D_v W}{\mu S_{min}}\right)^{.8}$	θ_2 °F	$\left(\frac{\theta_2}{100}\right)^4$	θ_3 °F	θ_4 °F	$\left(\frac{\theta_m}{100}\right)^4$	$1-\alpha_{G1,S1}$	A	ε_{G1}	ε_{G0}	B	$1-\alpha_{G0,S0}$	C	(B + C)	q_L'	p
58A	100	.00281	494	8280	354.4	355.2	4410	.389	$.0775p^2$	.640	.695	.341p	.344	$-.465p + .134p^2$	$.135p^2 - .124p$	201	.683
59	"	.00328	494	8280	355.9	358.4	4460	.391	$.0779p^2$	.640	.695	.341p	.345	$-.465p + .135p^2$	$.135p^2 - .124p$	202	.681
64	"	.000975	494	8280	388.0	384.0	5120	.387	$.0771p^2$	.637	.693	.340p	.343	$-.465p + .134p^2$	$.134p^2 - .125p$	226	.722
65	"	.00124	494	8280	388.1	385.0	5150	.387	$.0771p^2$	.637	.693	.340p	.343	$-.465p + .134p^2$	$.134p^2 - .125p$	228	.722
66	"	.00202	495	8320	384.4	382.0	5050	.387	$.0771p^2$	.637	.693	.340p	.343	$-.465p + .134p^2$	$.134p^2 - .125p$	224	.716
68	50	.00296	496	8350	386.1	385.1	5100	.573	$.1140p^2$	.435	.492	.241p	.528	$-.465p + .206p^2$	$.206p^2 - .224p$	226	.724
69	"	.00373	497	8390	376.0	375.0	4890	.574	$.1141p^2$	.435	.492	.241p	.529	$-.465p + .207p^2$	$.207p^2 - .224p$	218	.711
73	"	.00311	495	8320	370.9	368.3	4740	.575	$.1142p^2$	.434	.491	.240p	.527	$-.465p + .206p^2$	$.206p^2 - .225p$	209	.706
74	"	.00369	496	8350	367.6	367.1	4680	.575	$.1142p^2$	.434	.491	.240p	.527	$-.465p + .206p^2$	$.206p^2 - .225p$	211	.704
75	"	.00497	496	8350	362.9	365.1	4610	.575	$.1142p^2$	.434	.491	.240p	.527	$-.465p + .206p^2$	$.206p^2 - .225p$	207	.700

and temperatures according to the methods previously outlined. Column 10 gives the value of A expressed in terms of the emissivity of the steel by substitution of the value of $1-\alpha_{Gl,Sl}$ in the relation

$$A = 0.199 \times 10^{-8} p^2 (1 - \alpha_{Gl,Sl}) \qquad (109)$$

Similarly, Columns 13 and 15 give the values of the factors B and C. Column 16 tabulates the sum of B and C, which may be taken to operate upon Column 8 since the values of θ_3 and θ_4 are so nearly alike.

Column 17 presents the value of q_L' obtained by dividing Column 16 of Table IX by 5.89 in order to express this quantity on the basis of a square foot of inner tube surface. Finally, Column 18 presents the value of p obtained by solution of the equality between $A\theta_2^4 + (B + C)\theta_m^4$ and q_L'.

These values of p are plotted against the reciprocal of $(K/D_v)(C\mu/K)^{0.4}(D_vW/\mu S_{min})^{0.8}$ in Figure 44. The vertical dotted lines in this figure correspond to those in Figure 43, where $\theta_4 - \theta_3 = 0$ and the equality between q_{RW} and q_L' is strictly satisfied. The values of 0.695 and 0.705 which are obtained are considered to be excellent checks.

The good agreement between the two values obtained for the emissivity of steel, and the fact that these values lie nicely within the range of reported data,(26) and (28), offer confirmation to the entire process of obtaining the emissivity of steam by extrapolation of the data on water vapor.

It is concluded, therefore, that the emissivity of the steel walls of the annulus is 0.70, and this value is employed in the subsequent evaluation of the radiation equations for the plain annulus.

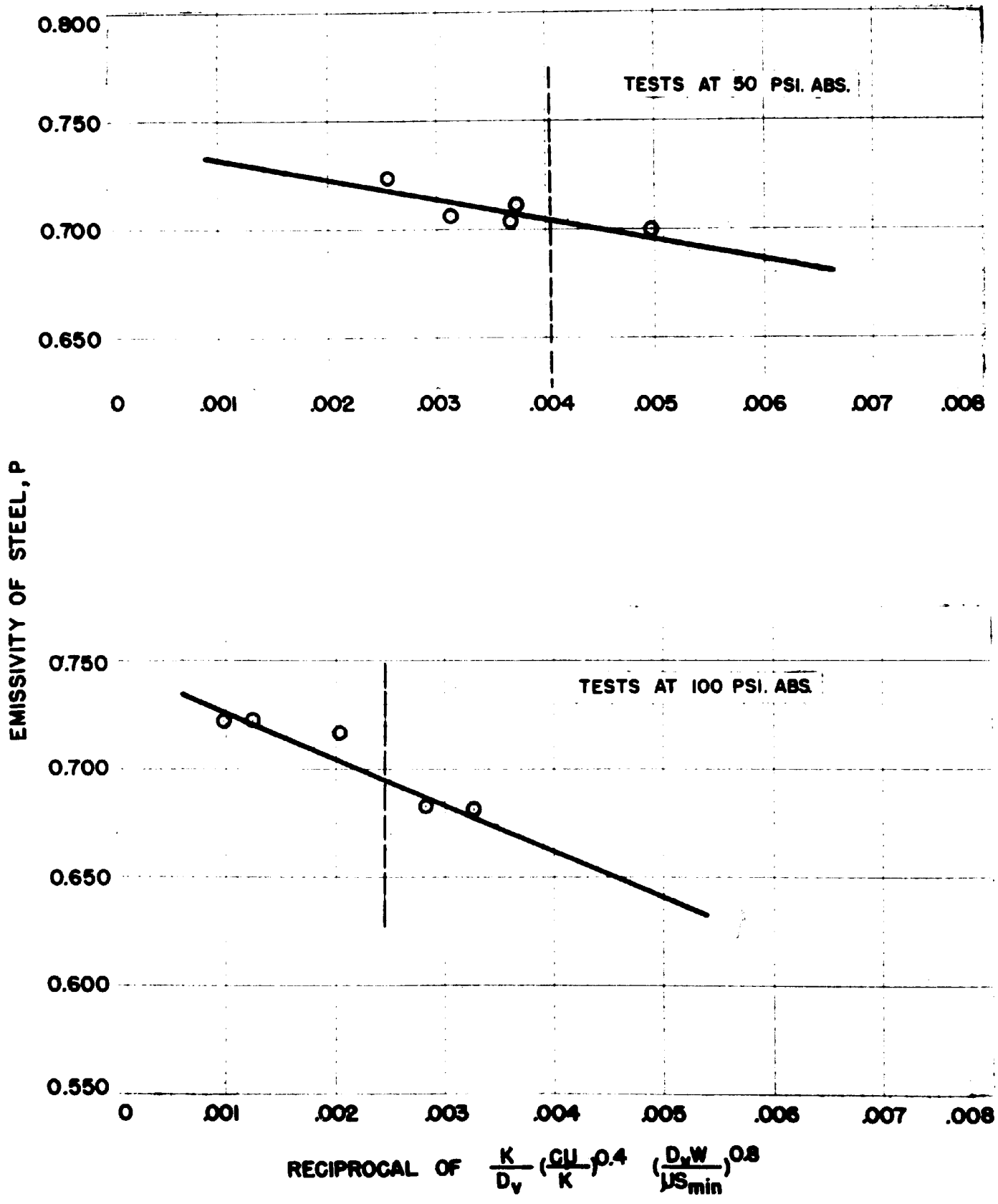

FIGURE 44

EMISSIVITY OF STEEL

(a) Radiation Analysis - vii. Final Radiation Equations

Having now obtained a value for the emissivity of the steel walls of the plain annulus, it is possible to evaluate the radiation constants A to J for any set of pressure and temperature conditions.

The numerical values for these constants at eight different pressure-temperature conditions are computed in Table XX.

Column 1 of this table lists the quantities which are evaluated. Columns 2 to 5 inclusive refer to a pressure of 50 psi. abs.; Columns 6 to 9 inclusive, to 100 psi. abs.; all Columns refer to an inner tube temperature Θ_2 of 500°F.

In Columns 2, 3, 6, and 7 the steam temperature Θ_3 and the outer wall temperature Θ_4 are the same and equal to 300°F. or 400°F. as indicated. In Columns 4, 5, 8, and 9 the wall temperature Θ_4 is 40°F. higher than the steam temperature, which again is 300°F. or 400°F. as indicated.

The first nine entries of Column 1 are absorptivity and emissivity quantities required for the evaluation of the factors A, B, C, D, E, F, G, H, and J as required by Equations (109) to (117) inclusive. These quantities are evaluated by the methods previously indicated, i.e., from the relations of Table XVI and Figure 34.

The remaining nine entries of Column 1 are the radiation factors. It will be noticed that opposite each factor, and under each column, two figures appear. The first of these figures is the value of the factor as computed from the equation for it and employing absorptivities and emissivities correct for the pressure and temperatures

TABLE XX

NUMERICAL EVALUATION OF THE RADIATION CONSTANTS

A, B, C, D, E, F, G, H AND J

1	2	3	4	5	6	7	8	9
	Pressure = 50 psi. abs. θ_2 = 500°F.				Pressure = 100 psi. abs. θ_2 = 500°F.			
Quantity	$\theta_4 - \theta_3 = 0$		$\theta_4 - \theta_3 = 40$		$\theta_4 - \theta_3 = 0$		$\theta_4 - \theta_3 = 40$	
	θ_3 = 300	θ_3 = 400	θ_3 = 300	θ_3 = 400	θ_3 = 300	θ_3 = 400	θ_3 = 300	θ_3 = 400
$1 - \alpha_{G1,S1}$	.597	.588	.597	.588	.415	.393	.415	.393
ϵ_{G1}	.446	.434	.446	.434	.642	.638	.642	.638
ϵ_{G0}	.500	.489	.500	.489	.700	.695	.700	.695
$1 - \alpha_{G0,S0}$	.500	.511	.513	.519	.300	.305	.318	.323
$\alpha_{G0,S0}$	.500	.489	.487	.481	.700	.695	.682	.677
$\alpha_{G1,S1}$	.403	.412	.403	.412	.585	.607	.585	.607
$\alpha_{G1,G1}$	.782	.766	.782	.766	.844	.847	.844	.847
$\alpha_{G0,G0}$	.800	.783	.800	.783	.871	.867	.871	.867
$1 - \alpha_{G0,G0}$	.200	.217	.200	.217	.129	.133	.129	.133
A x 10^8	.058 .061	.057 .060	.058 .061	.057 .060	.041 .041	.038 .038	.041 .041	.038 .038
B x 10^8	.171 .173	.167 .169	.171 .173	.167 .169	.239 .238	.237 .236	.239 .238	.237 .236
-C x 10^8	.229 .233	.227 .231	.227 .231	.226 .230	.268 .273	.267 .272	.264 .272	.263 .271
D x 10^8	.052 .055	.053 .056	.052 .055	.053 .056	.075 .075	.078 .078	.075 .075	.078 .078
E x 10^8	.168 .174	.165 .171	.164 .171	.162 .169	.236 .238	.234 .236	.229 .235	.228 .234
-F x 10^8	.232 .230	.228 .225	.232 .230	.228 .225	.317 .319	.315 .316	.317 .319	.315 .316
-G x 10^8	.118 .116	.118 .116	.118 .116	.118 .116	.118 .116	.118 .116	.118 .116	.118 .116
H x 10^8	.057 .057	.056 .056	.057 .057	.056 .056	.081 .081	.080 .080	.081 .081	.080 .080
J x 10^8	.047 .059	.048 .060	.048 .060	.049 .061	.028 .035	.029 .036	.030 .037	.030 .037

involved. These figures, however, require some slight adjustment to compensate for inconsistencies in the emissivity and absorptivity data and also in the previous adjustment process. The second figure therefore is the adjusted value of the factor.

The key to the adjustment process is the heat balance on any ray which requires that its fractions total zero (when an emitted ray is given a negative sign, as in this analysis). Reference to Table XVIII will indicate that this concept leads to the requirement that, at any pressure-temperature condition,

$$A + D + G = 0 \qquad (124)$$

$$F + B + H = 0 \qquad (125)$$

$$E + C + J = 0 \qquad (126)$$

The calculated factors are therefore adjusted slightly to conform to these three equations. The adjustment is arbitrary, but in most cases it is small in amount.

The adjusted factors, i.e., the second figures in Columns 2 to 9 inclusive, are plotted against temperature in Figures 45, 46, 47, 48, 49, and 50. (The multiplier 10^{-8} is omitted in these figures and henceforth, it being understood that all temperatures are divided by 100 before being raised to the fourth power.) Figures 45 and 46 present the factors A, B, C, and B + C at 50 psi. abs. and 100 psi. abs., respectively. Figures 47 and 48 present the factors D, E, F, and E + F; and Figures 49 and 50, the factors G, H, J, and H + J.

A requirement of the second law of thermodynamics is that when all temperatures, θ_2, θ_3, and θ_4, are identical

$$A + B + C = 0 \qquad (127)$$

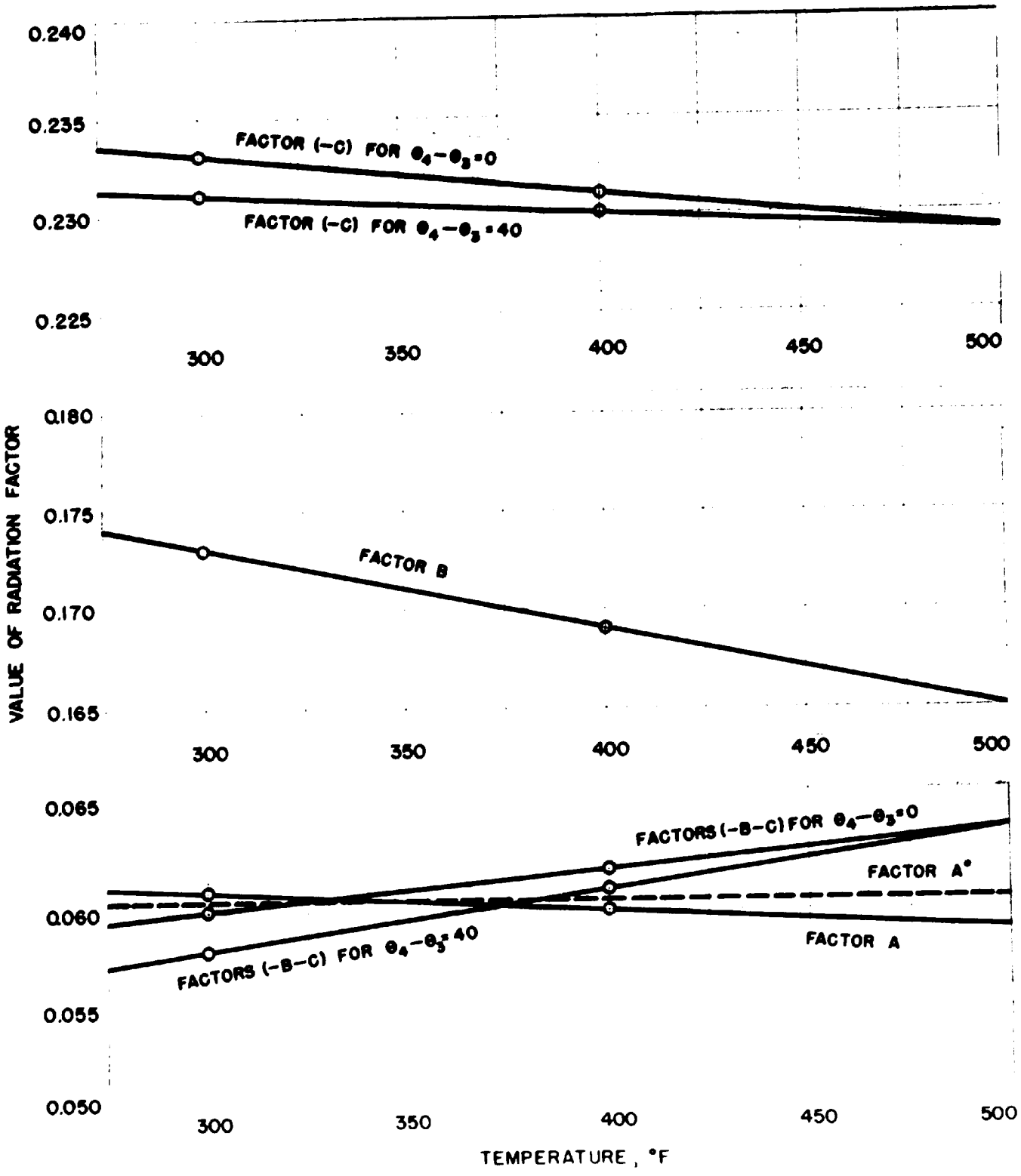

FIGURE 45

RADIATION FACTORS A, B, AND C

(SUPERHEATED STEAM AT 50 PSI. ABS.)

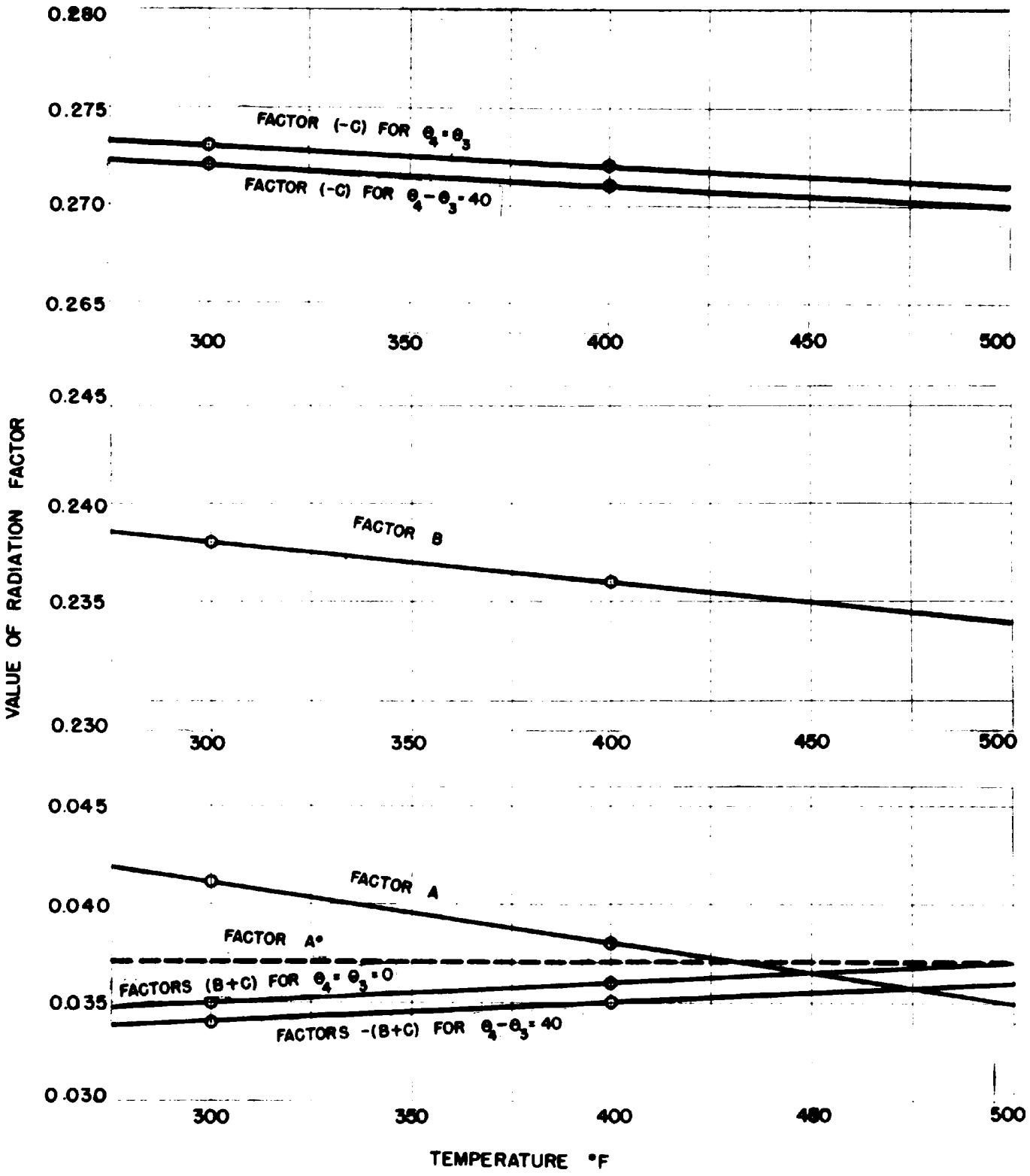

FIGURE 46.

RADIATION FACTORS A, B AND C
(SUPERHEATED STEAM AT 100 PSI ABS)

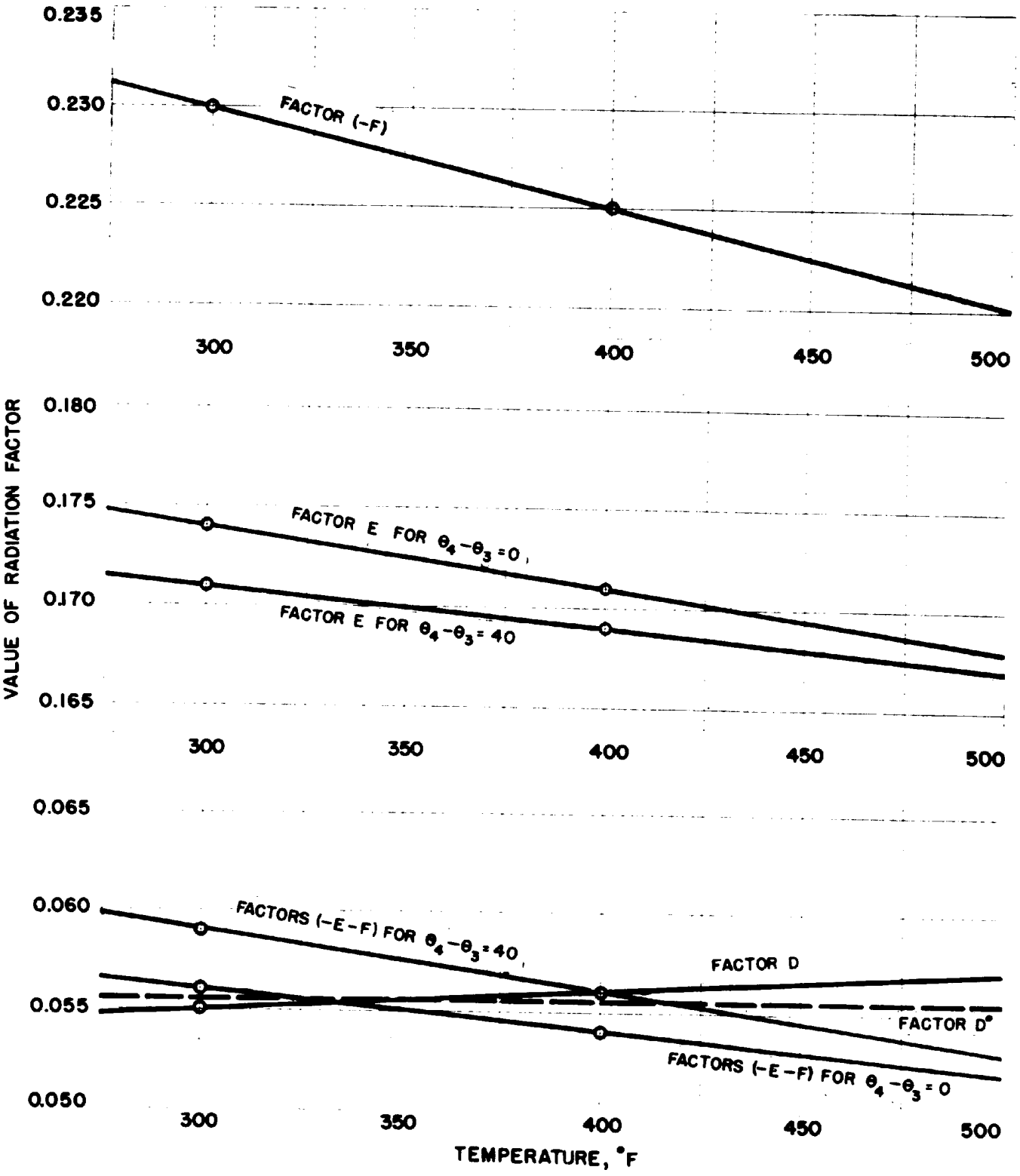

FIGURE 47

RADIATION FACTORS D,E, AND F

(SUPERHEATED STEAM AT 50 PSI. ABS.)

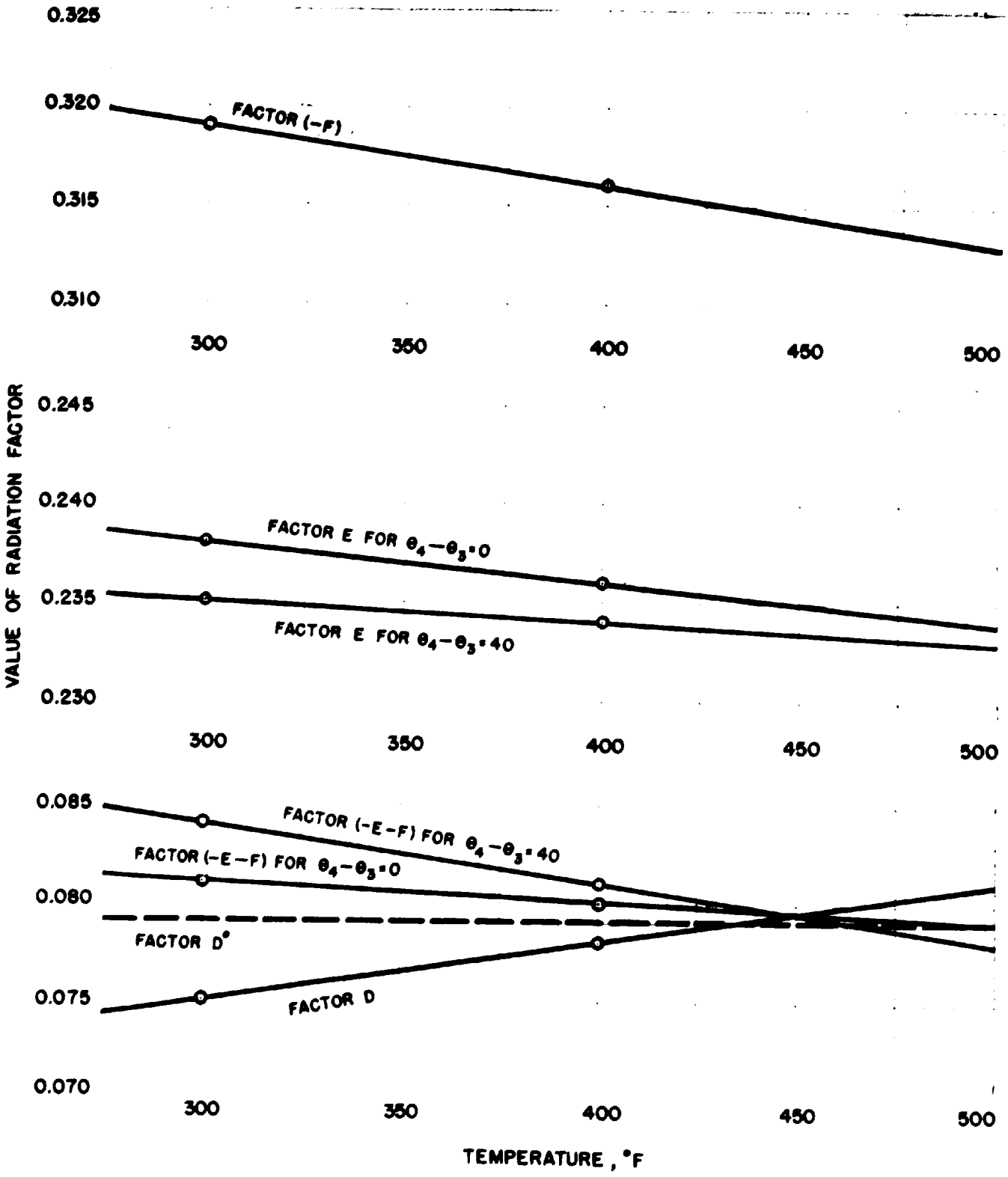

FIGURE 48

RADIATION FACTOR D, E, AND F

(SUPERHEATED STEAM AT 100 PSI. ABS.)

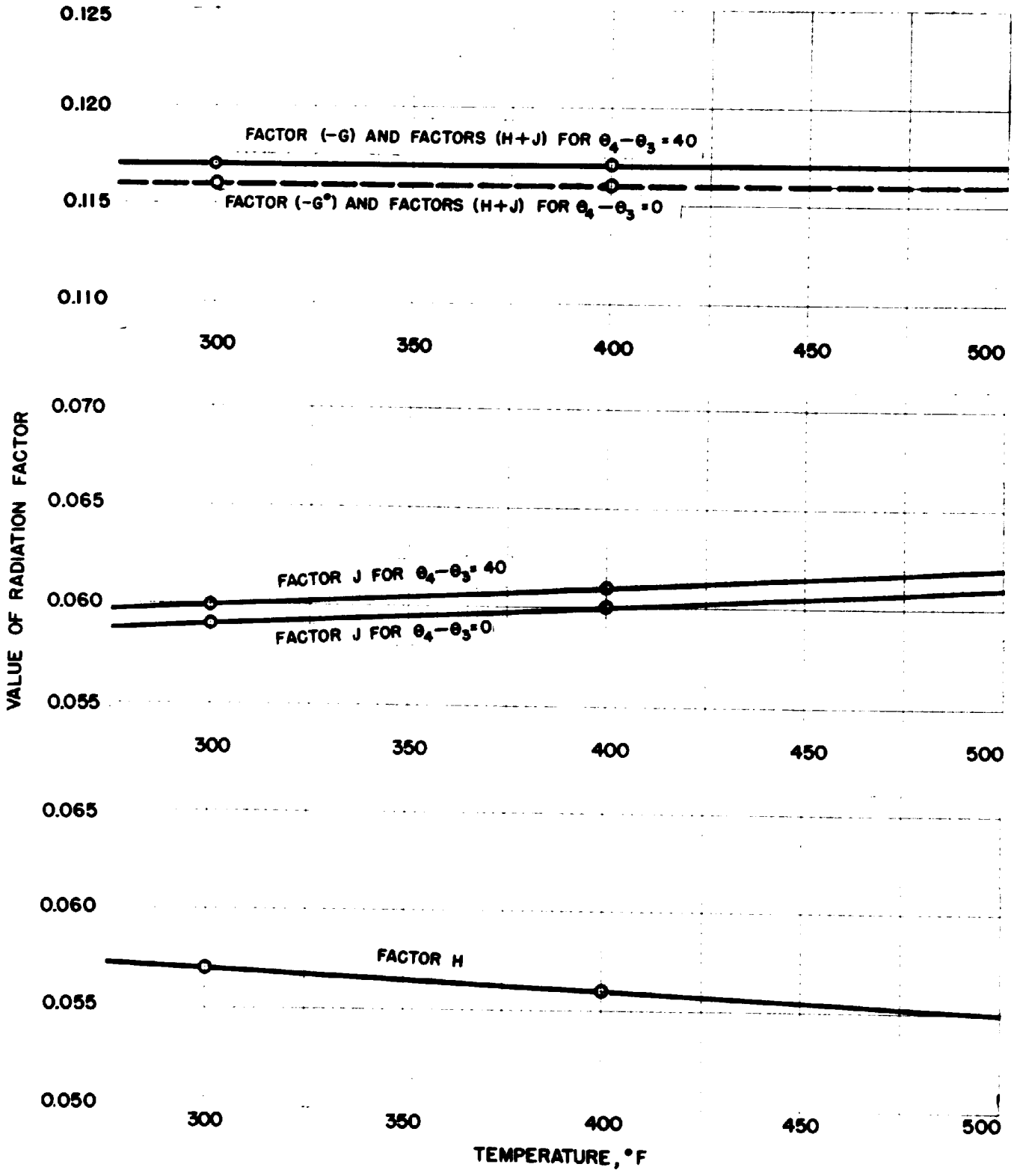

FIGURE 49

RADIATION FACTORS G, H, AND J

(SUPERHEATED STEAM AT 50 PSI. ABS.)

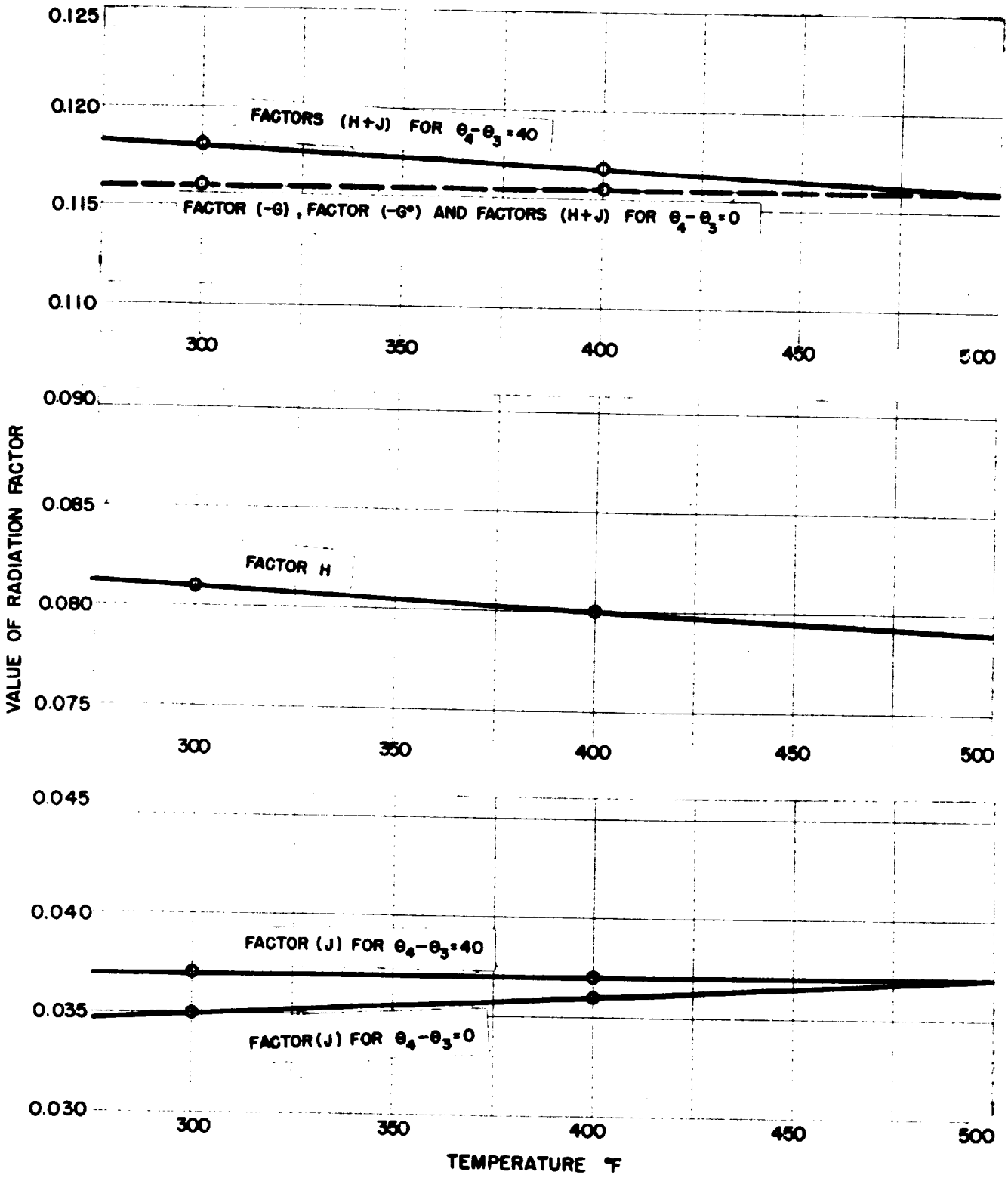

FIGURE 50.

RADIATION FACTORS G, H, AND J
(SUPERHEATED STEAM AT 100 PSI ABS)

$$D + E + F = 0 \qquad (128)$$

$$G + H + J = 0 \qquad (129)$$

Thus, when $\theta_3 = \theta_4 = 500°F.$, Equations (127), (128), and (129) should be satisfied. Examination of Figures 45 through 50 indicates that these relationships are approximately but not exactly satisfied. Since this is a very critical test of the relative magnitudes and the temperature consistency of the factors, the agreement is considered satisfactory. However, in the light of the slight disagreement with the requirements of Equations (127), (128), and (129) at 500°F., and the slow change in the values of all the factors with temperature, it is considered satisfactory to assume all factors constant with temperature and to adjust the factors A, D, and G to A^o, D^o, and G^o as shown in the figures. The values of A^o, D^o, and G^o are chosen to represent the averages respectively between A and B + C, D and E + F, and G and H + J, and at the same time to satisfy the requirement of Equation (124) that

$$A^o + D^o + G^o = 0$$

The factors A^o, D^o, and G^o are therefore taken as functions of pressure only and have the values:

	Pressure, 50 psi. abs.	Pressure, 100 psi. abs.
A^o	.0605	.0370
D^o	.0555	.0790
$-G^o$	.116	.116

Values of the other factors, i.e., B, C, E, F, H, and J, are unnecessary in view of the simplifications which have been made. This is because B + C may be taken as $-A^o$, E + F as $-D^o$, and H + J as $-G^o$, and these

quantities may be considered, with negligible error, to operate on the average of the fourth powers of θ_3 and θ_4.

Thus the final simplified radiation equations for the plain annulus become:

$$q_{RT} = G^{\circ} \left[(\theta_2/100)^4 - (\theta_m/100)^4 \right] \qquad (130)$$

$$q_{RW} = A^{\circ} \left[(\theta_2/100)^4 - (\theta_m/100)^4 \right] \qquad (131)$$

$$q_{RG} = D^{\circ} \left[(\theta_2/100)^4 - (\theta_m/100)^4 \right] \qquad (132)$$

where

$$(\theta_m/100)^4 = 1/2 \left[(\theta_3/100)^4 + (\theta_4/100)^4 \right] \qquad (133)$$

and the numerical values of A°, D°, and G° are given above.

(a) Radiation Analysis - viii. Evaluation of the Radiation Heat Transfer

The evaluation of the radiation heat transfer in the plain annulus may now be carried out with Equations (130), (131), (132), and (133) and the values of the constants G°, A°, and D° as given above. This is done in Table XXI.

Columns 1 and 2 of Table XXI give the test number and type of tube. Columns 3, 4, and 5 report the values of θ_2, θ_3, and θ_4; the inner tube, steam, and outer wall temperatures respectively, all in degrees Rankine. The values are obtained from Columns 5, 6, and 7 of Table IX by adding 460.

Columns 6, 7, and 8 give the values of $(\theta_2/100)^4$, $(\theta_3/100)^4$, and $(\theta_4/100)^4$; Column 9, the value of $(\theta_m/100)^4$, which represents the

the mean of Columns 7 and 8. Column 10 presents the "radiation driving force," $(\theta_2/100)^4 - (\theta_m/100)^4$, obtained from Columns 6 and 9.

The radiation quantities q_{RG}, q_{RW}, and $-q_{RT}$, the net radiation received by the steam, by the outer wall, and from the inner tube, are presented in Columns 11, 12, and 13. These quantities are evaluated from Equations (130), (131), and (132) with the proper numerical values of G°, A°, and D°. Since Equations (130), (131), and (132) are all on the basis of one square foot of inner tube surface, it is necessary to multiply the constants G°, A°, and D° by 5.89 (see Table I), which represents the total heat transfer surface of the inner tube.

Column 14 presents the logarithmic mean temperature difference, $(\theta_2 - \theta_3)_{lm}$, as previously computed in Table IX, Column 10. This value is used to calculate the radiation coefficient h_R, which is reported in Column 16. The coefficient h_R has been defined by the equation

$$q_{RT} = h_R (A_o + \phi A_f) (\theta_2 - \theta_3)_{lm} \qquad (36)$$

where $(A_o + \phi A_f)$ represents the effective area of the inner tube. The coefficient is calculated from Columns 13 and 14 of Table XXi and Column 22 of Table IX, which gives the effective area term, $(A_o + \phi A_f)$. In the case of the bare tube, the finned area is zero and $(A_o + \phi A_f) = A_o = 5.89$ square feet.

It is to be noted that the coefficients h_R for the bare tube vary only over the range of 3.06 to 3.51, with a calculated average value of 3.30. This is a perfect check with the value obtained graphically in Figure 26, which also was 3.30. Further as a matter of interest, the values of the radiation coefficients are plotted against $(\theta_2 - \theta_3)_{lm}$ in

TABLE XXI

RADIATION HEAT TRANSFER CALCULATIONS

1	2	3	4	5	6	7	8	9	10	11	12	13	14	15
Test Number	Type of Inner Tube	θ_2, °R.	θ_3, °R.	θ_4, °R.	$(\theta_2/100)^4$	$(\theta_3/100)^4$	$(\theta_4/100)^4$	$(\theta_m/100)^4$	$\left(\frac{\theta_2}{100}\right)^4 - \left(\frac{\theta_m}{100}\right)^4$	q_{RG}	q_{RW}	q_{RT}	$(\theta_2-\theta_3)_{lm}$	h_R
Column Reference →		Table IX, 5	Table IX, 6	Table IX, 7	Table XXI, 3	Table XXI, 4	Table XXI, 5	Table XXI, 7, 8	Table XXI, 6, 9	Table XXI, 10 Table II, 3	Table XXI, 10 Table II, 3	Table XXI, 10 Table II, 3	Table IX, 10	Table IX, 22 Table XXI, 13, 14
58	BARE	953	815	815	8250	4410	4410	4410	3840	1785	840	2625	137	3.26
58A	"	954	814	815	8285	4390	4410	4400	3885	1810	845	2655	138	3.26
59	"	954	816	818	8285	4430	4480	4455	3830	1780	835	2615	137	3.26
59A	"	953	815	818	8250	4410	4480	4445	3805	1770	830	2600	137	3.22
60	"	954	816	826	8285	4430	4660	4545	3740	1740	815	2555	137	3.17
60A	"	957	816	826	8390	4430	4660	4545	3845	1790	840	2630	139	3.21
61	"	952	810	811	8215	4350	4330	4340	3875	1270	1380	2650	138	3.26
61A	"	957	798	811	8390	4070	4330	4200	4190	1370	1490	2860	156	3.11
62	"	955	804	807	8320	4180	4240	4210	4110	1340	1460	2800	148	3.22
62A	"	957	796	807	8390	4010	4240	4125	4265	1395	1520	2915	162	3.06
63	"	955	801	814	8320	4120	4390	4255	4065	1330	1450	2780	151	3.13
63A	"	958	791	814	8425	3920	4390	4155	4270	1395	1520	2915	161	3.08
64	"	954	846	844	8285	5175	5075	5125	3160	1470	690	2160	106	3.46
65	"	954	848	845	8285	5175	5100	5138	3147	1460	685	2145	106	3.44
66	"	955	844	842	8320	5080	5030	5055	3265	1520	710	2230	111	3.42
67	"	956	851	848	8355	5250	5170	5210	3145	1030	1120	2120	105	3.43
68	"	956	846	843	8355	5130	5060	5095	3260	1070	1160	2230	108	3.51
69	"	957	836	835	8390	4890	4860	4875	3515	1150	1250	2400	119	3.43
70	"	954	841	836	8285	5010	4890	4950	3335	1090	1190	2280	114	3.40
71	"	955	841	836	8320	5010	4890	4950	3370	1570	735	2305	115	3.40
72	"	956	830	828	8355	4750	4700	4725	3630	1690	790	2480	125	3.37
73	"	955	831	828	8320	4775	4700	4738	3582	1170	1275	2445	124	3.35
74	"	956	828	827	8355	4700	4680	4690	3665	1200	1305	2505	127	3.35
75	"	956	823	825	8355	4590	4630	4610	3745	1225	1330	2555	132	3.29
76	LONGITU-DINAL FIN	954	886	876	8285	6155	5895	6025	2260	1300	610	1910	65.6	1.15
77	"	956	884	874	8355	6105	5840	5975	2380	1370	640	2010	69.6	1.11
78	"	955	877	868	8320	5925	5680	5805	2515	1445	680	2125	74.0	1.08
79	"	954	880	872	8285	6000	5785	5895	2390	965	1055	2020	69.7	1.07
80	"	954	873	869	8285	5820	5705	5765	2520	1020	1110	2130	75.7	1.01
81	"	955	858	861	8320	5420	5500	5460	2860	1160	1260	2420	88.9	0.94
82	"	955	844	839	8320	5060	4950	5005	3315	1905	895	2800	103.5	1.00
83	"	954	856	852	8285	5370	5270	5320	2965	1705	800	2505	92.1	0.98
84	"	954	858	859	8285	5425	5450	5440	2845	1640	765	2405	88.9	0.94
85	"	952	833	841	8215	4810	5000	4905	3910	1585	1720	3305	110.2	1.04
86	"	953	835	853	8250	4855	5300	5080	3170	1285	1395	2680	109.2	0.84
87	"	954	835	860	8285	4855	5475	5165	3120	1265	1375	2640	105.9	0.84
88	"	954	911	904	8285	6900	6685	6795	1490	857	403	1260	41.8	1.28
89	"	954	912	903	8285	6930	6650	6790	1495	860	405	1265	40.5	1.27
90	"	955	908	899	8320	6800	6530	6665	1655	953	447	1400	46.0	1.21
91	"	951	880	871	8180	6000	5755	5880	2300	930	1015	1945	68.8	1.10
92	"	950	881	873	8145	6025	5810	5920	2225	900	980	1880	66.5	1.07
93	"	952	881	875	8215	6025	5865	5945	2270	920	1000	1920	67.4	1.04

TABLE XXI, CONTINUED

RADIATION HEAT TRANSFER CALCULATIONS

1	2	3	4	5	6	7	8	9	10	11	12	13	14	15
Test Number	Type of Inner Tube	θ_2, °R.	θ_3, °R.	θ_4, °R.	$(\theta_2/100)^4$	$(\theta_3/100)^4$	$(\theta_4/100)^4$	$(\theta_m/100)^4$	$\left(\frac{\theta_2}{100}\right)^4 - \left(\frac{\theta_m}{100}\right)^4$	q_{RG}	q_{RT}	q_{RT}	$(\theta_2-\theta_3)_{lm}$	h_R
Column Reference →		Table II, 5	Table II, 6	Table II, 7	Table XXI, 3	Table XXI, 4	Table XXI, 5	Table XXI, 7,8	Table XXI, 6,9	Table XXI, 10 Table II, 3	Table XXI, 10 Table II, 3	Table XXI, 10 Table II, 3	Table II, 10	Table II, 22 Table XXI, 13, 14
94	"STAR" FIN	953	896	904	8250	6455	6685	6570	1680	966	454	1420	45.2	1.32
95	"	952	893	906	8215	6375	6745	6560	1655	953	447	1400	45.4	1.23
96	"	953	873	900	8250	5820	6560	6190	2060	1185	555	1740	58.2	1.23
97	"	951	859	885	8180	5450	6145	5800	2380	965	1050	2015	65.6	1.17
98	"	952	852	902	8215	5275	6625	5950	2265	917	998	1915	74.0	0.95
99	"	954	840	899	8285	4980	6530	5755	2530	1085	1115	2140	86.1	0.86
100	"	951	901	904	8180	6595	6685	6640	1540	885	415	1300	41.3	1.48
101	"	951	894	901	8180	6400	6595	6500	1680	966	454	1420	46.5	1.37
102	"	954	883	900	8285	6080	6560	6320	1965	1130	530	1660	52.7	1.24
103	"	961	899	911	8460	6530	6900	6715	1745	707	768	1475	48.1	1.23
104	"	960	893	911	8425	6375	6900	6635	1790	725	790	1515	55.5	1.03
105	"	960	885	910	8425	6130	6865	6500	1925	780	845	1625	59.8	1.00
106	"	957	907	913	8390	6770	6955	6865	1525	618	672	1290	39.6	1.37
107	"	959	899	912	8460	6530	6930	6730	1730	700	760	1460	48.8	1.17
108	"	959	923	926	8460	7265	7355	7310	1150	661	311	972	31.4	1.46
109	"	959	924	927	8460	7300	7390	7345	1115	641	301	942	30.6	1.42
110	"	961	919	925	8460	7130	7325	7230	1230	708	332	1040	34.4	1.29
111	"	961	848	905	8460	5165	6710	5940	2520	1020	1110	2130	83.1	0.91
112	"	962	840	911	8495	4980	6900	5940	2555	1035	1125	2160	96.6	0.77
113	HELICAL FIN	955	899	899	8320	6530	6530	6530	1790	1030	485	1515	50.6	1.406
114	"	954	901	903	8280	6595	6650	6620	1660	955	450	1405	49.5	1.405
115	"	954	907	905	8280	6770	6710	6740	1540	885	415	1300	44.0	1.65
116	"	953	908	906	8250	6800	6745	6770	1480	850	400	1250	42.4	1.740
117	"	955	904	902	8320	6680	6625	6655	1665	960	450	1410	46.4	1.460
118	"	954	882	908	8280	6065	6800	6430	1850	750	815	1565	64.1	1.175
119	"	955	878	882	8320	5965	6065	6015	2305	930	1015	1945	67.6	1.250
120	"	956	878	859	8350	5965	5450	6225	2125	860	935	1795	65.5	1.110
121	"	954	868	876	8280	5680	5905	5790	2490	1010	1095	2105	74.1	1.200
122	"	956	866	876	8350	5630	5905	5770	2580	1045	1135	2180	77.2	1.087
123	"	955	866	878	8320	5630	5965	5795	2525	1020	1110	2130	73.5	1.09
124	"	956	864	878	8350	5575	5965	5770	2580	1045	1135	2180	75.8	1.042
125	"	956	863	879	8350	5550	5990	5770	2580	1045	1135	2180	74.6	1.03
126	"	951	883	882	8175	6090	6065	6080	2095	1205	565	1770	62.3	1.36
127	"	954	884	886	8280	6115	6170	6140	2140	1230	580	1810	62.0	1.34
128	"	955	884	890	8320	6115	6280	6195	2125	1225	575	1800	60.9	1.17

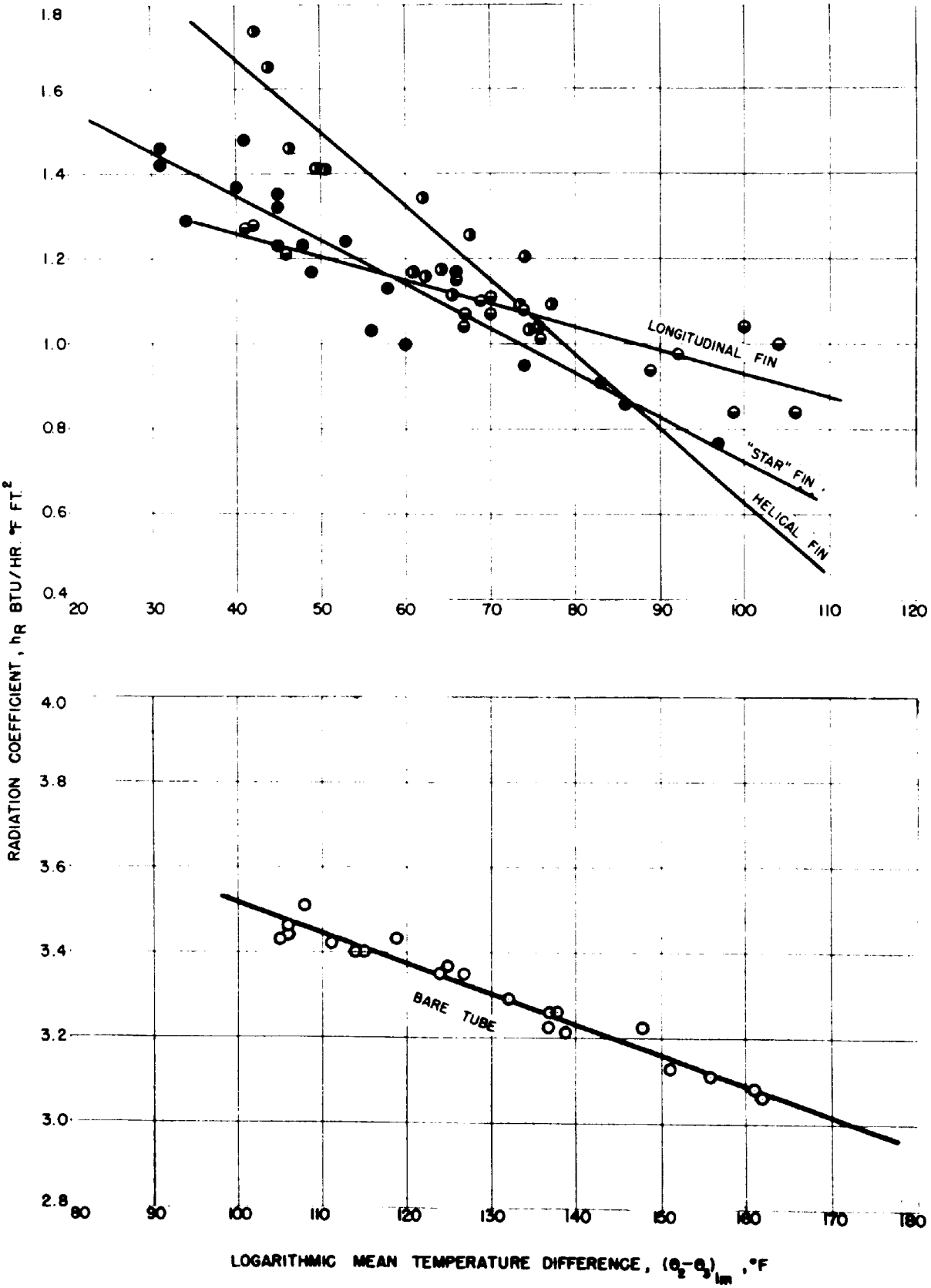

FIGURE 51

RADIATION COEFFICIENTS

Figure 51. The rather good correlation for the bare tube is considered largely fortuitous since the parameter Θ_4 (or its mathematical equivalent Θ_m) is missing. Figure 51, however, does show the consistent downward trend of the radiation coefficient with increasing values of $(\Theta_2 - \Theta_3)_{lm}$. This is as would be expected from Figure 27 of McAdams (28), which shows the variation of the radiation coefficient h_R (for two black bodies) as functions of their temperatures.

Table XXI also reports the radiation calculations for the modified annuli. The procedure which has been presented in the previous divisions of this section for the plain annulus is general, and may be applied as well to the modified annuli. In these cases, however, the number of "typical rays" which must be considered is much greater than for the plain annulus because of the added complexity of the geometry. Also, the problem of evaluating the angle factors and the mean beam length, while fundamentally unchanged, is vastly complicated by the new geometry. For these reasons, the rigorous evaluation of the radiation transfer in the modified annuli is too tedious for engineering purposes and a simplified approach is very desirable.

For practical purposes of radiation calculations, the extension of the surface of the inner tube by fins may be interpreted as increasing the effective emissivity of the inner tube without changing the effective geometry of the system (18). Thus, the fin tubes may be considered for purposes of radiation calculations as bare tubes of increased emissivity. Since no simple method is known for estimating the degree to which the effective emissivity is increased, it is arbitrarily assumed that all the fin tubes behave as bare tubes with unit emissivity.

With this assumption, the radiation heat transfer in the modified annuli may now be computed by Equations (130), (131), and (132) with suitable modification of the constants G^o, A^o, and D^o. Examination of the origin of the constants of these equations indicates that in each of them, the emissivity of the inner tube appears to the first power. The constants may be modified by multiplying them by the ratio 1/0.700 to account for the increased effective emissivity, and by 5.10, the surface area of 13.0 feet of the bare tube. The radiation heat transfer from the inner tubes of the modified annuli is therefore given by the application of Equations (130), (131), and (132) with the constants G^o, A^o, and D^o each multiplied by 7.29.

The calculations for the modified annuli are presented in Table XXI along with those for the plain annulus. The radiation coefficients are found to vary from

0.84 to 1.28 for the longitudinal fin, with a calculated average value of 1.05 Btu/hr.°F.ft.^{2}

0.86 to 1.48 for the star fin, with a calculated average value of 1.24 Btu/hr.°F.ft.^{2}

1.03 to 1.74 for the helical fin with a calculated average value of 1.30 Btu/hr.°F.ft.^{2}

The calculated average values compare favorably with those previously obtained graphically, i.e., 1.0 for the longitudinal fin, 1.0 for the star fin, and 0.8 for the helical fin.

The radiation coefficients for the fin tubes are also plotted against $(\theta_2 - \theta_3)_{lm}$ in Figure 51. The same downward trend with $(\theta_2 - \theta_3)_{lm}$, observed with the bare tube, is evident. To compare these coefficients for the fin tubes with that obtained for the bare tube, it is necessary first to reduce them all to the same basis, i.e., to the basis

of the bare tube. This is done by multiplying each coefficient by the ratio of the effective surface of the fin tube to the surface of the corresponding length of bare tube, i.e.,

For the longitudinal fin tube:

$$(h_{Rb})_{av} = 1.05\ (30.30/5.10) = 6.21 \text{ Btu/hr.°F.ft.}^2$$

where 30.20 is the effective area of the longitudinal fin tube evaluated at an h_R of 1.05 Btu/hr.°F.ft.^{2}

For the "star" fin tube:

$$(h_{Rb})_{av} = 1.24\ (29.89/5.10) = 7.26 \text{ Btu/hr.°F.ft.}^2$$

where 29.89 is the effective area of the "star" fin at an h_R of 1.24 Btu/hr.°F.ft.^{2}

For the helical fin tube:

$$(h_{Rb})_{av} = 1.30\ (35.99/5.10) = 9.18 \text{ Btu/hr.°F.ft.}^2$$

Thus the relative values of the radiation coefficients, all on the basis of bare tube area, are:

Bare Tube:	3.30	Btu/hr.°F.ft.^{2}
Longitudinal Fin Tube	6.27	"
"Star" Fin Tube	7.26	"
Helical Fin Tube	9.18	"

compared with the following as obtained through the previous graphical analysis:

Bare Tube	3.30	Btu/hr.°F.ft.^{2}
Longitudinal Fin Tube	5.94	"
"Star" Fin Tube	5.86	"
Helical Fin Tube	5.85	"

The higher coefficients for the fin tubes on this basis are due partly to their higher effective emissivity (unity instead of 0.700) but also to the lower $(\theta_2 - \theta_3)_{lm}$ range under which the fin tubes are operated (see Figure 51).

(b) Convection Analysis

It now is possible to obtain the convection heat transfer coefficients by the simple operation of subtracting the radiation coefficients from the composite heat transfer coefficients of Table IX. This subtraction and other calculations dealing with the analysis of the convection coefficients are presented in Table XXII.

This table presents the test number and the type of inner tube in Columns 1 and 2. Column 3 reports the composite coefficient as calculated in Table IX;and Column 4,the radiation coefficient as obtained in Table XXi. The convection coefficient, h, is given in Column 5 and is obtained by subtracting Column 4 from Column 3.

As has been discussed earlier, it is expected that the convection coefficients for heat transfer in turbulent motion at the inner surface of plain and modified annuli may be correlated by the equation

$$h = N \frac{K}{D_v} \left(\frac{C\mu}{K}\right)^{0.4} \left(\frac{D_v W}{\mu S_{min}}\right)^n \qquad (26)$$

where N and n are unknown constants depending upon the geometry of the annulus. A method for evaluating the constant n for each annulus is suggested when Equation (26) is rearranged to the form

TABLE XXII

ANALYSIS OF THE CONVECTION HEAT TRANSFER COEFFICIENTS

1	2	3	4	5	6	7	8	9	10
Test Number	Type of Tube	Composite Coefficient h'	Radiation Coefficient h_R	Convection Coefficient h	$K\left(\frac{C\mu}{k}\right)^{0.4}$	$\frac{h}{K\left(\frac{C\mu}{k}\right)^{0.4}}$	Reynolds Number $\left(\frac{D_v W}{\mu S_{min}}\right)$	Reynolds Number Exponent n	$\frac{K\left(\frac{C\mu}{k}\right)^{0.4}}{D_v\left(\frac{C\mu}{k}\right)^{0.4}}$ times $\left(\frac{DW}{\mu S}\right)^n$
Column Reference →		Table IX,23	Table XXI,15	Table XXIII, 3,4	Table IX,3,6 Figures 15, 17	Table I, 14 Table XXII,5,6	Table VIII,14	Figures 52,53, 54,55	Table XXII, 7,8,9
58	BARE	9.90	3.26	6.64	0.0212	65.9	27,600	0.80	359
58A	"	11.00	3.26	7.74	.0212	76.9	27,500	"	356
59	"	8.74	3.26	5.48	.0212	54.4	22,600	"	305
59A	"	9.80	3.22	6.58	.0212	65.3	22,200	"	301
60	"	5.93	3.17	2.76	.0212	27.4	10,600	"	163
60A	"	7.11	3.21	3.90	.0212	38.8	10,900	"	166
61	"	7.15	3.26	3.89	.0186	44.0	13,700	"	161
61A	"	8.06	3.11	4.95	.0184	56.6	14,300	"	163
62	"	6.00	3.22	2.78	.0185	31.6	10,700	"	145
62A	"	6.68	3.06	3.62	.0183	41.6	10,700	"	144
63	"	5.29	3.13	2.16	.0184	24.7	7,040	"	104
63A	"	5.69	3.08	2.61	.0183	30.0	7,270	"	106
64	"	26.17	3.46	22.71	.0212	226.0	102,000	"	1025
65	"	20.86	3.44	17.42	.0212	173.0	76,000	"	807
66	"	13.93	3.42	10.51	.0211	104.9	41,600	"	496
67	"	15.97	3.43	12.54	.0195	135.4	52,600	"	552
68	"	12.40	3.51	8.89	.0193	96.8	34,600	"	391
69	"	9.62	3.43	6.19	.0191	68.1	22,100	"	268
70	"	16.28	3.40	12.88	.0211	128.4	55,000	"	614
71	"	15.31	3.40	11.91	.0211	118.9	43,400	"	512
72	"	10.30	3.37	6.93	.0211	69.2	23,400	"	308
73	"	10.66	3.35	7.31	.0190	81.1	27,700	"	322
74	"	9.35	3.35	6.00	.0190	66.5	22,500	"	271
75	"	7.97	3.29	4.68	.0188	52.4	15,700	"	201
76	LONGITUDINAL FIN	9.39	1.15	8.24	.0217	32.2	20,300	0.80	714
77	"	7.78	1.11	6.67	.0217	26.1	16,300	"	598
78	"	6.70	1.08	5.62	.0216	22.0	12,100	"	470
79	"	5.71	1.07	4.64	.0201	19.6	9,950	"	374
80	"	4.35	1.01	3.34	.0199	14.2	7,100	"	283
81	"	3.02	0.94	2.08	.0196	9.00	4,460	"	202
82	"	5.82	1.00	4.82	.0211	19.4	10,600	"	413
83	"	4.52	0.98	3.54	.0212	14.1	8,080	"	334
84	"	3.28	0.94	2.34	.0213	9.31	4,800	"	221
85	"	3.20	1.04	2.16	.0190	9.64	5,460	"	219
86	"	2.31	0.84	1.47	.0191	6.53	3,670	"	160
87	"	1.93	0.84	1.09	.0191	4.84	2,470	"	117
88	"	14.12	1.28	12.84	.0221	49.3	36,600	"	1162
89	"	11.00	1.27	9.73	.0221	37.3	26,700	"	905
90	"	9.98	1.21	8.77	.0221	34.7	22,400	"	786
91	"	8.71	1.10	7.61	.0201	32.1	19,600	"	642
92	"	7.17	1.07	6.10	.0201	25.7	14,200	"	497
93	"	5.40	1.04	4.36	.0201	18.4	9,840	"	370
94	"SPAR" FIN	13.48	1.32	12.16	0.0219	43.7	12,000	0.91	1536
95	"	9.81	1.23	8.58	.0218	31.0	8,650	"	1050
96	"	6.48	1.13	5.35	.0215	19.6	5,500	"	689
97	"	7.38	1.17	6.21	.0196	25.0	6,700	"	747
98	"	5.16	0.95	4.21	.0194	17.1	5,010	"	573
99	"	2.85	0.86	1.99	.0192	8.16	2,880	"	342
100	"	21.90	1.48	20.42	.0220	73.0	20,800	"	2361
101	"	15.63	1.37	14.26	.0218	51.7	14,800	"	1720
102	"	8.85	1.24	7.61	.0216	27.8	7,650	"	935
103	"	10.44	1.23	9.21	.0205	35.4	10,200	"	1152
104	"	7.02	1.03	5.99	.0204	23.1	8,190	"	939
105	"	5.38	1.00	4.38	.0202	17.1	5,820	"	681
106	"	13.50	1.37	12.13	.0208	46.0	13,500	"	1511
107	"	8.56	1.17	7.39	.0205	28.4	9,430	"	1075
108	"	22.28	1.46	20.82	.0224	73.2	26,000	"	2950
109	"	20.00	1.42	18.58	.0224	65.3	22,100	"	2550
110	"	14.64	1.29	13.35	.0223	47.2	14,500	"	1711
111	"	3.79	0.91	2.88	.0194	11.7	3,730	"	437
112	"	2.38	0.77	1.61	.0192	6.61	2,710	"	324
113	HELICAL FIN	14.35	1.41	12.94	.0219	42.6	24,500	0.91	3020
114	"	17.75	1.41	16.34	.0219	53.7	31,200	"	3735
115	"	22.30	1.65	20.65	.0221	67.3	35,400	"	4210
116	"	25.50	1.74	23.76	.0221	77.4	40,500	"	4800
117	"	15.10	1.46	13.64	.0220	44.6	23,900	"	2948
118	"	15.25	1.18	14.07	.0201	50.4	22,600	"	2554
119	"	11.75	1.25	10.50	.0201	37.6	18,600	"	2137
120	"	9.32	1.11	8.21	.0201	29.4	13,600	"	1612
121	"	9.32	1.20	8.12	.0198	29.5	14,600	"	1690
122	"	7.88	1.09	6.79	.0198	24.7	12,800	"	1492
123	"	7.30	1.09	6.21	.0198	22.6	10,600	"	1265
124	"	6.29	1.04	5.25	.0197	19.2	9,220	"	1107
125	"	5.64	1.03	4.61	.0197	16.8	7,580	"	930
126	"	21.15	1.56	19.59	.0217	65.0	29,200	"	3495
127	"	13.56	1.34	12.22	.0217	40.6	20,500	"	2519
128	"	8.81	1.17	7.64	.0217	25.3	12,300	"	1582

$$\frac{h}{\frac{K}{D_v}\left(\frac{C\mu}{K}\right)^{0.4}} = N\left(\frac{D_v W}{\mu S_{min}}\right)^n$$

This equation indicates that if $h/(K/D_v)(C\mu/K)^{0.4}$ is plotted against the Reynolds number, on logarithmic paper, a straight line will result and its slope will be equal to n. (Actually the constant N may also be evaluated from such a plot but it can better be obtained by a second method.)

The quantity $h/(K/D_v)(C\mu/K)^{0.4}$ is computed for each test in Columns 6 and 7 of Table XXII. The Reynolds number, $(D_v W/\mu S_{min})$, obtained from Table XVIII, Column 4, is also tabulated in Column 9.

Figures 52, 53, 54, and 55 present the logarithmic plots of $h/(K/D_v)(C\mu/K)^{0.4}$ vs. $(D_v W/\mu S_{min})$. It is to be noted that the bare tube data, presented in Figure 52, form a satisfactory straight line which extends over the Reynolds number range of 7000 to 100,000. The slope of this line is 0.80 as expected. The data for the longitudinal fin tube presented in Figure 53 form two straight lines. The line representing the data in the true turbulent region of Reynolds number greater than 6000 to 7000, has a slope of 0.80, again as expected. Two lines are also required in the case of the "star" fin tube data presented in Figure 54. The "turbulent region" line in this case has a slope of 0.91, indicating a higher rate of increase of heat transfer coefficient with Reynolds number than in the case of the bare and the longitudinal fin tubes. Figure 55 presents the data for the helical fin tube. In this case all the points are within the true turbulent region and a single line suffices for their representation. The slope of this line is also 0.91, the same

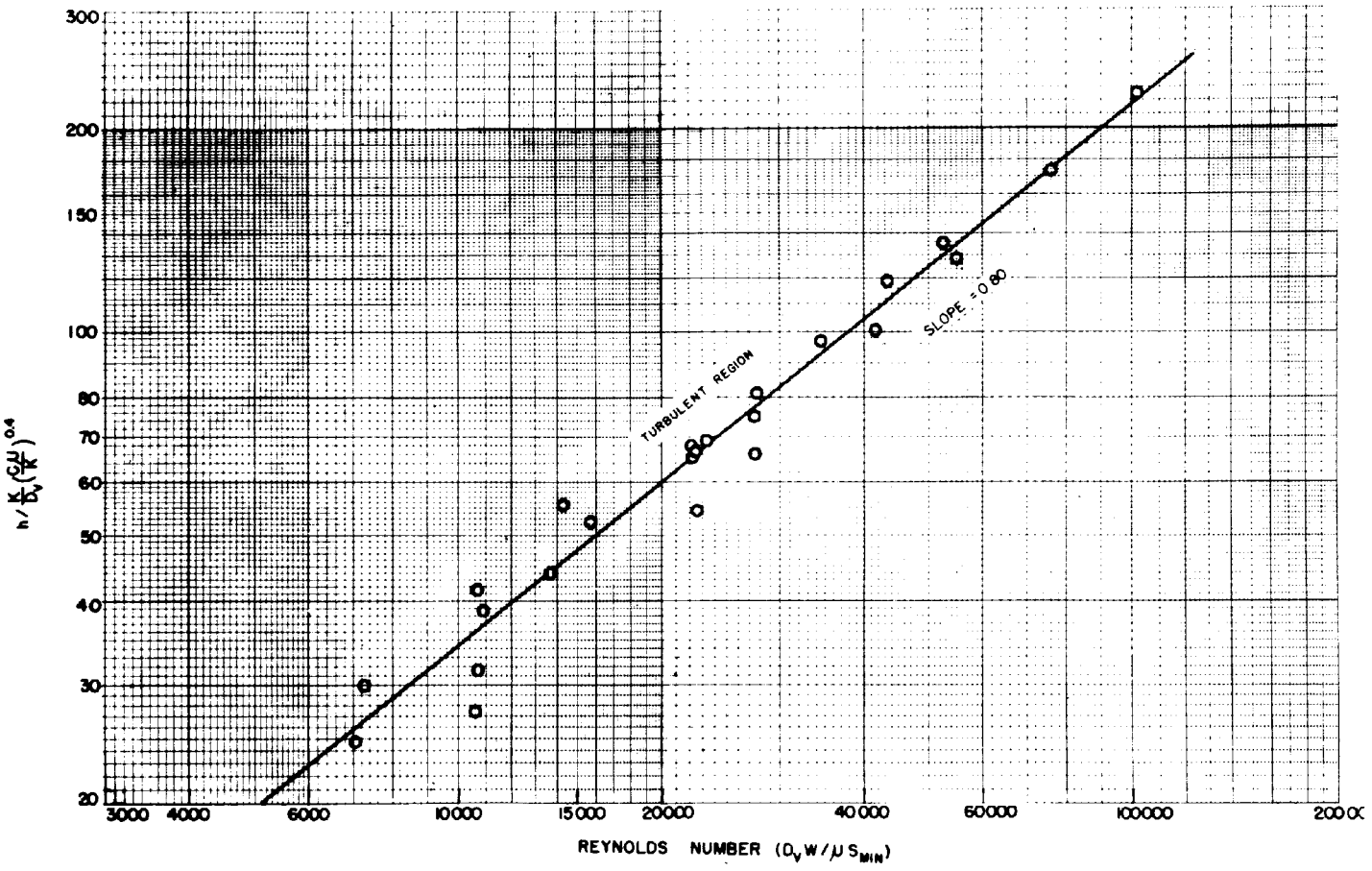

FIGURE 52

$h / \frac{K}{D_v} \left(\frac{C\mu U}{K}\right)^{0.4}$ VS. REYNOLDS NUMBER FOR BARE TUBE

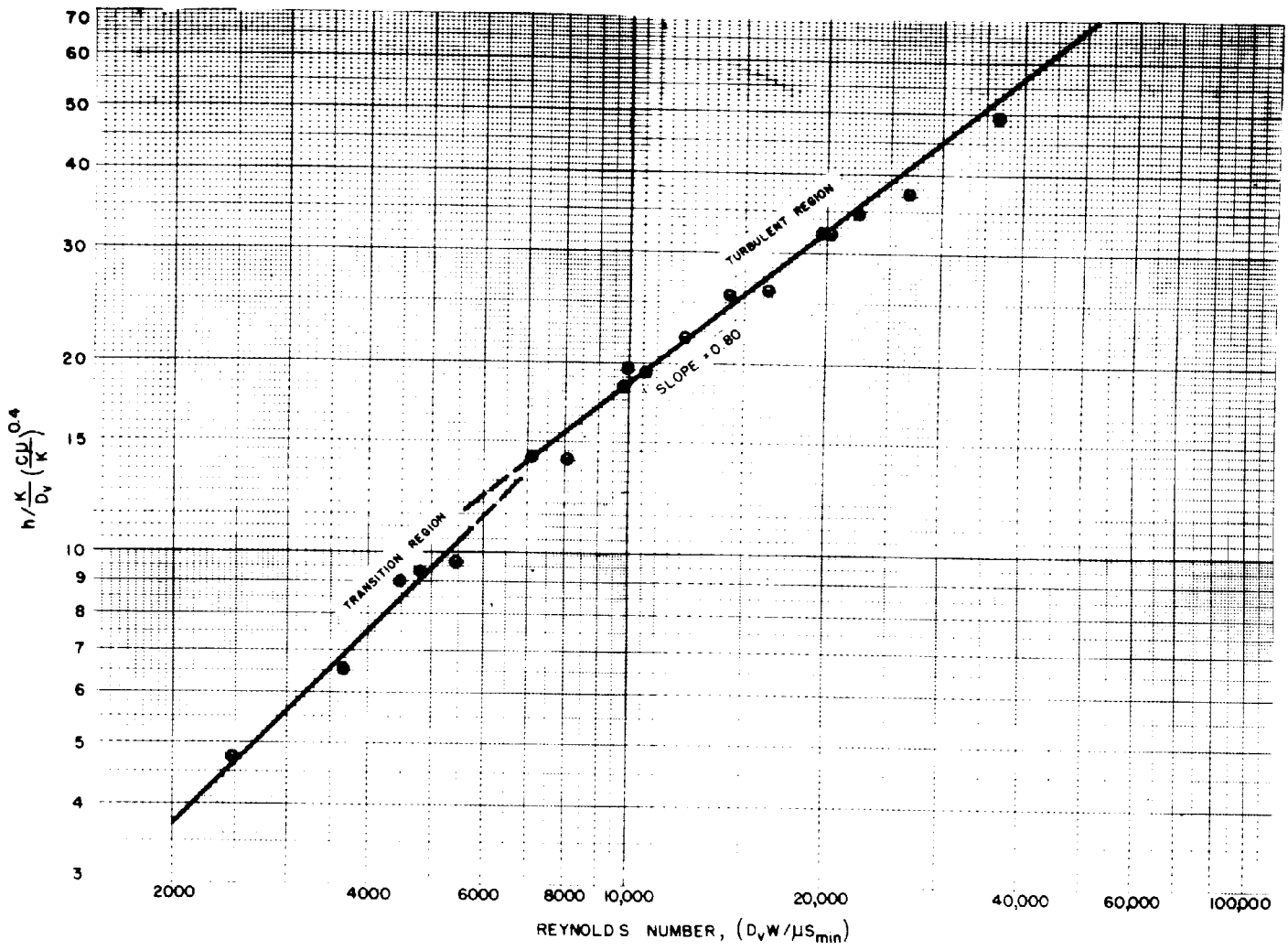

FIGURE 53

$h/\frac{K}{D_v}(\frac{C\mu}{K})^{0.4}$ VS. REYNOLDS NUMBER FOR LONGITUDINAL FIN.

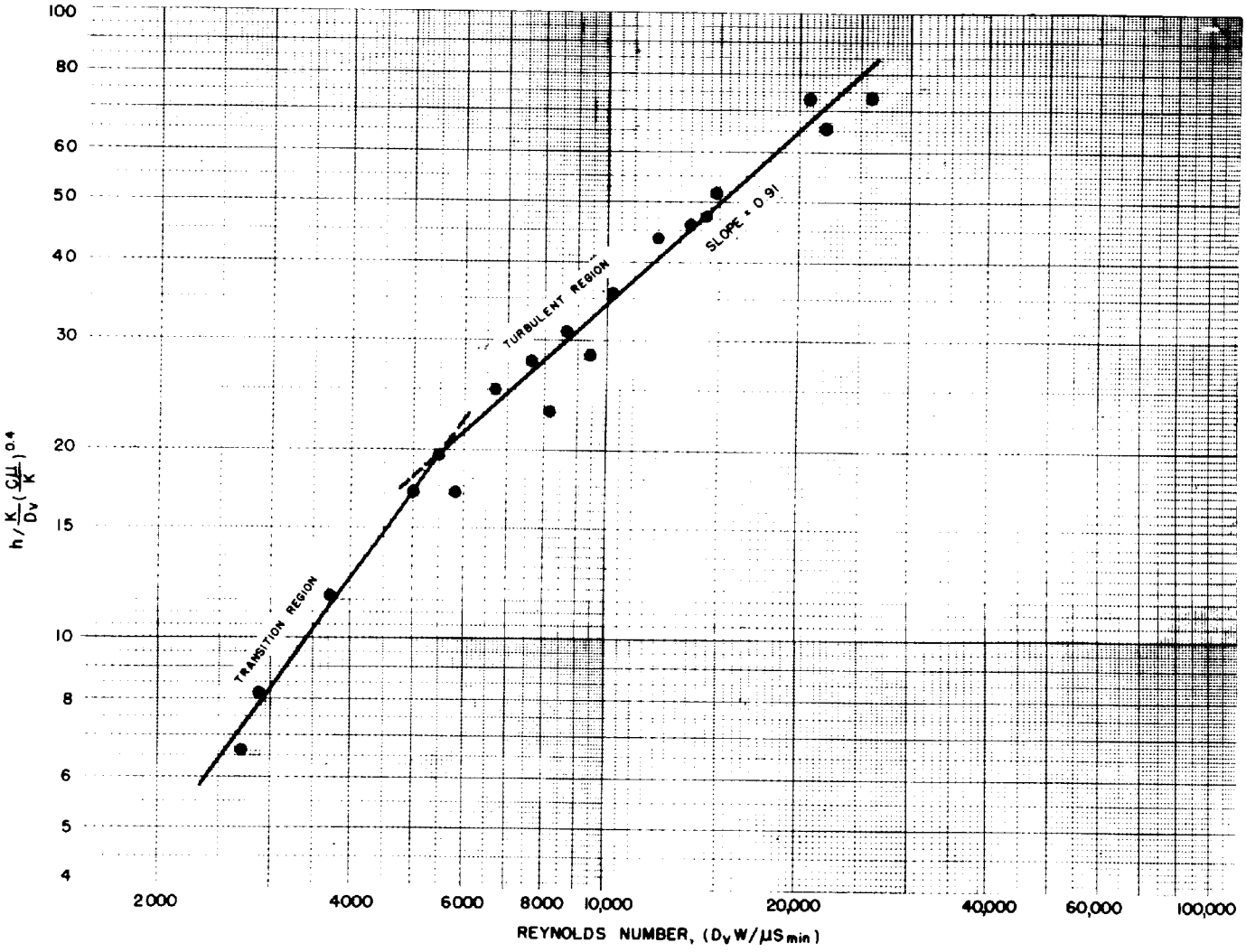

FIGURE 54

$h/\frac{K}{D_v}(\frac{C\mu}{K})^{0.4}$ VS. REYNOLDS NUMBER FOR STAR FIN

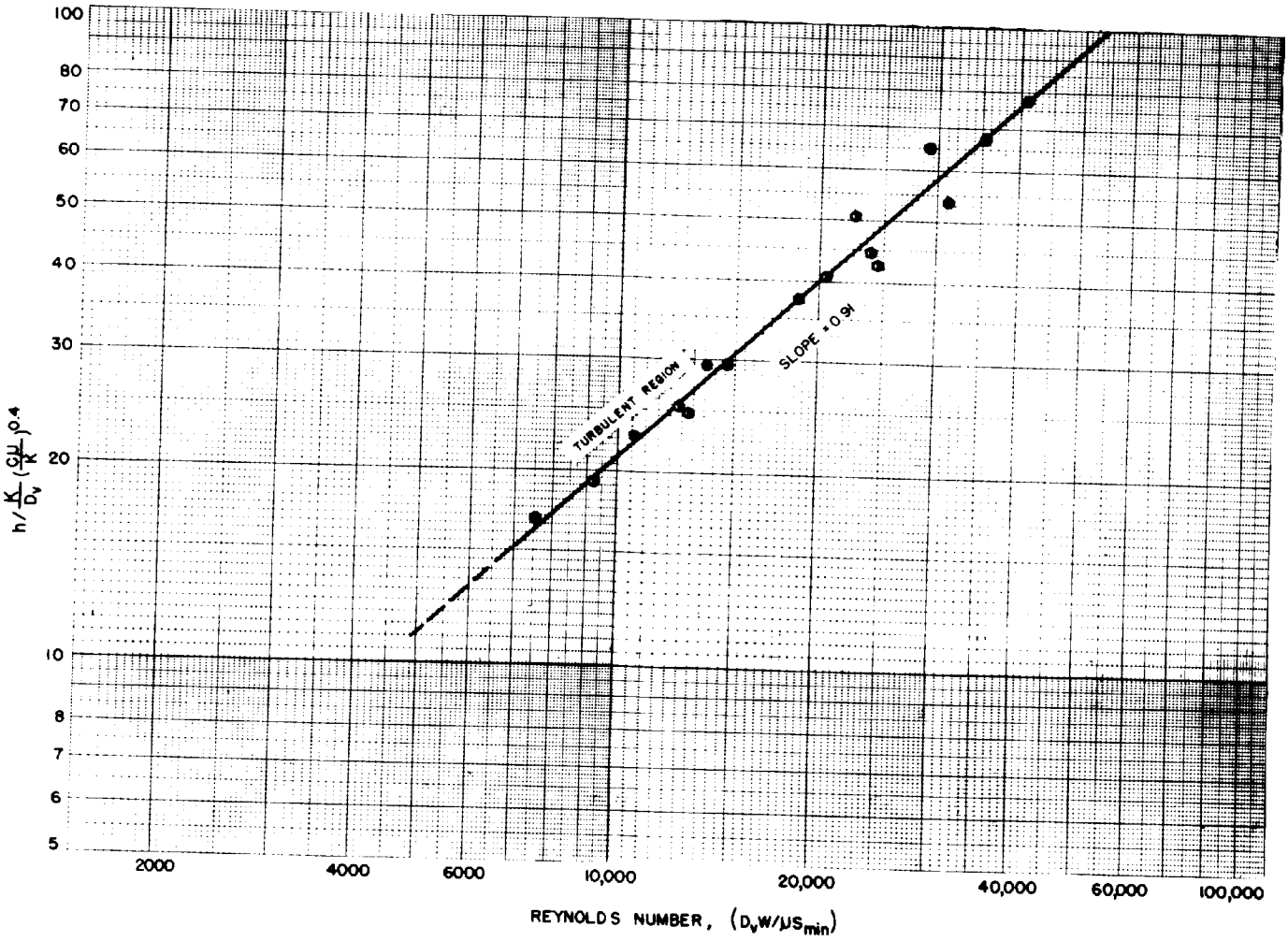

FIGURE 55

$h/\frac{K}{D_v}(\frac{CJ}{K})^{0.4}$ VS. REYNOLDS NUMBER FOR HELICAL FIN

as for the "star" fin tube.

Summarizing, the values of n, the exponent of the Reynolds number in Equation (26) are found to be

Bare Tube	0.80
Longitudinal Fin Tube	0.80
"Star" Fin Tube	0.91
Helical Fin Tube	0.91

These values are entered in Column 9 of Table XXII.

The constant N of Equation (26) is determined as follows: Values of $(K/D_v)(C\mu/K)^{0.4}\ (D_vW/\mu S_{min})^n$ are computed for each test using the appropriate values of n from Column 9. These values are listed in Column 10 of Table XXII. According to Equation (26) a plot of h, the convection coefficient (in the turbulent flow range) against the quantity $(K/D_v)(C\mu/K)^{0.4}\ (D_vW/\mu S_{min})^n$ should yield for each tube a straight line of slope equal to the "N" for the tube. Moreover, if the data are correct, this line should extrapolate through the origin of the coordinates. The data in the transition region are not expected to fall on the same line.

The values of Columns 5 and 10, i.e., the convection coefficients and the quantity $(K/D_v)(C\mu/K)^{0.4}\ (D_vW/\mu S_{min})^n$, are plotted in Figures 56, 57, 58, and 59. Figure 56 represents the data of the bare tube, all of which is within the region of true turbulent flow. It is seen that the data are well represented by a straight line which extrapolates exactly through the coordinate origin. This may be taken as corroboration of both the values of the composite coefficients and the entire procedure for calculating the radiation coefficients. The slope of the line of

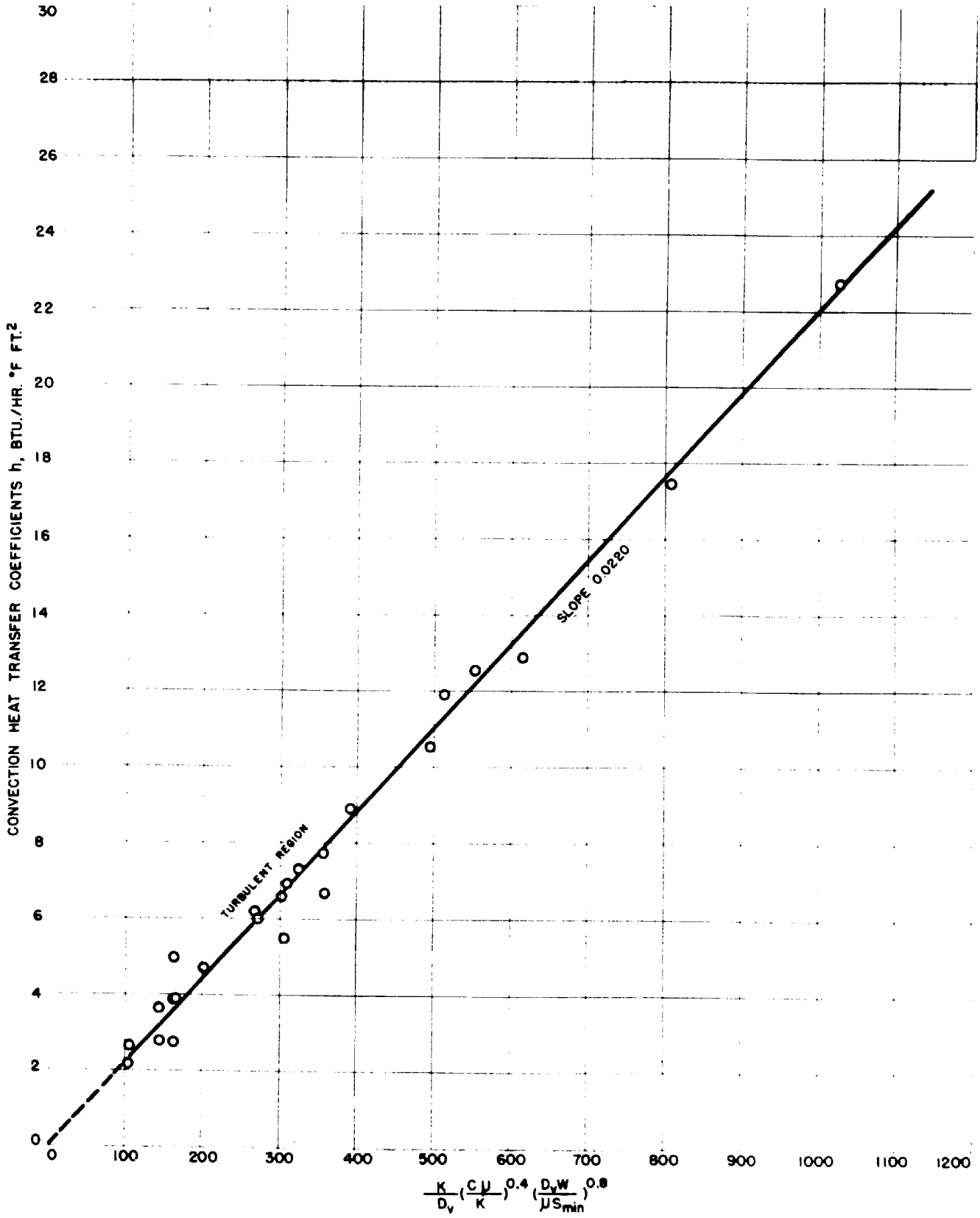

FIGURE 56

CONVECTION HEAT TRANSFER COEFFICIENTS FOR THE BARE TUBE

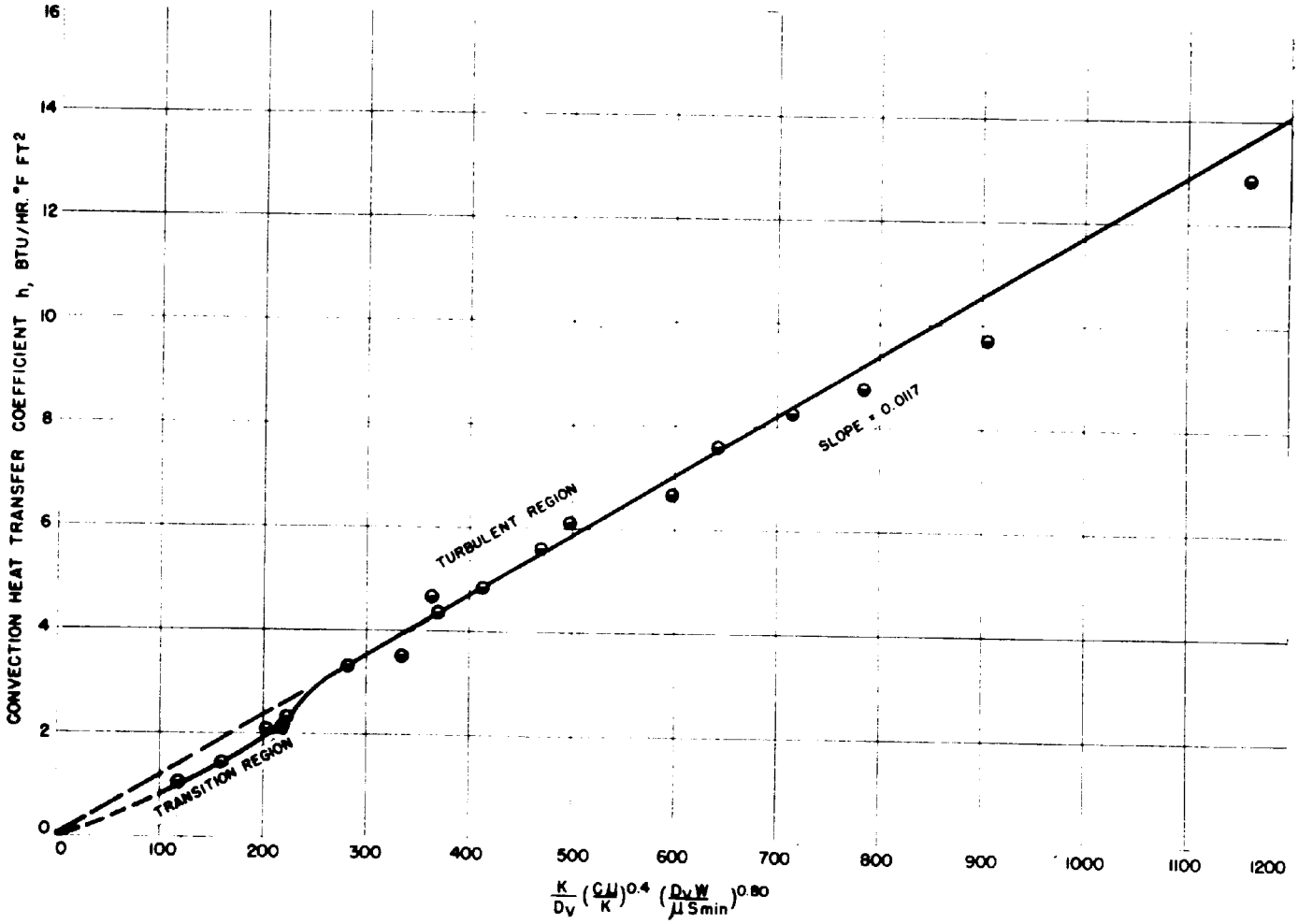

FIGURE 57

CONVECTION HEAT TRANSFER COEFFICIENTS FOR THE LONGITUDINAL FIN TUBE

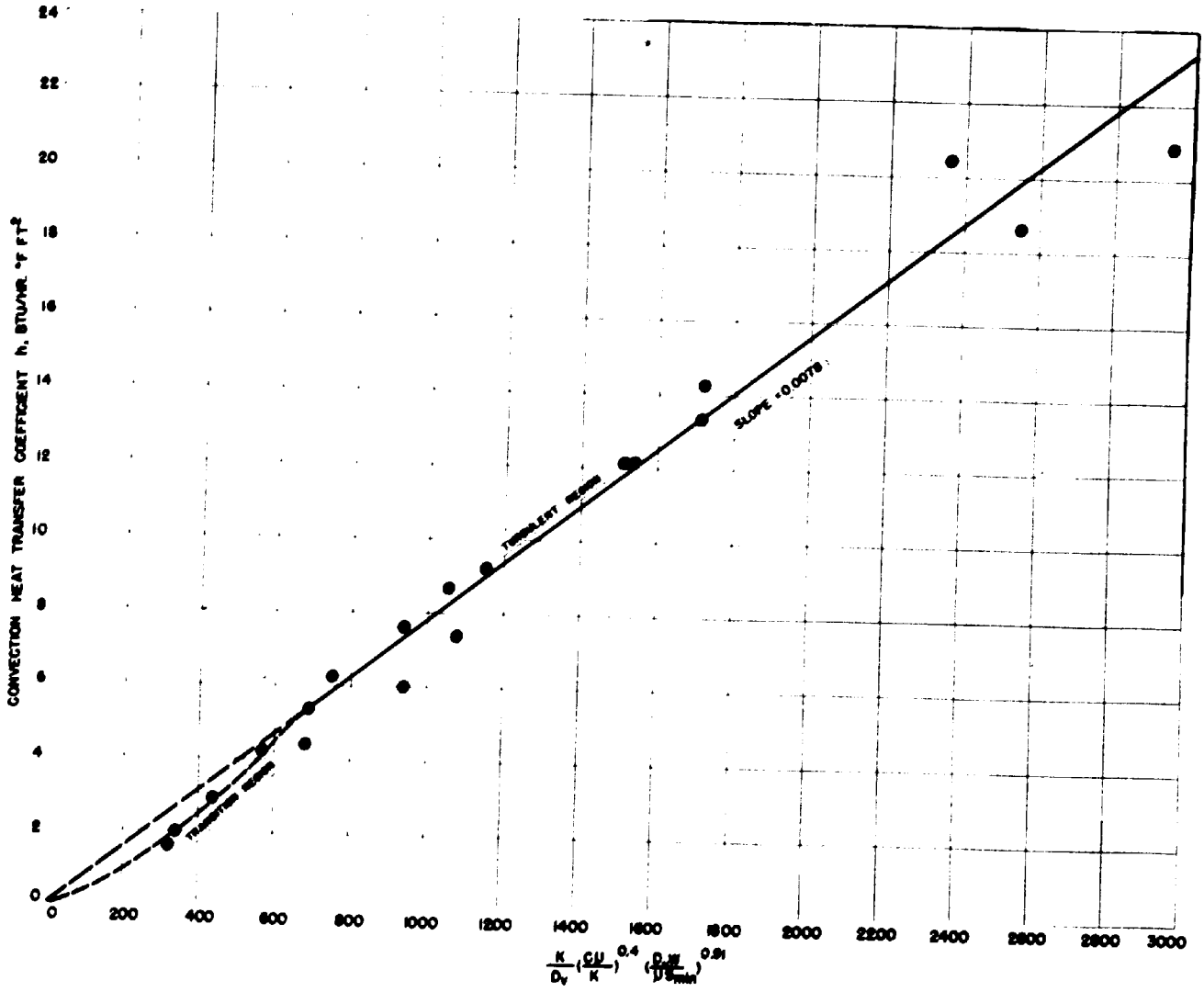

FIGURE 58

CONVECTION HEAT TRANSFER COEFFICIENTS FOR THE "STAR" FIN TUBE

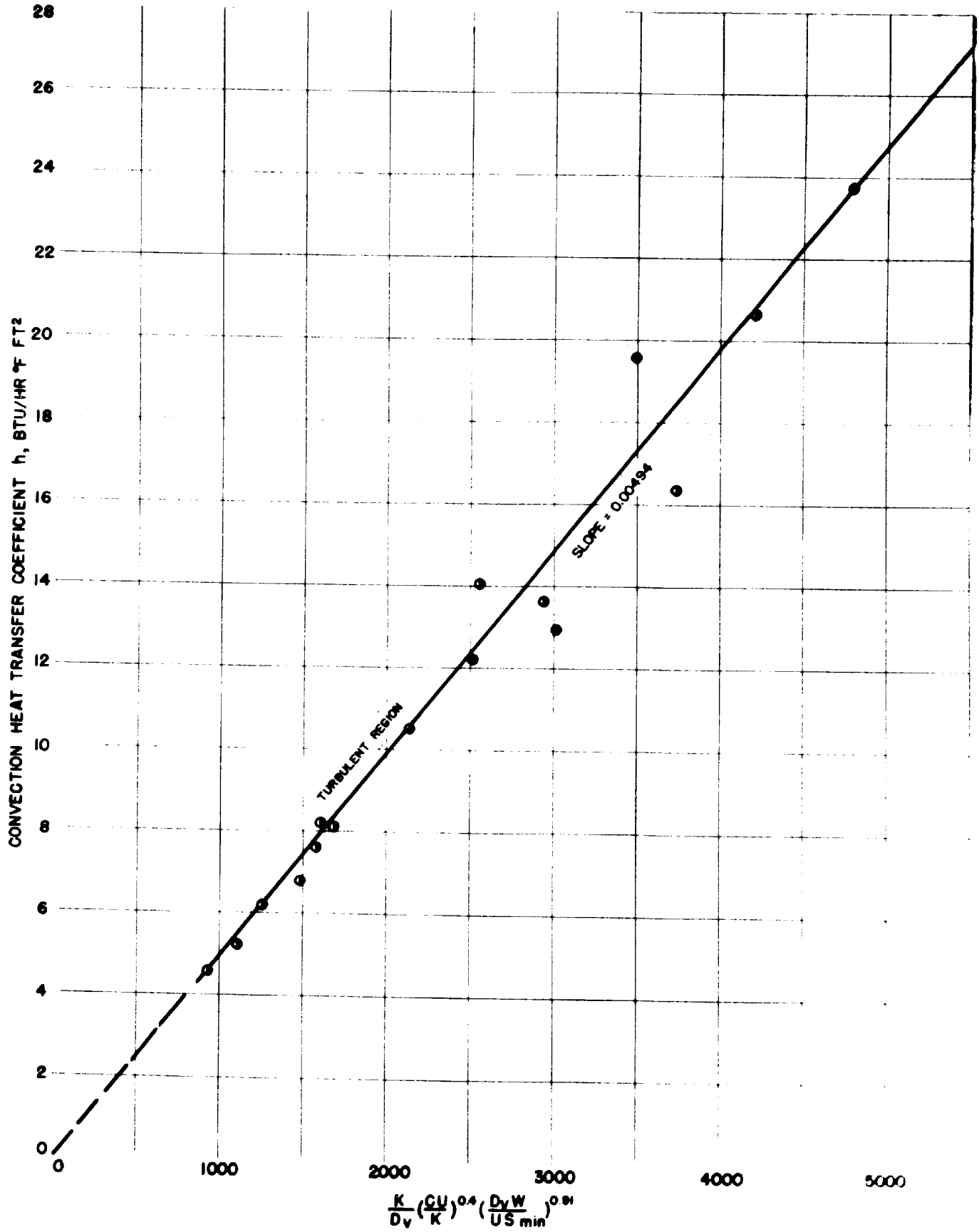

FIGURE 59
CONVECTION HEAT TRANSFER COEFFICIENTS FOR THE HELICAL FIN TUBE

Figure 56 is 0.0220, which is the value of the constant N for the bare tube annulus.

The data of the longitudinal fin tube are plotted in Figure 57. Disregarding the points which lie within the transition flow region, these data are also well represented by a straight line which may be extrapolated through the origin. The slope of this line is 0.0117, which is the value of the constant N for the longitudinal fin tube annulus.

Similarly, Figures 58 and 59 are plots of the data for the "star" and the helical fin tubes. It is to be noted in the case of these two tubes that the abscissa is $(K/D_v)(C\mu/K)^{0.4}(D_vW/\mu S_{min})^{0.91}$ rather than $(K/D_v)(C\mu/K)^{0.4}(D_vW/\mu S_{min})^{0.80}$ as for the bare and the longitudinal fin tubes. The data plotted in these figures are also correlated by straight lines which extrapolate through the origin. The "N" values are 0.0078 for the "star" fin tube and 0.00494 for the helical fin tube.

Summarizing, the convection heat transfer coefficients for true turbulent flow at the inner tube of the various annuli are correlated by the equations:

Bare Tube - Plain Annulus

$$h = 0.0220\,(K/D_v)(C\mu/K)^{0.4}(D_vW/\mu S_{min})^{0.80} \qquad (134)$$

Longitudinal Fin Tube - Modified Annulus

$$h = 0.0117\,(K/D_v)(C\mu/K)^{0.4}(D_vW/\mu S_{min})^{0.80} \qquad (135)$$

"Star" Fin Tube - Modified Annulus

$$h = 0.0078\,(K/D_v)(C\mu/K)^{0.4}(D_vW/\mu S_{min})^{0.91} \qquad (136)$$

Helical Fin Tube - Modified Annulus

$$h = 0.00494\ (K/D_v)(C\mu/K)^{0.4}(D_v W/\mu S_{min})^{0.91} \qquad (137)$$

These equations compare well with those obtained earlier, Equations (51), (52), (53), and (54), on the assumption of constant radiation coefficients. The present set, however, are considered the more reliable, since they take cognizance of the variation in radiation coefficients.

The only opportunity to check these results with those of the literature is for the plain annulus. In this case, the form of the equation and the exponents of the Prandtl and the Reynolds numbers, agree with those which are recommended by Wiegand (45) and others (27) and (29). The multiplying constant, 0.0220, does not agree with that proposed by Wiegand, which for this annulus would be

$$0.023\ (D_2/D_1)^{0.45} = 0.023\ (4.026/1.500)^{0.45}$$

$$= 0.0359.$$

On the other hand, the constant agrees well with that employed in the Dittus-Boelter "circular pipe" Equation (7), i.e., 0.023, which both McMillen (29) and Martinelli (27) found to satisfy their data better than the Wiegand equation.

3. PRESSURE DROP

The pressure drop data as reported in Column 11 of Table VII may be correlated in terms of the friction factor f, and the Reynolds number. The friction factor has been defined by Equation (24) and is

reported in Column 13 of Table VIII. The method of calculating this quantity from the pressure drop has been discussed. Reynolds numbers for each of the tests are also recorded in Table VIII, Column 14.

The relationship between the friction factors and the Reynolds number is shown in Figure 60, which is a logarithmic plot of f vs. $(D_v W/\mu S_{min})$. Figure 60 includes, in addition to the data of Table VIII, the supplementary friction factor data which are computed and recorded in Table 1A of Appendix A.

The data are seen to form three well defined bands, the bare tube and the longitudinal fin tube data forming a band at a low value of f, the helical fin tube data at an intermediate value of f, and the "star" fin tube data at a high value of f.

The extensive scattering of the friction factors for the bare tube and the longitudinal fin tube is to be expected in the light of the very small absolute values of the pressure drops and the experimental difficulties involved in their accurate measurement. (The absolute values of the pressure drops for these tubes vary from 0.009 to 0.696 inches of water with most of the values below 0.15 inches of water -- see Table VIII, Column 11).

The line through the data for the bare tube and the longitudinal fin tube is not drawn specifically to represent the data, but is rather the line recommended by Rouse (35) for a circular pipe of roughness corresponding to that of 2-1/2-inch, new, steel pipe. (The equivalent diameter of the plain annulus is approximately 2-1/2 inches.) The line was chosen as that along which the data might most reasonably be expected to fall, It is seen that, despite the scattering, this line does indicate

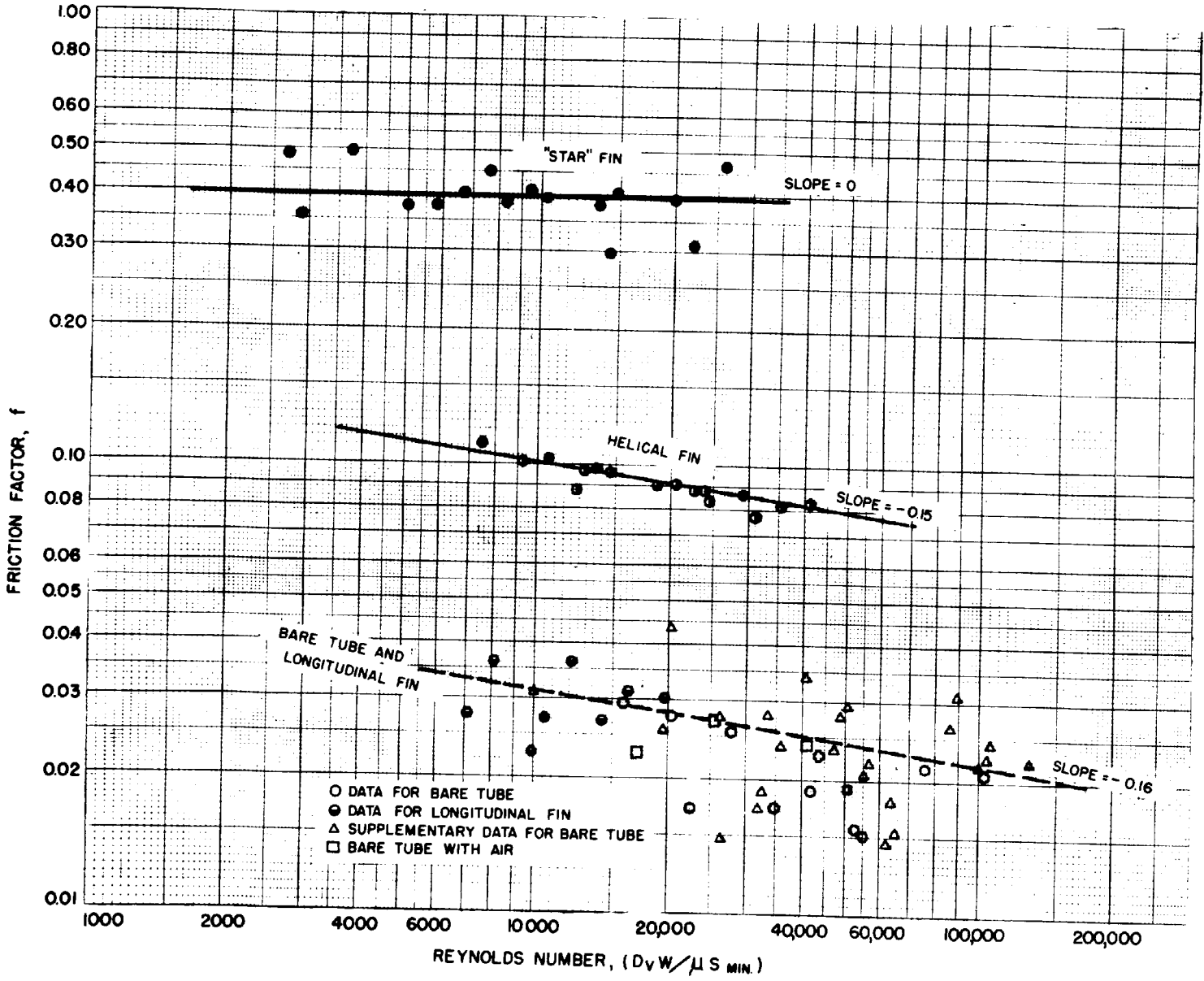

FIGURE 60
FRICTION FACTOR DATA FOR ALL TUBES

the proper value and trend of the data.

The curves through the "star" fin tube data and the helical fin tube data are drawn to represent the experimental points.

The friction factor data for the tubes may therefore be represented by the following equations, which are those of the curves of Figure 60.

Bare Tube - Plain Annulus

$$f = 0.133\ (D_v W/\mu S_{min})^{-0.16} \qquad (138)$$

Longitudinal Fin Tube - Modified Annulus

$$f = 0.133\ (D_v W/\mu S_{min})^{-0.16} \qquad (139)$$

"Star" Fin Tube - Modified Annulus

$$f = 0.395 \qquad (140)$$

Helical Fin Tube - Modified Annulus

$$f = 0.402\ (D_v W/\mu S_{min})^{-0.15} \qquad (141)$$

VIII. COMPARATIVE UTILITY OF SURFACES

Experimental values of the composite heat transfer coefficients have been obtained for the transfer of heat from bare and extended metallic surfaces to superheated steam. These coefficients have been analyzed in detail and separated into their radiation and convection components. Procedures and equations have been presented for the calculation of both the radiation and the convection coefficients for a plain and three modified annuli. These equations correlate the coefficients in terms of the properties of the superheated steam and the flow rate for each of the geometrical arrangements.

Data have also been obtained, analyzed and correlated for the pressure drop due to flow of superheated steam through these various annuli. The equations presented permit the prediction of the pressure drop in terms of the properties of the steam and the flow rate for each geometrical arrangement.

Information is now at hand therefore to predict both the heat transfer and the pressure drop performance of a steam superheater unit, similar in type or containing the elements of any of those studied. There remains, however, the problem of determining which of the several types of surface arrangement is the most advantageous from the viewpoint of its industrial utility.

It is first necessary to state those requirements of a heat exchange surface, or arrangement, which are considered desirable from the utilitarian viewpoint. Briefly, the requirements are:

(1) The surface and its arrangement should permit, under a minimum temperature differential, the transfer of heat to a fluid at a high rate, in an equipment of small volume, with a low expenditure of energy for fluid circulation.

(2) The cost of the equipment per unit of volume, and its maintenance, should be low.

The requirement of item (2), while of great importance, deals with capital cost of equipment and is beyond the scope of this discussion. Item (1) really lists two separate requirements:

(a) That the surface should permit a high heat flux per unit temperature differential per unit of energy expended in circulation of the fluid; and

(b) That the surface should permit a high heat flux per unit temperature differential and per unit of equipment volume.

It would appear desirable to define two separate "performance coefficients" to measure the extent to which the requirements of (a) and (b) are satisfied. So far as (a) is concerned, an "energy performance coefficient" might be defined as

$$P_E = \frac{q}{\Delta T \Delta E} \qquad (142)$$

where P_E = energy performance coefficient, BTU/watt hr. °F.

ΔE = power consumption in circulation of the fluid, watts.

q = heat transfer rate, BTU/hr.

ΔT = temperature differential available for heat transfer, °F.

The requirements of (b) may be measured by the definition of a "volume performance coefficient" as

$$P_V = \frac{q}{L \Delta T S} \qquad (143)$$

where P_V = volume performance coefficient, BTU/hr. ft.^{3} °F.

q = heat transfer rate, BTU/hr.

L = length of equipment, ft.

S^* = total cross section of equipment, ft.^{2}

ΔT = temperature differential available for heat transfer.

The relative utility of the various surface arrangements may now be studied by equations (142) and (143) and in the light of the relationships which have been obtained experimentally. The experimental data show that in most cases the bulk of the heat transfer is by convection. For this reason, and in the interests of simplicity, it will be assumed throughout this analysis that all the heat is transferred by the convection mechanism. This does not suggest that radiation may be neglected in heat exchanger design, but only that it is not too important when evaluating the relative performance characteristics of the surfaces. A second assumption which will be made is that all extended surfaces are so proportioned that their fin efficiencies approach one.

Considering first the energy performance coefficient P_E, equation (142) may be written as

$$P_E = \frac{hA\Delta T}{\Delta T \Delta E}$$

$$= \frac{hA}{\Delta E} \qquad (144)$$

where h = convection heat transfer coefficient, BTU/hr. °F. ft.^{2}

A = heat transfer area, ft.^{2}

---

* i.e., $S = \frac{\pi (4.026)^2}{576}$ for the present equipment.

The power consumption ΔE may be evaluated as

$$\Delta E = \frac{FW\ (746)}{3600\ (550)} \quad \text{watts} \tag{145}$$

where F = energy dissipated due to friction, ft. lbs./ft. of fluid

W = flow rate, lbs./hr.

3600 = seconds/hr.

550 = ft. lbs./HP

746 = watts/HP

Introducing equation (24), the definition of the friction factor

$$F = \frac{fV^2L}{2\beta D_v} \tag{24}$$

$$= f\ \frac{W^2}{S_{min}^2}\ \frac{v^2\ L}{2\beta D_v} \tag{146}$$

where f = friction factor

S_{min} = minimum cross section available for flow, $ft.^2$

v = specific volume of fluid, $ft.^3/lb.$

and the other symbols have their usual significance.

Combining equations (144), (145) and (146)

$$P_E = (5300\ \beta\ S_{min}^{\ 2}\ D_v)\ \frac{h\ (A/L)}{fW^3v^2} \tag{147}$$

The experimental work has shown that the heat transfer coefficients and the friction factors for the various "annuli" may be represented by:

$$h = N\ \frac{K}{D_v}\left(\frac{C\mu}{k}\right)^{0.4}\left(\frac{D_vW}{\mu S_{min}}\right)^n \tag{26}$$

and $$f = a\left(\frac{D_vW}{\mu S_{min}}\right)^b \tag{148}$$

where N, n, a and b depend upon the type of "annulus".

Substituting these values of h and f in equation (147) results in:

$$P_E = \left(5300\ \beta\ \frac{N}{a}\ D_v^{n-b}\ S_{min}^{2-n+b}\ \frac{A}{L}\right) \frac{K}{v^2 \mu^{n-b}} \left(\frac{C\mu}{k}\right)^{0.4} W^{n-3-b} \qquad (149)$$

The relationship may be made more useful by expressing the flow rate per unit of total equipment cross section, S; i.e.,

$$P_E = \left(5300\ \beta\ \frac{N}{a}\ D_v^{n-b}\ S_{min}^{2-n-b}\ \frac{A}{L}\ S^{n-3-b}\right) \left(\frac{K}{v^2 \mu^{n-b}} \left(\frac{C\mu}{k}\right)^{0.4}\right) \cdots \cdots \left(\frac{W}{S}\right)^{n-3-b} \qquad (150)$$

Equation (150) now gives the energy performance coefficient in terms of geometrical variables, fluid properties, and fluid flow rate based upon the total equipment cross section. Since the values of N, a, D_v, S_{min}, $\frac{A}{L}$, S, n and b are known for each of the annuli studied, their performance coefficients may be evaluated in terms of the fluid properties and the mass velocity based on the empty equipment shell, $\left(\frac{W}{S}\right)$.

This is done in Figure 61 which presents plots of the energy performance coefficients vs. the mass velocity for the various surfaces at two pressure-temperature conditions of superheated steam; 50 psi abs. and 381 °F., and 100 psi abs. and 328 °F. Examination of Figure 61 indicates the relative performance coefficients, P_E, to decrease in the order: longitudinal fin tube, bare tube, helical fin tube and "star" fin tube.

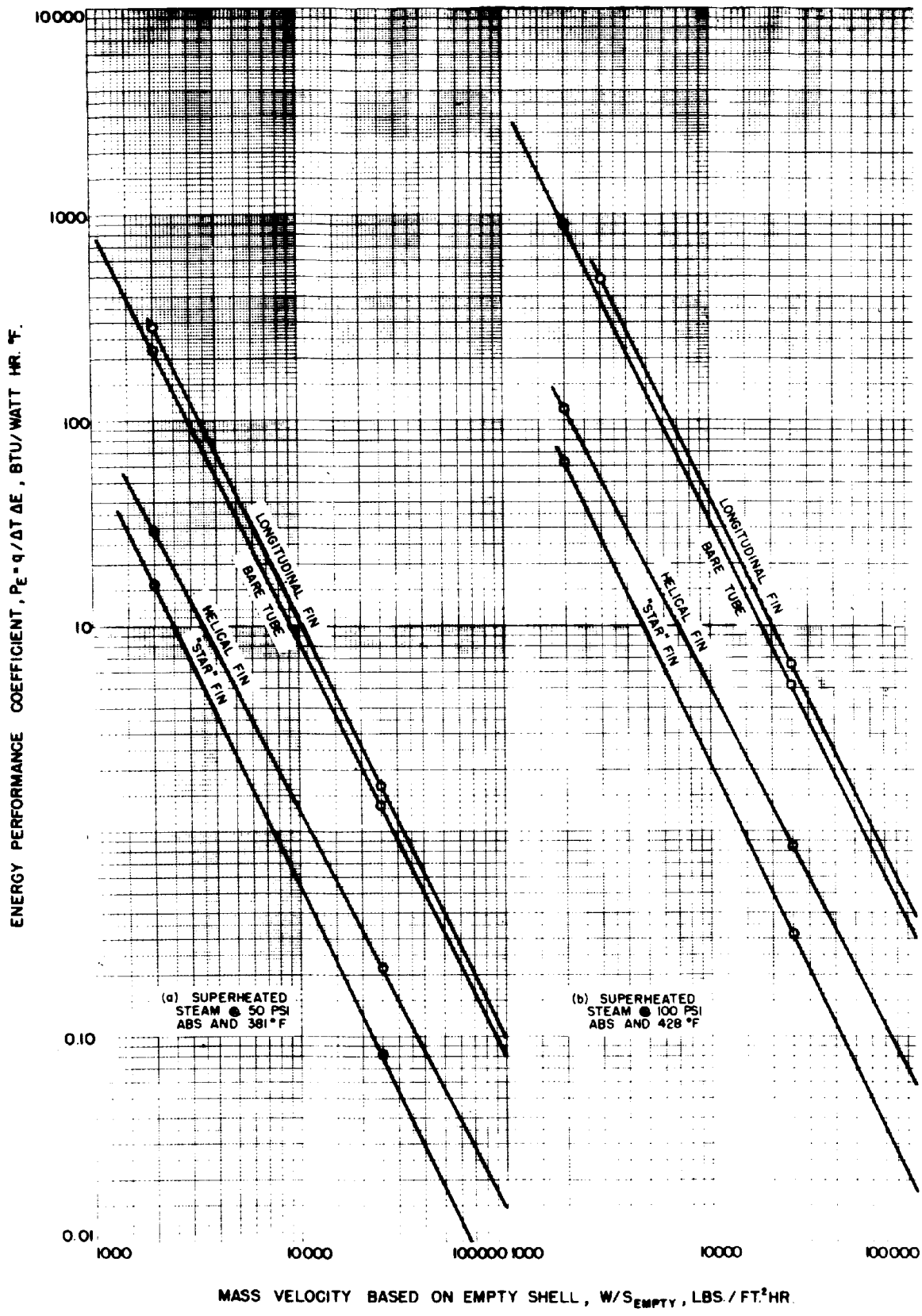

FIGURE 61

ENERGY PERFORMANCE COEFFICIENTS OF VARIOUS TYPES OF SURFACES FOR SUPERHEATED STEAM

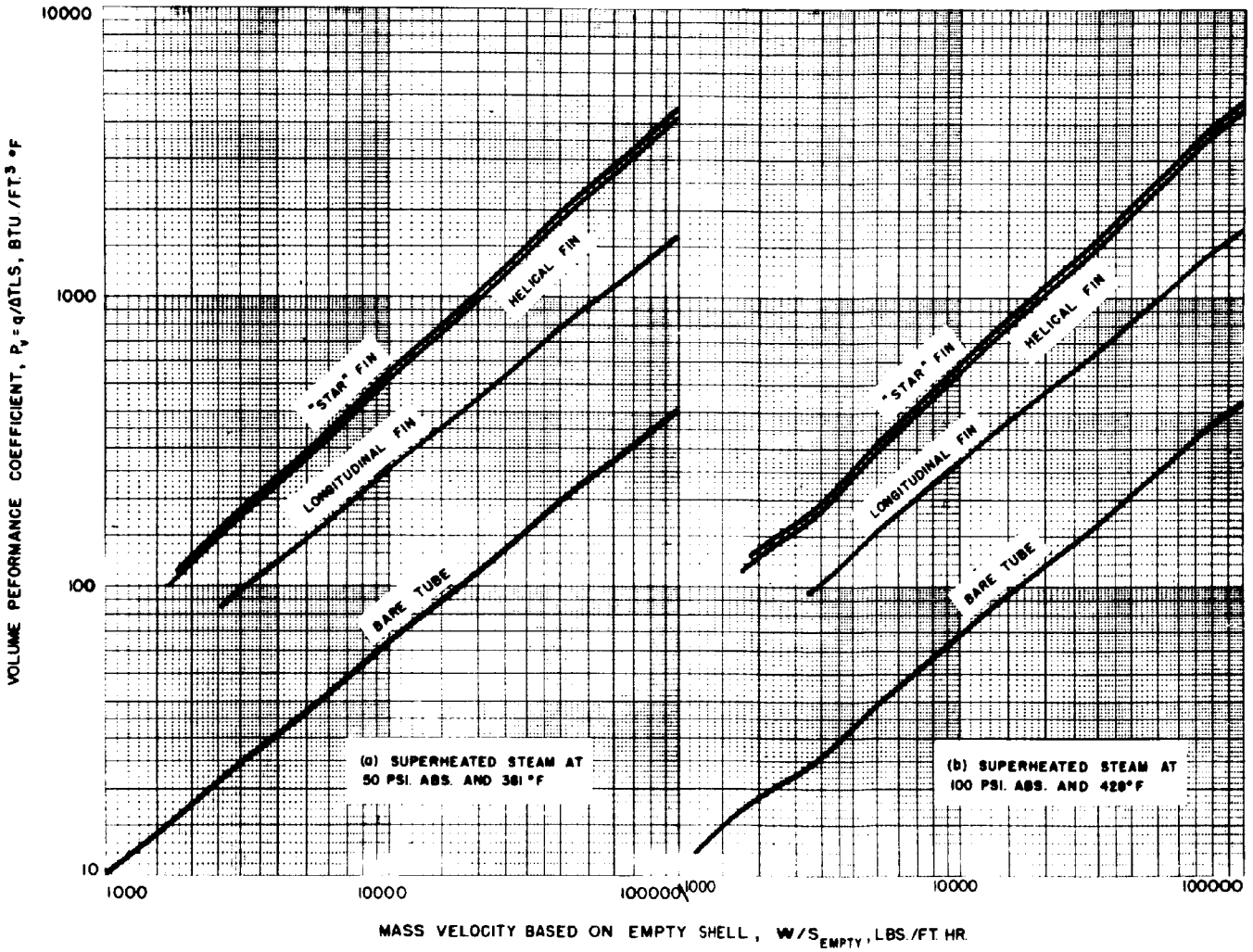

FIGURE 62

VOLUME PERFORMANCE COEFFICIENTS OF VARIOUS TYPES OF SURFACES FOR SUPERHEATED STEAM

Roughly speaking the coefficients for the longitudinal and the bare tubes are ten times greater than those for the helical and the "star" tube. This situation holds approximately at all flow rates and for both pressure-temperature conditions studied. The conclusion is therefore, that, so far as ability to transfer heat at low energy consumption is concerned, the longitudinal fin tube and the bare tube are far superior to the others.

Turning attention now to the volume performance coefficient P_v, equation (143) may be rewritten as

$$P_v = \frac{hA\Delta T}{L\Delta TS}$$

$$= \frac{hA}{LS} \qquad (151)$$

where h = convection heat transfer coefficient, BTU/ft.^{2} hr.°F.

A = heat transfer area, ft.^{2}

Substituting for h the relation,

$$h = N \frac{k}{D_v} \left(\frac{C\mu}{k}\right)^{0.4} \left(\frac{D_v W}{\mu S_{min}}\right)^n \qquad (26)$$

$$P_v = \frac{N\,(A/L)}{S\,D_v^{1-n}\,S_{min}^{n}} \frac{k}{\mu^n} \left(\frac{C\mu}{k}\right)^{0.4} W^n \qquad (152)$$

The equation may be rearranged slightly to express the flow rate in terms of mass velocity through the empty equipment shell.

$$P_v = \frac{N\,(A/L)}{(SD_v)^{1-n}\,S_{min}^{n}} \frac{k}{\mu^n} \left(\frac{C\mu}{k}\right)^{0.4} \left(\frac{W}{S}\right)^n \qquad (153)$$

The values of the volume performance coefficient, P_V, may be calculated for the various tubes from Equation (153) at any pressure-temperature condition and for any flow rate, since values of N, A/L, S, D_v, S_{min}, and n are all known. To present the picture fully, Figure 62 has been prepared. This figure is essentially a plot of Equation (153) for each annulus and at two pressure-temperature conditions: 50 psi. abs. and 381°F., and 100 psi. abs. and 428°F.

Figure 62 indicates the relative performance coefficients, P_V, to be almost in the inverse order to that obtained in Figure 61; i.e., P_V decreases in the order: "star" fin, helical fin, longitudinal fin, and bare tube. The star and the helical fin give coefficients approximately nine time those for the bare tube,and the longitudinal fin coefficients are approximately three times those for the bare tube. These ratios hold fairly constant over the flow range and at both pressure-temperature conditions. The result indicated by Figure 62 is that the "star" and the helical fin tubes are far superior, and the longitudinal fin tube considerably superior, to the bare tube, in respect to their ability to transfer heat in an equipment of small volume.

The reasonable conclusion of this analysis is that surfaces transversely oriented to the flow (e. g., the "star" and the helical fin tubes) possess great merit for use in installations where power consumption is secondary to compactness of equipment. On the other hand, surfaces oriented parallel to the direction of flow (e.g., the bare and the longitudinal fin tubes) are most suitable for installations where volume of equipment is secondary to power consumption.

IX. CONCLUSIONS

The final conclusions of this study may be summarized as follows:

1. A versatile experimental unit for the determination of gas-phase heat transfer coefficients has been designed, constructed, and successfully operated.

2. An analysis has been made of the role played by the conduction, convection, and radiation mechanisms in the general problem of heat transfer between the bounding walls of an annulus and a fluid flowing in an annular space.

3. The literature related to turbulent heat transfer and pressure drop in annuli has been briefly reviewed, and the present state of knowledge of these phenomena has been discussed.

4. A critical analysis has been made of the available data on the viscosity, thermal conductivity, and specific heat of superheated steam in the range of pressure and temperature from 14.7 to 200 psi. abs. and from 212 to 600°F. The most reliable values of these properties, and of the Prandtl number, have been presented and the discrepancies between these and other published values discussed.

5. Experimental values of the gas-phase heat transfer coefficients and the friction factors have been obtained for superheated steam flowing in a plain annulus and in three modified annuli. The plain annulus is that formed between a 1-1/2-inch O. D. tube and a 4.026-inch I. D. shell. The modified annuli are those between 1-1/2-inch O. D. tubes supporting three different types of extended surfaces and the 4.026-inch I. D.

shell. The extended surfaces are formed with longitudinal, helical, and "star" fins. The heat transfer section is 15.0 feet long in the case of the plain annulus, and 13.0 feet long for the modified annuli. The Reynolds number of the steam was varied from about 5000 to 102,000 over the temperature range of 294°F. to 460°F. at the two pressures of 50 and 100 psi. abs. Temperature differences between the heated inner tube and the steam were varied from 30°F. to 160°F. The gas-phase heat transfer coefficients, based upon the total exposed surface, were found to range from 2.85 to 26.2 Btu/hr.°F.ft.^{2} The friction factors were found to vary from about 0.02 for the plain annulus to about 0.40 for the modified annulus incorporating the "star" fin tube.

6. A simple graphical method has been devised for separating the "composite" gas-phase heat transfer coefficient into its radiation and convection components. This method gives the average radiation coefficient directly and the convection coefficient by difference. The method indicates that from 6.6 to 59 percent of the total heat transfer is by the mechanism of radiation.

7. The average radiation heat transfer coefficients have been obtained by the method of (6.) and are as follows:

Bare Tube - Plain Annulus	3.3 Btu/hr.°F.ft.^{2}
Longitudinal Fin Tube - Modified Annulus	1.0 Btu/hr.°F.ft.^{2}
"Star" Fin Tube - Modified Annulus	1.0 Btu/hr.°F.ft.^{2}
Helical Fin Tube - Modified Annulus	0.8 Btu/hr.°F.ft.^{2}

8. The convection heat transfer coefficients have been obtained by the method of (6.). These values range from 1.61 to 23.76 Btu/hr.°F.ft.^{2}

and have been correlated by the following Dittus-Boelter type equations:

Bare Tube - Plain Annulus

$$h = 0.022\ (K/D_v)(C\mu/K)^{0.4}\ (D_vW/\mu S_{min})^{0.80} \qquad (51)$$

Longitudinal Fin Tube - Modified Annulus

$$h = 0.0117\ (K/D_v)(C\mu/K)^{0.4}(D_vW/\mu S_{min})^{0.80} \qquad (52)$$

"Star" Fin Tube - Modified Annulus

$$h = 0.00795\ (K/D_v)(C\mu/K)^{0.4}(D_vW/\mu S_{min})^{0.91} \qquad (53)$$

Helical Fin Tube - Modified Annulus

$$h = 0.00514\ (K/D_v)(C\mu/K)^{0.4}(D_vW/\mu S_{min})^{0.91} \qquad (54)$$

9. A second, more rigorous method has also been described for the separation of the composite heat transfer coefficients into their radiation and convection components. This method involves a detailed theoretical analysis of the radiation process. The method is general and has been applied with reasonable rigor to the case of the plain annulus and with simplifications to the modified annuli.

10. The available data on the emissivity of water vapor in air have been extrapolated by means of a theoretical equation to yield reliable values for the emissivity of superheated steam.

11. The emissivity of the steel walls of the plain annulus has been determined by analysis of the data. The two values so obtained, 0.695 and 0.705, are excellent checks and in agreement with reported values. This

agreement offers confirmation to the procedure and to the steam emissivity figures obtained by extrapolation.

12. The radiation heat transfer coefficients have been obtained by the method of (9.). For the plain annulus, the values were found to vary from 3.06 to 3.51 Btu/hr.°F.ft.^{2} with an average value of 3.30, this constituting a perfect check with that obtained by the simple graphical method.

13. The radiation coefficients for the modified annuli have been obtained by the method of (9.) and by assuming the extension of the inner tube surface to raise the effective emissivity of the inner tube to unity without influencing the effective geometry of the system. The radiation coefficients obtained range from:

Longitudinal Fin Tube - Modified Annulus

0.84 to 1.28, with an average value of 1.05 Btu/hr.°F.ft.^{2}

"Star" Fin Tube - Modified Annulus

0.86 to 1.48, with an average value of 1.24 Btu/hr.°F.ft.^{2}

Helical Fin Tube - Modified Annulus

1.03 to 1.74, with an average value of 1.30 Btu/hr.°F.ft.^{2}

These values constitute satisfactory checks with those obtained by the simple graphical method.

14. The convection heat transfer coefficients have been obtained by the method of (9.) and have been correlated by the following Dittus-Boelter type equations:

Bare Tube - Plain Annulus

$$h = 0.022\ (K/D_v)(C\mu/K)^{0.4}(D_vW/\mu S_{min})^{0.80} \quad (134)$$

Longitudinal Fin Tube - Modified Annulus

$$h = 0.0117\ (K/D_v)(C\mu/K)^{0.4}(D_vW/\mu S_{min})^{0.80} \quad (135)$$

"Star" Fin Tube - Modified Annulus

$$h = 0.0078\ (K/D_v)(C\mu/K)^{0.4}(D_vW/\mu S_{min})^{0.91} \quad (136)$$

Helical Fin Tube - Modified Annulus

$$h = 0.00494\ (K/D_v)(C\mu/K)^{0.4}(D_vW/\mu S_{min})^{0.91} \quad (137)$$

These equations are considered more reliable than those obtained by the method of (6.), although the check is good.

15. The friction factors for the various annuli have been correlated against Reynolds number as follows:

Bare Tube - Plain Annulus

$$f = 0.133\ (D_vW/\mu S_{min})^{-0.16} \quad (138)$$

Longitudinal Fin Tube - Modified Annulus

$$f = 0.133\ (D_vW/\mu S_{min})^{-0.16} \quad (139)$$

"Star" Fin Tube - Modified Annulus

$$f = 0.395 \quad (140)$$

Helical Fin Tube - Modified Annulus

$$f = 0.402\ (D_vW/\mu S_{min})^{-0.15} \quad (141)$$

16. The convection heat transfer data and the pressure drop data have been interpreted in terms of "performance coefficients" to indicate the relative utility of the various surface arrangements which the annuli represent. Surfaces oriented transversely to the flow (e.g., the "star" and the helical fin tubes) have been found to possess great merit for use in installations where power consumption is secondary to compactness of equipment. On the other hand, surfaces oriented parallel to the direction of the flow (e.g., the bare and the longitudinal fin tubes) have been found most suitable for installations where volume of equipment is secondary to power consumption.

APPENDIX A

SUPPLEMENTARY PRESSURE DROP DATA AND CALCULATIONS

Table 1A presents supplementary pressure drop data not reported in Table II. These data are from preliminary runs which furnished unsatisfactory heat transfer information. A detailed explanation of the table is unnecessary since it is patterned closely after Tables II and VIII which have already been discussed.

The flow velocity (Column 14) and the pressure drop (Column 19) are plotted, along with values from Table VIII, in Figure 24 . Similarly, values of the friction factor (Column 21) and the Reynolds number (Column 22) are included in Figure 60.

TABLE IA

SUPPLEMENTARY PRESSURE DROP DATA AND CALCULATIONS

1	2	3	4	5	6	7	8	9	10	11	12	13	14	15	16	17	18	19	20	21	22
							FLOW RATE								PRESSURE DROP						
Test Number	Type of Inner Tube	Operating Pressure	Diameter Orifice Plate	Differential Across Orifice	Manometer Fluid	Effective Specific Gravity Manometer Fluid	Steam Temperature at Orifice	Specific Volume of Steam	Orifice Factor	Flow Rate	Average Steam Temperature	Specific Volume of Steam	Flow Velocity	Panel Board Temperature	Manometer Differential	Manometer Fluid	Effective Specific Gravity Manometer Fluid	Pressure Drop	Steam Viscosity	Friction Factor	Reynolds Number
Symbols, Units →		psi. abs.	in.	in.	---	ρ_m,	t_3, °F	v, ft^3/lb	F_b, -	W, lbs/hr	t_3, °F	v, ft^3/lb	V, ft/min	t_p, °F	in.	---	ρ_m, --	Δp, in. H_2O	μ, $\frac{lb}{ft\text{-}hr}$	f, --	$\left(\frac{D_p W}{\pi \mu_{min}}\right)$
Column Reference →		Data	Data	Data	Data	Table IA, 3,5 Figure 20	Data	---	See Text	Table IA, 5, 7,9,10	Data	---	Table I, 17 Table IA,11, 13	Data	Data	Data	Table IA, 15,17 Figure 21	Table IA,16, 18	Table IA, 12 Figure 14	Table I, Table IA,11 13,19	Table I,14,17 Table IA,11 20
20	BARE	50	1.250	13.1	A'	0.993	355	9.49	338	393	319	9.02	776	78.8	1.09	B	.0417	.0456	.0344	.0873	31,700
20A	"	"	"	13.3	"	.995	345	9.37	"	397	306	8.85	770	75.2	1.23	"	.0401	.0495	.0339	.0188	32,600
21	"	"	"	8.78	"	.993	354	9.48	"	319	312	8.93	625	80.4	1.11	"	.0425	.0472	.0340	.0275	26,100
22	"	"	"	5.35	"	.992	356	9.50	"	246	307	8.87	478	81.3	1.04	"	.0429	.0445	.0339	.0434	20,200
22A	"	"	"	4.90	"	.995	356	9.50	"	236	307	8.87	459	74.0	0.606	"	.0396	.0240	.0329	.0856	19,400
28	"	"	1.750	13.7	"	.994	347	9.39	675	804	318	9.02	1590	78.8	4.08	"	.0417	.170	.0343	.0154	65,100
29	"	"	"	10.0	"	.994	349	9.42	"	682	318	9.01	1350	78.9	3.92	"	.0418	.164	.0343	.0207	55,200
30	"	"	"	7.41	"	.994	350	9.43	"	583	318	9.01	1150	78.1	3.30	"	.0415	.137	.0343	.0235	47,200
31	"	"	"	4.38	"	.994	352	9.45	"	442	316	8.99	870	77.7	1.94	"	.0413	.080	.0342	.0239	35,900
32	"	100	"	20.5	A"	.989	382	4.82	"	1384	364	4.69	1420	80.9	8.96	"	.0426	.382	.0368	.0225	104,000
33	"	"	"	14.9	"	.989	383	4.82	"	1190	364	4.69	1220	79.5	9.19	"	.0420	.386	.0368	.0310	89,100
35	"	75	"	9.80	A"'	.991	374	6.42	"	829	349	6.20	1120	79.5	3.48	"	.0420	.146	.0360	.0181	63,600
36	"	"	"	7.72	"	"	376	6.43	"	736	351	6.21	1000	80.7	3.30	"	.0427	.141	.0362	.0220	56,500
37	"	"	"	5.81	"	"	378	6.45	"	632	352	6.22	862	81.7	3.11	"	.0431	.134	.0362	.0280	48,400
38	"	"	"	4.04	"	"	379	6.46	"	531	351	6.22	724	82.9	2.59	"	.0437	.113	.0362	.0340	40,600
39	"	"	"	2.74	"	"	382	6.49	"	438	350	6.21	597	83.5	1.43	"	.0439	.063	.0361	.0280	33,600
40	"	"	"	1.67	"	"	383	6.49	"	341	345	6.16	461	83.7	.447	"	.0440	.0197	.0358	.0148	26,300
41	"	50	"	13.1	A'	.993	362	9.58	"	785	334	9.23	1590	84.5	3.54	"	.0444	.157	.0351	.0146	62,000
45	"	125	"	27.7	A"	.987	405	3.93	"	1780	391	3.86	1500	83.3	11.71	"	.0438	.514	.0383	.0222	129,000
46	"	"	"	18.9	"	"	407	3.94	"	1470	393	3.86	1240	84.3	8.54	"	.0444	.379	.0385	.0241	106,000
47	"	"	"	12.5	"	"	408	3.94	"	1190	393	3.87	1010	84.7	6.22	"	.0444	.276	.0385	.0266	85,800
48	"	"	"	7.85	"	"	402	3.91	"	949	384	3.82	794	84.5	2.48	"	.0443	.110	.0380	.0274	69,200
49	"	"	"	4.15	"	"	402	3.91	"	689	382	3.81	575	83.9	2.27	"	.0441	.100	.0379	.0294	50,300
50*	"	50	"	19.80	A'	.993	392	6.31	"	1190	374	6.17	1610	81.6	9.39	"	.0430	.319	.0616	.0192	50,400
51*	"	"	"	11.52	"	"	395	6.32	"	910	375	6.17	1230	82.5	7.26	"	.0435	.234	.0616	.0242	40,900
52*	"	"	"	4.36	"	"	396	6.34	"	558	371	6.15	751	83.1	4.14	"	.0437	.0985	.0614	.0272	25,200
53*	"	"	"	1.97	"	"	396	6.34	"	376	367	6.11	504	83.5	2.75	"	.0439	.037	.0612	.0229	17,000

* indicates air used instead of steam.

APPENDIX B

SUPPLEMENTARY HEAT TRANSFER DATA AND CALCULATION OF THE STEAM OUTLET TEMPERATURE, G_2*

Preliminary heat transfer tests and their analysis indicated that the steam temperature G_2, as measured at the outlet from the exchanger, is not representative of the stream as a whole. This was confirmed beyond any doubt by temperature profiles taken at this point with a "travelling" thermocouple. The temperature profiles obtained were unsymmetrical with respect to the pipe axis and variable with flow rate.

Various attempts were made to equalize the gradient by the insertion of baffles, but these were unsuccessful since the baffle designs were limited to those which would not cause a significant pressure drop.

It was finally decided that the best way to obtain the true "mixed" temperature at the point, G_2, was to measure the temperature at a downstream point where the gradient did not exist, and obtain a measure of G_2 by correction for the heat loss between these points. The downstream location G_3 (see Figure 8) was selected and tested for uniformity of temperature with the travelling thermocouple. The temperature profiles at this location indicated that complete mixing had occurred and that reliable measurements could be obtained.

The supplementary data which were taken to permit the calculation of the mixed temperature at the steam outlet location are presented

in Table 1B. This table also includes the detailed calculation of G_2*, the mixed temperature, from the measured quantities.

Columns 1 and 2 of Table 1B give the test number and the type of tube. Columns 3 to 7, inclusive, report temperature data as follows:

Column 3: G_2, the steam outlet temperature; this value is not reliable.

Column 4: G_3, the steam temperature at the downstream location; this value is reliable.

Column 5: W_3, the outside temperature of the 4-inch pipe, near the exchanger outlet and point G_2.

Column 6: W_4, the outside temperature of the 4-inch pipe, near the spray chamber inlet and point G_3.

Column 7: S_m, the surface temperature of the insulation at a point midway between G_2 and G_3.

Column 8 presents the mean temperature of the pipe wall, W_m, and is obtained by averaging Columns 5 and 6. Column 9 gives the temperature differential causing the heat loss, $W_m - S_m$; Column 10, the mean temperature of the insulation obtained by averaging Columns 7 and 8.

Column 9 gives the heat loss between points G_2 and G_3. This is obtained by a method identical with that used in calculating the heat loss from the heat exchanger (see pages 89-91). The heat loss, q_{DL}, may be approximated (28) from the equation

$$q_{DL}' = \frac{kA_{lm}}{L} (W_m - S_m) \qquad \text{(B-1)}$$

which represents the conductive heat transfer rate from the outside wall of the 4-inch piping to the surface "skin" of the insulation. In this

TABLE IB

SUPPLEMENTARY HEAT TRANSFER DATA AND CALCULATION OF STEAM OUTLET TEMPERATURE, G_2^*

1	2	3	4	5	6	7	8	9	10	11	12	13	14	15	16
		TEMPERATURE DATA					CALCULATION OF G_2^*, STEAM OUTLET TEMPERATURE								
Test Number	Type of Inner Tube	Measured Steam Outlet	Steam After Orifice Plate	Downstream Outside of Outer Wall		Downstream Surface Insulation	Mean Downstream Wall	Differential for Heat Loss	Mean Temperature Insulation	Heat Loss	Steam Flow	Specific Heat of Steam	Temperature Drop	Computed Steam Outlet	Error in Measured Steam Outlet
Symbols, Units		G_2	G_3, °F	W_3, °F	W_4, °F	S_m, °F	W_m, °F	$W_m - S_m$, °F	T_k, °F	q_{DL} Btu/hr	W lbs/hr	C_3 Btu/lb°F.	$G_2^* - G_3$, °F	G_2^*, °F	$G_2 - G_2^*$, °F
Column Reference		Data	Data	Data	Data	Data	Table IB, 5,6	Table IB,7,8	Table IB, 7,8	Figure EI	Table VIII,7	Table IB,4 Figure 16	Table IB,11, 12,13	Table IB, 4,14	Table IB, 3,15
58	BARE	---	363.3	365.8	351.8	109	359	250	234	1550	364	0.556	7.65	371.0	---
58A	"	380.5	365.4	369.3	360.9	107	365	258	236	1600	362	.556	7.96	373.4	7.1
59	"	---	363.9	367.1	353.8	110	360	250	235	1550	298	.555	9.39	373.3	---
59A	"	384.2	365.6	370.8	360.7	108	366	254	237	1580	293	.555	9.71	375.3	8.9
60	"	---	358.9	366.1	347.5	110	357	247	234	1530	139	.554	19.89	378.8	---
60A	"	394.2	364.0	373.4	356.3	108	365	257	237	1600	144	.553	19.97	384.0	10.2
61	"	385.4	360.7	364.8	347.0	110	356	246	233	1520	178	.500	17.07	377.8	7.6
61A	"	375.9	354.9	370.8	349.2	106	360	254	233	1570	182	.501	17.22	372.1	3.8
62	"	382.3	352.4	360.5	338.5	108	348	240	228	1470	137	.500	21.45	373.9	8.4
62A	"	377.5	347.9	358.3	339.8	105	349	244	227	1500	135	.501	22.13	370.0	7.5
63	"	386.2	347.1	361.4	329.1	108	348	240	228	1470	89.6	.501	32.8	379.9	6.3
63A	"	387.8	345.8	362.0	334.1	105	348	243	227	1490	91.4	.501	32.5	378.3	9.5
64	"	400.2	395.4	396.4	372.7	116	384	268	250	1700	1410	.537	2.25	397.7	2.5
65	"	401.7	395.4	396.2	372.1	117	384	267	250	1700	1045	.536	3.03	398.4	3.3
66	"	401.3	391.6	392.7	365.5	117	379	262	248	1660	570	.538	5.42	397.0	4.3
67	"	405.1	397.7	398.2	369.7	115	384	269	250	1710	721	.494	4.80	402.5	2.6
68	"	403.6	393.0	395.9	365.0	116	380	264	248	1670	473	.495	7.14	400.1	3.5
69	"	399.1	383.8	385.7	353.0	113	369	256	241	1600	297	.496	10.87	394.7	4.4
70	"	396.6	388.5	389.3	374.9	117	382	265	250	1680	749	.540	4.16	392.7	3.9
71	"	398.2	388.3	389.7	374.0	117	381	264	249	1670	590	.540	5.26	393.6	4.6
72	"	396.6	378.8	379.5	363.0	117	371	254	244	1600	309	.544	9.51	388.3	8.3
73	"	392.1	379.9	379.9	363.0	115	371	256	243	1610	370	.497	8.74	388.6	3.5
74	"	392.3	376.1	378.5	358.4	114	368	254	241	1590	299	.497	10.70	386.8	5.5
75	"	392.8	371.6	375.1	352.5	114	364	250	239	1560	207	.498	15.15	386.8	6.0
76	LONGITUDINAL FIN	448.1	440.8	440.6	434.7	118	438	320	278	2130	695	.519	5.90	446.7	1.4
77	"	448.3	439.9	440.1	423.5	118	432	314	275	2070	555	.519	7.20	447.1	1.2
78	"	446.6	435.7	436.3	417.6	118	427	309	272	2030	410	.520	9.52	445.2	1.4
79	"	449.3	437.0	438.8	417.3	115	428	313	271	2060	338	.489	12.46	449.5	-0.2
80	"	448.9	431.2	435.5	409.3	113	422	309	267	2010	238	.490	17.17	448.4	0.5
81	"	444.9	418.0	427.7	393.7	110	411	301	260	1940	146	.486	27.4	445.4	0.5
82	"	430.7	417.8	419.3	399.5	118	409	291	263	1890	346	.526	10.38	428.2	2.5
83	"	440.0	421.3	425.2	400.0	118	413	295	265	1920	266	.525	13.74	435.0	5.0
84	"	445.9	419.2	426.4	397.5	118	412	294	265	1920	158	.526	23.1	442.3	3.6
85	"	433.3	406.3	415.1	382.1	117	399	282	258	1810	173	.493	21.2	427.5	5.8
86	"	440.4	400.4	418.6	375.5	118	397	279	257	1790	117	.494	31.0	431.4	9.0
87	"	448.1	394.4	422.0	367.1	117	395	278	256	1780	78.5	.495	45.8	440.2	7.9
88	"	461.5	457.6	447.6	442.6	122	445	323	283	2170	1300	.513	3.25	460.9	0.6
89	"	462.9	458.0	458.4	442.5	123	450	327	286	2210	950	.513	4.53	462.5	0.4
90	"	460.8	455.0	455.0	438.9	123	447	324	285	2180	793	.514	5.35	460.4	0.4
91	"	443.2	436.5	437.1	419.3	121	428	307	274	2020	666	.489	6.20	442.7	0.5
92	"	446.0	437.0	437.6	418.5	120	428	308	274	2030	480	.489	8.65	445.7	0.3
93	"	449.3	436.1	437.9	415.8	120	427	307	273	2020	335	.489	12.40	448.5	0.8

TABLE IB, CONTINUED

SUPPLEMENTARY HEAT TRANSFER DATA AND CALCULATION OF STEAM OUTLET TEMPERATURE, t_2^*

1	2	3	4	5	6	7	8	9	10	11	12	13	14	15	16
		TEMPERATURE DATA					CALCULATION OF t_2^*, STEAM OUTLET TEMPERATURE								
Test Number	Type of Inner Tube	Measured Steam Outlet	Steam After Orifice Plate	Downstream Outside of Outer Wall		Downstream Surface Insulation	Mean Downstream Wall	Differential for Heat Loss	Mean Temperature Insulation	Heat Loss	Steam Flow	Specific Heat of Steam	Tempera-ture Drop	Computed Steam Outlet	Error in Measured Steam Outlet
Symbols, Units →		t_2	t_3, °F	w_3, °F	w_4, °F	s_w, °F	w_m, °F	$w_m - s_w$, °F	T_k, °F	Q_{DL} Btu/hr	W lbs/hr	C_3 Btu/lb°F	$t_2^* - t_3$, °F	t_2^*, °F	$t_2 - t_2^*$, °F
Column Reference →		Data	Data	Data	Data	Data	Table IB, 5,6	Table IB, 7,8	Table IB, 7,8	Figure BI	Table VIII, 7	Table IB, 4 Figure 16	Table IB, 11,12,13	Table IB, 4,14	Table IB, 3,15
94	"STAR" FIN	479.7	462.7	468.1	441.7	133	455	322	294	2210	290	.512	14.89	477.6	2.1
95	"	480.1	457.6	466.3	434.7	133	451	318	292	2170	208	.514	20.30	477.9	2.2
96	"	480.0	444.9	461.6	419.2	128	440	312	284	2100	130	.514	31.44	476.3	3.7
97	"	478.2	446.1	459.2	419.8	126	440	314	283	2110	154	.488	28.06	474.2	4.0
98	"	478.3	434.2	455.3	427.6	124	441	317	283	2130	114	.489	38.18	472.4	5.9
99	"	475.5	408.1	445.5	377.9	121	412	291	267	1900	64.5	.493	59.75	467.9	7.6
100	"	476.0	466.0	468.4	447.8	132	458	326	295	2240	305	.512	8.66	474.7	1.3
101	"	476.8	463.6	467.0	444.0	132	456	324	294	2220	356	.512	12.18	475.8	1.0
102	"	481.8	455.3	465.6	432.8	132	449	317	291	2160	182	.514	23.10	478.4	3.4
103	"	491.2	465.2	475.0	449.1	116	462	346	289	2350	246	.487	19.61	484.8	6.4
104	"	490.8	454.2	469.8	440.4	117	455	338	286	2280	196	.488	23.82	478.0	12.8
105	"	490.8	446.0	463.1	427.8	114	445	331	280	2210	138	.488	32.82	478.8	12.0
106	"	487.4	467.7	479.3	453.5	118	466	348	292	2380	329	.487	14.85	482.6	4.8
107	"	490.0	460.2	473.0	443.6	120	458	338	289	2300	228	.487	20.71	480.9	9.1
108	"	487.4	476.1	487.1	464.4	123	456	333	290	2270	651	.509	6.85	483.0	4.4
109	"	489.4	476.7	487.6	465.0	123	456	333	290	2270	554	.509	8.06	484.8	4.6
110	"	491.8	473.7	484.4	459.7	123	472	349	298	2420	355	.510	13.36	487.1	4.7
111	"	491.3	427.0	461.4	406.0	118	434	316	276	2090	84.5	.490	50.5	477.5	13.8
112	"	489.8	402.0	457.0	381.1	116	419	303	268	1980	60.7	.493	66.1	468.1	21.7
113	HELICAL FIN	466.0	457.5	461.0	454.2	121	458	337	290	2290	546	.514	8.16	465.7	0.3
114	"	466.2	460.0	462.7	456.5	122	460	338	291	2300	697	.513	6.44	466.4	-0.2
115	"	466.2	461.2	462.8	458.6	123	461	338	292	2300	791	.512	5.68	466.9	-0.7
116	"	466.0	461.8	463.8	459.2	123	462	339	293	2310	912	.512	4.95	466.8	-0.8
117	"	468.2	460.3	463.8	456.5	123	460	337	292	2300	553	.513	8.44	468.7	-0.5
118	"	461.3	452.0	454.0	445.8	121	450	329	286	2230	490	.488	9.75	461.8	-0.5
119	"	463.2	450.3	455.4	443.9	122	450	328	286	2220	400	.488	11.4	461.7	1.5
120	"	468.3	451.2	458.0	443.1	123	451	328	287	2230	294	.488	16.3	467.5	0.8
121	"	463.6	446.3	449.9	437.5	119	444	325	282	2180	311	.488	14.4	460.7	2.9
122	"	465.9	448.6	452.8	436.6	120	445	325	283	2180	272	.488	16.4	461.0	4.9
123	"	468.2	445.5	455.1	436.3	121	446	325	284	2190	225	.488	20.0	465.5	2.7
124	"	469.1	444.1	455.1	434.1	122	445	323	284	2180	195	.488	22.9	467.0	2.1
125	"	470.5	441.3	455.8	430.6	121	443	322	282	2170	159	.489	27.9	469.2	1.3
126	"	456.2	450.5	452.0	446.1	122	449	327	286	2210	696	.515	6.74	457.2	-1.0
127	"	462.8	451.6	456.0	447.0	121	452	331	287	2240	448	.515	9.71	461.3	1.5
128	"	470.0	451.5	459.4	444.4	121	452	331	287	2240	269	.515	16.2	467.7	2.3

equation:

q_{DL}' = approximation to the heat loss, Btu/hr.

k = mean thermal conductivity of the insulation, Btu. in/ft^2 hr. °F.

L = thickness of insulation, in.

A_{lm} = logarithmic mean area normal to the direction of heat flow, ft^2.

$(W_m - S_m)$ = temperature difference across the insulation, °F.

As mentioned on page 89, this equation does not take into account heat loss through the supporting stands of the equipment and connecting piping. These losses may be estimated as equivalent to the loss through three rectangular steel supports of cross section A_s and length L_s;

i.e.

$$q_{DL}'' = \frac{3k_s A_s}{L_s} (W_m - S_m) \qquad \text{(B-2)}$$

where

q_{DL}'' = heat loss from stands and connecting pipes, Btu/hr.

k_s = thermal conductivity of steel, Btu ft./ft.^{2}hr.°F.

A_s = cross-sectional area normal to heat flow, ft.^{2}

L_s = length of travel to a point where the metal temperature is equal to S_m, ft.

Combination of equations (B-1) and (B-2) leads to

$$q_{DL} = q_{DL}' + q_{DL}'' = \left(\frac{k A_{lm}}{L} + \frac{3k_s A_s}{L_s}\right) (W_m - S_m) \qquad \text{(B-3)}$$

where

q_{DL} = calculated heat loss from the downstream piping section.

Numerical values may be substituted into equation (B-3) as follows:

$$A_{lm} = \frac{6.62}{12} (\pi)\ 24 = 41.5 \text{ ft.}^2$$

where

6.62 = logarithmic mean diameter of insulation, in.

24.0 = effective length of unit, ft.

$L = 2.375$ in.

$k_s = 26.0$ Btu ft./hr. ft.^{2} °F.

$L_s = 1.50$ ft. (estimated)

$A_s = 1.25$ in.^{2} = 0.0087 ft.^{2} (estimated)

This leads to

$$q_L = (17.5\ k + 0.451)\ (W_m - S_m) \qquad \text{(B-4)}$$

The thermal conductivity of the insulation is dependent upon its average temperature, T_K, in accordance with the relationship shown in Figure 20 (a) which represents the manufacturer's data.

Equation (B-4), along with Figure 20 (a), may be used to calculate the heat loss with an estimated uncertainty of 10 or 15 per cent. Because of this uncertainty, a blank test was conducted in which no heat was transferred in the exchanger, and the thermocouple at G_2 gave a true reading of the temperature of the steam at the exchanger outlet. The difference between the temperatures at points G_2 and G_3 was then a measure of the heat loss. This test gave the following results:

q_{DL} (observed) = 1330 Btu/hr.

$(W_m - S_m)$ = 195°F.

T_K = 200°F. = average temperature of the insulation.

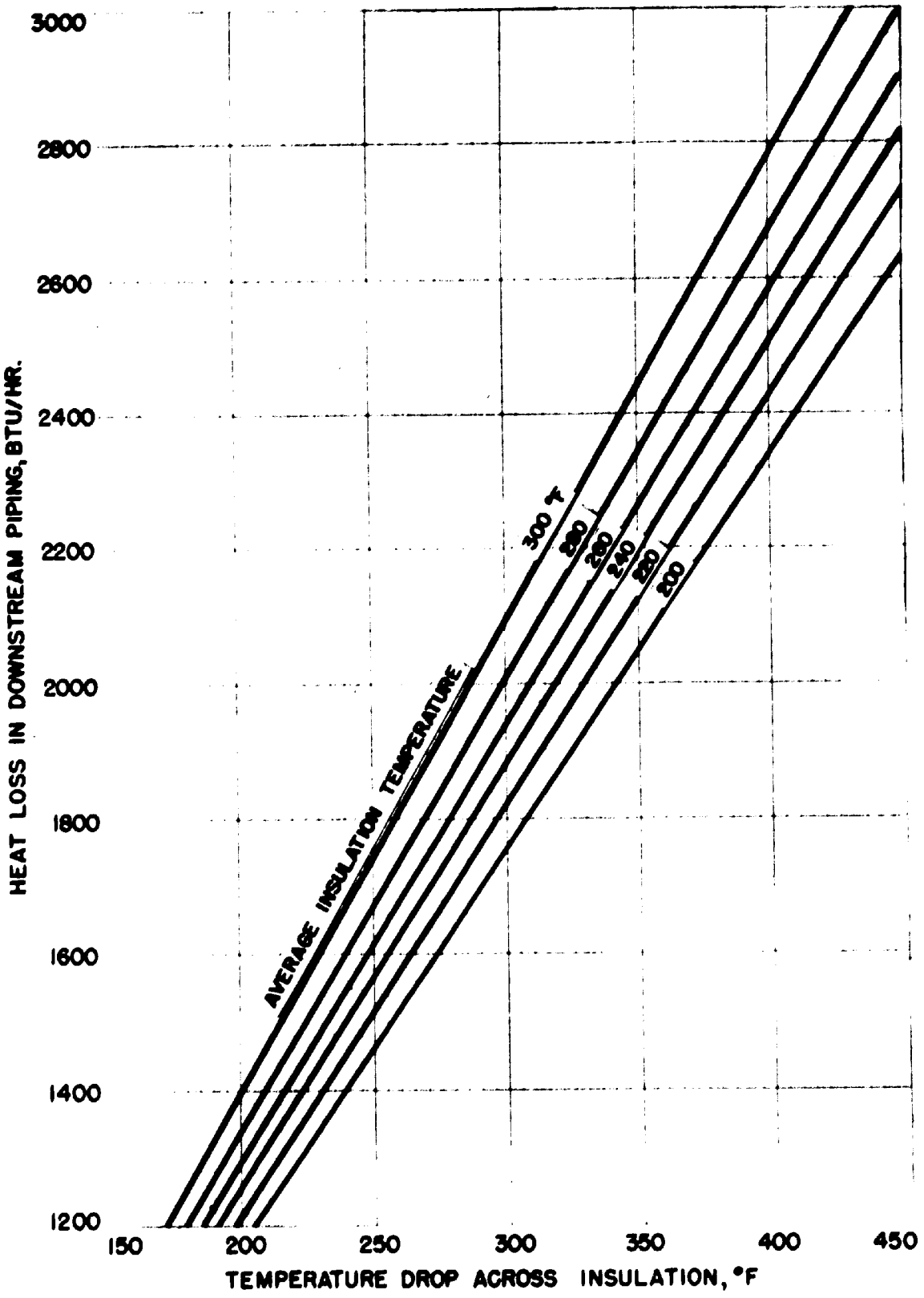

FIGURE. B-1

HEAT LOSS IN DOWNSTREAM PIPING

It is believed that the value of q_{DL}, obtained from this test, is within about 10 per cent of the true value. Calculating q_{DL} from equation (B-4) and Figure 20 (a) for the conditions of the test,

$$q_{DL} = \left[17.5\ (0.31) + 0.451\right]\ 195$$
$$= 1144 \text{ Btu/hr.}$$

which differs from the measured value by 15 per cent. The average of the two values, i.e., $q_{DL} = 1255$, is however within 10 per cent of both the measured and the computed values and is probably within about 5 per cent of the true value. Equation (B-4) may be modified therefore to give

$$q_{DL} = \frac{1255}{1144}\ (17.5\ k + 0.451)\ (W_m - S_m) \qquad (B\text{-}5)$$

The relationship of equation (B-5) is presented in chart form in Figure 1B. The quantity q_{DL}, reported in Column 11 of Table 1B, is obtained from this chart using values of T_K and $(W_m - S_m)$ from Columns 9 and 11. Column 12 of Table 1B indicates the steam flow rate, W, as recorded in Table VIII, Column 7. Column 13 gives the specific heat of steam, C_3, taken at the temperature G_3, of Column 4.

The temperature drop of the steam in flowing from point G_2 to point G_3 is presented in Column 14 as $G_2^* - G_3$, where G_2^* indicates the true temperature at G_2, the steam outlet from the exchanger. This calculation is carried out in accordance with the equation

$$G_2^* - G_3 = q_{DL}/W\ C_3 \qquad (B\text{-}6)$$

from Columns 11, 12 and 13.

Column 15 reports the final computed value of the true steam outlet temperature G_2^* as obtained by adding Columns 4 and 14. This

value is considered more reliable than could be obtained by direct observation at the point G_2. As a matter of interest, Column 16 reports the difference between the measured value of the temperature at the point G_2 and the calculated value, G_2*. This quantity ranges from 21.7 to -1.0 °F. being smaller at the higher flow rates.

APPENDIX C

CALCULATION OF THE SALT FLOW RATE

Because of difficulties encountered in the operation of the salt seal pot system, the salt flow rate was not directly observed. The flow rate, however, was kept at the maximum output of the pump at all times and since the temperature (and, therefore, the properties) of the salt was held constant at about 500°F., the salt flow rate was constant in all tests.

Early in the experimental program, a special test was conducted with the salt system filled with water at 99°F. The piping circuit was identical to that used throughout the later tests with salt. The maximum output of the pump through the piping system was determined, in terms of water flow, by calculation from the observed differential across the orifice plate.

The data obtained in the water test and the calculation of the water flow rate follow:

Diameter of orifice plate 1.000 inch

Diameter of pipe 2-1/2-inch i.p.s.

Differential across orifice plate = 19.7 cm. mercury under water

= 19.7 (12.55) = 247 cm. water

Flow equation - MacLean (25)

$$Q' = 0.00003656\, F_b R_F \sqrt{h/\rho_w} \qquad \text{(C-1)}$$

where

h = differential, cm. water

ρ_w = specific gravity water at 99°F. = 0.993

F_b = basic flow factor for 1.000-inch orifice in 2-1/2-inch i.p.s. pipe

= 210.65

R_F = Reynolds number factor

= 1.000

Q' = flow rate, $ft^3/sec.$ under flowing conditions

Solving for the flow rate

$$Q' = 0.121 \ ft^3/sec.$$

This flow rate corresponds to a velocity through the 1.000-inch I.D. inner tube of the exchanger of

$$V_w = \frac{0.121}{\pi} (576) \qquad (C\text{-}2)$$

$$= 22.1 \ ft/sec.$$

where V_w = water velocity, f.p.s. through the 1.000-inch I.D. tube.

It is now necessary to compute the velocity which would be realized by molten salt when flowing in the same system. The pertinent properties of the salt at 500°F. as given by Kirst (17) are

specific gravity, ρ_s	1.89
absolute viscosity, μ_s	4.20 centipoises
kinematic viscosity, $\frac{\mu_s}{\rho_s}$	2.22 centistokes

The fundamental flow equation for a liquid may be written (28) as

$$(X_2 - X_1) + \frac{P_2 - P_1}{\rho'} + \frac{V_2^2 - V_1^2}{2\beta} - W + \Sigma F = 0 \qquad (C\text{-}3)$$

where

X = the height in feet above an arbitrary datum

P = the fluid pressure, lbs/ft^2

V = the lineal velocity of the fluid, ft/sec.

W = the mechanical energy input to the fluid, ft.lbs/lb.

ΣF = the total energy dissipated as friction, ft.lbs/lb.

ρ' = the fluid density, lbs/ft^3

β = dimensional constant, $32.1740 \frac{\text{mass lbs.}}{\text{force lb.}} \frac{ft^2}{\text{sec.}}$

The subscripts 1 and 2 refer to conditions at the arbitrarily selected points 1 and 2.

Selecting point 1 in the discharge pipe of the pump at the elevation of the salt surface in the reservoir, and point 2 in the free surface at the same elevation,

$$X_2 - X_1 = 0$$

$$P_2 - P_1 = -P_1 = -H\rho'$$

where H is the head developed by the pump in ft. of salt

$$V_2^2 - V_1^2 = -V_1^2$$

$$W = 0$$

Also, ΣF may be written (35) as

$$\Sigma F = \frac{fV^2 N_e}{2\beta D} \qquad (C\text{-}4)$$

where

f = friction factor

N_e = equivalent length of the piping system expressed in terms of 1.000-inch I.D. tube, ft.

D = diameter of 1.000-inch tube, ft.

Combining equation (C-4) with (C-3) and inserting the values indicated above,

$$-H - \frac{V_1^2}{2\beta} + \frac{fV^2N_e}{2\beta D} = 0 \qquad \text{(C-5)}$$

Combining the second and third terms of equation (C-3) and rearranging,

$$H = \frac{fV^2N_e'}{2\beta D} \qquad \text{(C-6)}$$

where

N_e' = new equivalent length, ft.

The friction factor, f, may be expressed (34) as

$$f = a\left(\frac{DV\rho'}{\mu'}\right)^{-0.2} \qquad \text{(C-7)}$$

where

a = a constant

μ' = the fluid viscosity, lbs./ft.sec.

Combining equations (C-6) and (C-7)

$$H = \frac{a}{2\beta}\frac{V^{1.8}}{D^{1.2}}\left(\frac{\mu'}{\rho'}\right)^{0.2}$$

i.e.

$$H = bV^{1.8}\left(\frac{\mu'}{\rho'}\right)^{0.2} \qquad \text{(C-8)}$$

where

$$b = \frac{a}{2\beta D^{1.2}}\text{, a constant.}$$

Equation (C-8) may also be written as

$$H = cQ^{1.8}\left(\frac{\mu}{\rho}\right)^{0.2} \qquad \text{(C-9)}$$

where

Q = flow rate in gpm

$(\frac{\mu}{\rho})$ = kinematic viscosity, centistokes

c = a new constant

Equation (C-9) represents for any fluid the relationship for the salt piping system between the head supplied at point 1, the flow rate, Q, and the kinematic viscosity of fluid. There remains now the problem of obtaining the corresponding relationship for the pump.

Ippen (20a), in his recent study of the influence of physical properties of fluids on centrifugal pump performance, demonstrates that:

(a) The effect, upon the head-capacity curve, of a small change in kinematic viscosity (as from that of water at 99°F. to salt at 500°F.) is completely negligible.

(b) The effect, upon the head-capacity curve, of a change in density (as from that of water at 99°F. to salt at 500°F.) is completely negligible provided the discharge head is expressed in feet of fluid being handled.

On this basis, therefore, the pump may be expected to perform along the same fluid head-capacity curve with molten salt as it does with water. The characteristic head-capacity curve for the Taber centrifugal pump may be represented over a short range of capacity by the equation

$$H = H_o \left(1 - \frac{Q}{400}\right) \qquad \text{(C-10)}$$

where

H = discharge head in feet of fluid being pumped

Q = pumping rate, gpm

H_o = discharge heat at zero capacity

This relation has been obtained empirically from the head-capacity curve supplied by the Taber Pump Company.

Combining equation (C-9) for the piping system and equation (C-10) for the pump,

$$\frac{H_o}{c}\left(1 - \frac{Q}{400}\right) = Q^{1.8}\left(\frac{\mu}{\rho}\right)^{0.2} \qquad \text{(C-11)}$$

Equation (C-11) may now be applied (a) to water at 99°F., and (b) to salt at 500°F.

$$\text{(a)} \quad \frac{H_o}{c}\left(1 - \frac{0.121}{400}\right) = 0.121^{1.8}\,(0.700)^{0.2} \qquad \text{(C-12)}$$

$$\text{(b)} \quad \frac{H_o}{c}\left(1 - \frac{Q_s}{400}\right) = Q_s^{1.8}\,(2.22)^{0.2} \qquad \text{(C-13)}$$

where

0.700 = kinematic viscosity of water at 99°F., $\frac{\mu_w}{\rho_w}$

Q_s = salt flow rate at 500°F., gal/min.

Upon division of equation (C-13) by equation (C-12),

$$\frac{\left(1 - \frac{Q_s}{400}\right)}{\left(1 - \frac{0.121}{400}\right)} = \left(\frac{Q_s}{0.121}\right)^{1.8}\left(\frac{2.22}{0.700}\right)^{0.2} \qquad \text{(C-14)}$$

which may be solved for Q_s, the salt flow rate. Trial and error solution of equation (C-14) results in

$$Q_s = 47.8 \text{ gal/min.}$$

from which the salt velocity in the 1.000-inch I.D. exchanger tube is obtained as 19.5 ft/sec. (compared with the measured water velocity of 22.1 ft/sec.).

This computed value of the salt velocity is considered reliable since its calculation, based upon a reliable measure of the water velocity, is made without serious assumptions.

NOMENCLATURE

α = absorptivity

β = dimensional constant, 32.1740 (mass lbs)ft/(force lbs)sec^2

ϵ = emissivity

θ = average temperature, °F., see text

λ = wave length of radiation

μ = viscosity, lbs/ft-hr

μ_f = viscosity of fluid evaluated at the film temperature, lbs/ft-hr

μ_w = viscosity of fluid evaluated at the wall temperature, lbs/ft-hr

ρ_w = density, lbs/ft^3

σ = Stefan-Boltzmann constant, 0.173 $Btu/hr(°R)^4$

ϕ = fin efficiency

A = heat transfer surface, ft^2

A_o = area of bare tube exposed between fins, ft^2

A_f = area of finned surface, ft^2

$(A_o + \phi A_f)$ = effective heat transfer surface of fin tube, ft^2

A, A^o = radiation factors, see text

A' refers to a manometer fluid system embodying water-saturated air at 50 psi. trapped over water

A" refers to a manometer fluid system embodying water-saturated air at 100 psi. trapped over water

B refers to a manometer fluid system embodying turpentine with dissolved carbon tetrachloride trapped over water

B = radiation factor, see text

C = radiation factor, see text

C = specific heat, Btu/lb°F

C refers to a manometer fluid system embodying gasoline trapped over water

d = orifice plate diameter, in

D_1 = diameter at the inner wall of the annulus, ft

D_2 = diameter at the outer wall of the annulus, ft

D' = equivalent diameter of a plain annulus

= $D_2 - D_1$, ft

D_e', D_e'', D_r, D_v = equivalent diameters of modified annuli, ft, see text

D, D^o = radiation factors, see text

E = orifice efficiency factor

E = emissive power, Btu/ft^2-hr

E = radiation factor, see text

F = radiation factor, see text

F = radiation angle factor

F = energy dissipated due to friction, feet of flowing fluid

F_b' = basic orifice flow factor equal to $345.92\ Ed^2$

F_e = factor for expansion of orifice plate with temperature

F_b = $1.04\ F_b'$

f = friction factor

f' = $4f$ = friction factor

G = mass velocity, lbs/ft^2-hr

G, G^o = radiation factors, see text

G_1 = steam temperature at heat exchanger inlet, °F.

G_2 = measured steam temperature at heat exchanger outlet, °F

G_2^* = calculated steam temperature at heat exchanger outlet, °F

H = radiation factor, see text

h = convection heat transfer coefficient, Btu/hr°F ft^2

h_R = radiation heat transfer coefficient, Btu/hr°F ft^2

h' = $h + h_R$ = composite heat transfer coefficient, Btu/hr°F ft^2

h_w = differential heat across orifice plate, in.water

Δh = increase in enthalpy of the fluid in the inner tube, Btu/lb

ΔH = increase in enthalpy of the annular fluid, Btu/lb

J = radiation factor, see text

K,k = thermal conductivity, Btu-ft/hr°F ft^2

k_s = thermal conductivity of steel, Btu-ft/hr°F ft^2

L = length, ft

L = radiant beam length, ft

L_1 = salt temperature at heat exchanger inlet, °F

L_2 = salt temperature at heat exchanger outlet, °F

m = exponent of Prandtl Number in equation for convection heat transfer coefficient

N = constant in equation for convection heat transfer coefficient for modified annuli

n = exponent of Reynolds number in equation for convection heat transfer coefficient for modified annuli

P = pressure, psi. abs.

P = partial pressure of radiating component, atmos.

ΔP = pressure drop, in. of water

P_E = energy performance coefficient for heat transfer surface, Btu/watt-hr°F

P_V = volume performance coefficient for heat transfer surface, Btu/hr-ft^3°F

p = emissivity (or absorptivity) of the steel walls of the annulus

Q_s = rate of flow of steam, ft^3/hr

q = heat transfer rate, Btu/hr

q = total heat transfer from the inner tube of the annulus, Btu/hr

q_{RT} = net radiant heat transfer from the inner tube, Btu/hr

q_{CTG} = convection heat transfer from the inner tube to the annular fluid, Btu/hr

q_{RG} = net radiant heat transfer to the annular fluid, Btu/hr

q_{RW} = net radiant heat transfer to the outer wall of the annulus, Btu/hr

q_L = heat loss from the heat exchanger, Btu/hr

q_{DL} = heat loss from the downstream piping, Btu/hr

R_f = Reynolds number factor in orifice flow equation

S = total cross-sectional area of heat exchanger, ft^2

S_{min} = minimum free cross section of heat exchanger available for flow, ft^2

S_{max} = maximum free cross section of heat exchanger available for flow, ft^2

T = temperature, °F or °R

ΔT = temperature differential available for heat transfer, °F

V = lineal velocity, ft/sec

V_{max} = lineal velocity through minimum free cross section of heat exchanger, ft/min

v = specific volume of steam, ft^3/lb

w = rate of flow of the fluid in the inner tube, lbs/hr

W = rate of flow of the annular fluid or steam, lbs/hr

W_1 = temperature of heat exchanger shell near steam inlet, °F

W_2 = temperature of heat exchanger shell near steam outlet, °F

W_3 = temperature of downstream piping near steam outlet, °F

W_4 = temperature of downstream piping near blower inlet, °F

Note: See text for explanation of nomenclature not included in this list.

BIBLIOGRAPHY

(1) Boelter, L. M. K., Cherry, V. H., and Johnson, H. A., Heat Transfer Notes, Univ. of Calif. Press (1942)

(2) Carpenter, F. G., Colburn, A. P., Schoenborn, E. M., and Wurster, A., Trans. Amer. Inst. Chem. Engrs., 42, 165, 1946

(3) Colburn, A. P., Gunter, A. Y., Amer. Inst. Chem. Engrs., 40, 200, 1944

(4) Colburn, A. P., Trans. Amer. Inst. Chem. Engrs., 29, 174, 1933

(5) Davis, E. S., Trans. Amer. Soc. Mech. Eng., Oct. 1943, 755

(6) DeLorenzo, B., and Anderson, E. D., Amer. Soc. Mech. Eng., Heat Transfer Symposium, 1944

(7) Dittus, F. W., and Boelter, L. K., Univ. of Calif., Public. in Engrg., 2, 443, 1930

(8) Dorsey, N. E., Properties of Ordinary Water Substances, Reinhold Publishing Company, New York, p. 73

(9) Dufinez, M., and Marcus, P., M. S. Thesis, Carnegie Inst. Tech., 1938

(10) Foust, A. S., Christian, G. A., Trans. Amer. Inst. Chem. Engr., 36, 541, 1940

(11) Gardner, K. A., Trans. Amer. Soc. Mech. Engr., 621, 1944

(12) Gunter, A. Y., and Shaw, W. A., Trans. Amer. Soc. Mech. Engr., 64, 1942

(13) Hawkins, G. A., Solberg, H. L., and Potter, A. A., Trans. Amer. Soc. Mech. Engr., 57, 395, 1935

(14) Hawkins, G. A., Solberg, H. L., and Potter, A. A., Trans. Amer. Soc. Mech. Engr., 62, 677 (1940)

(15) Hawkins, G. A., Sibbitt, W. L., Solberg, H. L., Unpublished work on loan from Professor F. G. Keyes

(16) Katz, D. L., Hope, R. E., and Datsko, S. C., Refrig. Engrg., April, 1946

(17) Kirst, W. E., Nagle, W. M., and Castner, J. B., Trans. Amer. Inst. Chem. Engr., 3, 1, 1940

(18) Hottel, H. C., Personal Communication, August, 1948

(19) Hottel, H. C., and Egbert, R. B., Amer. Inst. Chem. Engr., 38, 531, 1942

(20) Hottel, H. C., and Egbert, R. B., Trans. Amer. Soc. Mech. Engr., 297, 1941

(20a) Ippen, A. T., Amer. Soc. Mech. Eng., Paper No. A-45-47, Nov. 27, 1945

(21) Jakob, M., Trans. Amer. Inst. Chem. Engr., 42, 1015, 1946

(22) Jordan, H. P., Proc. Inst. Mech. Engr., (London), Parts 3-4, 1317, 1909

(23) Keenan, J. H., and Keyes, F. G., Thermodynamic Properties of Steam, John Wiley and Sons, Inc., New York, 1944

(24a) Keyes, F. G., Mass. Inst. of Tech., Personal Communication, 1947

(24b) Keyes, F. G., Smith, L. B., Gerry, H. T., Proc. Am. Acad. of Arts and Sci., Vol. 70, p. 319, 1936

(25) MacLean, A. D., The Orifice Meter, Pittsburgh Equitable Meter Co., Pittsburgh, Pennsylvania

(26) Marks, L. S., Mechanical Engineers Handbook, McGraw-Hill Co., 1941

(27) Martinelli, R. C., Weinberg, E. B., Morrin, E. H., and Boelter, L. M. K., N.A.C.A., ARR., Oct., 1942

(28) McAdams, W. H., Heat Transmission, McGraw-Hill Book Company, New York, 1942

(29) McMillen, E. L., and Larson, R. E., Trans. Amer. Inst. Chem. Engr., 40, 177, 1944

(30) Monrad, C. C., and Pelton, J. F., Trans. Amer. Inst. Chem. Engr., 38, 593, 1942

(31) Mueller, A. C., Trans. Amer. Inst. Chem. Engr., 38, 613, 1942

(32) Nikuradse, J., Forschungsheft, 356, 1932

(33) Pierce, B. O., A Short Table of Integrals, Ginn and Co., 1929

(34) Perry, Chemical Engineers' Handbook, McGraw-Hill Book Company, New York, 1941.

(35) Rouse, H., Elementary Mechanics of Fluids, Wiley, 1946

(36) Schiller, W., Forschung auf dem Gebiete des Ingenieurwesens, March - April, 1934, Vol. 5, p. 73.

(37) Sieder, E. N. and Tate, G. E., Ind. Eng. Chem., 28, 1429 (1930).

(38) Sigwart, K., Forschung auf dem Gebiete des Ingenieurwesens, May - June, 1937, Vol. 7, p. 125.

(39) Speyer, H., Forschung auf dem Gebiete des Ingenieurwesens, 1925, No. 273.

(40) Thompson, T. J., Foust, A. S., Trans. Amer. Inst. Chem. Engrs., 36, 555 (1940).

(41) Timroth, D. L. and Vargaftik, N. B., Journal of Physics (Moscow) 1940, Vol. 2, No. 2, p. 101.

(42) Timroth, D. L., Journal of Physics (Moscow) 1940, Vol. 2, p. 419.

(43) Van Hengel, G. H., Detroit Edison Company, Personal Communications.

(44) Wiegand, J. H. and Baker, E. M., Trans. Amer. Inst. Chem. Engrs., 38, 569 (1942).

(45) Wiegand, J. H., Trans. Amer. Inst. Chem. Engrs., 41, 147 (1945).

(46) Wiegand, J. H., PhD Thesis, Univ. of Michigan, 1941, pp. 219, Pub. No. 306, University Microfilms, Ann Arbor, Mich.

(47) Zerban, A. H., PhD Thesis, Univ. of Michigan, 1940.